Centrobin functions in centriole duplication, primary ciliogenesis and genome maintenance

Yetunde Blessing Adesanya

Centre for Chromosome Biology,
School of Natural Sciences,
National University of Ireland Galway

A thesis submitted to the National University of Ireland Galway for the degree of Doctor of philosophy

October 2017

Supervisor: Prof. Ciaran G. Morrison

Centre for Chromosome Biology

Table of contents

Table of contents ..... **I**

List of figures ..... **IV**

List of tables ..... **VI**

Abbreviations ..... **VII**

Declaration ..... **X**

Acknowledgements ..... **XI**

Abstract ..... **XIII**

1 Introduction **1**
1.1 Centrosomes and centrioles **1**
1.1.1 Evolutionary conservation of centrosome and centrosomal proteins 1
1.1.2 Centrosome functions 2
1.1.2.1 Microtubule organising centre (MTOC) 2
1.1.2.2 Basal body for cilia/flagella formation 3
1.1.2.3 Signalling hub 3
1.1.3 Structure of the centrosome 4
1.1.4 The cell cycle and centrosome replication 7
1.1.4.1 Centriole disengagement 8
1.1.4.2 Procentriole assembly 9
1.1.4.3 Centrosome maturation 10
1.1.4.4 Centrosome separation 11
1.1.4.5 The link: cell cycle regulators in the centrosome duplication process 12
1.2 The DNA damage response **13**
1.2.1 DNA damage checkpoints 13
1.2.1.1 G1/S checkpoint 14
1.2.1.2 Intra-S checkpoint 14
1.2.1.3 G2/M checkpoint 15
1.2.2 Single strand break repair 16
1.2.3 Double strand break repair pathways 17
1.2.3.1 Homologous recombination (HR) repair 17
1.2.3.2 Non-homologous end joining (NHEJ) 20
1.3 Cilia **21**
1.3.1 Structure of the primary cilium 22
1.3.2 Functions of primary cilia 25
1.3.3 Formation and disassembly of cilia 27
1.3.4 Ciliopathies 31
1.4 Centrobin **33**
1.5 Aims of this project **35**
1.6 Model systems **36**

2 Materials and Methods **37**
2.1 Materials **37**
2.1.1 Chemicals and solutions 37
2.1.2 Molecular Biology Reagents 39
2.1.3 Antibodies 40
2.2 Biological materials and Tissue culture reagents **43**
2.2.1 Bacterial strains 43
2.2.2 Tissue culture reagents 44
2.2.3 Cell lines and culture conditions 44
2.3 Cell Biology methods **46**
2.3.1 Cell maintenance and proliferation analysis 46

2.3.2 Monoclonal antibody preparation 47
2.3.3 Stable cell line generation 48
2.3.4 Transient transfections 48
2.3.5 siRNA mediated knockdown 49
2.3.6 Serum starvation 49
2.3.7 Microscopy methods 49
2.3.7.1 Cell fixation 49
2.3.7.2 Immunofluorescence (IF) microscopy 50
2.3.7.3 Proximity Ligation Assay 50
2.3.7.4 Electron microscopy 51
2.3.8 Clonogenic survival assays 51
2.3.9 Flow cytometric analysis 52
2.4 Zebrafish embryo analysis 52
2.4.1 Zebrafish husbandry and manipulations 53
2.4.2 Immunofluorescence analysis 53
2.4.3 Whole mount in situ hybridisation (WMISH) 53
2.5 Protein Methods 54
2.5.1 Protein extraction and preparation 54
2.5.2 SDS-PAGE 54
2.5.3 Semi-dry and wet transfer 55
2.5.4 Immunoblotting technique 55
2.5.5 Immunoprecipitation 56
2.6 Nucleic acid methods 56
2.6.1 RNA isolation and cDNA synthesis 56
2.6.2 Genomic DNA extraction 57
2.6.3 Plasmid DNA prep 57
2.6.4 Polymerase Chain Reaction (PCR) 57
2.6.5 5' RACE reaction 60
2.6.6 Restriction digestion of DNA 60
2.6.7 Modification of DNA ends 60
2.6.7.1 Generation of Blunt DNA ends 60
2.6.7.2 Phosphorylation of DNA ends 60
2.6.7.3 Dephosphorylation of DNA ends 61
2.6.8 Sticky or blunt end ligations 61
2.6.9 Assembly of CRISPR plasmids 61
2.6.10 Analysis of cloned DNA and sequencing 61
2.6.11 Agarose gel electrophoresis 62
2.6.12 DNA purification methods 62
2.6.12.1 Gel extraction and Column clean-up 62
2.6.12.2 Ethanol precipitation 62
2.6.12.3 Phenol/chloroform precipitation 62
2.6.13 Preparation of chemically competent *E. coli* 63
2.6.14 Transformation of chemically competent *E. coli* 63
2.7 Computer programmes and Bioinformatic tools 63

3 A role for centrobin in centriole duplication and biogenesis 65
3.1 Introduction 65
3.2 Bioinformatic analysis of centrobin 67
3.3 Production and characterisation of monoclonal anti-centrobin antibody (6D4F4) 70
3.4 Localisation of centrobin at stages of the cell cycle 71
3.5 Cloning and overexpression of *CNTROB* and EGFP-CNTROB 72
3.6 Disruption of human *CNTROB* locus in hTERT-RPE1 cells using CRISPR/Cas9 74
3.7 *CNTROB* nulls show normal centrosome composition 78
3.8 Centrobin-deficient cells show normal proliferation 82

3.9 Centrobin-deficient cells show centriole duplication defects....84
3.10 Discussion....86

4 Centrobin regulates primary ciliogenesis in vertebrate systems....89
4.1 Introduction....89
4.2 Dynamics of centrobin localisation in ciliated cells....91
4.3 Centrobin loss reduces ciliation frequency in human cells....92
4.4 *Drosophilia* centrobin supports human ciliogenesis....94
4.4.1 Cloning and transient expression of *Drosophila* centrobin....95
4.4.2 Expression of *Drosophila* centrobin rescue ciliogenesis in hTERT-RPE1 centrobin nulls....97
4.5 Zebrafish centrobin acts as a positive regulator of ciliogenesis....99
4.5.1 5'RACE, homology and sequence analysis of zebrafish centrobin....99
4.5.2 Zebrafish centrobin controls effective primary cilium formation....101
4.5.3 Loss of zebrafish centrobin results in microcephaly-like phenotypes....102
4.5.4 Centrobin regulates normal organogenesis in zebrafish....104
4.6 Ultrastructural analysis of primary cilia in centrobin null cells....107
4.7 Centrobin, CP110 and ciliogenesis....108
4.7.1 Centrobin loss results in accumulation of negative regulators of ciliation....108
4.7.2 Centrobin interacts with CP110....110
4.8 Mapping of the centrobin region required for ciliation....111
4.9 Roles of centrobin in ciliary assembly....114
4.9.1 Centrobin may participate in ciliary IFT transport assembly....114
4.9.2 Overexpression of centrobin causes ARL13B protrusions....115
4.10 Effect of *CNTROB* loss on cellular CPAP levels....115
4.11 Discussion....118

5 A role for centrobin in the DNA damage response....121
5.1 Introduction....121
5.2 Reduced DNA damage-induced centrosome amplification in centrobin-deficient cells 123
5.3 Centrobin-deficient cells are sensitive to genotoxic stress....124
5.4 Centrobin ablation results in defective DSB repair....126
5.4.1 Reduced RAD51 focal recruitment in centrobin-deficient cells....126
5.4.2 Centrobin null cells show defective RAD51 and γ-H2AX foci formation after IR-induced double strand breaks....127
5.4.3 Centrobin-deficient cells are sensitive to MMS-induced DNA damage....130
5.4.4 *CNTROB* KO cells show effective G2/M checkpoint activation after IR....132
5.5 Centrobin-deficient cells show sensitivity to PARP inhibition....132
5.6 Dynamics of centrobin localisation in damaged human cells....134
5.7 Discussion....136

6 Conclusions and future perspectives....140

7 References....144

8 Appendix....159
8.1 Supporting data....159
8.2 Scientific communications....164
8.2.1 International oral and poster presentations....164
8.2.2 National oral and poster presentations....164
8.2.3 Publications/submissions....165

List of figures

Figure 1.1: Centrosome and centriole structure 5
Figure 1.2: The interplay between the cell cycle and centrosome duplication.....8
Figure 1.3: DSB repair via Homologous recombination (HR).....19
Figure 1.4: DSB repair via non-homologous end joining 21
Figure 1.5: Structure of the primary cilium.....23
Figure 1.6: Primary cilium and hedgehog (Hh) signal transduction 26
Figure 1.7: Physical stages in the intracellular and extracellular pathways of ciliogenesis.....28
Figure 1.8: Summary of factors that control cilium assembly and disassembly 30
Figure 3.1: Schematic of human *CNTROB* genomic locus. 68
Figure 3.2: Comparative analysis of the human *CNTROB* gene and its orthologues from other species.....70
Figure 3.3: Characterisation of a novel mouse monoclonal centrobin antibody. 71
Figure 3.4: Centrobin localisation at different stages of the cell cycle. 72
Figure 3.5: Cloning of full-length human *CNTROB* cDNA.....73
Figure 3.6 Transient expression of full-length human *CNTROB* cDNA.....74
Figure 3.7: Generation of *CNTROB* knockout hTERT-RPE1 cells. 76
Figure 3.8: Sequencing confirmation of specific genome manipulations *CNTROB* knockout clones after CRISPR/Cas9.....77
Figure 3.9: Localisation of centriole and centriolar satellite markers in wild-type hTERT-RPE1 and *CNTROB* null cells. 79
Figure 3.10: Loss of centrobin has no effect on localisation and composition of centrosomal proteins and alpha-tubulin in interphase *CNTROB* KO hTERT-RPE1 cells. 80
Figure 3.11: Loss of centrobin has no effect on localisation and composition of centrosomal proteins and alpha-tubulin in mitotic *CNTROB* KO hTERT-RPE1 cells.....81
Figure 3.12: Centrobin-deficient cells show normal centrosome morphology 82
Figure 3.13: Stable re-expression of centrobin to generate rescue cell lines. 83
Figure 3.14: Centrobin null and rescue cell lines show no proliferation defect. 84
Figure 3.15: Loss of centrobin results in defective centriole duplication. 85
Figure 4.1: Centrobin localisation in ciliated and non-ciliated cells 92
Figure 4.2: siRNA-mediated depletion of centrobin results in reduced frequency of cilia.....93
Figure 4.3: Centrobin is a positive regulator of ciliogenesis in human epithelial cells.....94
Figure 4.4: *Drosophila* centrobin localises to centrosomes in human cells 96
Figure 4.5: *Drosophila* centrobin rescues ciliogenesis in centrobin null hTERT-RPE1 cells .98
Figure 4.6: Human and zebrafish centrobin share high protein sequence identity.....100
Figure 4.7: Loss of zebrafish centrobin results in reduced cilia frequency and length 102
Figure 4.8: Morphological aberrations in centrobin-deficient zebrafish embryos 103
Figure 4.9: Laterality defect revealed by *spaw* randomisation in zebrafish centrobin morphant embryos. 104
Figure 4.10: Impaired cardiac looping in *cntrob*-deficient embryos.....105
Figure 4.11: Increased pancreas mislocalisation in *cntrob* deficient embryos.....106
Figure 4.12: Centrobin deficient centrioles dock to ciliary vesicle but fail to extend their axoneme.....107

Figure 4.13: CP110 stabilisation at the mother centriole partly contribute to ciliogenesis defects in centrobin-deficient cells 109
Figure 4.14: Centrobin directly interacts with CP110 via its C-terminal 111
Figure 4.15: Deletion analysis shows that the N-terminal CPAP-binding region of centrobin is dispensable for ciliogenesis 113
Figure 4.16: Defective smoothened localisation in residual ciliated centrobin null cells 114
Figure 4.17: Overexpression of centrobin causes ARL13B protrusion in hTERT-RPE1 115
Figure 4.18: CPAP localisation and expression in centrobin-deficient cells 117
Figure 5.1: DNA-damage induced centrosome amplification is reduced in *CNTROB* KO cells 124
Figure 5.2: Centrobin-deficient cells are sensitive to IR- and MMS-induced DNA damage 125
Figure 5.3: Centrobin is required for efficient DNA-damage induced RAD51 foci formation 127
Figure 5.4: Centrobin-deficient cells show defective RAD51 and γ–H2AX foci formation after IR treatment (Automated microscopy analysis) 129
Figure 5.5: *CNTROB* KO cells show defective RAD51 and γ–H2AX foci formation after MMS treatment (Automatic microscopy analysis) 131
Figure 5.6: FACS analysis shows effective G2/M checkpoint activation in *CNTROB* KO cells 132
Figure 5.7: Centrobin null cells are sensitive to PARP inhibition 133
Figure 5.8: Centrobin was not detected at DSBs sites in hTERT-RPE1 cells 135
Figure 5.9: Current model of centrobin involvement in DNA-damage response 138

List of tables

Table 2.1 Common buffers and reagents....37
Table 2.2 List of plasmids used in this study....39
Table 2.3 Commercially available kits used in this study....40
Table 2.4 List of primary antibodies used for this study....41
Table 2.5 List of secondary antibodies used in this study....43
Table 2.6 Cell lines and culture conditions used in this study....44
Table 2.7 Antibiotics used for the selection of stable human cell lines....46
Table 2.8 Pharmacological drugs used in this study for treatment of hTERT-RPE1....46
Table 2.9 List of components of the Hybridoma growth medium....48
Table 2.10 Cell plating numbers for clonogenic survival assays in 6 cm^2 dishes....52
Table 2.11 SDS-PAGE gel composition used for protein detection....55
Table 2.12 PCR conditions for Sigma Taq and KOD Hot Start....58
Table 2.13 PCR programme cycling conditions....58
Table 2.14 List of oligonucleotides used in this study....58
Table 2.15 Bioinformatics and statistical tools used in this study....63
Table 3.1: Comparative analysis of predicted human *CNTROB* isoforms....68
Table 4.1: Zebrafish ESTs used in this study and their homology to the human centrobin alpha using tblastn for 2 sequences....99

Abbreviations

53BP1	p53 binding protein 1
aa	Amino acids
APC/C	Anaphase promoting complex/cyclosome
APS	Ammonium persulphate
Arl13B	ADP-ribosylation factor-like 13B
ATM	Ataxia telangiectasia, mutated
ATP	Adenosine-5‟-triphosphate
ATR	ATM-Rad3 related
ATRIP	ATR-interacting protein
APLF	Aprataxin-and-PNK-like factor
APTX	Aprataxin
BBS	Bardet-Biedl syndrome
BLAST	Basic local alignment search tool
Bld10	Basal body 10
bp	Base pair(s)
BRCA1	Breast cancer associated gene1
BRCA2	Breast cancer associated gene 2
BSA	Bovine serum albumin
CDC	Cell division cycle
CDK	Cyclin-dependent kinase
CDK5RAP2	Cyclin-dependent kinase5 regulatory associated protein 2
cDNA	Complementary DNA
Cas9	CRISPR associated protein 9
Centrobin	Centrosomal BRCA2 interacting protein
Cep	Centrosomal protein
CHK	Checkpoint kinase
C-Nap1	Centrosomal Nek2-associated protein 1
CPAP	Centrosomal P4.1-associated Protein
CRISPR	Clustered regularly interspaced short palindromic repeat
DDR	DNA damage response
DEPC	Diethylpyrocarbonate
DMSO	Dimethylsulfoxide
DNA-PK	DNA-dependent protein kinase
dNTP	Deoxyribonucleotide-5‟-triphosphate
DSB	Double-strand break
dsDNA	Double-stranded DNA
ECL	Enhanced chemiluminesence
EDTA	Ethylenediaminetetraacetic acid
EGTA	Ethylene glycol tetraacetic acid
EH	Epidermal growth factor receptor pathway substrate 15 homology
EHD1	EH domain-containing protein 1
EM	Electron microscopy
FACS	Fluorescence-activated cell sorting
FANCD2	Fanconi anaemia, complementation group D2
FBS	Foetal bovine serum
FITC	Fluorescein isothiocyanate
γ-TURC	γ-tubulin ring complex
GFP	Green fluorescent protein
Hh	Hedgehog
HR	Homologous recombination
hTERT-RPE1	Human telomerase reverse transcriptase- retinal pigment epithelial
HU	hydroxyurea
IF	Immunofluorescence microscopy
IFT	Intraflagellar transport

IR	Ionizing radiation
kb	Kilobase pair(s)
Kif	Kinesin Family Member
Kiz	Kizuna
LB	Luria-Bertani medium
LIP8	Lysosomal trafficking regulator-interacting protein 8
MAP	Microtubule associated protein
MARK4	MAP/microtubule affinity-regulating kinase 4
MCPH	Microcephalin
MDM2	Mouse double minute 2
MMS	Methyl methanosulphate
MRE11	Meiotic recombination 11
MRN	MRE11-RAD50-NBS1 complex
MTOC	Microtubule-organising centre
NBS1	Nijmegen breakage syndrome 1
NCBI	National Center for Biotechnology Information
Nde1	Nuclear distribution gene E homologue 1
NEDD1	Neural precursor cell expressed, developmentally down-regulated 1
NEK	NIMA-related kinase
NHEJ	Non-homologous end joining
NIMA	Never-in-mitosis A
ODF2	Outer dense fiber protein 2
OFD1	Oral-facial-digital syndrome 1
PACT	Pericentrin- AKAP450 centrosome-localising domain
PARP	Poly (ADP-Ribose) polymerase
PBS	Phosphate buffered saline
PFA	Paraformaldehyde
PCM	Pericentriolar material
PCR	Polymerase chain reaction
PDGF	Platelet-derived growth factor
Pen/Strep	Penicillin/streptomycin
PIKK	Phosphoinositide 3-kinase related protein kinase
PLK	Polo-like kinase
PNK	Polynucleotide kinase
POC	Protein of Centriole
PP1	Protein phosphatase 1
Rad	Radiation sensitive
Rb	Retinoblastoma
RNA	Ribonucleic acid
RNAi	RNA interference
RNase	Ribonuclease
RPA	Replication protein A
RT	Room temperature
RT-PCR	Reverse transcription-PCR
SAC	Spindle assembly checkpoint
SAP	Shrimp alkaline phosphatese
SAS	Spindle assembly abnormal protein
SCC	Sister Chromatid Cohesion protein
SCF	Skp, Cullin, F-box containing complex
SDS	Sodium dodecyl sulphate
SDS-PAGE	SDS polyacrylamide gel electrophoresis
SEM	Standard error of the mean
SGO1	Shugosin 1
SHh	Sonic hedgehog
siRNA	Short interfering RNA
SPB	Spindle pole body

ss	Serum starved
ssDNA	Single-stranded DNA
STIL	SCL/TAL1 interrupting locus
TAE	Tris acetate EDTA
TEM	Transmission electron microscopy
TEMED	N,N,N‘,N‘-tetramethylethylenediamine
TG	Tris-glycine
TopBP1	Topoisomerase II DNA binding protein 1
Tris	Tris(hydroxymethyl)aminomethane
UV	Ultraviolet
v/v	Volume per volume
Wnt	Wingless-type MMTV integration site family
WT	Wild-type

Declaration

I, Yetunde Blessing Adesanya, confirm that the work presented in this thesis is my own. Experiments carried out in collaboration with others, notably Dr. Teresa Casar Tena, Philipp's lab, University of Ulm, Germany; Dr. David Gaboriau at FILM, Imperial College, London, UK; and undergraduate students (Ms. Gemma Hyland and Mr. Kambe Takanari) were clearly indicated in the corresponding figure legends. Also, I have not obtained a degree in this university or elsewhere information with the findings presented here.

Acknowledgements

First and foremost, I would like to thank Prof. Ciaran Morrison for believing in me and applying with me for the funding gave me an opportunity to do my PhD in his laboratory. I also sincerely appreciate all of your guidance, patience, support, and invaluable advice over the past four years. You have been an amazing supervisor and a great mentor.

I would also like to express my gratitude to the funding agency that supported my PhD project (funded by the Governement of Ireland Postgraduate Scholarship, project ID: GOIPG/2013/318).

I would like to thank all immediate-past and present members of the Morrison's lab for those suggestions, advice and insightful criticism in lab meetings. In particular, I would like to thank: Drs. Antonczak and Prosser for training me on the microscopes; Owen, Sandra and Lisa for being such wonderful colleagues and lab friends, it was such a great joy sharing the sitting area with all of you; to Anne-Marie, I am grateful for your assistance from the first day at the water dispenser, my drama at Moffetts and your kind heart and nice smiles that made my tough days shorter; Sinead King for helping me during my first few months with learning the experimental techniques; Ebtissal for being a friend and a sister, thanks for sharing in all of my scientific excitements and struggles; Shiva for being my late night lab partner and for helping with my immunoblot struggles; and Loretta for being such a great friend in the lab and in Amsterdam.

My other colleagues at the Centre for Chromosome Biology have also been wonderful companions over the years and I am greatful to all of you for creating such a great place to work, for all the fun and chats. Thanks to Janna, Karen and Ben for investing your precious time proofreading my write-ups. Thanks to Anna for those 'just in time' short notes and surprise little gifts, they helped a lot.

To Chituru, I have been blessed with you as a great friend and a sister since our undergraduate days in Dundalk. It has been such a pleasure to share my Galway adventures, the 'scientific ups and downs', and the 'Naija gists' at home and at work with you. Thank you so much Lucretia, I cannot imagine this journey without you. Mohammed, Ebtissal and family, thank you for making me feel welcome in your home and for being there on those tough thesis-writing days.

I am grateful to these special people in my life for all of their support and encouragement: Dr. Ronan Bree (DKIT) for making Biochemistry such a fun to learn and for his encouragements and visits during my PhD. You are such a great mentor and a model; Dr. Sinead Loughran and Dr. Frank Murray for believing in me and providing such amazing references; Dr. Ayodeji Oyelami, the Ogunleyes, and the Odunlamis thank you for the constant support and for being my 'personal people' all through this journey.

Rev (Dr.) & Mrs Adesanya, you have been my rock from the start. Mr & Mrs Adewale & Olatokunboh Adesanya, what can I say? You have been everything to me. I can never forget that envelope that changed the story, I have been so blessed to have you by my side always. To my princesses (Oluwapẹlumi, Oluwafiayọkunumi and Ọpẹyẹmi Adesanya), thank you for those calls, your prayers and your interests in my project. I am also grateful to all of my family members, from the oldest to the youngest of the Adesanyas and Olugbenros, I appreciate your encouragement, support and prayers. I love you all.

To Stephen, my darling husband, my 'bestest friendship', my proofreader, my bishop and my prayer warrior, thank you for being so patient, kind, loving, and understanding. I love you so much.

More than anyone else, I just want to say 'ọ̀nà, òtítọ́ ati ìyè, ẹ mà ṣeun l'ọpọlọpọ'.

Yetunde

Abstract

The centrosome is composed of numerous proteins that make up its core structure. Other proteins also transiently localise and interact with centrosomal proteins for functional modulation. Centrobin, one of the core centrosomal proteins, is involved in centriole biogenesis and elongation, ciliogenesis, and possibly, the DNA damage response. Although it was initially identified as a BRCA2-interacting protein that preferentially localises to the daughter centriole, its role in the DNA repair pathway or cilia formation has not been clearly defined.

To investigate the functions of centrobin in centriole duplication, ciliogenesis, and DNA repair processes, we generated a novel monoclonal anti-centrobin antibody and used CRISPR/Cas9 to disrupt *CNTROB* gene in the immortalized, non-transformed hTERT-RPE1 cell line. We confirmed successful gene targeting by western blot, immunofluorescence microscopy and sequencing of the genomic locus and cDNA. We noticed that loss of centrobin had no impact on cell cycle progression but resulted in an increase in acentric and monocentric cells. We also used clonogenic survival assays to show that centrobin-deficient cells had a severe decrease in viability after exposure to ionising radiation (IR) and methyl methanosulfonate (MMS) but not ultraviolet radiation (UV). Interestingly, these sensitivities to genotoxic stress agents were rescued by stable transgenic expression of centrobin in our cell line. To further investigate the involvement of centrobin in the DNA damage response, we studied the kinetics of RAD51 recombinase and γ–H2AX IR-induced foci (IRIF) formation after IR or MMS treatment of centrobin-deficient cells. We observed that the percentage of cells with RAD51 and γ–H2AX IRIF was reduced in centrobin-deficient cells after exposure to IR or MMS.

We also studied the roles of centrobin in primary cilia assembly and functions in vertebrate systems. Primary cilia are antenna-like microtubule-based sensory organelles for signal transduction and cell proliferation. Using immunofluorescence microscopy to study the localisation pattern of endogenous and Green Fluorescent Protein (GFP)-tagged centrobin, we noticed that, while centrobin was mainly retained on the daughter centrioles of proliferating cells, it localised to the mother centrioles of ciliated cells. We observed reduced ciliation frequency in *CNTROB* knockout cells, which was rescued by transient and stable transgenic centrobin. We also observed inappropriate accumulation of the negative regulators of ciliogenesis, CP110 and CEP97, in centrobin-deficient cells after serum deprivation. Further investigation revealed that centrobin and CP110 interact *in vivo* and that the microtubule binding- and CP110-interacting regions of centrobin fragments are required for ciliogenesis. Electron microscopy analysis of human centrobin-deficient cells showed that centrobin is crucial for axonemal extension from the ciliary bud.

Finally, we used antisense-morpholino oligonucleotides (MO) technology to deplete centrobin in zebrafish and study its ciliary roles in this vertebrate system. Our investigation revealed that centrobin depletion causes reduced cilium number and length of nodal cilia in the Kupffer's vesicle of zebrafish embryos. Furthermore, centrobin-depleted zebrafish embryos displayed microcephaly-like morphological abnormalities that are indicative of ciliary defects, thus identifying centrobin as a potential ciliopathy gene. To assess the roles of centrobin in organogenesis, we monitored left-right patterning and organ localisation in zebrafish embryos. We observed an increase in frequency of defective organ positioning which is a consequent of malfunctioning left-right patterning in the centrobin depleted embryos. Interestingly, these phenotypes were rescued by transgenic expression of MO-resistant transgenic centrobin.

In summary, our data identify centrobin as a positive regulator of ciliogenesis and a participant in the DNA damage response in vertebrates. Therefore, centrobin may be a molecular link between centriole duplication, cilia formation and DNA damage responses.

1 Introduction

1.1 Centrosomes and centrioles

The centrosome was first observed in the 1800s in independent work by early cell and developmental biologists, notably Theodor Boveri and Édouard Van Beneden. They both studied cell divisions in fertilized eggs of parasitic worms and discovered the existence of a spindle pole organiser during mitosis. Their works revealed that the spindle pole organiser is a permanent self-replicating organelle that duplicates prior to mitosis and acts as the main organising centre for cellular division (Van Beneden, 1876, Boveri 1887, reviewed by Scheer, 2014). The spindle pole organiser was later named centrosome, meaning a 'central organelle'. Until the invention of electron and immunofluorescence microscopy, the centrosome composition, organisation, mode of replication and its precise functions were not properly understood. It is now known to act as the major microtubule organising centre (MTOC) in proliferating animal somatic cells and, as the mother centriole, acts as the basal body for primary cilium formation in quiescent cells. In recent years, the centrosome biology field has gained scientific attention due to the implication of centrosomes in the pathogenesis of several human diseases.

1.1.1 Evolutionary conservation of centrosome and centrosomal proteins

The centrosome is highly conserved, at least among animal cells. Structurally, an unduplicated centrosome is made up of two microtubule-based centrioles with the microtubules arranged in a ninefold symmetry and embedded with a pericentriolar material (PCM). Centriole length differs among species, commonly ranging between 100 - 250 nm in diameter and 100 – 500 nm in length. For example, centrioles are considerably shorter in *Drosophila melanogaster* (*Drosophila*) and *Caenorhabditis elegans* (*C. elegans*) and are assembled from doublet and singlet microtubules, respectively (Carvalho-Santos et al. 2011, Azimzadeh 2014). Coincidentally, the majority of the organisms with genes encoding additional tubulin isoforms δ and ε tubulins can assemble triplet microtubules compared to α and β isoform in most organisms. However, *Drosophila* lack these tubulin isoforms but can assemble triplet microtubules in their germline cells (Fırat-karalar and Stearns 2014, Winey and O'Toole 2014).

The unicellular organisms evolutionarily closest to humans are the choanoflagellates which also nucleate a flagellum on a mature centriole that is surrounded by electron-dense material and organises microtubules (Azimzadeh 2014). The distal and subdistal appendages on the mother centrioles are conserved and in some ciliated ancestors, they act as transition fibres

and the basal foot, respectively. Interestingly, homologues of Cep164, a distal appendage protein, are expressed in flagellated protists. Similar to the subdistal appendages in proliferating higher organisms, the basal feet of the metazoans can anchor microtubules. Surprisingly, appendages are absent in *Drosophila* and *C. elegans*. However, several vertebrate centrosomal proteins are highly conserved in these species (Carvalho-Santos et al. 2011, Azimzadeh 2014). In general, vertebrate centrosomes are thought to have evolved from internalisation of basal bodies of unicellular organisms, although several eukaryotic cells including plants, some fungi, and mammalian oocytes lack apparent centriole structures (Bettencourt-Dias 2013). Furthermore, planarians also lack centrosomes, although most centrosomal genes are conserved in this organism. It is believed that planarians assemble multiple centrioles through a *de novo* pathway in their ciliated cells. Thus, inactivating the centrosomal genes in planarians has deleterious effect on effective ciliogenesis (Azimzadeh et al. 2012). Occasionally, there are divergent roles of centrosomal proteins among orthologues. For example, in *Drosophila* somatic cells, SPD-2 is dispensable for the centriole duplication process, while the human and *C. elegans* orthologues are required to co-ordinate and recruit PCM components for efficient centrosome replication (Dix and Raff 2007, Zhu et al. 2008). In summary, centrosomes can be said to be highly conserved small organelles that function in cellular microtubule organisation and ciliogenesis.

1.1.2 Centrosome functions

The structure and functions of the centrosome are evolutionarily conserved among eukaryotic cells (Nigg and Raff 2009, Carvalho-Santos et al. 2011). Its major functions are to organise microtubules in proliferating cells and to act as a basal body for cilia and flagella assembly. Recently, the roles of the centrosome as a signalling hub for the activation of cellular processes and its role in the pathogenesis of some diseases have been described (Fukasawa, 2007; Zhang et al. 2007; Bettencourt-Dias et al. 2011; Mullee and Morrison, 2016).

1.1.2.1 Microtubule organising centre (MTOC)

As the principal MTOC in proliferating cells, the centrosome is essential for MT nucleation. Thus, it helps to organise the microtubules that form the bipolar spindle during mitosis, and to orchestrate cell motility, adhesion, polarity and coordination of protein trafficking by the microtubule cytoskeleton (Doxsey et al. 2005; Bettencourt-Dias, 2013). The role of the centrosome in coordinating microtubules is facilitated by its association with γ-tubulin-ring complexes (γ-TuRCs) and the microtubule anchoring functions of the subdistal appendages (Delgehyr et al. 2005; O'Toole et al. 2012; Woodruff et al. 2014). The nucleated microtubules are polymerised from α and β-tubulin isoforms that grow from the minus (-) end towards the

plus (+) end in a GTP-dependent manner (Sept 2007). In *in vitro* experiments, it has been shown that microtubules can self-polymerise at high concentrations. However, the activity of the centrosome is required for their dynamic behaviour at different stages of the cell cycle (Sept 2007). While microtubules can be organised to form spindles through centrosome-independent pathways in higher plants and several fungi, the centrosome is essential for maintaining the integrity of genetic information (Azimzadeh and Marshall 2010, Azimzadeh 2014). Loss of centrioles in *Drosophila* results in delayed mitotic division, abnormal asymmetric neuroblast division and defective chemosensory neuronal cilia that lead to death early in development (Basto et al. 2006; Sir et al. 2013; Lattao et al. 2017).

1.1.2.2 Basal body for cilia/flagella formation

The mother centriole acts as the basal body that nucleates cilia or flagella in several organisms. It is believed that the eukaryotic centrioles were formed from internalisation of cilia at some stages during evolution (Azimzadeh 2014). During ciliogenesis, the basal body is first anchored to a ciliary vesicle that is continuous with the plasma membrane and allows for the growth of the ciliary axoneme. The ciliary membrane and the components of intra-ciliary transport are crucial for cell signalling. Cilia can be motile or immotile. Thus, they have a wide range of specialized functions that have evolved and are crucial in development, organ homeostasis and disease (reviewed by Nigg and Raff, 2009; Bettencourt-Dias et al. 2011; Carvalho-Santos et al. 2011; Hsiao et al. 2012; Izawa et al. 2015; also see section 1.3).

1.1.2.3 Signalling hub

Recent interest in the roles of centrosomes outside its known role as MTOC and basal body has revealed that it serves as a hub from which cellular signals emanate and that it also responds to intra-and extracellular cues. For example, several oncogenes and tumour suppressor proteins that regulate the cell cycle and facilitate DNA repair are localised to the centrosome (Fukasawa 2007, Nigg and Raff 2009, Izawa et al. 2015, Mullee and Morrison 2016). Interestingly, CDK1/Cyclin B activation for mitotic entry is first seen at the centrosome at prophase (Jackman et al. 2003). Kinases and phosphatases such as CDC25C, CDC25B, PLK1 and AuroraA, which participate in promoting cell cycle progression, have been shown to localise to the centrosome which acts as a signalling platform (Nigg, 2001; Busch et al. 2007; Zhang et al. 2007; Wang et al. 2014). CHE-1, a RNA polymerase II-binding protein and a protein that participate in DNA damage response (DDR), has been shown to accumulate at the centrosome after exposure to genotoxic stress. Depletion of CHE-1 results in centrosome hyperamplification and prevents centrosomal CHK1 and pericentrin interaction (Sorino et al. 2013). The activities of cell cycle regulators and DNA damage proteins at the centrosome support the role of the MTOC as a signalling hub (reviewed by Krämer et al. 2011; Mullee and Morrison, 2016).

1.1.3 Structure of the centrosome

A typical unduplicated centrosome is structurally composed of two cylindrical centrioles (namely, mother and daughter centriole) arranged orthogonally to each other. Each vertebrate centriole is made up of nine sets of circularly arranged triplet microtubules that form an elegant barrel (Azimzadeh and Marshall, 2010; Winey and O'toole, 2014). The triplet microtubules are known as the A, B and C-tubules (Figure 1.1). Microtubules impose polarity on the centriole: the microtubule plus ends are located at the distal end of the centrioles (Azimzadeh and Marshall 2010, Winey and O'Toole 2014). The proximal ends of the centrioles are embedded in the bulk of the pericentriolar material (PCM) and this is the region on which the cartwheel structures, that are crucial for procentriole assembly, are formed. The distal ends of the microtubule are surrounded by lower PCM volumes and exhibit doublet radial microtubules due to the shortened length of the C-tubules (Strnad and Gönzy 2008). The minor tubulins, δ and ε- isoforms, contribute immensely to the formation and integrity of the radial triplet microtubule structures of the centriole (Winey and O'Toole 2014). Figure 1.1 shows a schematic representation of centrosome structure.

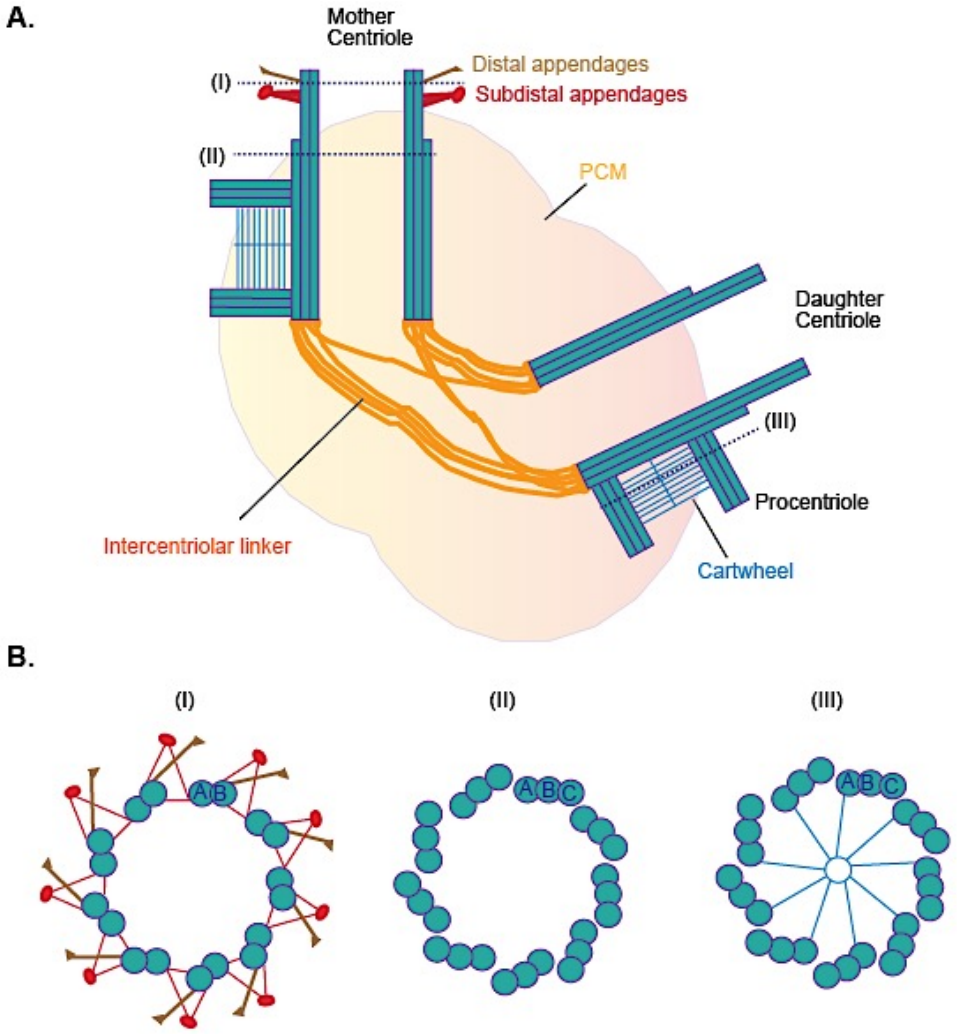

Figure 1.1: Centrosome and centriole structure

A. Schematic of a typical centrosome viewed from the side (side view) during S-phase. During S-phase, each procentriole is assembled on a carthwheel structure at the proximal ends of the mother and daughter centrioles that were licenced as they exited the previous mitosis. Each of the centrioles is composed of nine microtubule triplets. The daughter centriole lacks maturity markers, distal and subdistal appendages. Both parental centrioles are embedded in the PCM and are connected by flexible fibrous linkers. In human, the parental centrioles are approximately 450 nm long and 250 nm in diameter. The roman numerals designated I, II and II indicate the regions corresponding to the cross-sections in **B**. **(I)** Cross-sectional view of the distal part of the mother centriole with the doublet microtubules denoted as A and B. **(II)** Cross-sectional view of the central part of the mother centriole with nine triplet microtubes. Here, the shortened C-tubules can be viewed. In each of the triplet microtubules, the most internal tubule is called the A-tubule, followed by the B- and C-tubule. **(III)** Cross-section view of the proximal end of the procentriole region highlighting the cartwheel structure and the triplet microtubules (adapted from Bettencourt-Dias and Glover 2007; Bornens and Gonczy, 2014).

The centrioles are made of numerous proteins such as ninein, centrobin, centrosomal P4.1-associated protein (CPAP) and Sas6 that interact and stabilise tubulins (Delgehyr et al. 2005; Gudi et al. 2011; Zheng et al. 2016). The centrioles also organise the pericentriolar material

(PCM), an electron-dense, coiled-coil protein-rich structure that functions in microtubule nucleation and anchoring roles of the centrosome. Until recently, the PCM was thought to be amorphous, based on EM ultrastructure analysis. However, recent interest in its organisation and advances in microscopy have been used to characterise the dynamic structure of the PCM (Mennella et al. 2014; Woodruff et al. 2014). Pericentrin, γ-tubulin, CDK5RAP2 and AKAP450 are some of the large proteins localised to the PCM. The microtubule anchoring and nucleating activities of the PCM are mediated by γ-tubulin, a component of a tetrameric γ-TuSC (γ-tubulin small complex) complex. The γ-TuSC complex is made up of gamma complex protein 2 (GCP2) and 3 (GCP3), and two molecules of γ-tubulin (Moritz et al. 2000, Wiese et al. 2006). At least 6 γ-TuSC subcomplexes are held together by other members of the GCP family, including GCP4, GCP5 and GCP6, to form the γ-TuRC (γ-tubulin ring complex) structure (Moritz et al. 2000, Wiese et al. 2006). NEDD1 is a crucial recuitment factor of the γ-TuRC to the PCM but not for the complex assembly (Haren et al. 2006). Recent positional mapping of proteins has revealed a highly ordered organisation of PCM proteins around the centrioles, and that pericentrin and CDK5RAP2 are crucial for the assembly and organisation in this compartment (Lawo et al. 2012, Mennella et al. 2012). As the cell cycle progresses, the volume of the microtubule-nucleating PCM increases in a process that is synchronised with centriole maturation. This occurs prior to mitosis, a process that requires pericentrin activities to associate PCM and the centrioles (Fu and Glover, 2012; Lawo et al. 2012). The PCM components, pericentrin and γ-tubulin, interact directly; a toroidal pericentrin structure acts as a docking scaffold for microtubule-nucleating γ-tubulin ring complexes (Fu and Glover, 2012; Mennella et al. 2014; Woodruff et al. 2014). Interestingly, overexpression and depletion of pericentrin result in chromosome segregation and proliferative defects (Purohit et al. 1999, Wang et al. 2013b). Aside from PCM expansion during mitosis, which facilitates the increased microtubule nucleation for the formation of a bipolar spindle, PCM expansion also occurs after DNA damage (Antonczak et al. 2015). After DNA damage, PCM expansion allows for robust centrosome amplification induced by genotoxic stress.

In G1 cells, the proximal ends of the two centrioles are embedded in the highly organised PCM and tethered by filamentous centriole linkers. Centrosomal Nek2 associated protein 1 (C-Nap1), rootletin, Cep68 and LRRC45 are components of the filamentous centriole linkers. C-Nap1 and rootletin are phosphorylated by Never in mitosis A (NIMA) related kinase 2A (Nek2A) after Nek2A activation by PLK1 at late G2/early M phase of the cell cycle in a process known as ‘centrosome disjunction/separation’ (Fry et al. 1998; Yang et al. 2006; Pagan et al. 2014). C-Nap1 acts as a docking platform for filamentous rootletin, LRRC45 and Cep68 that connects the duplicated centrosomes during interphase. The centriole linker functions to ensure centrosome cohesion and forms the ciliary rootlet during cilia formation.

Centrosome separation via the dissolution of the centriole linker and loss of C-Nap1, rootletin and Cep68 from mitotic centrosome is crucial for generating the two centrosomes needed for faithful chromosome segregation. Overexpression of rootletin results in abnormal interphase nuclear morphology (Yang et al. 2006) and its loss in *Drosophila* affects sensory neuron functionality (Chen et al. 2015). siRNA-mediated depletion or gene ablation of C-Nap1 significantly affect centrosome cohesion, which causes reduced centriolar satellite numbers (Panic et al. 2015; Flanagan et al. 2017). Surprisingly, there was no impact on ciliation capacity and cellular migration speed in C-Nap1-deficient hTERT-RPE1 cells (Panic et al. 2015; Flanagan et al. 2017) but the direction of migration was affected (Panic et al. 2015). Also, C-Nap1-deficient cells show a mislocalisation of rootlein that may impact functionality of ciliary rootlet without detrimental impact on ciliary assembly, as revealed by unaltered ciliation frequency and defective migration (Panic et al. 2015; Flanagan et al. 2017).

Mother and daughter centrioles differ in age, structure and molecular composition. The mother centrioles of vertebrate cells have distal and subdistal appendages (*see* Figure 1.1A), which are added upon centriole maturation after the completion of one and a half cell cycle. The distal appendages confer ability of the mother centriole to attach to the plasma membrane during conversion to basal body. The distal appendages act as the transition fibre in ciliated cells (Ishikawa et al. 2005; reviewed by (Winey and O'Toole 2014). Interestingly, loss of centriolar distal appendages, Cep164 and Cep123, prevents ciliogenesis in human cells (Ishikawa et al. 2005, Graser et al. 2007, Sillibourne et al. 2013). Proximal to the distal appendages are the microtubule nucleating and anchoring proteins (such as ninein, centriolin, Cep170, Gal3 and ε-tubulin) of the subdistal appendages (Delgehyr et al. 2005; reviewed by Jana et al. 2014). The subdistal appendages become the basal foot after ciliogenesis and contribute to the basal body's microtubule organisation and to ciliary beating of motile cilia (Clare et al. 2014).

1.1.4 The cell cycle and centrosome replication

As reported by the one of the founding fathers of centrosome biology, Theodori Boveri, the centrosome duplicates prior to mitosis (Boveri 1887, reviewed by Scheer, 2014) but the mechanism of centriole duplication was not explained in his findings. Further advances in science and technology have facilitated the identification of the complex network of proteins that allow this highly co-ordinated centrosome duplication process. We now know that the centrosome and cell cycles are intricately linked to ensure that centrosome duplication is restricted to only once per cell cycle (Tsou and Stearns 2006, Nigg and Raff 2009, Hatch and Stearns 2010, Fırat-karalar and Stearns 2014). The mechanism of centriole duplication can be summarised as comprising four discrete steps, namely centriole disengagement, procentriole

assembly, centrosome maturation and centrosome separation. The major events during centrosome duplication and the corresponding stage of the cell cycle are summarised in Figure 1.2.

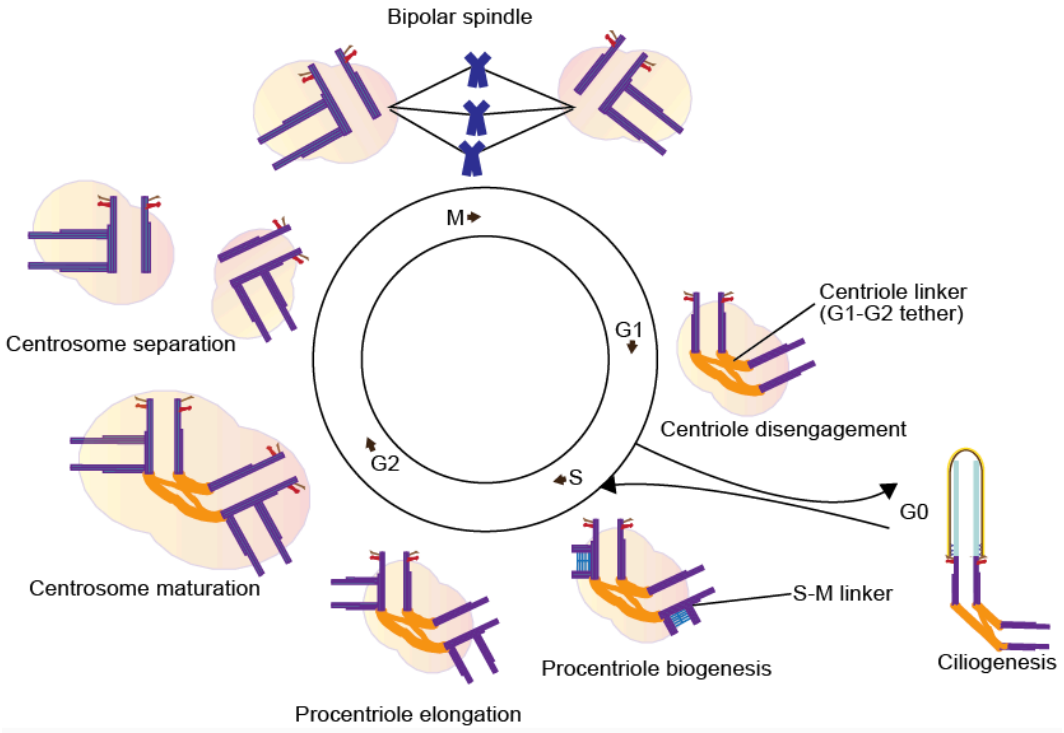

Figure 1.2: The interplay between the cell cycle and centrosome duplication

Schematic illustration of the major events during centrosome cycle at the indicated phases of the cell cycle. At the M/G1 transition, the mother and daughter centrioles are licensed (formation of 'G1-G2 tether') for procentriole nucleation during S-phase (centriole disengagement). During S-phase, two new procentrioles are assembled on cartwheel structures at the proximal ends of the parental centrioles (procentriole biogenesis). The perperndicularly arranged procentrioles are attached to their respective parental centrioles by a flexible 'S-M linker', and they continue to elongate throughout S and G2 phases (procentriole elongation). At this stage, the parental centrioles are still connected by the intercentriolar linker. During G2, the two centrosomes recruit additional PCM and the new mother centriole acquires distal and subdistal appendages (centrosome maturation). Prior to mitosis, the fibrous G1-G2 tether is degraded (centrososome separation) and the two centrosomes migrate to form the bipolar spindle during mitosis. When cell exit the cell cycle into G0 (quiescent phase), the centrosome can assemble a primary cilium (Adapted from Nigg and Raff, 2009).

1.1.4.1 Centriole disengagement

During metaphase, each of the centrosomes that form the bipolar spindle is composed of a pair of centrioles arranged in a tight orthogonal conformation (Figure 1.2). Centriole engagement/orthogonal configuration is thought to prevent centriole reduplication in the same cell cycle. At the end of mitosis or in early G1, the orthogonal arrangement of the centrioles is lost in a process known as 'centriole disengagement'. This process licences the centrioles for efficient centriole duplication at the proximal ends of each of the centrioles during S-phase (Tsou and Stearns 2006, Tsou et al. 2009). The involvement of Polo-like kinase 1 (PLK1) and

separase protease in centriole disengagement has been reported (Tsou and Stearns 2006, Tsou et al. 2009). The kinase and protease act during interphase and mitosis, respectively, to ensure centriole disengagement. Inhibition of both separase and PLK1 activities prevents centriole disengagement (Tsou et al. 2009). Interestingly, the chromosomal substrate for separase, SCC1, has been shown to localise to the centrosome and it is cleaved by the activities of separase in a PLK1-dependent manner (Schöckel et al. 2011). Another separase substrate, the PCM component, pericentrin, also contributes to centriole disengagement and its non-cleavable form prevents faithful centriole disengagement (Lee and Rhee 2012). Securin and Cyclin B1 regulate the activities of separase during chromatid sister separation, while additional proteins are required for centrosomal separase regulation (Tsou and Stearns 2006, Tsou et al. 2009, Fırat-karalar and Stearns 2014). Aki1 and astrin have been identified as modulators of the disengagement process, since depletion of these proteins results in premature centriole disengagement (Nakamura et al. 2009; Mardin and Schiebel, 2012). After centriole disengagement, the orthogonal link between the mother and daughter centriole is lost and the centriole pairs are tethered by an intercentriolar linkage that extends between the proximal ends (*see* Figure 1.2). This allows each of the centrioles to move apart and recruit their own distinct PCM clouds in preparation for procentriole assembly (Fry et al. 1998a, Bahe et al. 2005, Fry 2014) The intercentriole linker is a dynamic structure that is composed of rootletin, β-Catenin, Cep68, Cep215 and C-Nap1 (Fry et al. 1998a, Bahe et al. 2005, Bahmanyar et al. 2008, Pagan et al. 2014). The process for the assembly and disassembly of the centriole linker is described in section 1.1.4.4.

1.1.4.2 Procentriole assembly

Centriole disengagement licenses the centriole for procentriole nucleation during S-phase. Ultrastructural studies of the centrosome cycle revealed that procentrioles are assembled perpendicular to and at the proximal ends of the parental centrioles in a semiconservative manner (Vorobjev and Chentsov 1982). Procentriole biogenesis is a highly conserved process, at least, among eukaryotes. The procentriole assumes a orthogonal arrangement with the parental centriole and such association is maintained until centriole disengagement (Strnad and Gönzy 2008). At the initial stage of procentriole assembly, a central tube known as the cartwheel structure is formed at the proximal ends of each of the licensed centrioles (Figure 1.2). At present, the mechanism required for identifying the exact location on on which the cartwheel is assembled on a symmetric centriole is still unknown. However, a number of proteins have been shown to localise prior to the recruitment and formation of the cartwheel structure, thus indicating their potential involvement in determining the site of procentriole assembly. It is thought that Cep192 and Cep152 localise and interact with PLK4, the centriole biogenesis initiator, to coordinate the process and identify the origin of centriole duplication in ways that are reminiscent of the origin of DNA replication (Hatch et al. 2010,

Sonnen et al. 2013, Fırat-karalar and Stearns 2014, O'Rourke et al. 2014). Overexpression of PLK4 leads to the formation of 'centriole rosettes', which are characterised by the formation of several procentrioles on a single parental centriole, while the depletion of PLK4 obliterates centriole duplication (Kleylein-Sohn et al. 2007, Hatch et al. 2010, Sonnen et al. 2013).

Due to the relevance of PLK4 in centriole duplication, it is therefore not surprising that the cellular level of PLK4 is highly regulated through transcription, low protein half-life and ubiquitin-dependent proteolysis that limit its availability. This helps to ensure that centriole duplication occurs at a single site on the parental centriole (Kleylein-Sohn et al. 2007, Fırat-karalar and Stearns 2014, Lopes et al. 2015). Interestingly, the correct localisation of PLK4, Cep192, Cep152 and its interacting partner Cep63 have been shown to be crucial for recruitment of Sas-6, an important component of the cartwheel structure (Nigg and Stearns, 2011; Brown et al. 2013; Fırat-karalar and Stearns, 2014; Fu et al. 2015). Upon identification of centriole's 'origin of duplication' and successful cartwheel assembly, the procentriole undergoes centriole elongation in a proximal-to-distal direction until its reaches its full-length in G2-phase. Centrobin, Cep120 and CPAP participate in the centriole elongation process through their interactions with tubulin (Mahjoub et al. 2010; Gudi et al. 2011; Zheng et al. 2016). Emerging evidence has also revealed the functions of other proteins in procentriole formation and elongation process. For example, overexpression of centrobin and POC1 has been shown to result in the formation of overly long centriole-like structures; thus implicating them as participants in maintaining proficient centriole elongation (Keller et al. 2009; Gudi et al. 2011).

1.1.4.3 Centrosome maturation

Centrosome maturation occurs during the G2/M stage of the cell cycle (Figure 1.2). The process is marked by the recruitment of additional PCM proteins and assembly of the appendages on the new parental centriole which allow for its transition from daughter to a mother centriole (Azimzadeh and Marshall 2010). This process is regulated by a number of kinases, microtubule associated proteins (MAPs) and microtubule nucleating complexes. PLK1 and Aurora-A kinase activities are required for PCM expansion through recruiting several PCM components for increase in microtubule nucleation and organisation functions necessary for mitosis. PLK1 interacts directly with PCM components, which include γ-tubulin, pericentrin, CDK5RAP2, Cep192, and Aurora A. PLK1 inhibition prevents the accumulation of a γ-tubulin containing complex that is essential for mitotic PCM expansion, thus causing impaired microtubule nucleation (Lane and Nigg, 1996; Lee and Rhee, 2011; Joukov et al. 2014; Woodruff et al. 2014). Interestingly, in human cells, overexpression of pericentrin or CDK5RAP2 can result in PCM expansion, suggesting the ability of PCM proteins to undergo polymerisation independent of the mitotic kinase-driven expansion

(Loncarek et al. 2008b, Lawo et al. 2012). It is therefore believed that mitotic kinases, PLK1 and Aurora A, mediate rapid and spontaneous PCM assembly to allow for increased microtubule-nucleating activity at mitosis.

In addition to PLK1's involvement in PCM expansion during centrosome maturation, it is also an essential mitotic kinase that is required for the assembly of distal and subdistal appendages in human cells (Kong et al. 2014). Chemical inhibition of PLK1 blocked the recuitment of appendage proteins on the younger mother centriole, while the previously matured centriole was unaffected (Kong et al. 2014). Exogenous expression of activated PLK1 results in premature centriole disengagement and the accummulation of appendage proteins in S-phase or cycling daughter centrioles. The functionality of the prematurely-acquired appendages was determined by their ability to support ciliogenesis, thus leading to an increase in the number of biciliated cells (Kong et al. 2014).

1.1.4.4 Centrosome separation

Prior to mitosis, the two duplicated centrosomes are in close proximity and act as a single MTOC. As depicted in Figure 1.2, a fibrous linker, also called the G1-G2 tether, connects the proximal ends of the two parental centrioles in the duplicated centrosomes. The parental centrioles that served as template for procentriole assembly during the S-phase are attached to their respective procentrioles by a dynamic flexible S-M linker (Nigg and Stearns 2011). At late G2 phase, the G1-G2 tether is disassembled to allow for bipolar spindle assembly and faithful segregation of the chromosome. C-Nap1, rootletin, and Cep68 are some of the proteins that participate in maintaining centrosome cohesion (Fry et al. 1998; Yang et al. 2006; Pagan et al. 2014). A physiological agonist that promotes centriole linker disassembly and centrosome disjunctioning is the kinase, Nek2. It phosphorylates both C-Nap1 and rootletin to drive centrosome disjunction and centrosome migration to the spindle poles (Fry et al. 1998; Bahe et al. 2005; Yang *et al.* 2006; Kim et al. 2008; Hardy et al. 2014). A mechanistic explanation of the involvement of Nek2 is that it hyperphosphorylates the C-terminal of C-Nap1 to prevent its oligomerisation and interaction with the Cep135 (centrosomal protein of 135 kDa) and rootletin (Fry et al. 1998a); thereby disrupting the stability of the filamentous intercentriolar linker. On the other hand, centriole linker assembly and centriole cohesion require the interaction between the C-terminal end of a centriolar protein, Cep135, and C-Nap1, a protein that act as a platform for rootletin and other centriole linker proteins that form the fibrous linker (Fry et al. 1998; Bahe et al. 2005). A physiological antagonist of Nek2 activity is the PP1 phosphatase, specifically the PP1α isoform, which regulates centrosome cohesion through dephosphorylating C-Nap1 after mitosis. As a result, C-Nap1 is stimulated to play its role in the assembly of inter-centriolar fibrous linker complex

between the centrioles and reform a connection between the two parental centrioles (Meraldi and Nigg 2001, Mi et al. 2007).

1.1.4.5 The link: cell cycle regulators in the centrosome duplication process

DNA and centrosome replication are two important events during cell proliferation that facilitate faithful transmission of genetic information from a single mother cell to two genetically identical daughter cells. To ensure tight coordination of both processes, several cellular constituents are associated with regulation of the molecular events involved in both DNA and centrosome duplication.

The core regulators of the cell cycle are members of the Cyclin-dependent kinase (CDK) family. The CDKs are family of serine/threonine protein kinases that control both centrosome and cell cycle progression. CDK levels, activities and binding to the regulatory Cyclins are constantly changing in a regulated fashion depending on the stage of the cell cycle. During G1, the D-type Cyclins (Cyclin D1, D2, D3) and their interacting partners, CDK4 and CDK6 are activated through complex mitogenic signalling that promote the synthesis of Cyclin E and A (Sherr and Roberts 2004). Cyclins E, A1, A2 and their interacting partner, CDK2, coordinate the centrosome and cell cycle by phosphorylating their substrates to promote G1/S transition into S-phase (Sherr and Roberts 2004, Adon et al. 2010). For example, CDK2/Cyclin E complex promotes DNA synthesis by phosphorylating Rb and inhibiting CDK-inhibitory kinases (CKIs) that prevent cell cycle progression (Sherr and Roberts 2004). At the centrosome, CDK2 phosphorylates centrosomal NPM/B23 to promote centrosome licensing for S-phase duplication (Matsumoto and Maller 2004, Sherr and Roberts 2004). CDK2 also promotes the activation of PLK4 at the centrosome through a yet to be identified mechanism (Adon et al. 2010). The mitotic CDK1 can associate with Cyclins B1 and B2 and also the Cyclin A from S-phase. However, the CDK1/CyclinB1 complex is only activated upon entry of CDC25 phosphatase to the nucleus to block the inhibitory activities of WEE-1 and Myelin transcription factor 1 (MYT-1) on M-phase CDK1 (Sherr and Roberts, 2004; Wang et al. 2014). Interestingly, both CDK1/Cyclin B and CDC25C localise to the centrosome and their activated forms are seen at the centrosome at prophase, where their activation regulates the activities of some centrosomal components (Jackman et al. 2003; Busch et al. 2007; Fu et al. 2015).

In addition to the CDKs, the anaphase promoting complex or cyclosome (APC/C) also regulates cell cycle progression through the ubiquitination of key regulatory substrates to allow for their degradation (Nigg 2001). Perturbing the coordination between the centrosome and cell cycle can uncouple both cycles, as is observed in many cancer cells and after exposure to genotoxic stress (Badano et al. 2005; Fukasawa, 2007; Bettencourt-Dias et al. 2011).

1.2 The DNA damage response

To combat threats to the genome and its information posed by constant exposure to genotoxic stress which may be from endogenous or exogenous sources, cells have evolved mechanisms to detect damaged DNA and signals to facilitate its repair in a process collectively termed the DDR. Reactive oxygen species, originating from cell metabolism, and replication errors, such as stalled and collapsed replication forks, are some of the endogenous threats to the genomic DNA. External sources of damage to the genomic DNA include exposure to DNA-damaging agents like ionizing (IR), ultraviolet (UV) radiation and genotoxic chemicals such as alkylating agents (e.g methyl methanosulphate and mitomycin C). Irrespective of the source of genotoxic stress, DNA damage jeopardizes a chromosome's physical and informational integrity, which is essential for its correct segregation during mitosis and meiosis and which is essential for accurate expression of its genes. Thus, damage can result in genome instability, immunodeficiency, premature aging and cell death (reviewed by Ciccia and Elledge, 2010). Since DNA damage comes in multiple forms, cells have evolved multiple mechanisms for dealing with serious lesions. For example, erroneous insertions introduced by DNA polymerases during replication are a common source of single base insertions, mismatches or deletions. Normally these lesions are repaired by nucleotide, base excision or mismatch repair (NER, BER or MMR) (Katsura et al. 2009, Ciccia and Elledge 2010, Burgess and Misteli 2015, Chatterjee and Walker 2017). DNA damage caused by thymidine dimers introduced by UV radiation is repaired by NER (Chatterjee and Walker 2017). Double strand breaks (DSBs), which can be caused by ionizing radiation or chemotherapeutic drugs, are regarded as the most deleterious DNA lesion, as they can lead to gene fusions or chromosome rearrangement. DSBs are commonly repaired through two conserved pathways which are non-homologous end joining (NHEJ) or homologous recombination (HR) (reviewed by Burgess and Misteli, 2015; Chatterjee and Walker, 2017). Although DNA methylation, alkylation, oxidation or hydrolysis are commonly repaired by BER, they may be converted to DSBs when the adducts obstruct the replication or transcription machineries (Knipscheer et al. 2009, Chatterjee and Walker 2017).

1.2.1 DNA damage checkpoints

After exposure to genotoxic insult, the cell cycle is halted to allow cells sufficient time for the repair of DNA lesion in a process termed the DNA damaged-induced cell cycle checkpoint. This process helps to prevent the propagation of damaged DNA to the subsequent cell generations. Cell cycle checkpoints are activated between cell cycle phase transitions, and may be divided into: G1/S transition (G1/S), mid-S phase (Intra-S) or G2/M transition

(G2/M). The checkpoint kinases, CHK1 and CHK2, and tumour suppressor, p53, are important for efficient checkpoint activation in response to DNA damage (Dasika et al. 2000; Vogelstein et al. 2000; Bartek and Lukas, 2003; Satyanarayana and Kaldis, 2009; Stracker et al. 2009).

1.2.1.1 G1/S checkpoint

This checkpoint prevents entry into S-phase and ensures that damaged DNA is not replicated, thus preventing cell transformation and oncogenesis. Upon detection of damaged DNA by the sensor proteins, ATR and ATM, they activate the checkpoint kinases, CHK1 and CHK2, respectively. Both CHK1 and CHK2 can phosphorylate CDC25A; this inhibitory phosphorylation prevents the roles of CDC25A in CDK2 activation and interaction with Cyclin E (Bartek and Lukas, 2003; Satyanarayana and Kaldis, 2009; Stracker et al. 2009). Since CDK2/Cyclin E interaction is required for S-phase entry, activation of the ATM-CHK2-CDC25A or ATR-CHK1-CDC25A pathway in response to IR or UV and replication stress induces G1/S-phase cell cycle arrest (Falck et al. 2001). In addition, ATM and ATR also phosphorylate p53 on Ser15 in an independent pathway to induce cell cycle checkpoint arrest. CHK1 or CHK2 can also activate p53 by phosphorylating its amino residues, Thr18 and Ser20 (Vogelstein et al. 2000; Stracker et al. 2009). Activated p53 acts as a tumour suppressor and a gene transcription activator that upregulates expression of genes such as p21 and GADD45 (a growth arrest and DNA damage responsive gene). Also, phosphorylation of p53 on Ser15 prevents its interaction with MDM2 (mouse double minutes 2), ubiquitin ligase that targets it for degradation (Shieh et al. 1997). A p53-induced increase in the cellular levels of p21 also inhibits the CDK2/Cyclin B and CDK4/Cyclin D complexes to prevent entry into S-phase in response to DNA damage (Harper et al. 1995). After successful DNA repair or cell adaptation to the damaged DNA, the G1/S checkpoint is deactivated, similarly through a plethora of post-translational modifications that promote cell progression in a poorly-understood mechanism.

1.2.1.2 Intra-S checkpoint

The intra-S phase checkpoint is activated when cells enter S-phase with DNA damage or when cells acquire damage during S-phase. The DNA lesion is detected by the sensor proteins, which then signal to block replication progression. A requirement for ATM/ATR, BRCA1 and the MRN complex during S-phase checkpoint activation and signalling has been well established (D'Amours and Jackson, 2001; Usui et al. 2001; Falck et al. 2002; Stracker and Petrini, 2011). While ATM detects DSBs, ATR senses the presence and accumulation of ssDNA at stalled replication forks. Similarly, activation of ATR/ATM–CHK1/CHK2–

CDC25A pathway inactivates CDK2 which prevents CDC45 loading onto origin of replication (Chow et al. 2003; Watanabe et al. 1995). Some of the roles of CDC45 are the recruitment of DNA polymerase α to pre-replication complex and initiation of DNA replication, thus intra-S phase checkpoint activation inhibits additional DNA synthesis and origin firing (Takisawa et al. 2000; Falck et al. 2001). In an independent pathway, ATM also mediates the phosphorylation of SMC1 (Structural maintenance of chromosomes protein 1) and FANCD2 (Fanconi Anemia Complementation Group D2) in an NBS1-dependent pathway (Kitagawa et al. 2004, Ho et al. 2006) SMC1 phosphorylation leads to a loss of sister chromatid cohesion, while FANCD2 phosphorylation leads to BRCA1-mediated transcription of GADD45, which promotes intra-S checkpoint activation. Cell cycle progression is stimulated after cells adapt or recover from the damage that provoked the intra-S checkpoint by upregulating genes required for DNA replication in a process that requires the activities of the SCF^{FBW7} (Skp, Cullin, F-box and WD Repeat Domain Containing 7) E3 ubiquitin ligase complex and CDK2/Cyclin A (Coverley et al. 2002; Giráldez et al. 2014).

1.2.1.3 G2/M checkpoint

The G2/M checkpoint is operational during the late G2 phase, thus preventing mitotic segregation of damaged DNA. Similar to the G1/S- and intra S- checkpoints, the G2/M checkpoint activation is triggered by ATM/ATR-dependent phosphorylation of CHK2/CHK1, depending on the DNA damage type. CDC25C, a substrate of both CHK1 and CHK2, becomes phosphorylated at Ser216 and this inhibits its ability to dephosphorylation CDK1 on Thr14 and Tyr15 (Peng et al. 1997; Sanchez et al. 1997; Matsuoka et al. 1998; Donzelli and Draetta, 2003) CDK1 dephosphorylation by CDC25C phosphatase activates CDK1 for its mitotic roles. Furthermore, the phosphorylated CDC25C also binds to the 14-3-3 protein, an interaction that negatively regulates mitosis through transducting an inhibitory signal to CDK1 (Peng et al. 1997, Hermeking 2003). This inhibitory signal results from 14-3-3 preventing nuclear localisation of CDC25C and thereby sequestering its interaction with CDK1. In addition, WEE-1 kinase activity is upregulated upon detection of DNA lesions (Lindqvist et al. 2009). WEE-1 kinase phosphorylates CDK1 at Thr14 and Tyr15 to maintain the CDK1/Cyclin B complex in an inactive state, thus contributing to the inhibition of mitotic progression (Lindqvist et al. 2009).

Another mechanism through which cells prevent cell cycle progression is through the downregulation of PLK1 activity by the checkpoint kinases (Tang et al. 2006; Lindqvist et al. 2009). PLK1 is required for promoting nuclear localisation of CDC25C and for inhibitory phosphorylation of WEE-1 and MYT1 to drive entry into mitosis (Hermeking, 2003; Lindqvist et al. 2009; Zitouni et al. 2014). Similar to G1/S checkpoint, p53-induced

upregulation of p21 levels can results in p21 inhibition of CDK1/Cyclin B (Bunz et al. 1998). Upon successful DNA repair, the proficient checkpoint is deactivated through a PLK1-dependent phosphorylation of WEE-1, Aurora A and Claspin which promotes mitotic entry through an unknown mechanism (Lindqvist et al. 2009; Zitouni et al. 2014; Shaltieì et al. 2015). To downregulate p53-dependent activities that are required for G2/M arrest, TRIM24 and MDM2 ubiquitin ligase as well as Wip1 activities are required to promote cell cycle progression after checkpoint silencing (Honda and Yasuda, 2000., Lu et al. 2007, Jain et al. 2014).

1.2.2 Single strand break repair

Single strand breaks (SSBs) can result from oxidative damage to the deoxyribose and are primarily detected by the PARP proteins. In the presence of SSBs, the two zinc fingers of PARP1 are transiently activated to undergo conformational changes leading to synthesis of poly (ADP-ribose) (PAR) branched chain at the site of DNA lesions (Ciccia and Elledge, 2010; Genois et al. 2012; Chatterjee and Walker, 2017). Activated PARP acts on H1 and H2B histones to contribute to chromatin remodelling which act as a platform for recruitment of DNA repair proteins. Then, the PAR chains undergo rapid disassembly by PAR glycohydrase (PARG) within minutes of SSB detection; this disassembly allows for restoration, detection and signalling of the next SSB by PARP proteins (Ciccia and Elledge 2010, Chatterjee and Walker 2017). XRCC1-interacting endonucleases APE1 (Apurinic/apyrimidinic endonuclease 1), APTX (Aprataxin), APLF (Aprataxin-and-PNK-like factor), and FEN1 (Flap endonuclease 1) remove the damaged DNA in a process dependent upon PARP1 and PCNA and the ssDNA gap is filled by DNA polymerase β (Lan et al. 2004; Mortuse- wicz et al. 2006; McKinnon and Caldecott, 2007; Caldecott, 2008).

While PARP can bind to damaged ssDNA, it has a lower affinity for SSBs compared to DSBs (D'Silva et al. 1999). RPA complex can also bind to ssDNA to prevent DNA degradation by DNA endonucleases and recruit DNA repair factors to the site of DNA lesion. RPA recruits RAD17 complex and the RPA and RAD17 complexes subsequently recruit RAD9-RAD1and HUS1 (9-1-1) complex. Once recruited, the 9-1-1 complex stimulates ATR-dependent activation of CHK1 as well as recruiting ATR/ATR-interacting protein (ATRIP) to ssDNA breaks. ATR then undergoes autophosphorylation on Thr 1989 in response to many forms of genotoxic stress, including DNA cross-links, base modifications, and stalling of replication forks, while ATM is primarily responsive to DSBs (Zou and Elledge, 2003; Ball et al. 2005; Liu et al. 2011). TOPBP1 has also been shown to play a key role in ATR signalling to mediate repair of the ssDNA. It was previously believed that its recruitment is dependent on its interaction with the 9-1-1 complex; a recent finding has shown that its recruitment to the

site of damage is mediated by interaction between TOPBP1-BRCT2 domain and ssDNA-bound RPA complex (Lee et al. 2007; Acevedo et al. 2016). The ATR pathway activation leads to cell cycle delay and subsequent recruitment and activation of DNA polymerases α, δ and ε for repair of damaged DNA, thus maintaining genome integrity (Maréchal and Zou 2015).

1.2.3 Double strand break repair pathways

As implied by the name, DSBs involve damage to both strands of phosphodiester backbone within close proximity, and they are highly toxic to cells. They can arise from exposure genotoxic stresses such as IR or various chemical agents. DSBs may be particularly difficult to repair and unresolved DSBs can result in genetic instability arising from loss of genetic information or gene rearrangement. In eukaryotic cells, there are two major pathways for the repair of DSBs - homologous recombination (HR) and non-homologous end joining (NHEJ) (Chatterjee and Walker 2017). One of the earliest events in the identification of DSB involves chromatin modifications that trigger a cascade of events to signal for DNA repair (Chatterjee and Walker 2017).

1.2.3.1 Homologous recombination (HR) repair

Homologous recombination (HR) is an essential, error-free DNA repair mechanism that is predominantly used during S and G2 phases due to the requirement of a sister chromatid or the homologous chromosome for repair of the DSB. HR is a highly important mode of DSB repair and HR defects have been associated with increased mutagenesis, cancer predisposition and developmental defects (Morrison et al. 2000, Ciccia and Elledge 2010, Genois et al. 2012, Chatterjee and Walker 2017). At the onset of HR activation, the MRN complex, composed of MRE11, RAD50, and NBS1, binds to the free ends of the DNA lesion and recruits ATM to the site of DNA damage (Stracker and Petrini, 2011; Chatterjee and Walker, 2017). The MRN complex, CtIP (CtBP-interacting protein), BRCA1 and activated ATM trigger nucleolytic degradation of the DSBs to form ssDNA around the 5' ends of the lesion. An extended region of 3' overhang ssDNA is then formed by the exonuclease activities of DNA2 and EXO1 or BLM. The ssDNA-binding protein, RPA (RPA1, RPA2 and RPA3) complex, immediately accumulates at the ssDNA overhangs to stabilise the region for repair. RAD51-ssDNA nucleofilaments are assembled in a process that displaces RPA from the ssDNA and requires the activities of PALB2 and BRCA2 (West, 2003). BRCA2 and RAD51 interact directly, and the interaction between RAD51 and the BRCA2 C-terminus is important for HR. Upon assembling to the damage site, RAD51 searches for homologous sequence and mediates invasion of a nearby homologous duplex DNA to form a D-loop. RAD54

contributes to the activity of RAD51-dependent strand invasion process and also removes RAD51 to expose the 3' OH (hydroxyl) ends to prime DNA synthesis by DNA polymerases δ, φ and μ (Mazin et al. 2010; Sebesta et al. 2013). DNA synthesis of the invading strand occurs in the 5'-3' region using the donor homologous strand as a template to replace the nucleotides resected at the damaged site in a process known as strand extension.

Two main pathways have been described for the final stage of the HR repair process. The synthesis dependent strand annealing (SDSA) pathway requires RTEL helicase which promotes reannealing of the processed DNA ends after displacement of the RAD51 nucleofilament, D-loop dissociation and minimal strand extension (West, 2003). In the DSB repair (DSBR) model, the newly repaired DNA can be captured and interlocked with the end of the loop branch to a form a double Holliday junction (HJ) that can be dissolved or resolved to separate the repaired DNA from the template strand. Different cellular mechanisms and resolvases have been shown to potentially process the HJ. Depending on the orientation of cleavage, GEN1 (Gen homologue endonuclease 1), the heterodimeric MUS81-EME1 complex and the SLX1-SLX4 complex have been shown to resolve the HJ to yield either crossover or non-crossover products. The BLM-TOPOIII-RMI1-RMI2 complex, which contains the BLM helicase, has been to result in HJ dissolution which exclusively favours formation of non-crossover recombinants (Wu and Hickson, 2003). To date, the mechanism for the preferential selection of pathway for the resolution or dissolution of HJ is yet to be fully understood. Figure 1.3 summarises the HR-mediated repair of DSBs.

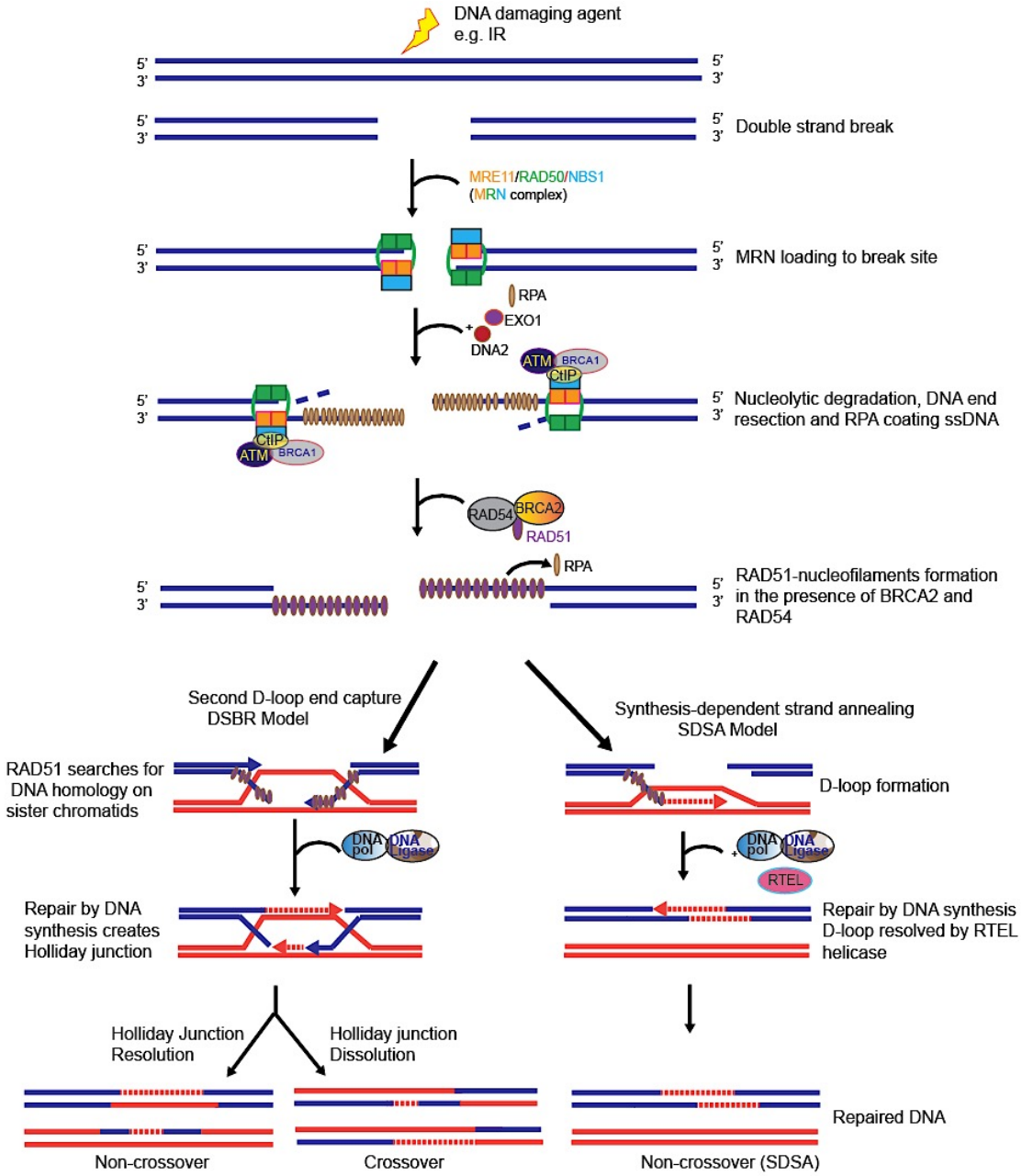

Figure 1.3: DSB repair via Homologous recombination (HR)

Schematic representation of major events in the HR-mediated repair of DSBs. Briefly, DSB is detected and resected by the MRN complex and CtIP in the presence of BRCA1 and ATM. Further resection in the 5'- 3' direction is carried out by DNA2 and EXO1. The single stranded DNA generated are immediately coated by RPA complex. Subsequently, RAD51 displaces RPA in a RAD54- and BRCA2-dependent manner to mediates homology search on the sister chromatids. The final stage of the repair process can be carried out using either SDSA or DSBR (see text for further details).

1.2.3.2 Non-homologous end joining (NHEJ)

NHEJ is the predominant choice of DSBs repair during G1/early S phase due to the absence of the sister chromatid DNA template that is required for successful HR pathway. Unlike HR, it is an error prone process due to the direct end-to-end ligation of the DNA lesion. NHEJ does not require DNA end resection; instead, it is instigated by the binding of heterodimeric Ku70/80 ring structure to the DNA break site (Jackson 2002, Davis and Chen 2013). Binding of Ku aligns, stabilises and prevents degradation of the DNA ends and also activates the PI3K component of DNA-PKcs which, in a complex with the Ku heterodimer, forms a functional DNA-PK holoenzyme that undergoes autophosphorylation to promote recruitment of other NHEJ repair proteins. The order of recruitment of the NHEJ DNA repair proteins is dependent on the complexity of the DNA damage (blunt or non-blunt ends) (Chatterjee and Walker 2017). Artemis, PNK (polynucleotide kinase), APLF, WRN (Werner syndrome), APTX and Ku initiate DNA end processing in an ATR/ATM-dependent manner, which is filled by the template-dependent polymerase, μ, or the template-independent polymerase, λ (Davis and Chen 2013, Chatterjee and Walker 2017). To complete the NHEJ repair process, XRCC4/LIG4 is recruited to the break site to promote the religation of the ends of the DNA strands with the help of the stimulatory factor XLF (XRCC4-like factor) (Lieber 2010, Chatterjee and Walker 2017). A summary of the major events in DSB repair via the NHEJ is shown in Figure 1.4.

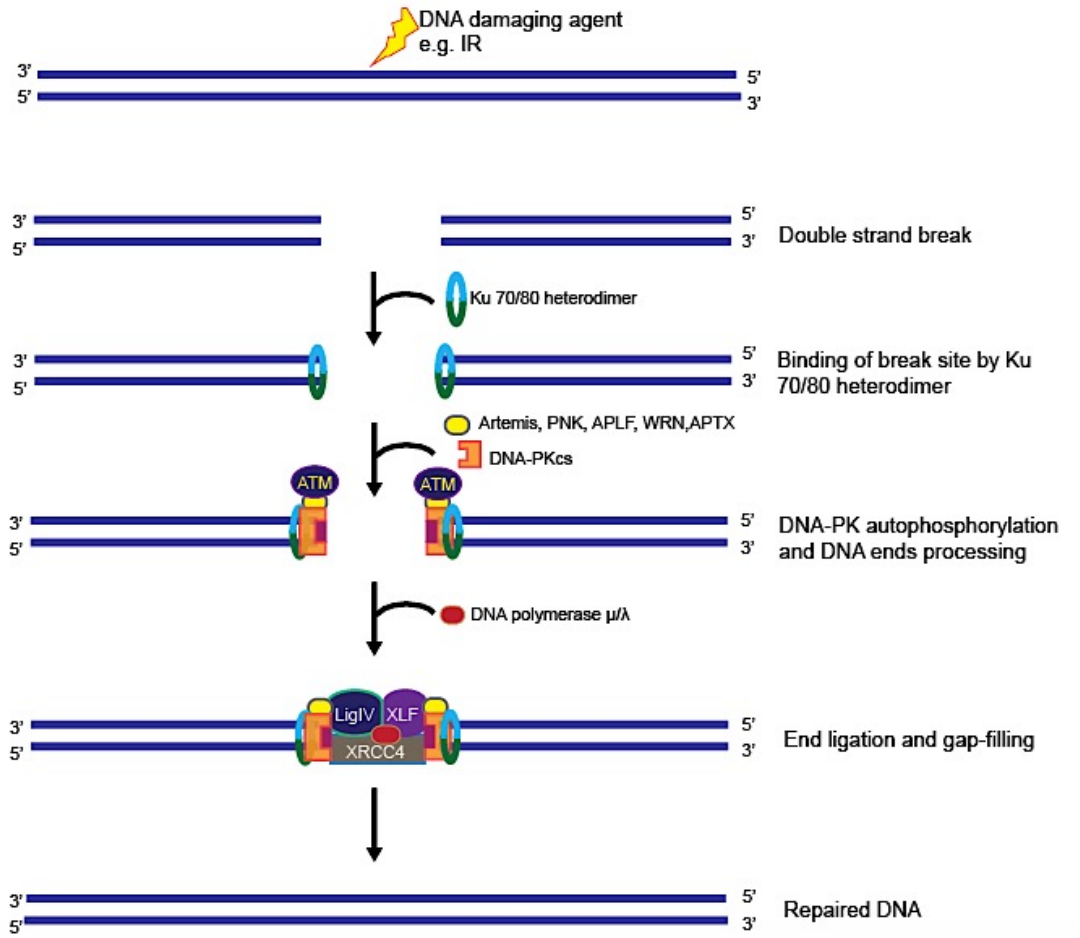

Figure 1.4: DSB repair via non-homologous end joining

Schematic showing the mechanism for DSB repair by NHEJ. Briefly, the damaged DNA ends are detected by the Ku 70/80 heterodimer to initiate the NHEJ pathway. The Ku complex recruits the catalytic substrate, DNA-PKcs, to form DNA-PK holoenzyme that facilitates the recruitment of Artemis, PNK, APLF, WRN and APTX complex. This complex is required for DNA end-processing in an ATR/ATM-dependent manner. The processed DNA is then filled by either DNA polymerase λ/μ. XRCC4 and DNA ligase IV complex facilitates the final end-joining (ligation).

1.3 Cilia

Cilia and flagella are essential and highly conserved organelles found on the cell surface of most eukaryotic cells. Cilia were described about a century ago in rabbit and human kidney cells (Zimmermann 1898), and in recent years, dysfunction in cilia-related proteins has been shown to result in human diseases, termed ciliopathies (Goetz and Anderson, 2010). Cilia have very well-established roles as motile and sensory organelles in various species (Pazour and Witman 2003, Kramer-Zucker et al. 2005, Shah et al. 2009, Goetz and Anderson 2010). Cilia are categorised based on their ability to move. Motile cilia have the ability to generate beats that are propagated from the base to the tip of the cilium. This beating propels fluid or facilitates cell motility, as it is seen in mammalian respiratory passages and spermatozoa,

respectively. In contrast to the motile cilia that can exist in groups or as single organelles as per the examples above, primary (immotile) cilia exist as single cellular projections that perform key sensory functions (Goetz and Anderson 2010). Primary cilia are important for a variety of vertebrate developmental and cellular functions. These include the detection of mechanical and chemical cues to induce intracellular responses that are necessary for processes such as embryogenesis and brain development (reviewed by Pazour and Witman, 2003; Gerdes et al. 2009; Goetz and Anderson, 2010). The primary cilium mediates these physiological roles through mechanisms such as the Hedgehog, Wnt and platelet-derived growth factor (PDGF) signalling pathways (Corbit et al. 2005; Schneider et al. 2005; Gerdes et al. 2009; Lancaster et al. 2011).

1.3.1 Structure of the primary cilium

Cilia, irrespective of the type, consist of nine circumferentially arranged pairs of microtubule doublets with the motile cilia having a central microtubule pair ('9+2 configuration'), which is absent in a primary cilium ('9+0 configuration'). Importantly, the primary cilia also lack the axonemal dynein that confers the mechanical force required for ciliary beating (Gibbons and Rowe 1965, Yagi et al. 2005). However, there are some exceptions to this configurational classification: for example, mouse nodal cilia are motile and exhibit the 9+0 microtubule arrangement, while kinocilia are non-motile and have the 9+2 doublets microtubule arrangement.

As shown in Figure 1.5, the primary cilium is assembled on a mother centriole that is docked to the plasma membrane (called the 'basal body' only when docked) during G1/G0. Primary cilia are resorbed prior to mitosis to allow the mother centriole to function as part of the centrosome (Izawa *et al.* 2015). A striking feature of the primary cilium is the microtubule-based axoneme that protrudes from the cell surface into the extracellular space (see Figure 1.5). The cylindrical array of doublet axonemal microtubules is arranged continuously from the nine doublet microtubules at the distal end of the basal body. Upon mother centriole conversion to a basal body, the distal appendages form the transition fibre that anchors the basal body to the plasma membrane. Ablation of one of the distal appendage proteins, such as Cep123, SCLT1, Cep83, FBF1, Cep164, and Odf2, prevents ciliogenesis in human cells (Daly et al. 2016; Graser et al. 2007; Ishikawa et al. 2005; Sillibourne et al. 2013; Tanos et al. 2013). The transition zone, the region where the basal body microtubules convert into the axonemal doublet microtubules, serves as a selective barrier that controls protein and lipid diffusion between the plasma and ciliary membranes. It consists of transition fibres, Y-links that connect axonemal microtubules to the ciliary membrane, and the ciliary necklace (Hsiao et al. 2012; Szymanska and Johnson, 2012). The exact organisation of the transition zone is unknown. It is thought that some nephronophthisis (NPHP) proteins and Meckel syndrome-

associated (MKS) proteins interact to form this region. Also, loss of transition zone proteins has been associated with perturbed basal body docking or defective Y-links formation in human ciliopathies such as NPHP and MKS (Garcia-Gonzalo et al. 2011, Szymanska and Johnson 2012).

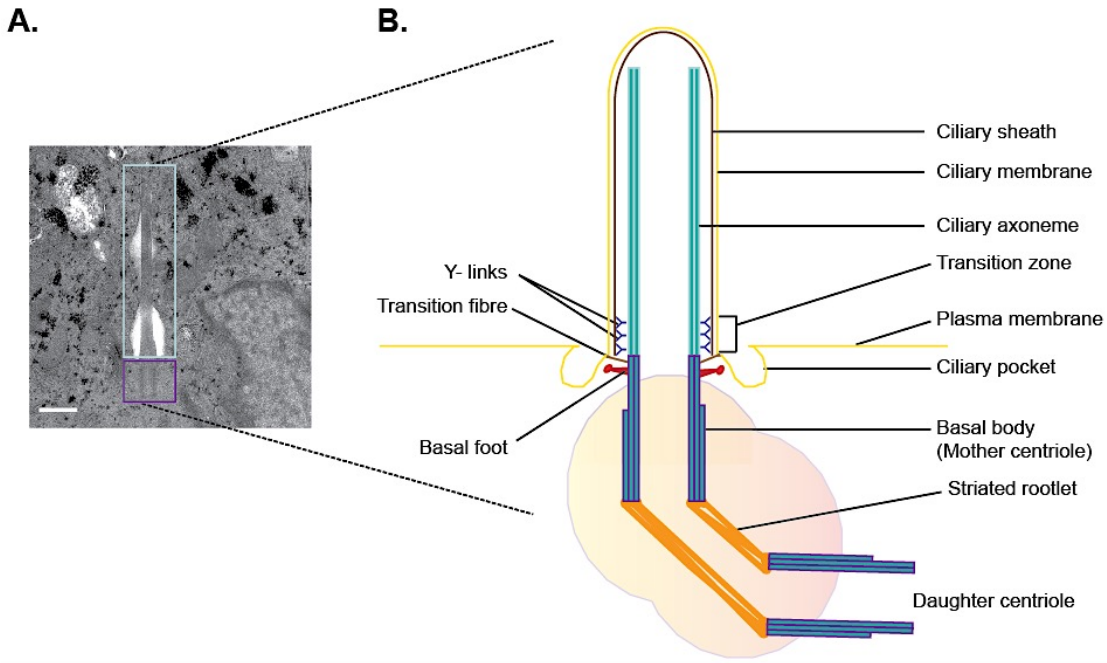

Figure 1.5: Structure of the primary cilium

A. Electron micrograph of a primary cilium of hTERT-RPE1 cell. Purple and green boxes indicate the basal body and axoneme region respectively. Scale bar, 500 nm. **B.** Schematic showing the structure of a basal body within the centrosome, the transition zone, the ciliary pocket, and the ciliary axoneme. The distal and subdistal appendages become transition fibres and basal feet, respectively. The ciliary membrane is continuous with the plasma membrane, but it is functionally distinct. Y-links and the transition fibres make the transition zone that controls protein and lipid movement into and out of the primary cilium (see text for further details).

The axonemal doublet microtubules, the A- and B- tubules, are polymerised from intracellular tubulin pools, with the growing (+) ends at the ciliary tip axoneme. Adjacent outer microtubules are interconnected by nexin links. The tip of the cilium contains singlet microtubules that contribute to motile and sensory functions (Fisch and Dupuis-Williams 2011). The ciliary microtubules undergo post-translational modifications, such as acetylation, detyrosination, polyglutamylation and glycylation, that promote axonemal stability (Hammond et al. 2008).

For axonemal growth to occur, ciliary proteins are transported to and from the cilia tip by intraflagellar transport (IFT). The IFT particles, which are composed of the IFT-particle subcomplexes, IFT-A and IFT-B, IFT motor proteins, and BBSomes, support bidirectional transport (retrograde and anterograde movement) of IFT cargoes along the axoneme. They are crucial for cilium assembly and maintenance (Pedersen and Rosenbaum, 2008; Hsiao et al.

2012). The anterograde IFT particle is powered by heterotrimeric kinesin-II complex and homodimeric OSM-3 that facilitate transport from the base of cilium to the distal tip, while retrograde transport is coordinated by oligomeric dynein-II complex which allows for movement from ciliary tip back to the cell body (Qin et al. 2004, Pedersen and Rosenbaum 2008, Fisch and Dupuis-Williams 2011). The kinesin-II complex is made up of two motor domains, Kif3A and Kif3B, and a non-motor domain known as kinesin-associated protein (KAP). On the other hand, the oligomeric dynein-II complex consists of four homodimeric subunits: a heavy chain DYNC2H1, a light chain, DYNC2LI1, an intermediate chain, WDR34 and a light chain DYNLL1 (reviewed by Qin et al. 2004; Pedersen and Rosenbaum, 2008). Both anterograde and retrograde transport are crucial for the assembly and disassembly of primary cilia, respectively. The IFT subcomplexes, IFT-A and IFT-B, are involved in retrograde and anterograde transport, respectively (Pedersen and Rosenbaum 2008, Goetz and Anderson 2010). The BBSome is formed from a biochemically stable complex of seven BBS gene products (BBS1, 2, 4, 5, 7, 8, and 9) (Jin and Nachury 2009, Wei et al. 2012). The BBS genes are highly conserved among ciliated organisms and mutation in at least 12 BBS genes in human can cause Bardet-Biedl syndrome (BBS) (Jin and Nachury 2009). Mutations in components of the IFT particles have been linked to a range of ciliopathies (Pazour et al. 2000; Hildebrandt et al. 2011).

The ciliary axoneme is located within the ciliary membrane which is made up of the ciliary pocket and sheath (Benmerah 2013). The ciliary membrane is contiguous with the plasma membrane, but is morphologically and functionally distinct due to the localisation and diffusion of specialised sensory and signalling receptors (Hu et al. 2010, Bloodgood 2012). This diffusion compartment limits the exchanges between the cilium and cytoplasm. The ciliary pocket is characterised by the invagination of membrane that is almost perpendicular to the axoneme and then folds toward and along the cilium. The presence of budding clathrin-coated and actin patches maintains the shape and integrity of the ciliary pocket, and also facilitates endocytosis at this region of the primary cilium (Benmerah, 2013). Recently, clustered cilia that shared the same ciliary pocket have been reported to have reduced levels of ciliary membrane proteins, implicating the ciliary pocket as a rate-limiting structure for trafficking ciliary proteins (Mahjoub and Stearns 2012). The ciliary sheath is formed from the ciliary vesicle and persists with the cilium structure. During ciliary morphogenesis, the extending axoneme lengthens, and the sheath enlarges to accommodate the shaft. The sheath and ciliary pocket are more prominent on cells whose basal bodies lies deep within the cytoplasm than those whose basal body is in the proximity of the plasma membrane (Sorokin, 1962).

1.3.2 Functions of primary cilia

In contrast to primary cilia that are present on almost all cells in the human body, motile cilia are restricted to the sperm, cells in the nervous system, and the epithelial cells of the airway and oviduct. Multiple motile cilia of the epithelial cells and nervous system are characterised by their ability to beat synchronously and direct extracellular flow of mucus, ovum movement through the fallopian tube, and cerebrospinal fluid through the cerebral ventricles (Pazour and Witman 2003, Goetz and Anderson 2010). In mammalian cells, primary cilia are commonly solitary where they act as sensors for extracellular chemicals, mechanical modulators and as photoreceptors in cells such as pancreas, kidney and eyes, respectively. Motile cilia of the human airway epithelia that facilitate mucus flow also act as chemosensors for the bitter taste receptor (Shah et al. 2009). The presence of chemosensor receptors on these motile cilia was demonstrated through the localisation of sensory-related gene products such as T2Rs (Taste receptor type 2 family), α-gustducin, PLC-β2 (phospholipase C β2), and an increase in intracellular Ca^{2+} levels of ciliated cells upon exposure to bitter compounds. These experiments show that motile cilia, like the primary cilia, can serve sensory functions.

As an extracellular sensor, the ciliary membrane is decorated with high numbers of transmembrane receptors and ion channels. These confer chemosensory and mechanosensory capabilities upon the primary cilia, and the involvement of primary cilia in several signalling pathways such as Wnt, SHh, and PDGF has been well described (Hooper and Scott 2005, Corbit et al. 2005). An example of the involvement of primary cilia in Hh signalling is seen in its diverse roles in animal embryo and bone development, tissue homeostasis and metabolism (Hooper and Scott 2005, Corbit et al. 2005). Sonic (SHh), Indian (IHh), and Desert (DHh) Hedgehog are the three known families of Hh signalling. All Hh proteins are synthesised as inactive precursors that possess an amino-terminal (HhN) region which mediates Hh signalling and a carboxy-terminal (HhC) intein-like domain that is later removed by autocatalytic cleavage (Perler et al. 1995, Perler 1998). The Hh signalling agonist mediates its effects by inhibiting the negative regulator of Hh pathway, patched (PTCH), a 12 transmembrane receptor. As shown in Figure 1.6, in the absence of Hh, PTCH represses the functions of Smoothened (Smo), a seven-transmembrane protein, that acts as the central positive mediator of Hh signalling. PTCH translocalises to the primary cilium when activated (Hooper and Scott 2005, Corbit et al. 2005). The stoichiometric binding of SHh to PTCH is regulated by Hh binding proteins such as the positive regulator, Hh-interacting protein (HHIP), and the negative regulator, Growth arrest-specific gene 1 (GAS1) (Hooper and Scott, 2005; Wong and Reiter, 2008, *see* Figure 1.6). Upon binding of Hh to PTCH1, the transmembrane receptor is internalised to allow for translocalisation of Smo from the intracellular vesicle to the primary cilium (Wong and Reiter 2008, Lu et al. 2015b, Sánchez

and Dynlacht 2016). Smo activation and translocalisation allows for the uncoupling of Glioma (GLI) proteins from their inhibitor, suppressor of fused (SUFU). The inhibitor blocks transcriptional activities and translocation of GLI proteins to the nucleus where they can activate the transcription of Hh target genes (Hooper and Scott 2005, Wong and Reiter 2008).

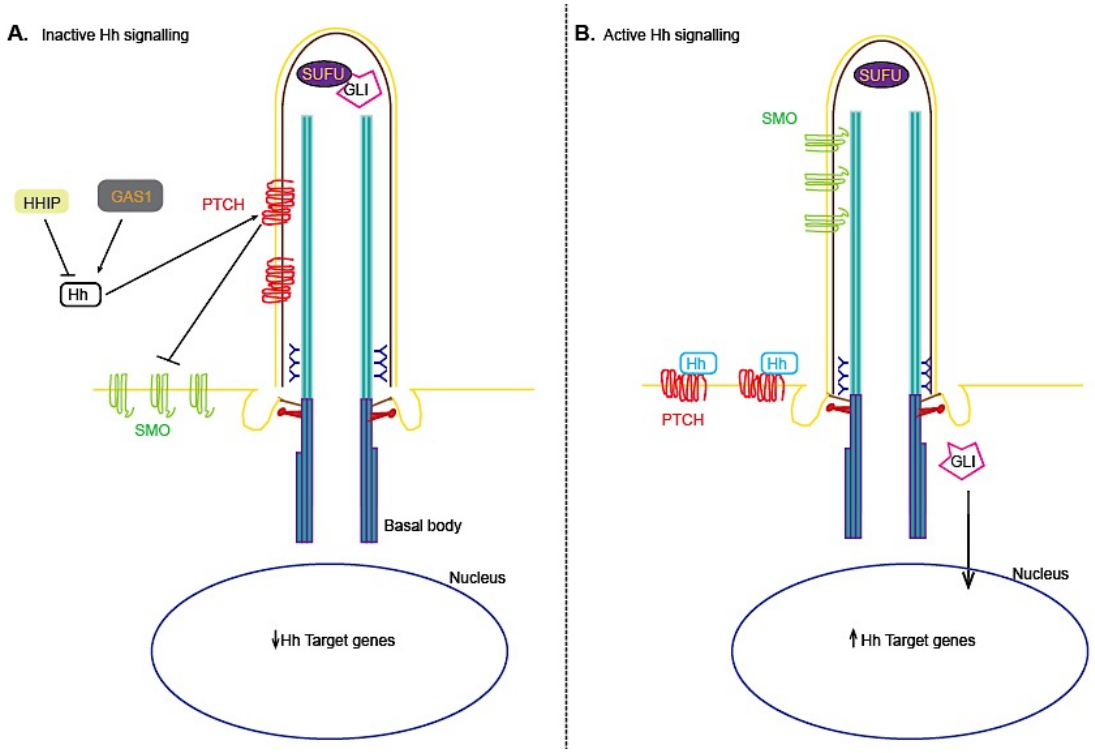

Figure 1.6: Primary cilium and hedgehog (Hh) signal transduction

A. In the absence of Hedgehog (Hh) ligand, Patched (PTCH) inhibits Smoothened (Smo) localisation the the primary cilium. Nuclear translocation of Glioma (GLI) protein is also inhibited by Suppressor of fused (SUFU) to repress transcription of Hh target genes. Hh-interacting protein (HHIP) acts as a positive regulator of Hh and Growth arrest-specific 1 (GAS1) as a negative control of the stoichiometric binding of Hh to PTCH. **B.** Binding of Hh to PTCH releases the inhibition of Smo. Smo translocates to the primary cilium and relieves SUFU inhibitory signal on GLI. GLI proteins then translocate to the nucleus to activate Hh target genes (Adapted from: Hooper and Scott, 2005; Wong and Reiter, 2008).

Primary cilia in osteocytes and osteoblasts have flow sensing capabilities that are reminiscent of those in the kidney (Hoey et al. 2012). This response to extracellular shear stress involves upregulation of intracellular Ca^{2+} osteogenic gene expression and protein secretion, which is lost upon treatment with siRNA to IFT proteins or choral hydrate-mediated primary cilia ablation (Hoey et al. 2012). Protein secretion is thought to act in paracrine manner that facilitates osteogenic gene expression in mesenchymal stem cells for efficient bone development (Hoey et al. 2012). In vertebrate models, primary cilia also establish the left-right asymmetry that is crucial for determining organ laterality and positioning during the early stage of embryonic development. During embryonic organogenesis, primary cilia

mediate asymmetric expression of genes such as *nodal* and *southpaw* (*spaw*). This is crucial for correct positioning of internal organs, such as the heart and pancreas which are located on the left (Long et al. 2003; Kramer-Zucker et al. 2005; Goetz and Anderson, 2010). In zebrafish, IFT mutant embryos show defective fluid flow and develop kidney cysts, hydrocephalus and laterality defects that correlate with reduced cilia frequency in the Kupffer's vesicle (KV, the equivalent of the mouse embryonic node). Defective cilia cause laterality defects which are marked by randomisation of the gut positioning or incorrect looping of the heart (Long et al. 2003; Kramer-Zucker et al. 2005).

In conclusion, the primary cilium serves as a hub for several signalling pathways that contribute to movement, differentiation, and proliferation. Structural alteration of this organelle can lead to severe multi-organ human disorders.

1.3.3 Formation and disassembly of cilia

Primary cilia are assembled at G0/G1 phase of the cell cycle and are disassembled to allow for basal bodies' centrosomal role in formation of the bipolar spindle. Therefore, cilia assembly occurs outside the cell cycle exit, and their disassembly corresponds with cell cycle re-entry. Defective assembly/disassembly timing may prevent cell cycle progression and proliferation (Seeley and Nachury 2010, Sánchez and Dynlacht 2016, Liang et al. 2016). Ultrastructural analysis of the basal body revealed the several steps that occur during ciliogenesis (Sorokin, 1962; 1968). Sorokin's findings established the extracellular and intracellular pathways of cilia assembly, which differ by direct docking of the basal body to the plasma membrane (extracellular) or indirect docking to the ciliary vesicle before fusing to the plasma membrane (intracellular) (*see* Figure 1.7).

At the initiation stage of ciliogenesis, the distal appendages on the mother centriole facilitate membrane fusion to the ciliary vesicle. For example, Cep164, Cep89 and Cep123, distal appendage proteins, are indispensable for membrane docking and ciliogenesis (Graser et al. 2007, Tanos et al. 2013, Sillibourne et al. 2013, Daly et al. 2016). Upon inducing ciliogenesis, small cytoplasmic vesicles that originate from the Golgi and the recycling endosome, termed distal appendage vesicles (DAVs), begin to accumulate in the vicinity of distal appendages of the mother centriole, where basal body docking occurs. Rabin8, a Rab GTPases and regulator of exocytosis, recruits TrappII (Transport protein particle II). Subsequently, TrappII activates Rab8a and Rab11, members of the Rab GTPase family, to promote the rapid localisation of cytoplasmic vesicles around the mother centriole (reviewed by Lu, Q. et al. 2015; Sánchez and Dynlacht, 2016). EHD1 (EH domain-containing protein 1) is then recruited to facilitate further vesicularization of the donor membrane and fusion with the ciliary vesicle. This allows for the formation of the ciliary membrane and sheath into which the extending axoneme grow into (Sorokin, 1962; Lu, Q. et al. 2015).

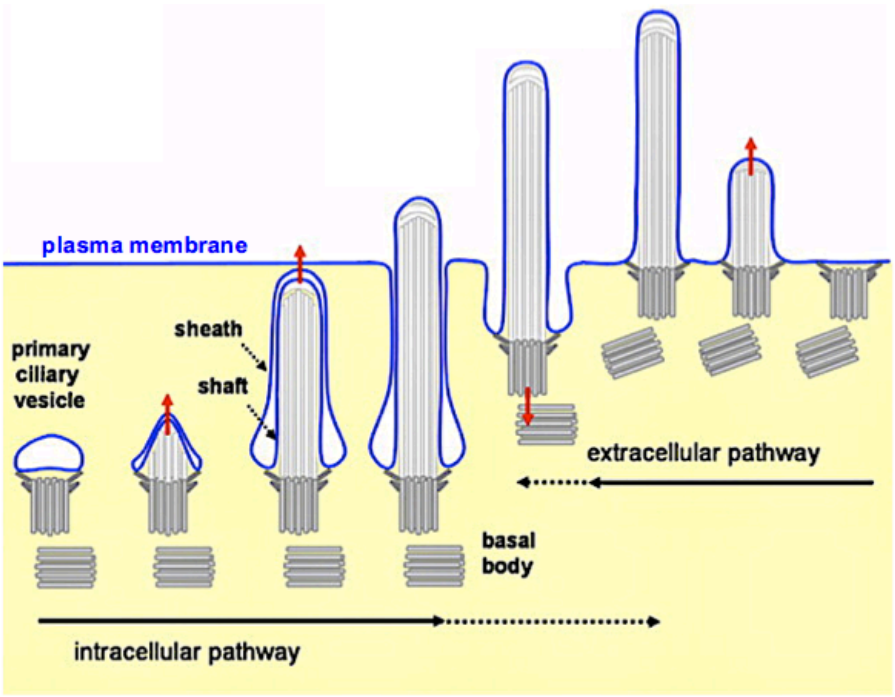

Figure 1.7: Physical stages in the intracellular and extracellular pathways of ciliogenesis

Schematic illustration of Intracellular (left) and extracellular (right) pathways of cilum assembly. In the intracellular pathway, the basal body associates with ciliary vesicles (CV) that form from distal appendage vesicles (DAVs). Further vesicularisation allows for the growth of the CV and the axoneme elongates within the CV. The CV then forms the cilia sheath pocket and membrane. The ciliary membrane is functionally distinct from the plasma membrane with which it eventually fuses to allow for cilium access to the cell surface. In the extracellular pathway, the basal body docks directly to the plasma membrane in a process that also requires the distal appendages. The axoneme then grows within the ciliary membrane into the extracellular space (Taken from Molla-Herman et al. 2010).

Upon docking of the basal body to the ciliary membrane, TTBK2 kinase is recruited to mediate removal of the CP110/Cep97 centriolar cap protein omplex that inhibits ciliogenesis (Spektor et al. 2007, Goetz et al. 2012). Interestingly, these proteins, CP110 and Cep97, regulate centriole length in proliferating cells. Depletion of either CP110 or Cep97 results in increased ciliation frequency in human cells while their overexpression prevents ciliogenesis (Spektor et al. 2007, Schmidt et al. 2009, Wu and Tang 2012, Zheng et al. 2016). Therefore, CP110 and Cep97 act as cap proteins on centrioles that negatively regulate formation of primary cilia. CP110 removal is mediated through a complex mechanism that involves the activities a number of proteins, such as the basal body-associated kinases, TTBK2 and MARK4, centrin2 and Neurl4 (Spektor et al. 2007; Goetz et al. 2012; Kuhns et al. 2013; Prosser and Morrison, 2015; Loukil et al. 2017). There remain several steps yet to be understood in the mechanisms underlying asymmetric CP110 removal from the mother centriole. Similar to CP110, aurora A and trichoplein also prevent ciliogenesis in proliferating cells and are removed from the basal body by proteolytic degradation upon induction of ciliogenesis (Inoko et al. 2012, Sánchez and Dynlacht 2016). Finally, the IFT particles

(described in section 1.3.1) facilitate axonemal membrane transport and interact with RabGTPase, another vital component of the membrane trafficking machineries (Wong and Reiter 2008, Kobayashi and Dynlacht 2011).

CPAP/CENPJ, an early initiation factor recruited during centriole duplication process, has been shown to be a positive regulator of ciliogenesis. Overexpression of CPAP in human osteosarcoma U2OS cells causes elongation of centrioles and increased level of primary cilium formation, while its depletion in neuronal cells prevents ciliation (Schmidt et al. 2009, Wu and Tang 2012, Zheng et al. 2016). More recently, CPAP has been implicated in primary cilium disassembly that is crucial for maintaining a pool of neural progenitor cells (NPCs) (Gabriel et al. 2016). Human fibroblast cells with specific *CPAP* Seckel syndrome mutations have overly long cilia and delayed cell cycle re-entry due to defective cilium resorption after serum stimulation (Gabriel et al. 2016). Interestingly, CPAP was also shown to interact with several cilium disassembly complex proteins, such as Nde-1, Aurora A, HDAC6 and the oral-facial-digital syndrome type 1 (OFD1) (Pugacheva et al. 2007, Kim et al. 2011, Tang et al. 2013), where it acts as a scaffold protein for localisation of the cilium disassembly complex (Gabriel et al. 2016).

While several steps in cilium disassembly remain unknown, it is believed that the disassembly process happen in two phases. The first phase of disassembly happens in G1 phase after serum stimulation. Cilia disassemble gradually as the cells progress through cell cycle until the second and final wave of disassembly, which occurs at G2/M to allow for bipolar spindle formation during mitosis (Sánchez and Dynlacht 2016). Aurora A has been reported to play a role in cilium resorption through its activation of INPP5E55 which promotes phosphatidylinositol (PtdIns(4)P) activities. PtdIns(4)P prevents TTBK2 recruitment to the basal body (Pugacheva et al. 2007, Inoko et al. 2012, Sánchez and Dynlacht 2016). Aurora A also phosphorylates histone deacetylase, HDAC6, to promote cilium disassembly through axonemal tubulin deacetylation and actin polymerisation (reviewed by Sánchez and Dynlacht, 2016). Trichoplein and HEF-1 participate in centrosomal stabilisation and activation of Aurora A to promote cilium disassembly during G2/M phases (Pugacheva et al. 2007, Inoko et al. 2012). Chemical inhibition or siRNA-mediated depletion of Aurora A promote primary cilium assembly and prevent cilium disassembly after serum stimulation in hTERT-RPE-1 cells. Also, microinjection of activated Aurora A promotes cilium disassembly in ciliated cells (Pugacheva et al. 2007). Interestingly, the mitotic kinase, PLK1, also promotes the activation of HEF1-Aurora A complex to activate the cilium disassembly process (Wang et al. 2013a, Sánchez and Dynlacht 2016).

The microtubule depolymerising kinesins, Kif2a and Kif24, facilitate axonemal tubulin depolymerisation during primary cilium disassembly. Upon serum stimulation, PLK1 phosphorylates Kif2a (Kim et al. 2015), while Nek2 phosphorylates Kif24 (Miyamoto et al. 2015) to ensure cilium disassembly and irreversible cell cycle progression (Wang et al. 2013a, Sánchez and Dynlacht 2016). Since IFT and BBSomes facilitate both anterograde and retrograde transport to assemble and maintain the ciliary axoneme, it is not surprising that they facilitate both cilia assembly and disassembly (Pedersen and Rosenbaum 2008, Krock and Perkins 2008, Wei et al. 2012). It is thought that an equilibrium between anterograde and retrograde IFT is essential for maintaining the cilium axoneme and that a cilium disassembles when the rate of retrograde movement from the ciliary tip to the base outweighs the rate of anterograde movement (Qin et al. 2004, Pugacheva et al. 2007, Pedersen and Rosenbaum 2008). A summary of the mechanisms for cilium assembly and disassembly is shown in Figure 1.8

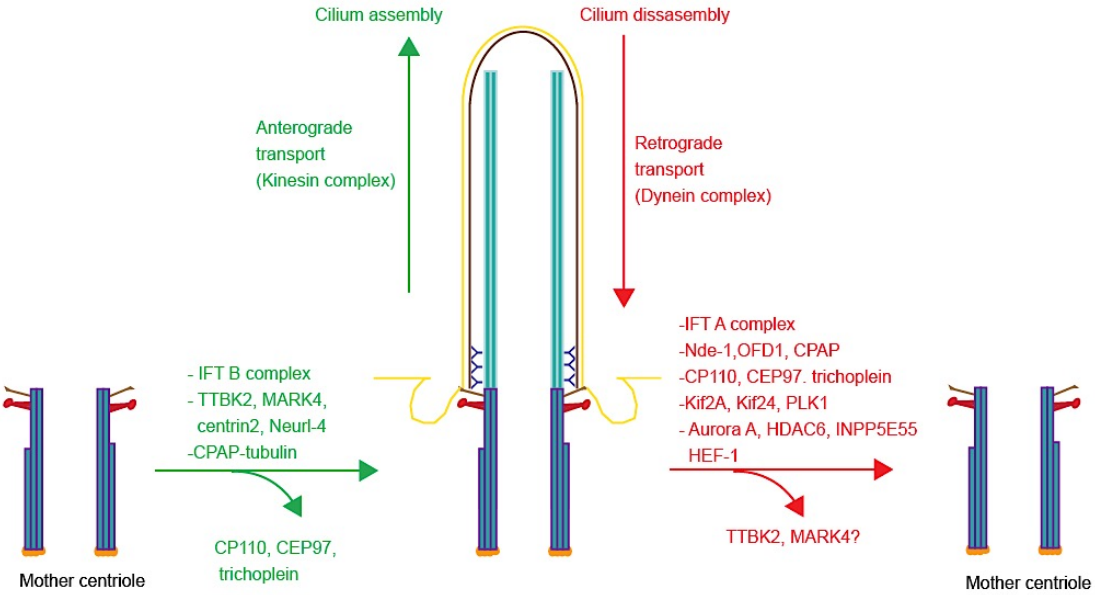

Figure 1.8: Summary of factors that control cilium assembly and disassembly

A schematic illustration of proteins that control ciliogenesis and cilium resorption. During primary cilium assembly (green labels), IFT-complexes are recruited to maintain a balance in anterograde and retrograde transport. TTBK2, centrin2 and Neurl-4 promote CP110 and CEP97 removal from basal body. MARK-4 also contributes to CP110 and trichoplein disappearance from the basal body to facilitate axonemal tubulin polymerisation. On the other hand, cilium disassembly requires the activities of Aurora A on HDAC6, INPP5E55 and HEF-1. HDAC6 promotes axonemal tubulin deacetylation and actin stabilisation. Kif2A and Kif24 facilitate microtubule depolymerisation. TTBK2, and possibly MARK-4 kinases are displaced from the basal body. CP110, trichoplein and CEP97 are then recruited back to act as centriole caps after axoneme disassembly. The IFT-A complex also contributes to cilium disassembly (Pedersen and Rosenbaum 2008, Sánchez and Dynlacht 2016).

1.3.4 Ciliopathies

Structural and functional differences occur between motile and primary cilia, although dysfunction in all cilia types has been reported in ciliopathies. Ciliopathies are a range of diseases that arise due to defects in of ciliary structure and functions. They manifest in different ways and affect multiple organs of the body (Goetz and Anderson 2010, Diiorio et al. 2014). Developmental and degenerative disorders such as NPHP, Polycystic Kidney Disease (PKD), BBS, MKS, polydactyly and Joubert Syndrome are common examples of cilia-related human diseases (Hildebrandt et al. 2011). Primary cilia are present on almost, if not all, human cells, and because of their relevance in transducing signals from extracellular stimuli to control proliferation, differentiation, transcription, mobility and tissue morphology, it is therefore not surprising that ciliopathies affect multiple organs in most vertebrates and are pleiotropic in nature.

A number of proteins that localise to the primary cilium participate in the pathogenesis of ciliopathies. For example, mutations in *PKD1* and *PKD2* which encode polycystin-1 and polycystin-2, cause Autosomal Dominant Polycystic Kidney Disease (ADPKD), an inheritable disorder that results in renal cyst development (Yoder et al. 2002). Both proteins localise to the primary cilia and act as mechanosensors or ion channels, especially, in renal tubular cell differentiation and maintenance (Yoder et al. 2002). Polycystin-2 expression is controlled during embryonic development, where it contributes to the determinination of axial left-right laterality through its activities at the nodal cilia (Pazour et al. 2000; Yoder et al. 2002; Hildebrandt et al. 2011). *PKD1* and *PKD2* are required to maintain the correct number of centrosome and their loss causes superciliated cells. Abnormal centrosome number in these cell line results in chromosome segregation defects during mitosis, chromosome instability and polyploidy (Pazour and Witman 2003, Bettencourt-Dias et al. 2011, Mahjoub and Stearns 2012, Sánchez and Dynlacht 2016). Further study of PKD pathogenesis has also revealed that mutations in *Tg737*/*IFT88* result in shortened cilia and renal cysts that phenocopy human ADPKD in mice (Pazour et al. 2000).

NPHP is an autosomal recessive kidney disease caused by mutations in *NPHP* causative genes (*NPHP1-11* and *NPHP-like 1* (*NPHPL1*). With the exception of *NPHPL1*, all of the *NPHP*-causative gene products localise to the centrosome and primary cilium. Mutations in *NPHP* genes show different clinical symptoms. For example, mutations in *NPHP2,* which encodes inversin, result in enlarged kidney and also cause *situs inversus*, which is characterised by random localisation of internal organs (Hildebrandt et al. 2011; Hurd et al. 2011). This disorder is due to the role of inversin in planar cell polarity and wnt signalling during embryogenesis. Mutations in *NPHP4* and *-5* genes cause retinal-renal ciliopathies; their gene products also colocalise at both the photoreceptor and renal epithelial cilia (Hurd et

al. 2011). These gene products interact with the retinal ciliopathy gene product, retinitis pigmentosa GTPase regulator (*RPGR*). The majority of the *NPHP* gene products also localise to the primary cilium and directly interact with one another and with components of the Hh and Wnt signalling pathway. Defects in any one of these genes results in NPHP, and thus it has been proposed that the *NPHP* gene products form supramolecular complexes that are crucial for cilia assembly and function (Hurd et al. 2011). Furthermore, NPHP10/SDCCAG8 interacts with OFD1 protein and its truncation contributes to the pathology of renal-retinal ciliopathies (Otto et al. 2010). SDCCAG8 depletion results in kidney cysts, hydrocephalus, body axis defects and multiple developmental defects in zebrafish (Otto et al. 2010).

Bardet-Biedl syndrome (BBS) is an autosomal recessive ciliopathy that affects multiple system characterised by retinal dystrophy, renal anomalies, obesity, cognitive impairment, diabetes mellitus, infertility and polydactyly (Hildebrandt et al. 2011). Mutations in 16 genes (*BBS1-12, 15, 16, MKS1, NPHP6/CEP290, NPHP10/SDCCAG8* and *SEPT7*) have been implicated in the development of BBS (Hildebrandt et al. 2011). Seven of these genes interact *in vivo* to form a stable complex known as BBSome, a complex composed of the BBS1, BBS2, BBS4, BBS5, BBS7, BBS8 and BBS9 and a BBS-interacting protein 10 (BBIP10) (Jin and Nachury 2009, Wei et al. 2012). The BBSome localises to primary cilia and centriolar satellites and it is essential for primary cilium biogenesis where it facilitates trafficking to and in the organelle. For example, the BBSome complex is required for the localisation of some of the receptor proteins (MRCH1, SSTR3 and dopamine receptor 1) to the primary cilium (Berbari et al. 2008). Interestingly, all members of the BBSome are essential for BBSome ciliary localisation and functionality as well as the ciliary localisation of Smo in human (Seo et al. 2011). In zebrafish, depletion of bbs2, bbs4 bbs5, bbs6, bbs7 or bbs8 causes loss of cilia in the Kupffer's vesicle (KV), which consequently gives rise to defective left-right patterning and abnormal retrograde melanosome transport (Yen et al. 2006, Wei et al. 2012).

While the majority of reported ciliopathies result from defective cilium assembly or functionality, it is unknown if aberrant cilium disassembly participates in the pathogenesis of these diseases. A recent study showed that premature chromatid separation syndrome (PCS; also known as mosaic variegated aneuploidy syndrome, MVA), a rare autosomal recessive disorder that causes an increase risk of cancer and ciliopathy-linked PKD and infantile NPHP, is a consequence of an increased rate of cilium disassembly. In this patient's skin fibroblast cells, constitutive activation of PLK1-Kif2a results in defective ciliogenesis that underlies the disease mechanism (Miyamoto et al. 2015, Sánchez and Dynlacht 2016). CPAP has been described as a microcephaly and ciliopathy gene that positively drives ciliogenesis. However, a recent identification of its role in cilium disassembly highlights its role in the pathogenesis of microcephaly and Seckel syndrome. In these patient-induced pluripotent stem (iPS) cells,

CPAP localisation was lost or reduced to cause abnormally long cilia, slower cilium disassembly kinetics and delayed cell cycle re-entry which promotes premature differentiation of NPCs that are necessary for maintaining neural stem cell pool. This contributes to the underdeveloped brain in microcephaly and Seckel syndrome (Gabriel et al. 2016).

1.4 Centrobin

Centrobin (Centrosomal BRCA2 interacting protein) was initially identified through a proteomic analysis of purified human centrosomes (Andersen et al. 2003). It was later identified through its interaction with the conserved C-terminal region of the BRCA2 tumour suppressor (Zou et al. 2005), although the centrobin-BRCA2 interaction could not be verified by independent experimental methods (Jeffery et al. 2010). If indeed they interact *in vivo*, the relevance of such interaction remains unknown. Centrobin has been shown to be ubiquitously expressed at varying levels in almost all cells (Zou et al. 2005, Fagerberg et al. 2014). Through immunofluorescence and immunogold electron microscopy, centrobin was shown to preferentially localise to the daughter centriole of proliferating human cells. However, in mouse hippocampal cells, centrobin localised to both the mother and daughter centrioles (Shin et al. 2015). Centrobin interacts with tubulin and its centrosomal and cytosolic pools are essential for microtubule nucleation at the centrosome and in the cytosol (Gudi et al. 2011, Shin et al. 2015).

During centrosome duplication, centrobin is recruited to the procentriole during the early stage of the process and is essential for the localisation of other centriole duplication proteins such as CPAP and CP110 (Gudi et al. 2011). Cep152 interacts with and recruits centrobin to site of centriole biogenesis, and siRNA-mediated depletion of centrobin shows that it is essential for centriole biogenesis, but not for centrosomal microtubule nucleation activities (Zou et al. 2005). A combination of siRNA-mediated centrobin depletion and HU-induced cell cycle arrest prevents centrosome amplification that results from uncoupling centrosome and cell cycle. Furthermore, centrobin depletion in HeLa cells prevented centriole overduplication caused by the overexpression of PLK4. Based on these experiments, centrobin was described as an essential centriole duplication factor. Centrobin is required for the localisation of CPAP, and both proteins interact with and stabilise microtubules during procentriole assembly and elongation (Gudi et al. 2011, Zheng et al. 2016). Unlike human cells, *Drosophila* centrobin is dispensable for centriole duplication, since its RNAi-mediated depletion or *Cnb* hemizygosity did not affect the centriole duplication process in *Drosophila* neuroblasts and *Drosophila* S2 cells (Januschke et al. 2013).

A potential role for centrobin in PCM organisation has been previously reported (Jeffery et al. 2013). Centrobin-depleted cells have been shown to have increased levels of PCM proteins, including γ-tubulin, AKAP450 and pericentrin, and the centriolar satellite protein, PCM-1, at the centrosome. Interestingly, this increase in PCM protein recruitment correlates with an observed increase in the level of microtubule nucleation, thereby implicating centrobin as a modulator of PCM components and microtubule nucleation activity of the centrosome. Previous findings have shown that centrioles are essential for maintaining the organisation and distribution of the PCM (Bobinnec et al. 1998, Basto et al. 2006). Nek2 and PLK1 phosphorylate centrobin at its N-terminus to mediate opposing effects on microtubule-stabilising activities of centrobin (Lee et al. 2010, Park and Rhee 2013). While PLK1 phosphorylation of centrobin promotes its microtubule stabilising activity, Nek2 activities on centrobin antagonise its microtubule stabilising activity. Centrobin modulation by these kinases is proposed to allow for microtubule organisation dynamics during interphase and mitosis and directly impact cell morphology and mobility.

Based on the siRNA experiments, it is unclear if centrobin is essential for viability. HeLa or U2OS cells depleted of centrobin were capable of comparable proliferation to control cells (Gudi et al. 2011, Park and Rhee 2013). Another study has shown the dependency on p53 status for centrobin depletion to induce G1/S cell cycle arrest. Depletion of centrobin in p53-proficient lung cancer cells (A459) resulted in a G1/S cell cycle arrest, while the growth rate of p53-deficient lung cancer cells (H1299) was unaffected (Song et al. 2010). RNAi-mediated depletion of centrobin resulted in p38-dependent activation of p53 (Ser 15 and Ser 33). Thus, cell proliferation arrest in centrobin-depleted cells was inhibited by downregulation of p38 expression and activities. In *Drosophila*, centrobin is crucial for successful asymmetric cell division and some allelic combinations of centrobin mutations have been reported to result in cell death (Januschke et al. 2013).

Mass spectroscopy analysis of the *Trypanosoma brucei* flagellum-transition zone revealed the localisation of the trypanosome centrobin orthologue (TZP104.4) to the transition zone compartment, although siRNA-mediated depletion of the orthologue did not give an obvious phenotype in the organism (Dean et al. 2016). Work in *Drosophila* has indicated centrobin as a negative regulator of ciliogenesis in specialised sensory neurons (Gottardo et al. 2015), but any ciliary functions in vertebrates remain to be described. However, in rat spermatozoa, centrobin has been shown to localise to the marginal ring of the spermatid acroplaxome, manchette and the centrosome during spermatogenesis (Liska et al. 2009). Mutation caused by retroviral DNA insertion into the rat *Cntrob* gene located on the *hypodactylous* locus contributes to impaired limb development and male infertility (Liska et al. 2009, 2013). This mutation of the rat *Cntrob* gene results in the expression of a C-terminally truncated form of

centrobin which did not affect its localisation to the centrosome and spermatid acroplaxome, but abrogated its interaction with keratin 5. Interestingly, transgenic rats expressing exogenous centrobin rescued the abnormal rescued limb malformation, but not the malformation in the sperm head and tail of *hypodactylous* rats (Liska et al. 2009, 2013).

As a potential interacting protein of the tumour suppressor gene product, BRCA2, centrobin was studied for a role in breast cancer susceptibility in the Chinese Han population (Wang et al. 2012). This analysis showed that some genetic nucleotide polymorphisms of the human *CNTROB* can be associated with breast cancer susceptibility. Furthermore, a recent proteomic analysis (Gupta et al. 2015) of centrosome-cilium protein interactions identified centrobin as an interacting partner of FANCD2, an essential DNA inter-strand crosslink that has been shown to be mutated in some human ciliopathies (Johnson and Collis, 2016; Lachaud et al. 2016). To date, the mechanism through which centrobin participates in breast cancer prognosis is unknown. It is equally unclear if centrobin directly participates in cellular DNA damage responses.

1.5 Aims of this project

The distinct localisation of centrobin in interphase cells and its having direct interaction with a number of key players in ciliogenesis and DNA repair pathways suggest its having potential roles in multiple processes. Knockdown of centrobin results in loss of centriole duplication in human carcinoma cell lines and also prevents centrosome amplification induced by genotoxic stress or PLK4 overexpression. The main aim of this project was to identify novel roles for centrobin at the centrosome, in primary cilia and in the DNA damage response. To determine these roles, we disrupted the human *CNTROB* in hTERT-RPE1 cells and used morpholino–mediated depletion in zebrafish to carry out reverse genetic analysis of centrobin. In human cells, we investigate the role of centrobin in maintaining centrosome integrity, proliferation and primary ciliogenesis. For better understanding of the relevance of centrobin in cilia formation, we depleted centrobin in zebrafish and monitored its effects on embryogenesis.

Another major objective of this project was to elucidate the roles of centrobin in the DNA damage response. We tested survival of centrobin-depleted human cells after treatment with genotoxic stress, namely UV, IR and MMS. We also monitored changes in the recruitment of some DNA repair machineries to DNA lesions, which indicated the involvement of centrobin in a particular DNA repair pathway.

In summary, this project identifies centrobin as a centrosomal protein that may provide a molecular link between the centrosome, DNA damage responses, and primary cilia formation.

This is of great importance as it may further clarify our understanding of poorly-understood human ciliopathies, cancer and other diseases.

1.6 Model systems

Human retinal pigmented epithelial (RPE1) cells immortalised by integration of human telomerase reverse transcriptase (hTERT) are karyotypically normal (Bodnar et al. 1998). These cells are commonly used to investigate centrosome structure and function, and primary cilium assembly pathways (Schmidt et al. 2009; Prosser and Morrison, 2015; Daly et al. 2016; Loukil et al. 2017). Generally, hTERT-RPE1 cells have lower gene targetting efficiency compared to cancer cell lines such as U2OS, HCT116 and HeLa cells (Mao et al. 2009, Katoh et al. 2017). However, the cell line proliferates efficiently and can assemble primary cilia when subjected to serum starvation. CRISPR/Cas9 or siRNA transfection technology was used to deplete the *CNTROB* gene product in our reverse genetic functional analysis.

The *Danio rerio* (zebrafish) model system has been extensively employed for investigating the functions of centrosomal and ciliary proteomes. Zebrafish are transparent, develop externally and are easy to manipulate embryonically and study morphological changes at all stages of the life cycle, thereby making the zebrafish an excellent model for understanding vertebrate development biology. We used zebrafish to determine developmental and physiological functions of centrobin that may result from its role in Kupffer's vesicle and nodal cilia formation. At the initial stage, we used 5' rapid amplification of cDNA ends (5' RACE) to identify the zebrafish centrobin (*cntrob*) gene locus and we designed antisense morpholino-oligonucleotides (MO) to disrupt translation of centrobin in wild-type zebrafish embryos. To eliminate the possibility of the known off-target effects of the MOs, we used two independent MOs and also rescued the phenotypes with MO-resistant centrobin cDNA.

2 Materials and Methods

2.1 Materials

2.1.1 Chemicals and solutions

In the course of this study, unless otherwise stated, we obtained all of the analytical grade chemicals, including organic solvents, acids and alcohols, from Sigma Aldrich (Arklow, Ireland), Fisher Scientific (Loughborough, UK), VWR (Dublin, Ireland), Invivogen (Toulouse, France), Lennox Supplies Ltd (Dublin, Ireland), Melford Laboratories Ltd. (Suffolk, UK) and Merck (Darmstadt, Germany). Western blotting detection system was obtained from GE Healthcare Life Sciences (Buckinghamshire, UK), and electron microscopy grade gluteraldehyde and paraformaldehyde were supplied by Electron Microscopy Sciences (Hatfield, UK). Acrylamide (37:5:1) protein gel solutions were purchased from Severn Biotech Ltd. (Worcestershire, UK). All buffers and hydrophilic reagents were prepared by dissolution in double distilled water (ddH_2O) or Milli-Q purified water collected from the ELGA Purelab flex 3 (ELGA LabWater, Veolia Water Systems, Kildare, Ireland) and were autoclaved or filtered, where appropriate. All chemical reagents and buffers used in this study are listed in Table 2.1.

Table 2.1: Common buffers and reagents

Solution/Reagent	Composition	Use
Blocking solution for immunofluorescence (IF) microscopy	1% BSA in 1x Phosphate buffered saline (1x PBS)	For blocking cells and diluting antibody during immunofluorescence staining
Blocking solution for western blot (WB)	5% dried semi-skimmed milk in 1x PBS, 0.1% Tween-20	For minimising non-specific binding of antibodies to nitrocellulose membrane during immunoblot
Cacodylate buffer	0.1 M Sodium cacodylate-HCl, pH 7.2	For washing cell pellets for transmission electron microscopy (TEM)
Cell lysis buffer	50 mM Tris HCl, pH 7.4; 150 mM NaCl; 5% Glycerol; 1 mM EDTA; 0.5% sodium deoxycholate and 1% IGEPAL	For cell lysis before immunoblot analysis
Crystal violet staining buffer	0.5% crystal violet; 6% glutaraldehyde in 1x PBS	For staining and visualising colonies formed from clonogenic survival assay
Coomassie brilliant blue	0.5% Coomassie in 35% methanol and 14% acetic acid	For visualising proteins on SDS-PAGE gel
Coomassie destaining solution	20% methanol; 10% acetic acid	For destaining Coomassie stained gels

Diethylpyrocarbonate (DEPC)-treated water	0.1% DEPC in Milli-Q H_2O	For dissolving RNA
DNA loading buffer (6x)	20% sucrose; 0.1M EDTA, pH 8.0; 0.25% Bromophenol blue; 0.25% xylene cyanol FF or 60% glycerol; 10 mM Tris-HCl, pH 7.5; 0.3% orange G	For loading DNA samples and to facilitate visual tracking of DNA migration during agarose gel electrophoresis
IF fixation buffer	4% Paraformaldehyde (PFA) in 1x PBS or methanol containing 5mM EGTA, pH 8.0 at -20°C	For fixing cells prior to IF microscopy staining
Immunoprecipitation (IP) buffer	50 mM Tris HCl, pH 7.4; 150 mM NaCl; 20% Glycerol; 1 mM EDTA, pH 8.0; 0.5% sodium deoxycholate and 1% IGEPAL	For immunoprecipitation of endogenous and tagged proteins
Luria-Bertani (LB) medium	1% Tryptone; 0.5% Yeast extract; 1% NaCl pH 7.0	For growth of bacteria (*Escherichia coli*) cultures
Mounting medium	0.3% N-Propyl gallate; 80% glycerol in 1x PBS	For mounting slides after IF staining
Permeabilisation buffer	0.15% Triton X-100 in 1x PBS	To permeabilise cells after fixation with PFA
1x PBS	137 mM NaCl; 2.7 mM KCl; 1.4 mM NaH_2PO_4, pH 7.4	For washing cells, preparing blocking solution during IF, IB and FACS
1x PBST	1x PBS; 0.25% Tween-20	For washing cells, preparing blocking solution during IB, IF and FACS
1x PBT	1x PBS; 0.25% Tween-20 and 1% BSA	For washing cells, preparing blocking and antibody solution during FACS
Ponceau S	0.5% w/v Ponceau S; 5% acetic acid	For staining nitrocellulose membrane during immunoblotting
Primary fixative (TEM)	2% glutaraldehyde and 2% paraformaldehyde in cacodylate buffer	Primary fixation of samples for electron microscopy
Primary antibody dilution buffer	1% milk in 1x PBST or 1% BSA in 1x TBST	For dilution and incubation of primary antibodies for western blot
RIPA buffer	50 mM Tris-HCl, pH 7.4; 150 mM NaCl; 0.25% sodium deoxycholate; 1% IGEPAL; 1 mM EDTA	For cellular protein extraction
Running buffer	1x TG; 1% SDS	For running polyacrylamide gel
5x protein sample buffer	150 mM Tris base, pH 6.8; 30% glycerol; 10% SDS; 0.1% Bromophenol blue; 25% β-mercaptoethanol	For loading protein samples on polyacrylamide gels
Secondary fixative (TEM)	1% Osmium tetroxide in cacodylate	Secondary fixation of samples for

	buffer	electron microscopy
Semi-dry TG transfer buffer	1x TG; 20% Methanol	For semi-dry transfer of proteins to nitrocellulose membrane during immunoblot
1x TAE	40 mM Tris; 20 mM Acetic acid; 1 mM EDTA	For running agarose DNA gels
1x Tail buffer	50 mM Tris-HCl, pH 8.8; 100 mM EDTA, pH 8.0; 100 mM NaCl; 1% SDS	For extraction of genomic DNA from mammalian cells
1x Tris-buffer saline (1x TBS)	40 mM Tris-base; 20 mM acetic acid; 1 mM EDTA	For dilution and incubation of phospho-primary antibodies for western blot
1x TBST	1x TBS; 0.1% Tween-20	For dilution and incubation of primary antibodies for western blot
1x TG transfer buffer	25 mM Tris base; 192 mM Glycine	Used in the preparing semi-dry and wet protein transfer buffer during western blot
Wet TG transfer buffer	1x TG; 20% Methanol; 0.01% SDS	For wet transfer of proteins to nitrocellulose membrane during immunoblot

2.1.2 Molecular Biology Reagents

Biological reagents used for DNA restriction digestion and subcloning, such as restriction enzymes, DNA ligase, DNA polymerase (Klenow Fragment I), T4 Polynucleotide Kinase and calf alkaline phosphatase were obtained from New England Biolabs (NEB, Hitchin, UK). Shrimp Alkaline Phosphatase was obtained from United States Biochemical (USB, Santa Clara, CA, USA). DNA size markers used were Quick-load 100 bp DNA ladder (NEB) or 1Kb Plus DNA ladder (Thermofisher Scientific, Loughborough, UK). RNA was extracted using TRIzol reagent (Total RNA Isolation) which was obtained from (Ambion, now Thermofisher Scientific). KOD polymerase was obtained from Novagen (Merck Millipore, Darmstadt, Germany). A list of cloning and expression vectors used is presented in table 2.2.

The PageRuler Plus prestained protein ladder (Fermentas, now Thermofisher Scientific) or the Colour protein standard, broad range marker (NEB) were used in this study as protein size markers.

Table 2.2: List of plasmids used in this study

Plasmid name	**Use**	**Source/References**
pGEM-T-Easy	For general subcloning, for assembly of gene fragments and for zebrafish mRNA *in vitro*	Promega (Madison, WI, USA)

	transcription	
pEGFP-C1/N1	For expression of various genes in mammalian cells	Clontech (Mountain View, CA, USA)
pX330	Cas9 nuclease and guide RNA for expression of CRISPR system	Cong et al. 2013 (Obtained from Addgene, Cambridge, MA, USA)
pGEX4T3	Expression of GST-fusion protein fragment in bacteria	GE Healthcare Life Sciences

A list of commercially available molecular biology kits used in this study is presented in Table 2.3.

Table 2.3: Commercially available kits used in this study

Kit Name	**Use**	**Supplier's name**
GenElute Plasmid Miniprep Kit	Small scale plasmid DNA extraction	Sigma-Aldrich
Nucleobond Xtra Midi (Endotoxin-free)	Large scale plasmid DNA extraction	Macherey-Nagel (Düren, Germany)
High Capacity RNA-to cDNA kit	cDNA synthesis	Applied Biosystems (Foster city, CA, USA)
QIAquick gel extraction kit	Extraction and purification of DNA fragments from agarose gel	Qiagen (Crawley, UK)
QIAquick PCR purification kit	Purification of DNA fragments after PCR	Qiagen
5'/3' RACE kit, 2nd generation	For the isolation and amplification of 5' cDNA ends	Roche (distributed by Sigma-Aldrich)

2.1.3 Antibodies

Primary and secondary antibodies were used for detecting protein of interest during WB, IF and fluorescence-activated cell sorting (FACS) analysis. Freeze-dried conjugated affinity-purified antibodies were resuspended as recommended by suppliers in 1x PBS or Milli-Q H_2O. Detailed lists of primary and secondary antibodies used throughout this study are shown in Table 2.4 and 2.5.

Table 2.4: List of primary antibodies used for this study

Antigen	Clone/ Catalog number	Host species	Dilution (WB)	Dilution (IF)	Manufacturer
Alpha-tubulin	B512	Mouse monoclonal	1:10000	1:2000	Sigma-Aldrich
Acetylated tubulin	6-11B-1 /T6793	Mouse monoclonal	1:10000	1:2000	Sigma-Aldrich
Arl13B	17711-1-AP	Rabbit polyclonal	1:2000	1:2000	ProteinTech (Manchester, UK)
ATM	Ab78	Mouse	1:1000		Abcam (Cambridge, UK)
5-bromo-2-deoxyuridine (BRDU)	B44/347580	Mouse		1:50 for FACS	BD Biosciences, NJ, USA
Centrin	20H5	Mouse monoclonal	1:1000	1:1000	EMD Millipore (Darmstadt, Germany)
Centrin 2	Poly6288	Rabbit polyclonal		1:500	Biolegend (San Diego, CA, USA)
Centrin 3	M01 3E6	Mouse monoclonal	1:1000		Abnova (Taipei, Taiwan)
Centrobin	Ab70448	Mouse polyclonal	1:1000	1:250	Abcam
Centrobin	6D4 F4	Mouse monoclonal	1:10000	1:250	Dr. David Gaboriau, CCB
Cep97	22050-1-AP	Rabbit monoclonal	1:2000	1:2000	Proteintech
Cep97	N-17	Goat monoclonal	1:1000		Proteintech
Cep135	ab75005	Rabbit polyclonal		1:750	Abcam
Cep135	1457 748	Rabbit polyclonal		1:1000	Dr. Alex Bird (Bird and Hyman 2008)
Cep164	IF3 G10	Mouse monoclonal		1:100000	Dr. David Gaboriau (Daly et al. 2016)
Cep290	IC3 G10	Mouse monoclonal		1:1000	Dr. David Gaboriau
CP110	12780-1-AP	Rabbit polyclonal	1:2000	1:2000	ProteinTech
CHK1	DCS-310	Mouse monoclonal		1:1000	Sigma-Aldrich
C-Nap1	6F2 C8	Mouse	1:2	1:2	David Gaboriau, CCB

		monoclonal			(Flanagan et al. 2017)
CPAP	11517-1-AP	Rabbit polyclonal	1:1000	1:1000	ProteinTech
Detyrosinated tubulin	Ab48389	Rabbit polyclonal	1:1000	1:500	Abcam
Gamma-H2AX	JBW 301	Rabbit polyclonal		1:1000	Cell Signaling (Danvars, MA, USA)
Gamma-tubulin	T3559	Rabbit polyclonal		1:1000	Sigma-Aldrich
Gamma-tubulin	SC-7396	Goat polyclonal		1:1000	Santa-Cruz (Dallas, TX, USA)
GAPDH	2118	Rabbit polyclonal	1:10000		Cell Signaling
GFP	Clone 7.1+13.1	Mouse monoclonal		1;1000	Roche (Basel, Switzerland)
GFP	1E10H7	Mouse monoclonal		1:15000	ProteinTech
Glutamylated tubulin	GT335	Mouse monoclonal	1:1000	1:1000	AdipoGen Life Sciences (Liestal, Switzerland)
hSas6	H00163786-B01P	Mouse polyclonal		1:500	Novus Biologicals
Kizuna	-	Rabbit polyclonal		1:1000	Dr. Naoki Oshimori (Oshimori et al. 2006)
Myc	9E10	Mouse monoclonal		1:500	Prof. Ciaran Morrison, CCB
Ninein	Ab4447	Rabbit polyclonal		1:250	Abcam
PCM-1	817	Rabbit polyclonal	1:10000	1:10000	Dr. Andreas Merdes (Dammermann and Merdes 2002)
Pericentrin	Ab4448	Rabbit polyclonal	1:2000	1:1000	Abcam
p-ATM s1981	Ab81292	Rabbit polyclonal	1:2000	1:2000	Cell Signaling
p-CHK1 S345	2348 133D3	Rabbit monoclonal	1:1000	1:1000	Cell Signaling
Rad51	PC130	Rabbit polyclonal	1:2000	1:2000	Calbiochem
Rootletin	NBP1-80820	Rabbit polyclonal	1:750		Novus Biologicals
Rootletin	C20	Goat polyclonal		1:250	Santa Cruz

	Sc 67824				
Smoothened (smo)	Ab38686	Rabbit polyclonal		1:500	Abcam

Table 2.5: List of secondary antibodies used in this study

Antigen	Label	Host species	Dilution (IB)	Dilution (IF)	Manufacturer
Mouse IgG	FITC (fluorescein isothiocyanate)	Goat	-	1:1000	Jackson ImmunoResearch (Suffolk, UK)
Mouse IgG	FITC	Donkey		1:50 for FACS	Jackson ImmunoResearch
Mouse IgG	Cy5	Donkey		1:250	Jackson ImmunoResearch
Mouse IgG	Alexa 488	Donkey		1:1000	Molecular Probes
Mouse IgG	Alexa 488-594	Donkey		1:1000	Jackson ImmunoResearch
Mouse IgG	HRP (Horseradish peroxidase)	Donkey	1:10000		Invitrogen (ThermoFisher Scientific)
Goat IgG	Cy5	Donkey		1:250	Bethyl Laboratory Inc. (Texas, USA)
Goat IgG	Rhodamine Red	Donkey		1:1000	Jackson ImmunoResearch
Goat IgG	HRP	Donkey	1:10000		Abcam (Ab7125)
Rabbit IgG	HRP	Goat	1:10000		Jackson ImmunoResearch
Rabbit IgG	FITC	Donkey		1:1000	Invitrogen

2.2 Biological materials and Tissue culture reagents

2.2.1 Bacterial strains

DNA transformation was carried out in *Escherichia coli* (*E. coli*) Top 10 strain (F^- *mcr*A Δ(*mrr-hsd*RMS-*mcr*BC) φ80*lac*ZΔM1*5* Δ*lac*X74 *nup*G *rec*A1 *ara*D139 Δ(*ara-leu*)7697 *gal*E15 *gal*K16 *rps*L(Str^R) *end*A1 λ^-) from Invitrogen. Ampicillin or kanamycin antibiotics (Sigma-Aldrich) were used for Top10 clone selection at final concentrations of 50 μg/ml or 30 μg/ml, respectively.

2.2.2 Tissue culture reagents

Most sterile plasticware used for cell culture was supplied by Corning (Riverfront Plaza, NY, USA), Greiner Bio-One (Kremsmünster, Austria) and Sarstedt (Numbrecht, Germany). Culture media used in this study were Dulbecco's modified Eagle's medium (DMEM); DMEM Nutrient Mixture F-12 Ham (Lonza, Basel Switzerland) and Roswell Park Memorial Institute (RPMI) 1640 media (Gibco, MA, USA). Fetal bovine serum (FBS), Trypsin, chicken serum (CS), penicillin-Streptomycin (Pen-Strep) and dimethyl sulfoxide (DMSO) were obtained from Sigma-Aldrich. Opti-MEM serum-free medium was purchased from Invitrogen, Life Technologies while lipofectamine 2000 and oligofectamine were products from Invivogen.

2.2.3 Cell lines and culture conditions

This study was specifically carried out using non-transformed hTERT-RPE1, which has approximately 24 h doubling time and shows a relatively stable diploid karyotype. HCT116 was used for interaction studies while U2OS, Jurkat and DT40 were used for testing antibody reactivity. A list of cell lines used during this study is shown in Table 2.6, along with the culture conditions. The antibiotics used for selection of stable hTERT-RPE1 cell lines in this study are listed in Table 2.7.

Table 2.6: Cell lines and culture conditions used in this study

Cell line	Brief description	Source	Culture medium
hTERT-RPE1	Non-transformed, h-TERT immortalised human retinal epithelial cell line	ATCC (Manassas, VA, USA)	DMEM F12
TP53$^{+/+}$ HCT116 (wild-type)	Human colorectal carcinoma cell line; clone 40-16 p53 $^{+/+}$	Bunz et al. 1998	DMEM
TP53$^{-/-}$HCT116	Human colorectal carcinoma cell line, p53 null cells; clone 379.2	Bunz et al. 1998	DMEM
U2OS	Human osteosarcoma cell line	ATCC	DMEM
Jurkat	Human T-lymphocyte clone E6.1, acute T cell leukemia cells	Sigma-Aldrich	RPMI-1640,
DT40	Chicken B-cell lymphoma cell line	Prof. Ciaran Morrison (NUI Galway)	RPMI-1640, 1% CS
6D4F4	Mouse hybridoma B lymphocytes cells producing monoclonal anti-centrobin antibody	Dr. David Gaboriau	*See* Table 2.9

All cells were cultured in a 95% air, 5% CO_2 incubator and their culture media were supplemented with 10% FBS and 1% pen-strep. Human cells were cultured at 37°C while chicken cells grow optimally at 39.5°C.

Table 2.7: Antibiotics used for the selection of stable human cell lines

Antibiotic	Final concentration	Source
Blasticidin	5 µg/ml	Invivogen
G418	1 mg/ml	Invivogen
Geneticin	1 mg/ml	Invitrogen

The various pharmacological treatments that were used on hTERT-RPE1 cells in different assays are listed in table 2.8.

Table 2.8: Pharmacological drugs used in this study for treatment of hTERT-RPE1

Drug	Stock concentration	Final concentration	Diluent	Use	Source
Hydroxyurea (HU)	1 M	4 mM	Milli-Q H_2O	To induce S-phase arrest	Sigma-Aldrich
ICRF-193	14 mM	0.25 – 1 µm	DMSO	For topoisomerase II inhibition	Sigma-Aldrich
Olaparib	50 mM	2.5 – 10 µM	DMSO	PARP inhibition	Selleckchem
Methyl methanesulphatonate (MMS)	1.3 g/ml	2.5-10 µg/ml	-	As DNA methylating agent	Sigma-Aldrich
ATM kinase inhibitor; KU 55933 (ATMi)	2 mg/ml	2-10 µM	DMSO	For inhibiting ATM kinase activity.	Santa Cruz
DNA-PK inhibitor, KU57788 (DNA-PKi)	1 mM	2.5-10 µM	DMSO	DNA-PK holoenzyme inhibition	Tocris, Abingdon, UK

2.3 Cell Biology methods

2.3.1 Cell maintenance and proliferation analysis

Cells used in this study were cultured under the conditions described in table 2.6. All human cells were maintained at exponential growth phase; cells were subcultured when they attained confluency of between 80-90%. hTERT-RPE1 and U2OS have doubling time of approximately 24 h while HCT116 and Jurkat cells have doubling time of 18 h and 20 h, respectively. To passage adherent cells, cells were trypsinised with 0.05% trypsin and 0.02% EDTA in 1x PBS at 37°C for 5 min. When cells were detached from the plate, trypsin was inactivated by the addition of fresh growth media before cells were subcultured into plates containing fresh growth media where they were maintained at confluency between 20-80%. Jurkat and DT40 were also maintained in exponential growth phase and were subcultured by

diluting 1:5 – 1:10 into 10 ml of fresh media and were maintained at less than $1x10^6$ cells/ml. Mycoplasma testing was performed every 3 months.

For freezing and long term storage, adherent cells were first trypsinised and centrifuged at 250 *g*. Supernatant was decanted and the pellet resuspended in a mixture of 70% FBS, 20% growth media and 10% DMSO and aliquoted into cryotubes. For freezing suspension cells, confluent cells were centrifuged at 250 *g*, the supernatant was removed and pellet was resuspended in small volume of 250-400µl of FBS supplemented with 10% DMSO. All human cells were placed in a Mr. Frosty Freezing Container (Thermo Scientific, Wilmington, DE, USA) at room temperature for overnight storage at -80°C before transfer into liquid nitrogen for long-term storage. To wake up cells, the contents of a frozen vial were warmed in a 37°C water bath and transferred into 5 ml of fresh growth media, cells were spun down and then transferred to a dish containing fresh growth media.

For proliferation analysis, hTERT-RPE1 cells were cultured in triplicate, starting from equal cell densities of $5x10^4$ cells in a 6-well dish. Cells were then counted every 24 h for 96 h. When cells approached confluency ($4x10^5$ cells), the cultures were diluted and the dilution factor was taken into account when calculating and plotting the cell numbers.

2.3.2 Monoclonal antibody preparation

Before I started my work in this laboratory, Dr. David Gaboriau (a Postdoctoral Researcher in the lab at the time) generated monoclonal antibodies to some centrosomal proteins. Among these were centrobin monoclonal antibodies. For centrobin antibody generation, a fragment of the human *CNTROB* cDNA encoding amino acids 113-361 was cloned into pGEX4T3 (GE Healthcare) and expressed in bacteria as a GST fusion protein. The centrobin fragment was purified from a glutathione column by thrombin cleavage and used for hybridoma preparation (Dundee Cell Products). Supernatants from 2 different hybridoma clones were compared for strong antigen identification. The best-performing clone, 6D4, was expanded and subcloned to give 6D4F4, which produces IgG1 kappa that was used for further experiments in this study.

To wake up hybridoma cells, cells were thawed in a 37°C water bath and thawed cells were resuspended slowly in 9 ml growth media (table 2.9) and was centrifuged for 5 min at 100 g at room temperature, the supernatant was decanted. Cells were then resuspended in 5 ml growth media and transferred into adherent T25 cell culture flask for overnight incubation at 37°C. On the next day, cells were expanded into a T75 cell culture flask and from then on, hybridoma cells were cultured in a T175 cell culture flask at 37°C with split every 2-3 days. When splitting cells, the supernatant was transferred to a 50 ml Falcon tube and cells and cell debris pelleted at 200 g for 5 min. The resulting supernatant was filtered through a 0.2 µm filter and stored at -80°C.

To generate purified monoclonal antibody, 6D4F4 hybridoma cells were sent to Proteogenix (Schiltigheim, France) in a Pateka G3 cell culture system at concentrations of 1-3x10^5 cells/ml and purified antibody was generated according to the company's protocol. The purified antibody was used for most centrobin analyses by IF and IB in this study.

Table 2.9: List of components of the Hybridoma growth medium

Components	Amount	Source
DMEM	500 mL	Lonza
L-glutamine	4 mM	Lonza
FBS	10%	Sigma-Aldrich
Pen-strep	1%	Sigma-Aldrich
Hybridoma Cloning Factor	2%	PAA (now GE Healthcare)
Hybridoma Fusion and cloning supplement	0.5x	Roche
Hypoxanthine supplement	1x	Sigma-Aldrich
Non-essential aminoacids	1x	Sigma-Aldrich

2.3.3 Stable cell line generation

To generate stably transfected hTERT-RPE1 cell lines, cells were plated to be 80-90% confluent on the following day in antibiotic-free growth media. For generation of *CNTROB* null cells using CRISPR/Cas9 technology, 4 µg of pX330-Ex1Tor pX330-Ex4 and 2 µg of pLOX-Neo plasmids were complexed with Lipofectamine 2000 (Invitrogen) in Opti-MEM (Gibco) for 20 min. For other stable cell lines, linearised plasmid was complexed with Lipofectamine 2000 and where indicated, with pLox-Bsr or pLox-Neo plasmids (Arakawa et al. 2001). The mixture was added to cells and incubated at 37°C for 4–6 h. After 24 h of recovery, cells were trypsinised and serial dilutions were performed into media containing the necessary antibiotic (see table 2.7) and incubated for at least 3 days, after which cells were incubated in antibiotic free growth media at 37°C until single colonies appeared after 10-14 days. Single colonies were picked and expanded using 3 mm Scienceware clonng discs (Sigma-Aldrich) into 48-well plates (Sarstedt). Cells were further expanded and screened by immunoblotting and immunofluorescence microscopy and DNA sequencing (Source Bioscience, Waterford, Ireland).

2.3.4 Transient transfections

For transient plasmid DNA expression, hTERT-RPE1, U2OS or HCT116 cells were plated to attain confluency of 70-80% on the day of transfection. The next day, cells were transfected with 1:2 DNA to lipofectamine 2000 ratio complexed in Opti-MEM serum-free medium for 20 min. The mixture was added to cells and incubated for 4 h before replacing with fresh

growth media. The cells were then incubated for theindicated time at 37°C before fixation for immunofluorescence (section 2.3.7) or immunoblot (section 2.5.5) to analyse protein expression levels.

2.3.5 siRNA mediated knockdown

hTERT-RPE1 cells were plated to attain 30-40% confluency in growth media without pen-strep. On the following day, 50 nmol of custom *CNTROB* siRNA from Sigma-Aldrich: 5' AAGGAUGGUUCUAAGCAUAUC 3' (Jeong et al. 2007), Silencer Select siRNA oligonucleotides specific to GAPDH or CP110 (Table 2.13) were obtained from Ambion and were complexed with Oligofectamine (Invitrogen) in Opti-MEM for 20 min before addition to cells. After 4 h incubation of cells-oligofectamine-siRNA complex at 37°C, media supplemented with 30% FBS was added to the mixture and cells were incubated for total of 48 h; where indicated, cells were transfected for 36 h and serum starved for 24 h as described in section 2.3.6 before analysis by immunoblotting or immunofluorescence microscopy.

2.3.6 Serum starvation

To induce primary cilia formation in hTERT-RPE1, cells were plated to be 70-80% confluent the next day. The following day, cells were washed twice with 1x PBS and once with serum-free DMEM F-12 before incubation in DMEM-F12 supplemented with 0.1% FBS and 1% pen-strep for up to 48 h. For microscopy analysis of modified tubulin, cells were incubated on ice for 30 min to depolymerise microtubule cytoskeleton before fixation for microscopy (section 2.3.7.1).

2.3.7 Microscopy methods

2.3.7.1 Cell fixation

Coverslips were sterilised by exposure to ultraviolet radiation under the laminar flow. Adherent cells were grown on sterile coverslips to attain 30-50% confluency before immunofluorescence (IF) microscopy, while suspension cells were incubated on poly-D-lysine slides for 15 min at room temperature to allow cells to adhere to the slide. Cell medium was aspirated and cells were by either methanol or paraformaldehyde treatment. For methanol fixation, cells were fixed and permeabilised in 95% methanol containing 5 mM EGTA at -20°C, for 10 min. Cells were then washed three times in 1x PBS before proceeding to staining for IF microscopy (section 2.3.7.2). For paraformaldehyde fixation, cells were fixed using 4% paraformaldehyde for 10 min at room temperature and were permeabilised with permeabilisation buffer (see Table 2.1) for 2 min. Cells were then washed thrice in 1x PBS

before staining for IF microscopy. To study zebrafish cilia by IF microscopy, 8 somite stage (ss) embryos were fixed overnight at 4ºC using 4% paraformaldehyde buffered in 1x PBS .

2.3.7.2 Immunofluorescence (IF) microscopy

The fixation procedure described in section 2.3.7.1 is dependent on the nature of the antibody. Prior to antibody staining, cells were incubated in IF blocking buffer (Table 2.1) for 30 min at room temperature. Cells were incubated with appropriate primary antibodies (see Table 2.4) diluted in IF blocking buffer for 1 h at room temperature, followed by three 5 min washes with 1x PBS. This was followed by incubation with appropriate fluorophore-labelled secondary antibodies (see Table 2.5) diluted in IF blocking buffer in a dark humid chamber at room temperature for 45 min. The slides or coverslips were washed three times for 5 min in 1x PBS and mounted in 80% v/v glycerol containing 3% N-propyl-gallate in 1x PBS. DNA was stained with Hoechst 33258 (Sigma Aldrich) and coverslips were sealed with nail varnish and stored at 4°C in the dark. Cells images were captured using an Olympus IX81 microscope (Hamamatsu C4742-80-12AG camera) with a 100× oil objective, numeric aperture (NA) 1.35 and a Z-step of 0.4 μm, using Volocity software v6.2.1 (Improvision Perkin-Elmer, Coventry, UK). Images are presented as maximum intensity projections of Z-stacks after deconvolution.

In collaboration with Dr. David Gaboriau at the Facility for Imaging by Light Microscopy, Imperial College, London, we performed automated microscopy imaging analysis for DNA damage foci counts. Cells were irradiated using a ^{137}Cs source and prepared for immunofluorescence microscopy as described above. IF slides were then sent to Imperial College, London for analysis. Automated microscopy imaging and analysis was carried out using a Nikon Ti Eclipse microscope (Nikon Instruments, Amsterdam, Netherlands), with a 60× objective, NA 1.4. Eighteen fields of view were acquired per slide, with 7 Z-slices and a Z-step of 0.7 μm. Images were processed as maximum intensity projections and were analysed using the General Analysis module of NIS-Elements (Nikon Instruments). The DNA signal was used to segment the nucleus and cells on the border of the field of view were excluded. Rad51 foci were counted using a spot detector and the number of Rad51 and γ−H2AX foci inside the nucleus per individual cell were exported.

2.3.7.3 Proximity Ligation Assay

hTERT-RPE1 cells were grown on a sterile coverslip and fixed in methanol containing 5 mM EGTA at -20°C for 10 min. Primary antibody staining was carried out as previously described for immunofluorescence. PLA was carried out using Duolink system (Olink) following the manufacturer's protocol. Fluorescence analysis was visualised on an Olympus IX81 microscope (Hamamatsu C4742-80-12AG camera) with a 100× oil objective, NA 1.35, using Volocity software (Perkin-Elmer).

2.3.7.4 Electron microscopy

After necessary cell treatment and incubation, hTERT-RPE1 cells were harvested from a T175 cell culture flask by trypsinisation and pelleting at 250 g for 5 min in a 1.5 ml eppendorf tube. Cells were washed twice in 1x PBS, and then twice in 0.1 M sodium cacodylate buffer, pH 7.2 (Sigma-Aldrich). Cell were then resuspended in primary fixative (see Table 2.1) and incubated overnight at 4°C. On the next day, cells were pelleted, washed twice in cacoodylate buffer and fixed in secondary fixative (see Table 2.1) for minimum of 2 h in the dark at room temperature until cell pellet turned black. Toxic osmium waste was neutalised in 2% ascorbic acid while cell pellets were washed 3 times in cacodylate buffer before dehydration through ethanol gradient (15 min each of 30, 60, and 90%). Cells were further dehydrated by 3 x 30 min incubations in 100% ethanol, after which ethanol traces were removed by 30 min incubation in propylene oxide (Sigma-Aldrich). Cells were then subjected to 4 h incubation in 50:50 propylene oxide to resin (TAAB, England, UK), followed by overnight incubation in a 25:75 propylene oxide to resin mixture. On the next day, cells were embedded in 100% Low Viscosity Resin for 6 h which was refreshed every 3 h and after 24 h before polymerising at 60°C for 48 h. The blocks were cut on a microtome (Reichert-Jung Ultracut E; Leica) into sections and stained with uranyl acetate and lead citrate before placing on copper grids for viewing on a transmission electron microscope (H-7000; Hitachi) which uses a ORCA-HRL; Hamamatsu Photonics camera. Images were processed using AMT version 6 (AMT Imaging).

2.3.8 Clonogenic survival assays

Clonogenic survival assays were performed to determine the sensitivity of hTERT-RPE1 cells to different DNA damaging agents. Cells were plated on a 6 cm tissue culture plate and assayed as previously described by Franken et al. (2006). Briefly, cells in exponential growth phase were trypsinised to detach cells from the culture plate and to ensure single-cell suspension. Cells were counted using a haematocytometer (Precicolor, HBG, Giessen-Lützellinden, Germany) and serially diluted to $1x10^4$ cells/ml, then plated in triplicate at the appropriate cell seeding concentrations in 6cm dishes, as indicated in Table 2.10. After 6 h incubation at 37°C to allow cells to adhere to the culture plate, cells were exposed to varying treatments and returned to the 37°C incubator for 10-14 days, when colonies appeared. The colonies were gently washed with 1x PBS and stained with crystal violet staining buffer for a minimum of 30 min at room temperature. Cell plating efficiency and surviving fractions were calculated as described by Franken et al. (2006), and were plotted as a percentage of viable cells normalised to the untreated control.

IR clonogenic assays employed a ^{137}Cs source (Mainance Engineering). For UV radiation clonogenic survival assay, cell medium was removed and cells were exposed to UV-C using a UVIlite filtered UV lamp source at 254 nm (UVItek, Cambridge, UK). To perform MMS

clonogenic survival assays, growth media containing dilution of 20 µg/ml MMS were used to make drug dilutions of MMS (Table 2.10) in which cells were incubated at 37°C for 16 h, after which spent media were removed, cells were washed twice with 1x PBS and conditioned growth media replaced. Stock dilutions of DNA-PKi, ATMi, ICRF-193 and olaparib were used to prepare the indicated drug concentrations in conditioned growth media in which cells were incubated until colonies formed.

Table 2.10: Cell plating numbers for clonogenic survival assays in 6 cm^2 dishes

IR dosage (Gy)	Cell plating number	UV dosage ($5J/m^2$)	Cell plating number	MMS/ATMi/ DNA-PKi dosage (µm)	Cell plating number	ICRF-193 (µm)	Cell plating number
0	400	0	400	0	300	0	400
2.5	800	5	2000	2.5	1000	0.25	1000
5.0	2000	10	5000	5	5000	0.5	5000
7.5	10000	20	20000	10	10000	1.0	10000

2.3.9 Flow cytometric analysis

Flow cytometry was used to determine cell cycle distribution profile. Exponentially growing cells were harvested by trypsinisation, washed in 1x PBS and pelleted by centrifugation at 250 g. The cell pellet was slowly resuspended in ice-cold 70% ethanol buffered in 1x PBS whilst vortexing to disperse cell clumps. Fixed cells were stored at -20°C for at least 2 h or overnight. Prior to flow cytometry analysis, cells were washed twice with 1x PBS and resuspended in 200 µg/ml RNase A and 40 µg/ml propidium iodide (Sigma-Aldrich) buffered in 1x PBS and incubated for 30 min at room temperature. The genomic DNA was stained with propidium iodide (PI) and the flow cytomeric analysis of cell DNA content was performed and analysed on an Accuri C6 Sampler and analysis software (BD Biosciences, New Jersey, USA).

2.4 Zebrafish embryo analysis

To investigate the roles of centrobin in an entire organism, we collaborated with the Dr. Teresa casa Tena of the Philipp's lab, University of Ulm, Germany for *in vivo* experiments. First, I carried out bioinformatics analysis and identified zebrafish *cntrob* locus using 5' RACE (sections 2.6.12 and 4.5.1) and also generated full-length *cntrob* and morpholino-resistant rescue plasmids for the zebrafish experiments. Dr Teresa casa Tena then designed morpholinos targeting *cntrob* mRNA and also carried out the zebrafish manipulations experiments as described in this section.

2.4.1 Zebrafish husbandry and manipulations

Zebrafish were housed in a fully automated, water circulating rack system (Tecniplast) and exposed to a 14 h light and 10 h dark cycle. Embryos from EK and AB wild-type strains were generated using natural matings and raised until the desired stage in an incubator set to 28.5ºC. Microinjections of MOs or capped RNAs were done with the help of an Eppendorf Femtojet and a Narishige micromanipulator at the 1-2 cell stage. MOs were designed based on submitted sequences and synthesized by Gene Tools (Philomath, USA). Two non-overlapping MOs were used, MO1 and MO2, targetting the ATG and 5'-UTR of *Cntrob* respectively (see Table 2.14). As control, the standard control MO was used. Capped RNAs for reconstitution experiments were *in vitro* transcribed from linearized plasmids using the mMessage mMachine SP6 kit (Ambion) according to the manufacturer's instructions. All husbandry and experiments herein have been approved by local authorities in Ulm, Germany and current European law.

2.4.2 Immunofluorescence analysis

Zebrafish embryos were processed for cilia staining as previously described Burkhalter et al. (2013). Zebrafish cilia were labelled by incubation with anti-acetylated tubulin antibody (Table 2.4) followed by 1x PBS washes. The embryos were then incubated with fluorescent-conjugated secondary antibody (see Table 2.5) to allow for primary antibody detection. After staining, zebrafish embryos were manually deyolked using forceps and the posterior part of the embryo was mounted in Vectashield (Vector Laboratory Ltd, Peterborough, UK) between two coverslips. Cilia were then analysed with a Leica TCS SP5II confocal microscope. Cilia length was measured from confocal stacks using Image J.

2.4.3 Whole mount in situ hybridisation (WMISH)

Zebrafish embryos were fixed at the desired stages as described by Burkhalter et al. (2013). After fixation, embryos were dehydrated in a methanol/PBT gradient and stored in 100% methanol at -20 ºC until further processing. For WMISH, embryos were gradually rehydrated and then processed according to standard protocols. WMISH probes against cardiac myosin light chain (*cmlc2*), insulin (*ins*) and southpaw (*spaw*) have been described before (Burkhalter et al. 2013). For detection of centrobin transcripts, a DIG-labelled in situ probe covering the whole *CNTROB* coding sequence was generated from the pGEM-T Easy plasmid after linearization with ApaI and using SP6 for in vitro transcription. Live embryos and those

processed by WMISH were imaged on a Leica M125 upright microscope equipped with a Leica IC80 HD camera.

2.5 Protein Methods

2.5.1 Protein extraction and preparation

To isolate cellular proteins for analysis, cells were harvested, washed in 1x PBS and pelleted at 250 g for 5 min. Cell pellets were resuspended in appropriate volume (20-50 µl) lysis buffer (50 mM Tris HCl, pH 7.4; 150 mM NaCl; 5% Glycerol; 1 mM EDTA; 0.5% sodium deoxycholate; 1% IGEPAL; protease inhibitor cocktail (Roche) and phosphatase inhibitor (Sigma)) for 20 - 40 min on ice with occasional vortexing. Samples were then centrifuged for 20 min at top speed at 4°C and the supernatant transferred to a fresh 1.5 ml eppendorf tube. Total protein concentration of the supernatant was determined by Bradford assay which is a dependent on binding of Coomassie Brilliant Blue G-250 dye to amino acids in an acidic medium that results in stoichiometric change in dye wavelength. To perform this assay, 1 µl of a protein sample was diluted in 1 ml of 1:1 milliQ H_2O:Bradford solution (Sigma-Aldrich) and incubated at room temperature for 5 min. The absorbance was measured at 595nm using a BioPhotometer (Eppendorf) or ThermoScientific Nanodrop 2000c Spectrophotometer (Nanodrop Products, Wilmington, DE, USA) and the protein concentration was interpolated based on BSA standard curve (y=0.0595x-0.0154 or y=0.0641x+0.0216) for the respective spectrophotometers. For the BSA standard curve, absorbance was plotted against increasing concentrations of the BSA protein.

2.5.2 SDS-PAGE

SDS-PAGE gel provides pore sizes through which protein samples are separated based on their molecular weights and the desired gel percentage (composition in Table 2.11) is dependent on the size of the protein of interest. To set a desired SDS-PAGE gel percentage (usually 6-15%), glass plate and gel combs were cleaned with distilled water followed by 100% ethanol which was wiped off with lint-free paper towels. The gel apparatus was set up and resolving gel was poured and gently overlaid with 100% isopropanol. After at least 20 min of allowing resolving gel to set, the isopropanol was removed, washed and blotted off with whatmann papers. The stacking gel was then poured, a clean gel comb was inserted and allowed to set for at least 20 min at room temperature. After polymerisation, gel was submerged in ddH_2O and the gel comb was gently removed, water was discarded and using synringe, the un-polymerised gel and water were removed and the gel wells were straightened and gently rinse with 1x TG running buffer. The gel apparatus chamber was filled with 1x TG running buffer and protein samples were loaded.

For loading on SDS-PAGE gel, appropriate protein concentration (20-80 µg of whole cell lysate) was transferred into a fresh tube and 5x protein sample buffer (Table 2.1) was added to the samples prior to boiling at 95°C for 5 min. The extract was either stored at -80°C or directly loaded on SDS-PAGE gel alongside a prestained broad range protein marker to estimate protein molecular size. Electrophoresis was performed at a constant current of 30-70 mA for 90-120 min in 1x TG running buffer using Hoefer or Bio-Rad Vertical Electrophoresis systems.

Table 2.11: SDS-PAGE gel composition used for protein detection

Reagent	Resolving gel	Stacking gel
30% Acrylamide mix (37:5:1)	6-15 %	5%
Tris-HCl pH8.8	375 mM	-
Tris-HCl pH6.8	-	125 mM
Sodium dodecylsulfate (SDS)	0.1%	0.1%
Ammonium persulfate	0.1%	0.1%
Tetramethylethylenediamine (TEMED)	0.04%	0.1%

2.5.3 Semi-dry and wet transfer

Following protein separation on SDS-PAGE gel, the gel was rinsed with water and equilibrated in 1x TG transfer buffer (see table 2.1) for 5-10 min. A pre-soaked nitrocellulose (0.45 µm pore size) membrane (GE Healthcare) was placed on 2 whatman papers (Hartenstein, Würzburg, Germany) pre-soaked in 1x TG transfer buffer. The equilibrated gel was gently placed on the membrane, then, another 2 pre-soaked whatman sheets was placed on the gel and air bubbles carefully rolled out. The membrane/gel sandwich was assembled on the appropriate transfer apparatus in a way that the membrane was closest to the anode and the gel to the cathode. Proteins were transferred from the SDS-PAGE gel to the nitrocellulose mambrane using Hoefer TE 77 semi-dry transfer unit (GE Healthcare) at 1 mA/cm^2 for 2 h or a BioRad TransBlot wet transfer unit (Watford, UK) at a constant current of 350mA for 3 h.

2.5.4 Immunoblotting technique

To visualise and assess transfer efficiency, membranes were washed 3 times in ddH_2O and then stained with Ponceau S solution (Table 2.1) for 5 min at room temperature. This was followed by several washes with ddH_2O until distinct protein bands were visible and a photograph of the stained membrane was taken as a reference. Blots were then incubated in WB blocking solution (Table 2.1) for 30-60 min at room temperature. This was followed by membrane incubation with the appropriate primary antibody (Table 2.4) dilution in 1% milk or 1% BSA in 1x PBST or 1x TBST for 1-2 h at room temperature or overnight at 4°C. To

remove unbound primary antibody, membranes were washed for 30 min with three 1x PBST buffer changes and incubated in HRP-conjugated secondary antibody (Table 2.5) in 1% milk or 1% BSA in 1x PBST for 45 min at room temperature. Membranes were then washed with 1x PBST for 45 min with three 1x PBST buffer changes. All of the above washes and incubations were carried out with constant agitation on a rocking platform. To facilitate protein detection, ECL (GE Healthcare) was used with strict adherence to the manufacturer's instructions. Briefly, membranes were covered with a 1:1 mixture of the ECL solutions and incubated for 3 min followed by autoradiograph film exposure and development on a CP 1000, AGFA film processor (Superior Radiographics Ltd, Madison, WI, USA).

2.5.5 Immunoprecipitation

After trypsinisation of HCT116 or hTERT-RPE1 cells, whole cell extracts were prepared by lysing cells in 1 ml of IP lysis buffer (Table 2.1) containing protease inbititor cocktail (Roche), 1 mM sodium orthovanadate, 5 mM sodium fluoride, 1:10000 dilution of benzonase nuclease (Sigma-Aldrich) and 1 mM PMSF for 45 min at 4°C on rotating wheel. Samples were centrifuged for 20 min at 14,000 rpm at 4°C to remove cell debris and supernatants were transferred to fresh 1.5 ml eppendorf tubes. Protein concentrations were determined by Bradford assay (section 2.5.1). Meanwhile, 20 µl of prewashed protein A/G beads (Santa Cruz) were incubated with 3-5 µg of primary antibody for 1-2 h at 4°C with gentle agitation. Beads-antibody complex was washed twice with IP lysis buffer followed by incubation with 3-5 mg total cell extracts for a further 2-4 h. After incubation, beads-antibody-protein complex was spun down at 250 g for 3 min and supernatant discarded while beads-antibody-protein complex were washed 4-6 times in lysis buffer. The complexes were then boiled in 5x protein sample buffer for 10 min and pelleted at 12,000 g before immunoblot analysis of bound proteins.

2.6 Nucleic acid methods

2.6.1 RNA isolation and cDNA synthesis

For total RNA extraction, exponentially growing hTERT-RPE1 cells were harvested from confluent 10 cm^2 dish by trypsinisation and were resuspended in 1 ml of TRIzol. After 5 min incubation at room temperature, 0.2 ml of chloroform was added and mixed by inverting the tube followed by 2 min incubation at room temperature. The sample was then centrifuged at 4°C for 15 min at 12,000 g and the upper aqueous phase was gently removed, while avoiding any material at the interphase, and transferred into a new microfuge tube. An equal volume of isopropanol was added, mixed by inverting the microfuge tube and incubating for 10 min at room temperature. The RNA was pelleted by centrifugation at 4°C, 12,000 g for 10 min and

the supernatant was removed. The pellet was washed with 500 µl 70% v/v ethanol in DEPC-treated water to remove excess salts. The sample was then centrifuged for 5 min at 4°C, 10,000 g, the supernatant was removed and the pellet was air-dried for approximately 10 min at room temperature. The RNA pellet was re-suspended in DEPC-treated H_2O and incubated at 55°C. RNA concentration was determined on ThermoScientific Nanodrop 2000c Spectrophotometer at 260 nm and samples stored at -80°C. Using 2 µg extracted RNA, cDNA was synthesised using High-Capacity RNA-to-cDNA kit (Applied Biosystems). The reactions were set up according to the manufacturer's instructions and the cDNA generated was used as a template in PCR reactions (section 2.6.4) for the amplification of specific cDNAs.

2.6.2 Genomic DNA extraction

Cells were harvested from a confluent 6 well dish into a 1.5 ml microfuge tube and incubated overnight at 37°C in a 500 µl Tail buffer (Table 2.1) containing 0.5 mg/ml Proteinase K (Sigma-Aldrich). On the following day, the cell lysate was subjected vigorous mixing on a thermomixer at 1400 rpm for 5 min after which 240 µl of 5 M NaCl was added to the tubes. Cell lysates were mixed for an additional 5 min before being centrifuged at 4°C, top speed for 10 min to remove precipitated proteins. The supernatants were transferred into new microfuge tubes and DNA was precipitated with 750 µl of isopropanol which was added and mixed by inverting the tubes. This was followed by centrifugation at top speed, after which the supernatant was removed and was followed by a wash in 500 µl of 70% ethanol. The pellet was air dried for approximately 10 min at room temperature and the DNA was resuspended and solubilised in 50 µl of Milli-Q H_2O at 37°C for at least 1 h. Genomic DNA was used for PCR amplification of specific sequences (section 2.6.4).

2.6.3 Plasmid DNA prep

Mini and midi plasmid DNA were prepared using the GenElute^{TM} or Nucleobond Xtra Midi (Endotoxin-free) kits, respectively. In these procedures, plasmids were isolated according to the manufacturer's instructions. For miniprep, a single bacterial colony was used to inoculate 5 ml of LB broth with appropriate antibiotic (see section 2.2.1) and incubated shaking overnight at 37°C. 4 ml of the overnight culture was used for miniprep DNA extraction while 100 ml overnight culture was used for midiprep extractions. The resulting plasmids were resuspended in 50 µl and 160 µl Milli-Q water respectively.

2.6.4 Polymerase Chain Reaction (PCR)

PCR was performed to amplify specific DNA sequence for sub-cloning into linearised vectors that was subsequently used for functional analysis. Usually, KOD Hot Start DNA Polymerase from Novagen, (Darmstadt, Germany) or Taq DNA polymerase from Sigma-Aldrich were the DNA polymerases used depending on the requirement for high fidelity. The annealing

temperature and magnesium concentration were optimised for each reaction and a representative PCR reaction is shown in Table 2.12.

Table 2.12: PCR conditions for Sigma Taq and KOD Hot Start

Reagent	Final concentration
PCR Buffer	1x
Primers	200 µM
dNTPs	200 nM
Mg^{2+}	1.5 mM
DMSO	1-5%
Plasmid/RT reaction/genomic DNA (Template)	10 ng/100 ng/1-2 µl
Enzyme	0.02 U/µl

All PCR reactions were performed on an Eppendorf Mastercycler Nexus Gradient (Hamburg, Germany) and typical program cycling conditions are listed in Table 2.13.

Table 2.13: PCR programme cycling conditions.

PCR step	Program cycling	Number of cycles
Initial denaturation	95°C – 2 min	1 cycle
Denaturation	95°C – 20 s	30 cycles
Annealing	50-65°C – 10 s	
Extension	70°C – 25 s/Kb	
Final Extension	72°C – 5 min	1 cycle

A list of primers and siRNA sequences used in this study are detailed in Table 2.14:

Table 2.14: List of oligonucleotides used in this study.

Lower cases indicate restriction enzyme sequences and bases required for restriction enzyme cleavage close to DNA fragment ends. The capital letters are regions complimentary to the region of interest to be amplified.

Primer name	Use	Sequence (5'→3')
CNTROB full fwd	Cloning full length human *CNTROB*	aaaaagaattctATGGCAACATCAGCTGAC
CNTROB full rev:		aaaaaggtaccTCATCTCCAGACTCCC
hCNTROB 765-EcoR1F	Cloning fragments of human *CNTROB* for functional analysis	tttagaattccGCCATGGCATCCAGTCTTTTCCGGGTCCC
hCNTROB-364 Sal1 R		tttgtcgacctACTGGGCCCAGGTCTGCCGTTCTTCTTCTAG
hCNTROB 183- EcoR 1 F		tttggaattctTTTCAGGGGCTGAGAGATGCATTGG
hCNTROB 452- EcoR 1 F		ttatgaattctGCTGTGCAGCTGGAGCAGCGGGTGAC

hCNTROB -452 Sal1 R		aatgtcgacGCCAGCTCCGACTCCAGCTGGATCCGC
hCNTROB 365- EcoR 1F		aaaagaattcaCAAGAGCACCAGCTTAAGGAACACTACCAGG
CNTROB Exon 1T Fwd	CRISPR gRNA targeting *CNTROB*	caccgGTCTAACCCTTCATGAGGCG
CNTROB Exon 1T Rev		aaacCGCCTCATGAAGGGTTAGACc
CNTROB Exon 4 Fwd		caccgGTTTGCATCTTACCTTGCGG
CNTROB Exon 4 Rev		aaacCCGCAAGGTAAGATGCAAACc
Cntrob ex1 SFwd	*CNTROB* CRISPR clone screening	GATCCTTGGCGTGGAGTCTTC
Cntrob ex1 SRev		AAACCTTACCCGTTCCCAGTG
Cntrob ex4 RevS		CGCCATTCTCCTGCCTCA
Cntrob ex4 FwdS		AGCCCTAACATTCTCTACC
GSP1_ZF5	5' RACE identification of zebrafish *Cntrob*	CAGCGGTGAGATCAGGAGAGGACAGAGCG
GSP2_ZF5		CACTTTCCATCTCCTCTATGTGCTTCCTGC
GSP3_ZF5		CCTCCACATGCACACGCAGATCAGACGCC
GSP4_ZF5		CGTCCGTGTGTCATGCGACTCTGTCTGG
ZF CNTROB full F	Cloning of full length zebrafish *Cntrob*	ATGTCTGTGAGCCGAGCTGCTGCTGATGG
ZF CNTROB full R		TCAGTGTTGTCCAGCTGTGGCTCCAGTG
ZF CNTROB full R3		TCAGTACAGAAACTCCAACCTGCTCAGCCC
ZF7 CNTROB HindIII frag F		AGCAAAAGCTTAGCAGAGAAGCAGATAAACACAGAG
ZF7 CNTROB mut F	Cloning of MO resistant zebrafish *Cntrob*	ATGTCAGTCAGTCGCGCTGCAGCAG
ZF CNTROB MO1	Gene specific MO-mediated depletion of zebrafish *Cntrob*	GTCTGTGAGATGTCTGTGAGCCGAG
ZF CNTROB MO2		ATGAGAGTTTGTTTACCGTCCGAGT
DCnb-Fwd	Cloning of *Drosophila* Cnb	ccctcaagcttCCATGAGTGATACCGATACGGACGAC
DCnb-Rev		gccttggtaccTCAGCACTTCCAAGGTGGAGGCTTACT
siCNTROB sense	Knockdown of centrobin	AAGGAUGGUUCUAAGCAUAUC
siCNTROB-antisense		GAUAUGCUUAGAACCAUCCUU
siCP110-sense	Knockdown of CP110	GCAAAACCAGAAUACGAGATT
siCP110-antisense		UCUCGUAUUCUGGUUUUGCAT
siGAPDH-sense	Knockdown of GAPDH	UGGUUUACAUGUUCCAAUATT
siGAPDH-antisense		UAUUGGAACAUGUAAACCATG

2.6.5 5' RACE reaction

To identify zebrafish *CNTROB* cDNA sequence, mRNA was extracted from zebrafish embryo at 8 hpf. 5' RACE was performed using Roche 5'/3 RACE kit, 2nd generation (Table 2.3) according to the manufacturer's protocol. The primers (Table 2.14) designed were based on EST sequences available (Gen bank numbers: CO356610.1, CT682788.2, CT670105.2, EB909336.1 and CK697594.1).

2.6.6 Restriction digestion of DNA

Restriction digestion patterns were predicted for DNA sequences using the NEBCutter bioinformatics tool or Serial Cloner 2-6 software (Table 2.15). NEB supplied all restriction endonucleases used. DNA digestion reactions were set up according to the manufacturer's protocol supplied and incubated at the recommended optimal temperature for the restriction enzyme for minimum of 2 h depending on the type (PCR amplicon, plasmid or genomic DNA) and amount of DNA being digested. Where necessary, restriction enzymes were heat-inactivated at manufacturer's recommended temperature and the digestions were analysed by agarose gel electrophoresis (section 2.6.10).

2.6.7 Modification of DNA ends

2.6.7.1 Generation of Blunt DNA ends

To facilitate ligation of incompatible cohesive DNA ends, the 5' and 3' overhangs were blunted using the DNA polymerase I Large (Klenow) Fragment. This enzyme has both 5'→3' polymerase activity which fill-in the 3' overhangs and 3'→5' exonuclease activity needed for the removal of 5' overhangs. Briefly, the reaction was carried out in the presence of any NEB restriction enzyme buffer, dNTPs (33 µM each) and 1 U of enzyme was used per µg of DNA. The reaction mixture was incubated at 25°C for 15 min. The enzyme was then deactivated by the addition of 10 mM EDTA and incubation at 75°C for 20 min. The reaction was cleaned-up (section 2.6.11) and used for blunt end ligation.

2.6.7.2 Phosphorylation of DNA ends

After PCR reaction, DNA inserts needed for ligation were subjected to 5' DNA end phosphorylation and removal of 3′ phosphates by T4 Polynucleotide Kinase (T4 PNK) from NEB. The reaction was carried out as per the manufacturer's instructions, briefly, 1x T4 DNA ligase buffer containing 1 mM ATP and 1 U T4 PNK per µg DNA were added to each purified PCR reaction and incubated at 37°C for 30 min. Enzyme inactivation was achieved by incubating the reaction mixture at 65°C for 20 min.

2.6.7.3 Dephosphorylation of DNA ends

To minimise re-circularisation of linear DNA needed for ligation, the linearised DNA vector was treated with calf-intestinal alkaline phosphatase (CIP) from NEB or recombinant shrimp alkaline phosphatase (rSAP) from USB Affymetrix to dephosphorylate the 5' ends of linear DNA. The enzymes were used according to the manufacturer's protocol. Briefly, after heat-inactivation and ice-cooling or spin column clean-up of restriction enzyme reaction, 1 U CIP or SAP per µg DNA was added to the digestion reaction and incubated at 37°C for 30 min. This was either followed by rSAP enzyme denaturation at 65°C for 10 min or a DNA clean-up (section 2.6.12) step for CIP.

2.6.8 Sticky or blunt end ligations

After recommended DNA purification step, the vector and insert fragment concentrations were determined on ThermoScientific Nanodrop 2000c Spectrophotometer and the amount required for ratios between 1:3 and 1:10 were calculated using Insilico Ligation Calculator (Heinrich-Heine-University of Düsseldorf, Germany). The ligations were performed in the smallest volume possible (usually between 10 – 20 µl) using 200-400 U of T4 DNA ligase supplemented with the buffer (containing 1 mM ATP) provided. Ligation reactions were incubated for 1-4 h at room temperature or overnight at 16°C. After ligation, DNA ligase was heat-inactivated by incubation at 65°C for 10 min and plasmids were transformed into *E. coli* (section 2.6.15) immediately or stored at 4°C. Control ligations were performed with either vector or insert only to quantify the number of background colonies.

2.6.9 Assembly of CRISPR plasmids

To build CRISPR targeting vectors used for generating knockout clones, oligonucleotides were annealed at 95°C for 5 min and then cooled slowly on the thermoblock. The oligos were then phosphorylated with T4 Polynucleotide Kinase (section 2.6.6.2). pX330 plasmid was obtained from Addgene (MA, USA), digested with BbsI restriction endonuclease and dephosphorylated with Calf Intestinal Phosphatase (section 2.6.6.3). Annealed and phosphorylated oligo nucleotides were then ligated to the digested pX330 plasmid and successful cloning was verified by commercial DNA sequencing.

2.6.10 Analysis of cloned DNA and sequencing

Usually, 300 ng of DNA from mini or midi prep was analysed by restriction digestion (section 2.6.6) and commercial DNA sequencing (Source Bioscience). Plasmid DNA sequencing was performed to ensure nucleic acid fidelity and in-frame insertion of DNA fragments following cloning. Typically, 100 ng of mini or miniprep and 10 pM sequencing primers were sent to Source Bioscience for Sanger sequencing and the output data were

analysed on Serial Cloner v2-6 (Table 2.15) to construct correct vector maps with the analysed sequences.

2.6.11 Agarose gel electrophoresis

Agarose gel is the standard method used to separate, identify, and in some cases, to purify DNA fragments. Usually, a 0.5-1.2% agarose gel was prepared using electrophoresis grade agarose (Sigma-Aldrich) in 1X TAE buffer (Table 2.1) containing 0.5 µg/ml ethidium bromide. The Hoefer HE33 or HE99x Horizontal Submarine Unit (ThermoFisher Scientific) were used according to the manufacturer's instructions for a maximum of 2 h. After completion of electrophoresis, separated DNA molecules were viewed on the gel using a Multi-Image Light Cabinet (ChemiImager 5500, AlphaImager, ProteinSimple, San Jose, CA, USA) and images were taken with a digital camera. For DNA extraction, bands of interest were excised from the agarose gel with a scalpel blade under UV light and the DNA was purified as described in section 2.6.12.1.

2.6.12 DNA purification methods

2.6.12.1 Gel extraction and Column clean-up

DNA was purified from agarose gel slices (section 2.6.10) using the Qiagen QIAquick Gel Extraction Kit according to the manufacturer's instructions. Typically, a gel slice was placed in a 2ml microfuge tube and bound DNA was eluted off the column in 20-40 µl of warm Milli-Q H_2O. Column clean-up was performed using QIAquick PCR purification kit according to the manufacturer's protocol and bound DNA elution was in 20-40 µl of warm milliQ H_2O.

2.6.12.2 Ethanol precipitation

For purifying linearised plasmid DNA before transfections, one-tenth volume of 3 M sodium acetate, pH 5.2 and 1 volume of 100% isopropanol were added to the DNA solution. The sample was vortexed and the DNA was pelleted at 4°C, top speed for 10 min. The supernatant was removed and the pellet was washed with 500 µl of 70% ethanol. The sample was then centrifuged at 4°C top speed for 5 min, the supernatant was also discarded and the pellet was air-dried at room temperature for 10 min. The pellet was resuspended in appropriate volume of milliQ H_2O and stored at -20°C.

2.6.12.3 Phenol/chloroform precipitation

Phenol/chloroform extraction and ethanol precipitation were carried out to concentrate nucleic acid samples or change the buffers in which DNA samples were dissolved. To perform this procedure, an equal volume of phenol:chloroform:isoamyl alcohol (25:24:1) was added to the DNA solution, mixed by vortexing and centrifuged for 10 min at top speed. The upper aqueous phase was removed while avoiding any material at the interphase, and placed

in a sterile microfuge tube. An equal volume of chloroform:isoamyl alcohol (24:1) was added to the aqueous phase, vortexed as before, and centrifuged for 5 min at 13,000 g. The upper aqueous solution was transferred into a sterile microfuge tube and the DNA solution was used for ethanol precipitation, as described in section 2.6.11.2.

2.6.13 Preparation of chemically competent *E. coli*

Chemically competent Top10 *E. coli* competent cells were prepared by inoculating an overnight mini culture into 500 ml of LB broth in a sterile 2 L flask which was incubated at 37°C with shaking until an OD_{600} between 0.4 and 0.6 was reached, usually about 2 h. The bacterial cells were chilled on ice before centrifugation at 6000 g for 10 min at 4°C. The pellet was resuspended in 250 ml of ice-cold 0.1 M $CaCl_2$ and incubated on ice for 30 min. The cells were then spun down again under the same conditions stated above and the pellet was resuspended in 50 ml of cold 0.1 M $CaCl_2$ supplemented with 15% glycerol before 50 µl aliquots were prepared in the cold room and flash frozen on dry ice. The competent cell aliquots were stored at -80°C.

2.6.14 Transformation of chemically competent *E. coli*

To transform competent cells, an aliquot of *E. coli* was thawed on ice and was transformed by heat shock as described in Sambrook et al. 1989. In general, 5-10 µl of a ligation reaction or 0.5 µl of plasmid DNA was added and gently mixed by tapping with the thawed *E. coli* under sterile conditions. The cells were placed on ice for 20 min, heat shocked for 90s at 42°C, followed by 2 min incubation on ice. After incubation, 900 µl Luria Broth (LB) was added to cells and were then incubated shaking (300-350 rpm) at 37°C for 1 h. Transformed cells were plated on LB plates containing the appropriate antibiotic (usually ampicillin or kanamycin antibiotics (Sigma-Aldrich) at final concentrations of 50 µg/ml or 30 µg/ml, respectively) and incubated overnight at 37°C. Transformed cells were resistant to the antibiotic and cells yielded colonies. These colonies were subsequently used to prepare broth cultures for DNA mini or midi-preparations after screening.

2.7 Computer programmes and Bioinformatic tools

A number of softwares and online bioinformatics tools were routinely used in this study. A list of such is shown in Table 2.15.

Table 2.15: Bioinformatics and statistical tools used in this study

Tool	Source	Use
Accuri C6 sampler and flow analysis software	BD Biosciences	For analysis of flow cytometry samples

Adobe illustrator CS6	Adobe Systems	For processing images and Figures
Adobe Photoshop CS6	Adobe Systems	For processing microscopy images
BLAST	http://www.ncbi.nlm.nih.gov/BLAST	For comparing DNA or protein sequences to database for analysis
ClustalW	www.ebi.ac.uk/clustalw	For Protein and DNA sequence alignment
Double Digest Finder	https://www.neb.com/tools-and-resources/interactive-tools/double-digest-finder	For determining buffer compatibility for restriction endonuclease
Expressed Sequence Tags (EST) database	http://www.ncbi.nlm.nih.gov/dbEST/	For analysing EST sequences in the database
Gene Tools	www.gene-tools.com	To design MO antisense oligos
GraphPad Prism 5.0c	Graphpad, La Jolla, CA, USA	For statistical analysis of acquired data
ImageJ	imagej.nih.gov/ij/	For processing and quantifying image signals
Ligation calculator	www.insilico.uni-duesseldorf.de/Lig_Input.html	For determining DNA amount needed for ligation ratios
NEBcutter	http://www.labtools.us/nebcutter-v2-0/	For identifying restriction enzyme sites on DNA sequence
NCBI gene database	http://www.ncbi.nlm.nih.gov/gene/	For obtaining gene (DNA or protein) sequences from the database
OligoCalc	http://biotools.nubic.northwestern.edu/OligoCalc.html	For calculating primer properties such as T_m, self-complimentarity etc.
Reverse Complement	http://www.bioinformatics.org/sms/rev_comp.html	To convert DNA sequence into its reverse, complement, or reverse-complement sequence
Serial cloner v2-6	serialbasics.free.fr/Serial_Cloner.html	For drawing DNA plasmid maps and identifying restriction sites on DNA sequence
Translation tool	Expasy.org	To translate nucleotide sequence to protein sequence
Volocity v6.21	Improvision/Perkin-Elmer	Acquistion and analysis of microscopy images

3 A role for centrobin in centriole duplication and biogenesis

3.1 Introduction

The formation of a bipolar mitotic spindle is essential for faithful segregation of chromosome between two newly formed daughter cells. The centrosome organises microtubules and ensures proper spindle assembly. As with DNA replication, centrosome duplication also follows a semi-conservative assembly that occurs strictly once per cell cycle (Tsou and Stearns 2006, Fu et al. 2015). Both processes are tightly linked and regulated by several key players in the cell cycle (Busch et al. 2007, Bourke et al. 2007, Adon et al. 2010).

Structurally, a typical G1 centrosome contains a pair of microtubule-based centrioles connected by a linker at the proximal ends and embedded in their functionally distinct proteinaceous pericentriolar material (PCM) (Lu et al. 2015a). The proximal ends of each of the G1/S centrioles nucleate a single cartwheel structure on which the procentriole is assembled and elongates during S and G2 phases of the cell cycle. Prior to mitosis, the linked mother centrioles are disconnected to allow for bipolar spindle formation (Azimzadeh and Marshall 2010, Nigg and Stearns 2011). The two newly duplicated centrosomes are then disengaged in late mitosis/early G1 in a process that requires the activities of PLK1 and separase (Tsou and Stearns 2006, Tsou et al. 2009). Centriole disengagement and the acquisition of PCM by the newly synthesised centriole act as the license for centrosome duplication in the subsequent round of the cell cycle (Loncarek et al. 2008a, Tsou et al. 2009, Hatch and Stearns 2010)

The two centrioles in a centrosome differ in age and maturity. Only the mother centriole carries the appendages which were conferred during G2 and M-phase of the cell cycle (Delgehyr et al. 2005; Azimzadeh and Marshall, 2010; Nigg and Stearns, 2011). The distal and the sub-distal appendages are located at the distal end of the mother centriole where they play essential roles in anchoring microtubules and primary ciliogenesis (Delgehyr et al. 2005; Ishikawa et al. 2005; Graser et al. 2007). Structural and numerical defects of the centrosome contribute to genome instability, aneuploidy and ciliopathy (Doxsey et al. 2005; Dodson et al. 2007; Nigg and Raff, 2009; Azimzadeh and Marshall, 2010; Pihan, 2013).

A complex network of proteins localise to the centrosome and participate in coordinating centrosomal activities during ciliogenesis and spindle assembly (Andersen et al. 2003).

Centrobin (Centrosomal BRCA2-interacting protein, also called *NIP2*[1]*, LIP8* and *PP1221*) was initially categorised as a centrosomal candidate in a proteomic screen for human centrosomal proteins (Andersen et al. 2003). It was later identified as a bona fide centrosomal protein that interacts with BRCA2 (Zou et al. 2005). Centrobin is a core centrosomal protein. It localises to the centrosome at all stages of the cell cycle and its localisation is not influenced by microtubule depolymerisation (Zou et al. 2005).

In human cells, depletion of centrobin was sufficient to prevent centrosome amplification induced by HU treatment or PLK4 overexpression and also led to increased numbers of monocentric and acentric cells (Zou et al. 2005). Based on these observations, centrobin was thought to be an essential centriole duplication factor that localises to the daughter centriole of interphase cells (Zou et al. 2005). During centriole biogenesis, centrobin is recruited to the procentriole by CEP152 and its activity is essential for regulating centriolar levels of CPAP/CENPJ during centriole elongation (Gudi et al. 2014). Centrobin interacts directly with CPAP and tubulin and thus is essential for both the biogenesis and elongation stages of centriole replication. Interestingly, overexpression of centrobin in interphase cells resulted in the formation of abnormally long centriole-like structures (Gudi et al. 2015).

Similar to Nek2 depletion, mice depleted of centrobin showed disorganised mitotic spindle organisation during embryogenesis and were arrested at the 4-cell stage (Sonn et al. 2009). Hypodactylous rats with a congenital abnormality that results in loss of digits endogenously express a truncated form of centrobin (Liska et al. 2009). The hypodactylous rats do not exhibit any proliferation defect; rather, they show deformed limbs and skeleton, abnormal spermatogenesis and growth retardation. Strikingly, re-introduction of centrobin into hypodactylous rats rescues all malformation phenotypes except the spermatogenesis defects (Liska et al. 2009, 2013). In *Drosophila* neuroblasts, centrobin distinguishes the mother and daughter centrioles and it is not essential for centriole duplication or maturation marked by mitotic PCM recruitment on the immotile daughter centriole. In this specialised cell type, centrobin regulates asymmetric division in neuroblasts through its ability to organise microtubules and PCM (Januschke et al. 2013). Loss of centrobin from the daughter centriole prevents it from organising aster microtubules and results in loss of PCM from the daughter centriole (Januschke et al. 2013).

To date, all published observations on the contributions of centrobin to centrosome functions in human cells were based on siRNA-mediated depletion of the protein. The use of siRNA-mediated protein depletion presents certain disadvantages, such as non-specific off-target

[1] *CNTROB* (NM_053051) located on chromosome 17 is different from *BNIP2* (NM_001320675.1) which is also called *NIP2* and is located on chromosome 15.

effects and incomplete knockdown efficiency that may lead to residual functional protein. To minimise these deficiencies, we decided to use CRISPR/Cas9 technology to disrupt the *CNTROB* locus in non-transformed hTERT-RPE1 (retinal pigmented epithelium) cells, which are considered to be karyotypically normal (Bodnar et al. 1998).

CRISPR/Cas9 endonuclease-mediated gene targeting is a highly efficient technique that facilitates gene manipulation at specific site. This technology mimics the bacterial defense system. It relies on guide RNA (gRNA) binding specifically to regions of interest to allow the Cas9 endonuclease to induce a double-strand DNA break upstream of the PAM (protospacer-adjacent motif) sequence that is adjacent to the gRNA (Ran et al. 2013, Mali et al. 2013). Generally, genotoxic insults that induces DSBs activate either the homologous repair (HR) or non-homologous end joining (NHEJ). During NHEJ repair, nucleotide insertion and/or deletion mutations at the break site may introduce a premature stop codon. This results in transcription of a highly unstable mRNA for protein translation that results in the functional ablation of the gene. On the other hand, activation of the HR repair pathway depends on the availability of a template DNA to allow for precise repair through integration of the template DNA into the genome. Recently, this precise repair has been successfully used to manipulate the genome of human embryos to correct heritable genetic mutations (Ma et al. 2017, Tang et al. 2017).

At the initial stage of this project, we generated a novel monoclonal antibody against centrobin as well as centrobin knockout and rescue cell lines which were useful reagents for investigating the roles of centrobin in centrosome-related functions such as DNA repair and ciliogenesis. In this chapter, we present bioinformatics analysis of human centrobin, cloning of human *CNTROB* cDNA, and novel monoclonal antibody characterisation. We analyse the centriolar and proliferative roles of centrobin in *CNTROB* null and rescue clones. We find that *CNTROB* is not an essential gene for cell proliferation and viability. Loss of centrobin does not significantly affect centrosome protein composition but results in a slight increase in acentric and monocentric cell populations.

3.2 Bioinformatic analysis of centrobin

We used the NCBI database for analysis of the human *CNTROB* locus. The *CNTROB* gene spans 17.8 kbp on the p-arm of chromosome 17 (Figure 3.1). Based on the current database, there are 6 confirmed human *CNTROB* isoforms (Table 3.1).

Figure 3.1: Schematic of human *CNTROB* genomic locus.

Exons are indicated as black boxes and exon numbers are indicated with Roman numerals. Introns and the untranslated regions (UTR) are shown with connecting lines and grey boxes respectively.

Zou et al. initially reported the presence of alpha and beta centrobin isoforms in human (Zou et al. 2005). The only difference between these isoforms is that the beta isoform contains an extra 66 nucleotides on exon 17, making it the longest transcript. To date, the alpha transcript is known as the predominant variant and has been the most widely studied. Expression of the beta isoform as a minor transcript was briefly described during initial centrobin characterisation (Zou et al. 2005). The expressions of other centrobin mRNA variants (model and known RefSeq with NM and XM accession number, respectively, see Table 3.1) have never been experimentally confirmed in the currently available literature. Aside from transcript X14 that lacks the expression of exons 1-5, variations between the isoforms are as a result of differences between either UTRs, exons II, XVII or XVIII (Figure 3.1). Since there is no experimental confirmation of these isoforms, it is unknown if these isoforms are expressed and are functionally relevant in a biological system. On the other hand, these isoforms may be products of computational gene prediction tools. Therefore, our study was based on the analysis of the alpha isoform of the *CNTROB* gene.

Table 3.1: Comparative analysis of predicted human *CNTROB* isoforms

Analysis of the 18 human *CNTROB* transcript variants. The transcript, CDS and amino acid length are shown.

Isoform name	NCBI accession number	Transcript length (bp)	CDS length (bp)	Confirmed or predicted Protein length (aa)
Alpha	NM_053051.4	4114	2712	903
Beta	NM_001037144.6	4180	2778	925
Gamma	NM_001330124.2	4117	2715	904
Delta	NM_001353202.1	4094	2616	871
Epsilon	NM_001353205.1	4121	2447	815
Zeta	NM_001353204.1	4119	2153	717
X1	XM_017024128	3612	2778	925
X2	XM_017024129	3083	2778	925

X8	XM_017024134	3703	2682	893
X9	XM_005256438	3640	2618	872
X11	XM_017024135	3712	2511	836
X13	XM_017024137	3660	2445	814
X14	XM_017024138.1	2390	2220	739
X15	XM_017024139.1	3746	2157	718
X17	XM_017024141.1	3082	2127	708
X18	XM_017024142.1	3809	2088	695
X19	XM_017024143.1	2838	1914	637
X20	XM_017024144.1	3869	1848	615

CNTROB gene orthologues have been identified in several vertebrates and *Drosophila.* Using the Clustal Omega sequence alignment tool, we determined the level of protein homology between human centrobin and its orthologues in other species. We observed the highest level of conservation (≥70%) between human and other mammalian centrobin orthologues. When the human centrobin was compared to its fish orthologues in this study (represented by zebrafish and herring), there was a high level of sequence identity in only some parts of the protein sequence, resulting in an overall moderate homology (30-40%). Our analysis revealed that the least homology (<30%) is between human and *Drosophila* centrobin (Figure 3.2). With the exception of *Drosophila*, all the other *CNTROB* orthologues in this study share synteny by localising between the *ATP1B2* and *TRAPPC1* gene loci on their respective chromosome (data not shown). However, these analyses suggest that *CNTROB* is moderately conserved among species used in this study. It also highlights the possibility of highly conserved domains with functional significance in centrobin and its orthologues.

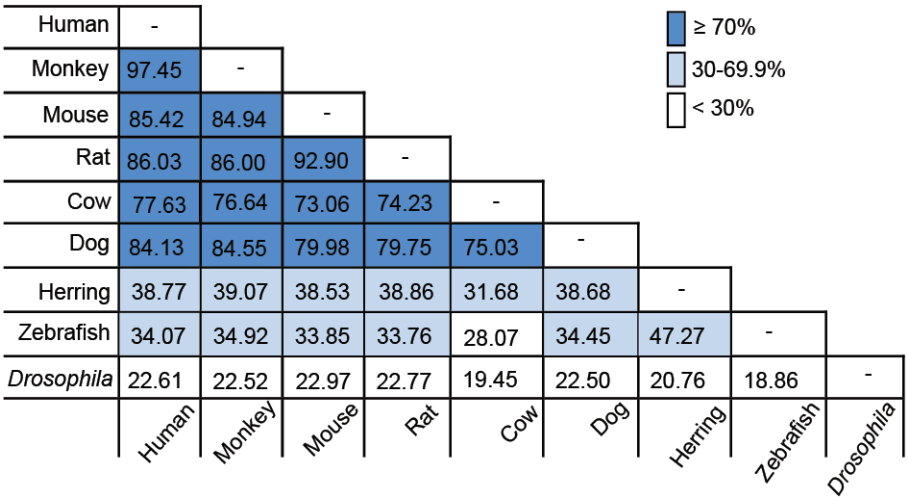

Figure 3.2: Comparative analysis of the human *CNTROB* gene and its orthologues from other species.

The level of conservation is measured by the % of identical amino acid residues found in the analysed sequences. The referred values do not account for computational errors associated with predicted protein sequence. The protein sequences used for this comparison and their NCBI protein database accession number are as follows: Human: NP_444279.2; Rhesus monkey: NP_001248135.1; Mouse: NP_766148.2; Rat: NP_001128117.1; Cow: XP_015314253.1; Dog: XP_005620061.1; Herring: XP_012673037.1; Zebrafish: MF461638 (this study; submission under review by NCBI); *Drosophila*: NP_647680.1.

3.3 Production and characterisation of monoclonal anti-centrobin antibody (6D4F4)

To study the functions of *CNTROB*, a monoclonal antibody (6D4F4) was raised in mouse against ~300 amino acids at the N-terminus of the human centrobin (Figure 3.3A). Dr. David Gaboriau generated the antigen used for generating this monoclonal antibody as previously discussed in section 2.3.2. The specificity of our novel antibody was confirmed by immunoblotting and immunofluorescence microscopy analysis after 48 h of treatment with siRNA to mediate protein knockdown. The *CNTROB* siRNA used in this has been previously established in an independent study (Jeong et al. 2007). After treatment, immunoblotting analysis conducted on the cell lysates of controls or si*CNTROB* showed that the antibody detects a band at ~120 kDa and the loss of this protein signal after knockdown verified the specificity of our monoclonal centrobin antibody. siRNA against GAPDH was used to confirm siRNA transfection while α-tubulin was used as loading control (Figure 3.3B). Furthermore, we used immunofluorescence microscopy to detect centrosomal localisation of the antigen recognised by our monoclonal anti-centrobin antibody. As shown in Figure 3.3C, after 50 and 100 nM si*CNTROB* treatment, the recognised protein levels were significantly reduced at the centrosome of hTERT-RPE1 while the centrosome marker used, γ-tubulin, was

retained with an unaltered intensity at the centrosome. These results confirm the specificity of our novel monoclonal anti-centrobin antibody (6D4F4).

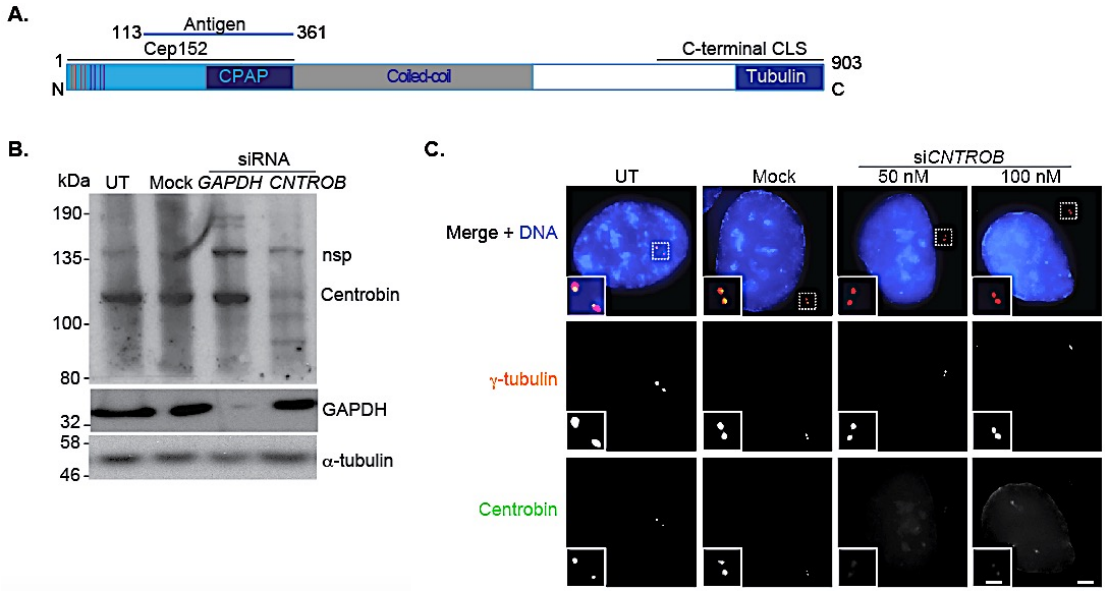

Figure 3.3: Characterisation of a novel mouse monoclonal centrobin antibody.

A. Schematic representation of full-length human centrobin showing the region used as an antigen for monoclonal antibody production. CPAP-, Cep152- and tubulin- binding regions and centrosome localisation signals at the C-terminal end of the protein (C-terminal CLS) are also shown. A Coiled-coil domain in the centre of the protein sequence is indicated by a grey box. Orange lines indicate PLK1 phosphorylation (T3, S4, 21, 22) while purple lines indicate Nek2 phosphorylation sites (T35, S36, 41, 45). **B.** Immunoblot confirming specificity of the novel antibody by siRNA-mediated centrobin knockdown in hTERT-RPE1 cells for 48 hours. siRNA against GAPDH was used as positive control and α-tubulin as a loading control. nsp denotes non-specific protein band. **C.** Immunofluorescence microscopy reveals that anti-centrobin antibody, 6D4F4, specifically detects centrobin (green) at the centrosome. γ-tubulin (red) was used to mark the centrosome, and DNA (blue). Scale bar, 5 µm and insets, 1 µm. (Monoclonal antibody was designed and generated by Dr. David Gaboriau).

3.4 Localisation of centrobin at stages of the cell cycle

Our monoclonal anti-centrobin 6D4F4 was next used to investigate the localisation of endogenous centrobin in asynchronous hTERT-RPE1 and chicken DT40 cells (Figure 3.4). Immunofluorescence microscopy analysis of centrobin in both of these cell lines revealed that centrobin is indeed a core centrosomal protein that is consistently localised to the centrosome at all stages of the cell cycle. Consistent with the observations reported by Zou *et al.* our immunolocalisation studies also revealed a specific pattern in the appearance of centrobin at different phases of the cell cycle (Figure 3.4A). We noticed that in majority of G1 cells, a single centrobin signal was present while during S/early G2 and mitosis, a second centrobin signal, which may occasionally be with one or two weaker centrobin signals, was observed.

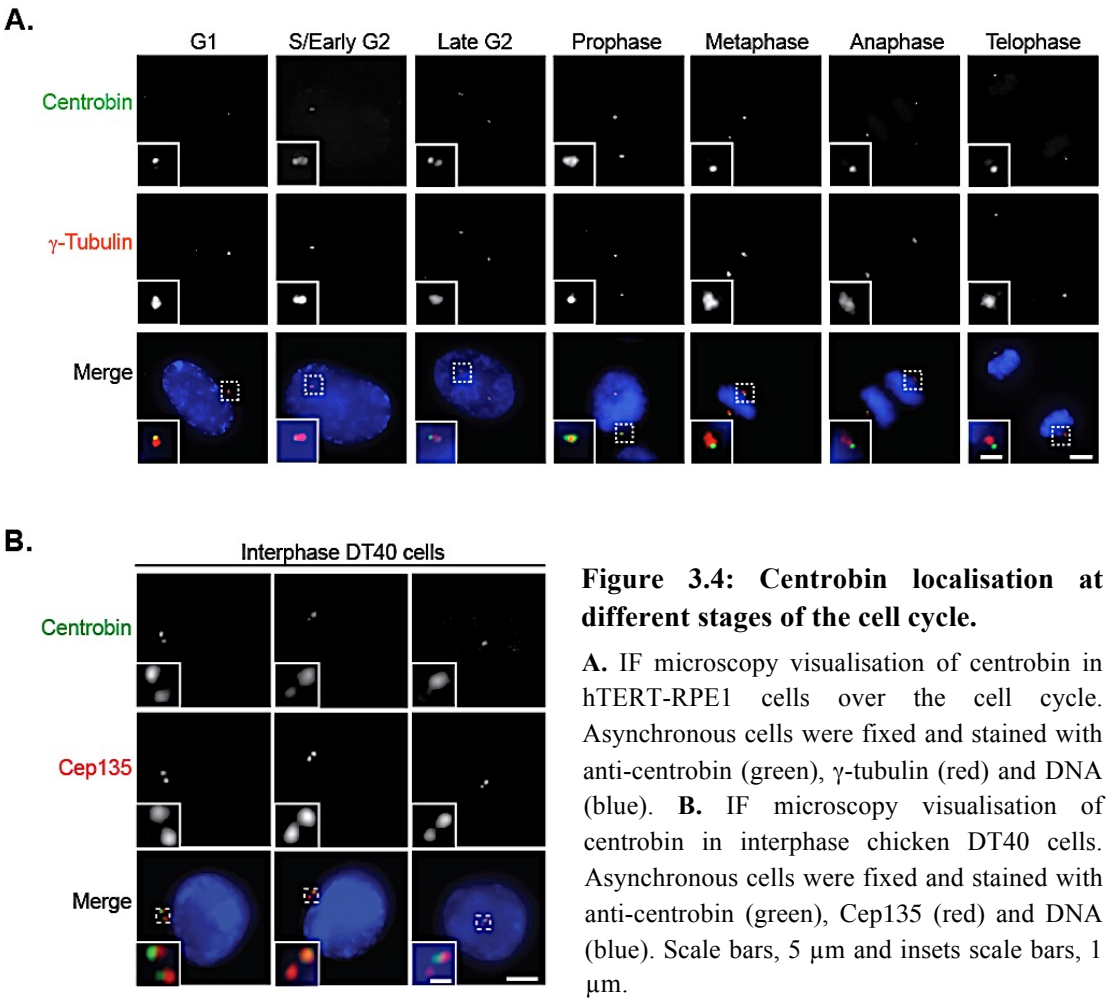

Figure 3.4: Centrobin localisation at different stages of the cell cycle.

A. IF microscopy visualisation of centrobin in hTERT-RPE1 cells over the cell cycle. Asynchronous cells were fixed and stained with anti-centrobin (green), γ-tubulin (red) and DNA (blue). **B.** IF microscopy visualisation of centrobin in interphase chicken DT40 cells. Asynchronous cells were fixed and stained with anti-centrobin (green), Cep135 (red) and DNA (blue). Scale bars, 5 µm and insets scale bars, 1 µm.

The weaker signals may indicate the presence of residual centrobin at the mother centrioles; although the mechanism through which centrobin is removed from the mother centriole during mitosis is yet unknown. This observed pattern confirms previous studies where centrobin was shown to localise to nascent procentrioles at very early stages of centriole duplication during the G1/S transition. It is then retained as a core centriolar protein that is preferentially visualised on the daughter centriole (Zou et al. 2005, Gudi et al. 2014).

3.5 Cloning and overexpression of *CNTROB* and EGFP-CNTROB

To investigate centrosomal functions of centrobin, we cloned the *CNTROB* cDNA into mammalian cloning and expression vectors. First, we designed primers to the 5' and 3' ends of *CNTROB* alpha transcript (NCBI accession number: NM_053051), with which we successfully performed RT-PCR as confirmed by agarose gel electrophoresis (Figure 3.5A). The amplicon was cloned into pEGFP-C1 backbone to yield a pEGFP-CNTROB plasmid

which features a neomycin resistance cassette. A number of pEGFP-CNTROB clones were sequenced to verify the cDNA sequence relative to NM_053051.

Although centrobin has a low endogenous expression level (Zou *et al.* 2005; Jeong *et al.* 2007), our initial immunoblot analysis of pEGFP-CNTROB after transient transfection of the plasmid into hTERT-RPE1 showed a low level of expression for the GFP-centrobin encoded by the plasmid (data not shown). Due to the very low expression level of GFP-centrobin in hTERT-RPE1 and the neomycin resistance of our *CNTROB* knockout cells (section 3.6), we decided to remove EGFP and neomycin promoter sequences from the pEGFP-CNTROB plasmid. We also decided to subclone a blasticidin resistance (*Bsr*) cassette (from pLoxP-BSR) into the plasmid for selection. The EGFP removal was achieved using AgeI and XhoI while the *Bsr* cassette (along with SV40 promoter) was subcloned by blunt end ligation to generate p*CNTROB-Bsr* (hereinafter referred to as pCNTROB) (Figure 3.5B).

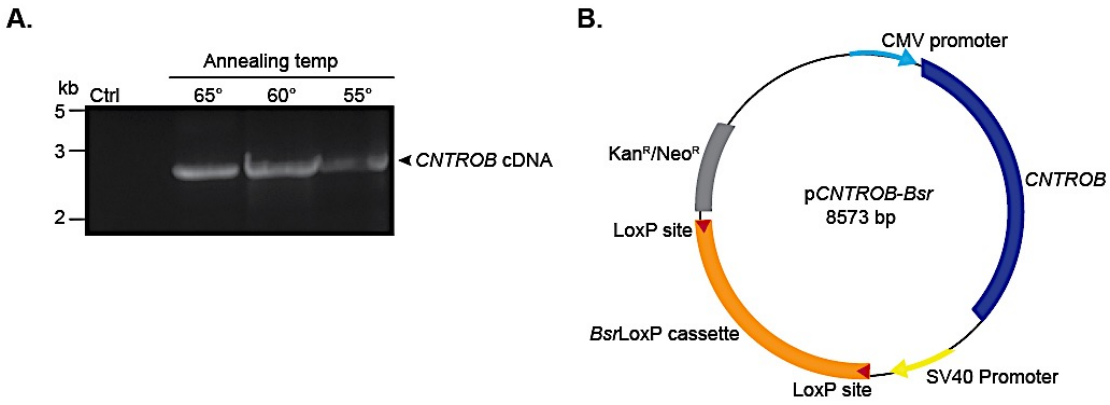

Figure 3.5: Cloning of full-length human *CNTROB* cDNA

A. PCR amplification of *CNTROB* from human cDNA yielded the expected ~2.8 kb product. Amplification was successful at various indicated annealing temperatures using primers designed from NM_053051 sequence. **B.** Schematic of p*CNTROB-Bsr* plasmid showing the CMV promoter, kanamycin and blasticidin resistance marker used for bacterial and mammalian selections.

To test the centrobin expression constructs, we transfected them into wild-type hTERT-RPE1 or U2OS cells for transient expression (Figure 3.6A-D). The expression levels of centrobin and GFP-centrobin were assessed by immunofluorescence and western blot (Figure 3.6A-D). Using pericentrin to mark the centrosome during immunofluorescence microscopy, we confirmed that centrobin protein expressed from pCNTROB and pEGFP-CNTROB plasmids localised to the centrosome (Figure 3.6A-B). We observed moderate expression of GFP-centrobin while the untagged centrobin was highly expressed in U2OS cells. The untransfected (UT) control and pCNTROB-transfected cells show centrosomal signals, but linear cytosolic structures were stained in the pCNTROB-transfected cells (Figure 3.6A). Also, there was no centrosomal localisation in the empty vector (pEGFP-C1) negative control compared to pEGFP-CNTROB-transfected cells (Figure 3.6B). Our immunoblot analysis was

consistent with the expected size of centrobin: we observed an increase in the level of centrobin in hTERT-RPE1 cells transfected with pCNTROB relative to the untransfected control and the levels declined over time (Figure 3.6C, lane 2-4). We also observed a ~140 kDa protein in the pEGFP-CNTROB-transfected hTERT-RPE1 cells (Figure 3.6C, lane 5-7). This also confirms the specificity of our monoclonal antibody, which recognises both the endogenous centrobin and centrobin expressed from cloned cDNA. Furthermore, anti-GFP antibodies specifically detected the ~140 kDa band only in the pEGFP-CNTROB transfected cells (Figure 3.6D, lane 5-7). We used α-tubulin as a loading control on the western blot analyses. These results show that the plasmids encode functional centrobin that localises to the centrosome in U2OS and hTERT-RPE1 (data not shown).

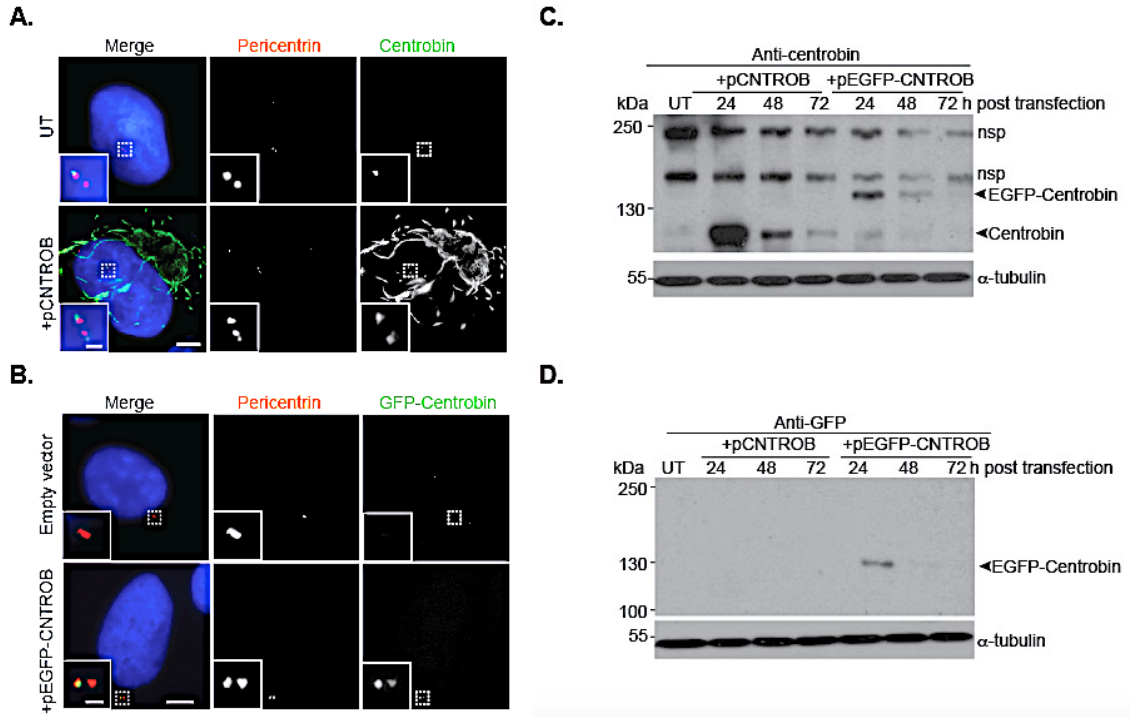

Figure 3.6 Transient expression of full-length human *CNTROB* cDNA

A. Immunofluorescence microscopy analysis of transient expression of pCNTROB and **B.** pEGFP-CNTROB in U2OS cells. Proteins expressed from both plasmids showed centrosomal localisation with pericentrin (red). Scale bars, 5 µm and insets, 1 µm. **C.** Immunoblot analysis of transient expression of pCNTROB and pEGFP-CNTROB in hTERT-RPE1 cells at indicated time points. Cell lysates were probed with anti-centrobin (6D4F4) or **D**. with GFP antibody. Centrobin and GFP-centrobin products run at approximately 120 and 140 kDa, respectively. nsp denotes non-specific bands.

3.6 Disruption of human *CNTROB* locus in hTERT-RPE1 cells using CRISPR/Cas9

To study the functions of centrobin in human cells, we generated centrobin knockout cells using CRISPR/Cas9 genome editing, a very robust and commonly used RNA- guided gene

editing technique. Using the guide RNA (gRNA) database (available at http://arep.med.harvard.edu/human_crispr/) provided by Mali et al. (2013), we selected 2 of the available 16 gRNA sequences that can potentially disrupt the *CNTROB* genomic locus. To ensure higher efficiency of disrupting all the *CNTROB* transcripts/isoforms, we designed gRNA against exons 1 and 4 (Figure 3.7A), which were chosen due to their proximity to the start codon and the 5' end of the locus. This was preferred as it reduces the likelihood of cells expressing a potentially stable coding transcript.

hTERT-RPE1 cells were transfected with pX330 plasmid containing one of the two gRNA sequences (the oligo sequences are listed in Table 2.14) along with a plasmid coding for neomycin antibiotic resistance. After 10 days of antibiotic selection with geneticin, colonies were individually selected and subsequently examined by western blot and IF microscopy for their loss of centrobin expression (Figure 3.7B-D). We screened 45 clones and obtained 4 clones that lacked detectable centrobin by western blot. A representative immunoblot for two clones that were analysed further is shown in Figure 3.7B. To ascertain the loss of centrobin at the centrosome, we used our monoclonal antibody and a commercially available polyclonal anti-centrobin antibody which was designed against the full-length protein for IF microscopy (Figure 3.7A, C and D). We observed the absence of centrobin signal at the centrosome, as visualised by γ–tubulin and PCM1 respectively. The polyclonal antibody was expected to facilitate the visualisation of any truncated form of centrobin protein since the full-length protein had been used as immunogen during antibody generation. These data showed that we successfully targetted the human *CNTROB* gene locus and ablated the gene expression in human hTERT-RPE1 cells.

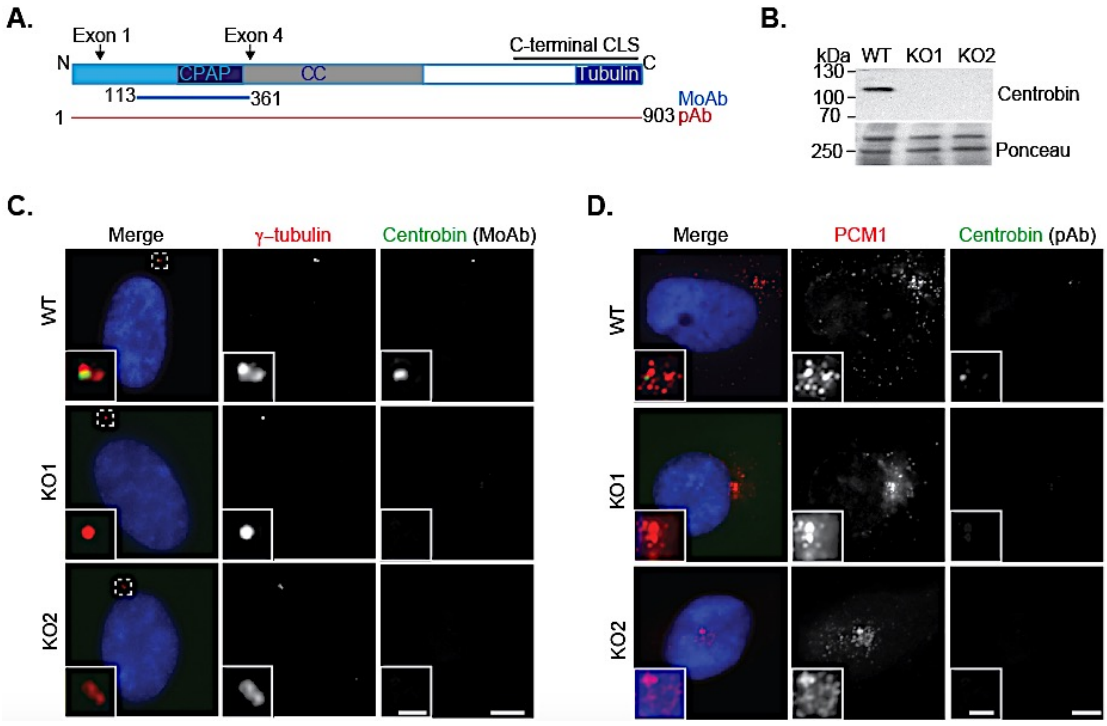

Figure 3.7: Generation of *CNTROB* knockout hTERT-RPE1 cells.

A. Schematic representation of centrobin protein showing regions used as antigen during monoclonal (6D4F4; MoAb) and commercially available polyclonal (pAb) anti-centrobin antibodies design; and are shown in blue and red lines respectively. Arrows indicate the guide RNA target sites used for disruption of CNTROB at exons 1 and 4. The coiled-coil domain is shown in grey box. CPAP and tubulin binding domains and the centrosome localisation signal are also shown. **B.** Western blot confirming loss of centrobin expression in wild-type and two hTERT-RPE1 *CNTROB* knockout (KO) clones. Ponceau was used as loading control. **C.** Immunofluorescence micrograph confirming loss of centrobin at the centrosome of *CNTROB* KO cells using our novel monoclonal antibody (MoAb, shown in green). γ–tubulin (red) was used to visualise the centrosome and DNA is shown in blue (stained with Hoechst). **D.** Immunofluorescence micrograph confirming loss of centrobin in *CNTROB*-KO cells using commercially available polyclonal antibody (pAB, shown in green). PCM1 (red) was used to visualise the centriolar satellites and DNA, shown in blue, was stained with Hoechst. Scale bars, 5 µm and insets, 1 µm.

To determine the exact nature of the Cas9-mediated DNA modification of the *CNTROB* locus, we carried out PCR reactions on genomic samples from wild-type and the four CRISPR knockout clones. The PCR amplicons were sequenced for the targetted regions on exon 1 and 4 using CRISPR screen primers (Table 2.14). The sequence traces of the PCR products (not shown) for wild-type cells and our positive CRISPR clones (clones lacking centrobin signals) revealed the exact alterations that occurred after the Cas9 activity.

From the sequencing data, we discovered that the genomic sequence of 3 of our 4 clones had 43 nucleotide deletions on exon 4. This deletion resulted in the removal of a splice site (Figure 3.8A-C). To ascertain the impact of the splice site removal after Cas9 cleavage, we analysed cDNA from one of these 3 clones. Our analysis revealed the loss of exon 4 during pre-mRNA splicing that leads to the introduction of a premature stop codon (Figure 3.8C).

This clone (interchangeably referred to as 'KO1'; 'KO'; or '*CNTROB* KO') was chosen for further experimental investigation in this project.

We sequenced the fourth of our CRISPR clones and we also observed 7 nucleotide deletions on the exon 1 genomic sequence which also led to premature stop codon (Figure 3.7A and D). We also used this clone (referred to as 'KO2') for some of our experimental investigations in which we found no significant difference in the phenotypes observed between KO1 and KO2. To investigate the homozygosity of the mutations, we cloned the PCR products into pGEM-T-Easy and all the clones (at least 5 clones were sequenced from each of the mutants using T7 and SP6 primers) revealed similar mutations. Also, the evidence that the same alterations occurred to DNA on both alleles was revealed by the presence of single peaks all through the DNA traces of total PCR products for the *CNTROB* CRISPR clones (Appendix 1, Appendix 2).

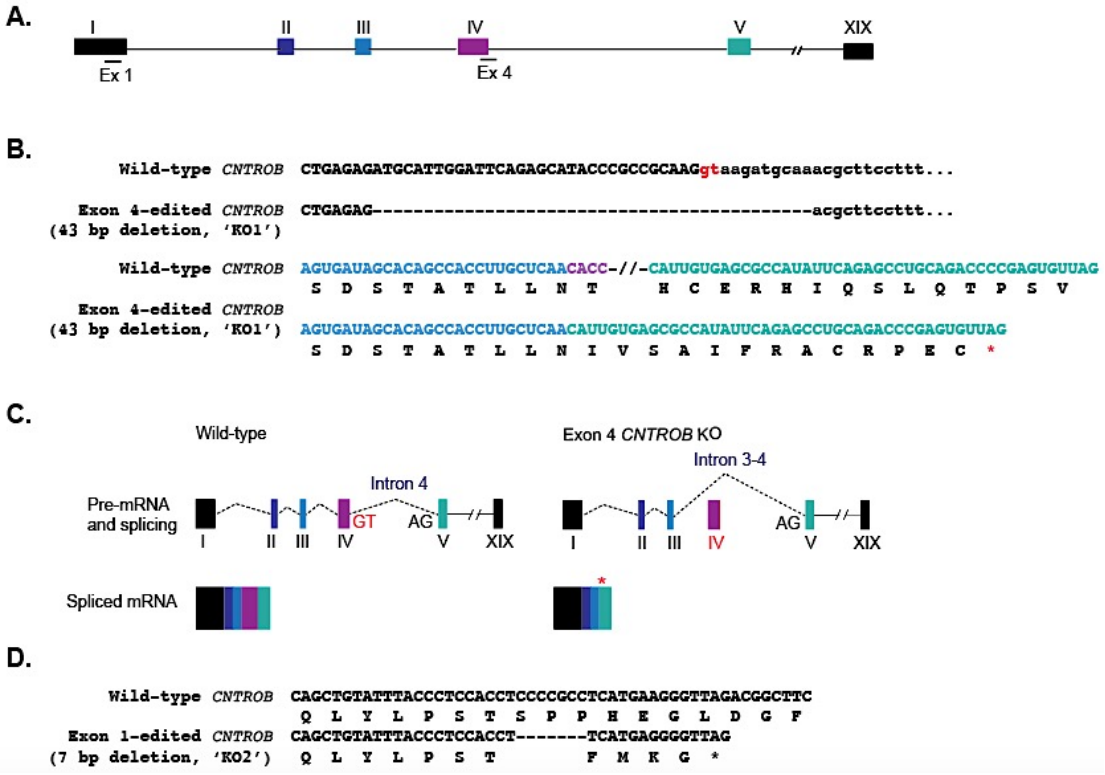

Figure 3.8: Sequencing confirmation of specific genome manipulations *CNTROB* knockout clones after CRISPR/Cas9

A. Schematic representation of *CNTROB* gene. The regions to which both gRNAs were designed are underlined below the exons, highlighting the targeted CRISPR exons. **B.** Upper panel shows nucleotide sequences obtained from genomic DNA PCR of wild-type and KO1 cells revealing 43 nucleotide deletion at the 3' end of exon 4 which includes an intron/exon junction indicated in small letters. Lower panel shows the cDNA and predicted protein sequence for KO1 (exon 4 gRNA). Sequences are coloured according to their respective exons and part of the wild-type exon 4 sequence is omitted. The loss of intron/exon junction (GT in red) led to loss of exon 4 in KO1 during splicing. Direct translation of exon 3 and 5 in KO1 introduces a premature stop codon shown with red asterisk. **C.** Schematic representation of pre-mRNA splicing process in KO1 indicates splicing-out of exon 4 to yield premature stop codon indicated by red asterisk in the mRNA transcript. **D.** Genome editing of

CNTROB locus sequence reveals loss of 7 nucleotides that resulted in premature stop codon in KO2 (exon 1 gRNA).

Generally, transcripts with a premature stop codon activate an mRNA decay pathway that leads to rapid reduction in their availability for the translational machineries (Jacobson and Peltz 1996). Furthermore, the predicted molecular weight of any truncated form of centrobin proteins produced as a result of these premature stop codons introduced by Cas9 activity are 23.7 kDa (198 aa) and 8.2 kDa (69 aa) for KO1 and KO2 respectively. We believe that the functionality of these truncated centrobin proteins, if produced, would be insufficient to play any roles of the full-length protein. Therefore, we concluded that our *CNTROB* KO cell lines are complete centrobin null cells.

3.7 *CNTROB* nulls show normal centrosome composition

The centrosome is composed of several hundreds of proteins that contribute to different stages of centrosomal duplication process and/or functions. To investigate the impact of centrobin deficiency at the centrosome, we used antibodies that recognise known centrosomal components. First, we analysed the integrity of the cartwheel assembly by staining for the distribution and localisation of Cep135 and hSas6. The centrosomal cartwheel and scaffold proteins are essential for procentriole assembly during centriole replication (Kleylein-Sohn et al. 2007, Strnad et al. 2007, Azimzadeh and Marshall 2010). As evident from immunofluorescence microscopy, Cep135 and hSas6 localisation and distribution in centrobin-deficient cells were comparable to those of wild-type cells (Figure 3.9).

For further investigation of centrosome structure in our *CNTROB* KO cells, we studied the dynamics of centriole linker, centriole distal end and mother centriole integrity by looking at the localisation pattern of C-Nap1, Cep97 and Kizuna, respectively (Figure 3.9). We observed that the integrity of these proteins at the centrosome were retained in the absence centrobin. Normally, C-Nap1 localises to and acts as a tether at the proximal ends of both parental centrioles while Cep97, along with its interacting partner CP110, localises to the distal end of the centrioles where they regulate centriole length and prevent ciliogenesis in cycling cells (Schmidt et al. 2009, Nigg and Stearns 2011). Importantly, a single kizuna signal was observed in both wild-type and *CNTROB* knockout clones. This indicates the presence of only one matured centriole in a typical G1 cell in *CNTROB* knockout cell populations. This observation confirmed published findings that highlighted centrobin as a major determinant of mother-daughter centriole function (Conduit 2013, Gottardo et al. 2015).

Next, we stained the cells with antibodies against Cep164, PCM1 and Centrin2, which allow us to visualise the distal appendages, centriolar satellites and the distal lumen, respectively. Representative examples of a typical stained G2 wild-type and centrobin-deficient cells are shown in Figure 3.9. We observed the presence of four centrin2 signals and the localisation of two Cep164 signals (1 strong and 1 weaker signal), which are indicative of distal appendages on the parental centrioles (Graser et al. 2007). Cep164 is a component of the distal appendage that resides only on the mother centriole and is essential for ciliogenesis (Graser et al. 2007, Daly et al. 2016). This result corroborates our observation that the daughter centriole in *CNTROB* null cells does not carry the distal and subdistal appendages, as we have shown with stainings with maturation markers, Cep164 and Kizuna. This result shows that centriole maturation is not affected in centrobin-deficient cells. As apparent from the IF analysis, the integrity and distribution of centriolar satellites were also undisturbed in centrobin-deficient cells, as indicated by PCM1 staining (Figure 3.9).

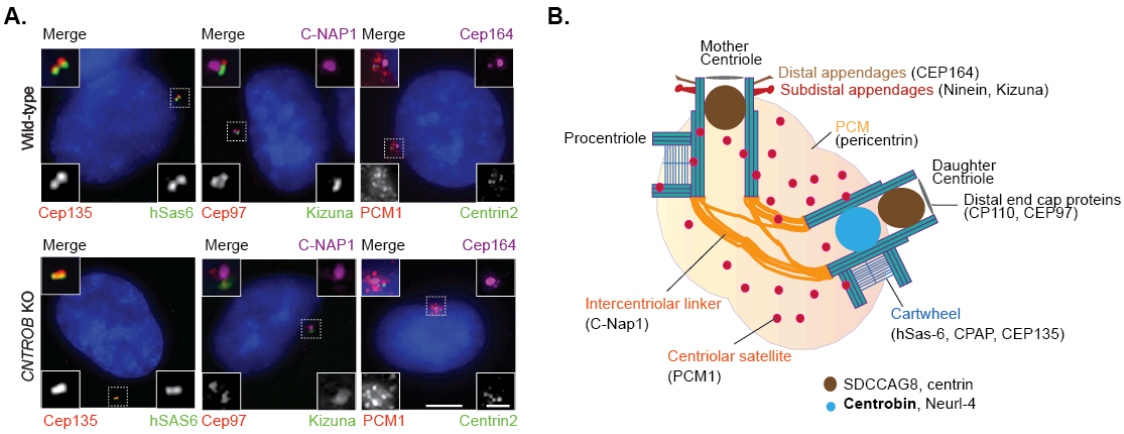

Figure 3.9: Localisation of centriole and centriolar satellite markers in wild-type hTERT-RPE1 and *CNTROB* null cells.

A. IF microscopy stainings of indicated centriole and centriolar satellite proteins indicated in asynchonous wild-type and *CNTROB* KO cells. Scale bar, 5 µm, inset scale bar, 1 µm. B. A schematic diagram showing the localisation of different centrosomal proteins in a typical S-phase centrosome. It highlights the mother and daughter centrioles, procentrioles, intercentriolar linker, centriolar satellites, PCM and the appendages.

Centrobin has been shown to play modulatory roles at the centrosome of both interphase and mitotic cells (Lee et al. 2010, Jeffery et al. 2013). To further understand the involvement of centrobin at these stages of the cell cycle, we cultured asynchronous hTERT-RPE1 and centrobin-deficient cells and visualised the localisation patterns of Cep135, CPAP, pericentrin, ninein, SDCCAG8 and α-tubulin in interphase (Figure 3.10) and mitotic (Figure 3.11) cells. Cep135 and CPAP are core centrosomal proteins that participate in the centriole duplication process (Schmidt et al. 2009; Azimzadeh and Marshall, 2010; Gudi et al. 2014, 2015). Interestingly, centrobin is known to regulate CPAP levels at the centrosome (Gudi et al. 2014, 2015). We also visualised the integrity and dynamics of the PCM through

pericentrin staining. The PCM serves as an essential hub for microtubule nucleation and organisation in interphase cells and during spindle assembly in mitotic cells. We observed no distortion in the localisation and distribution of this protein in our centrobin-disrupted cells. Next, we stained the cells with ninein, which marks subdistal appendages associated with mother centriole and SDCCAG8 marks the distal ends of both centrioles. Based on our immunofluorescence microscopy analysis, we detected no visible difference in the appearance of these centriole distal end markers in our centrobin-deficient interphase and mitotic cells.

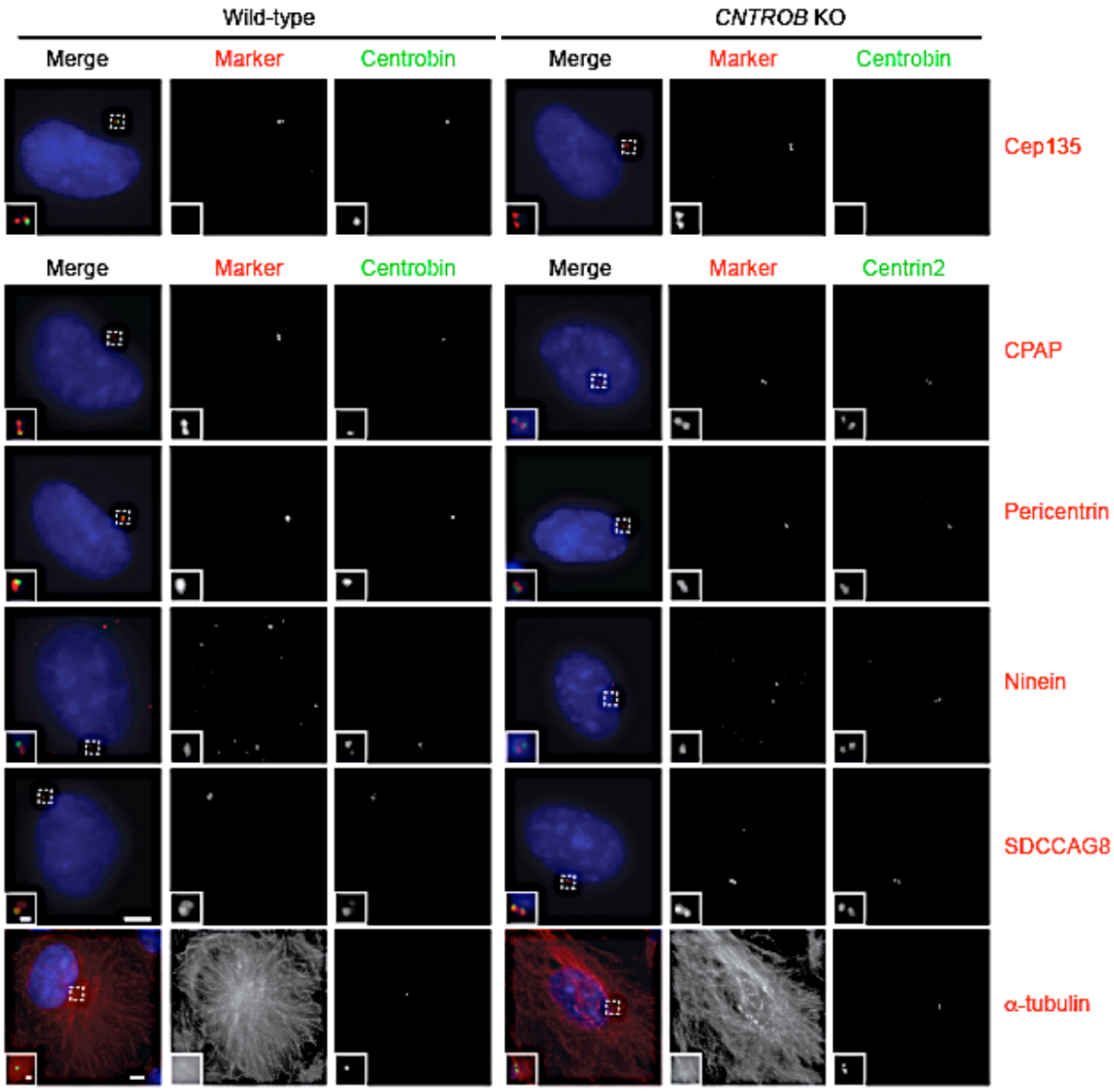

Figure 3.10: Loss of centrobin has no effect on localisation and composition of centrosomal proteins and alpha-tubulin in interphase *CNTROB* KO hTERT-RPE1 cells.

Wild-type and centrobin-deficient cells were fixed and stained with antibodies to Cep135, CPAP, pericentrin, ninein, SDCCAG8 and α-tubulin (all in red), as indicated, centrobin or centrin2 (in green) and DNA in blue. Scale bars, 5 µm and inset scale bars, 1 µm.

Because centrobin interacts with tubulin, we examined the organisation of microtubules in our cell lines using antibodies against α-tubulin. We observed a more even distribution of microtubules emanating from the centrosome in our wild-type while centrobin-depleted cells appeared more disorganised, without any definite organisation at the centrosome (Figure 3.10). While we observed minor difference in the tubulin conformation in interphase *CNTROB* null cells, we considered the possibility of this being a minor defect since our cells grow normally in culture. However, it might be interesting to look into microtubule repolymerisation/regrowth to determine the microtubule nucleating ability of the centrosome in our knockout cells.

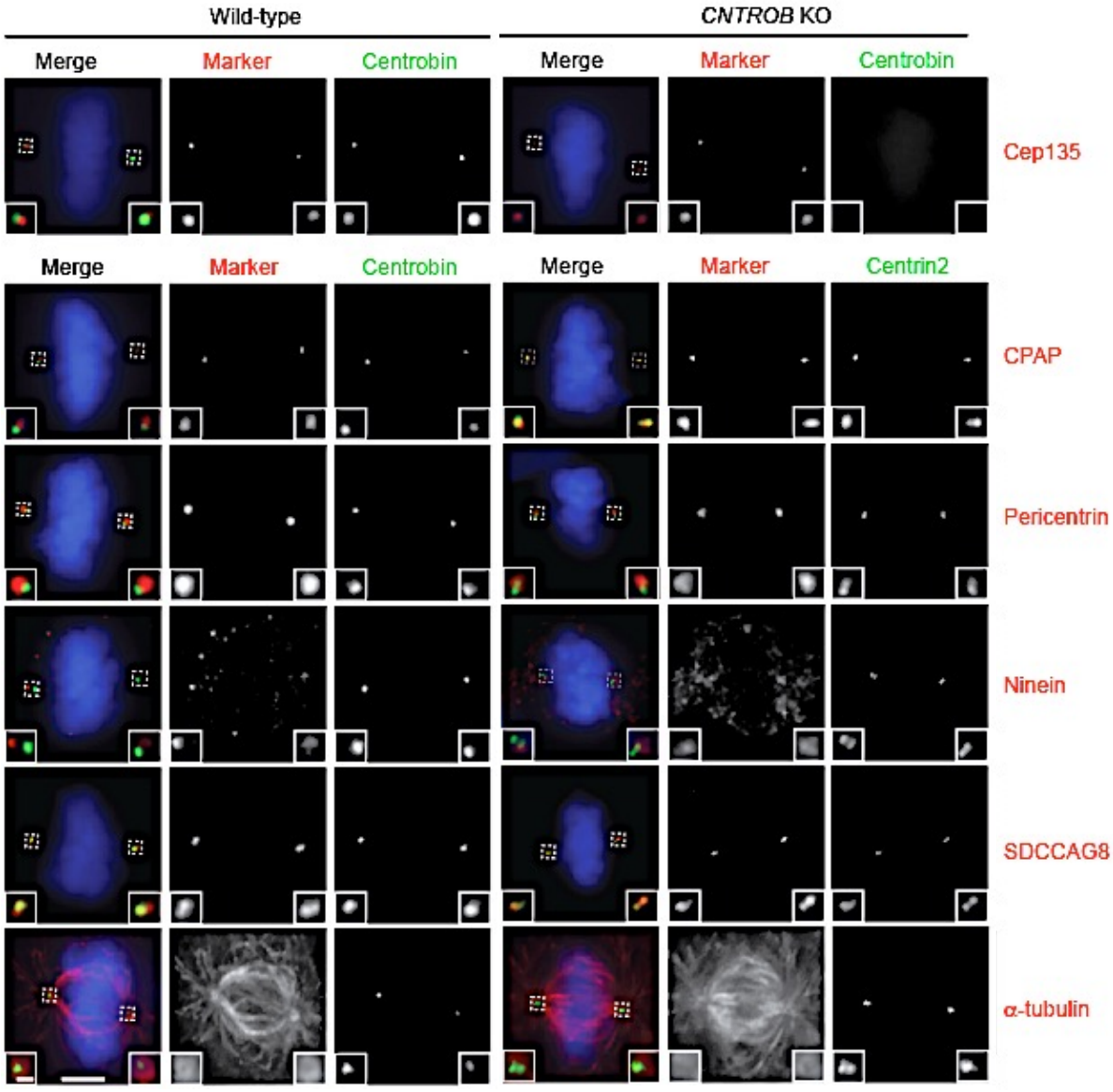

Figure 3.11: Loss of centrobin has no effect on localisation and composition of centrosomal proteins and alpha-tubulin in mitotic *CNTROB* KO hTERT-RPE1 cells.

Asynchronous wild-type and centrobin-deficient cells were fixed and stained with antibodies to Cep135, CPAP, pericentrin, ninein, SDCCAG8 and α-tubulin (all in red), as indicated, centrobin or centrin2 (in green) and DNA in blue. Scale bar, 5 μm and inset scale bar, 1 μm.

We next examined centrosomal/centriolar integrity in our wild-type and centrobin-deficient cells using electron microscopy (EM) to visualise the centrosome. Samples were prepared as described in section 2.3.7.4. We noticed no apparent anomaly in centrosome, appendages, microtubule nucleation and procentriole assembly in centrobin-deficient cells (Figure 3.12). Examples of centriole triplets, centrioles showing the mother centriole appendages and procentrioles are presented in Figure 3.12. This result recapitulates our observations by IF analysis.

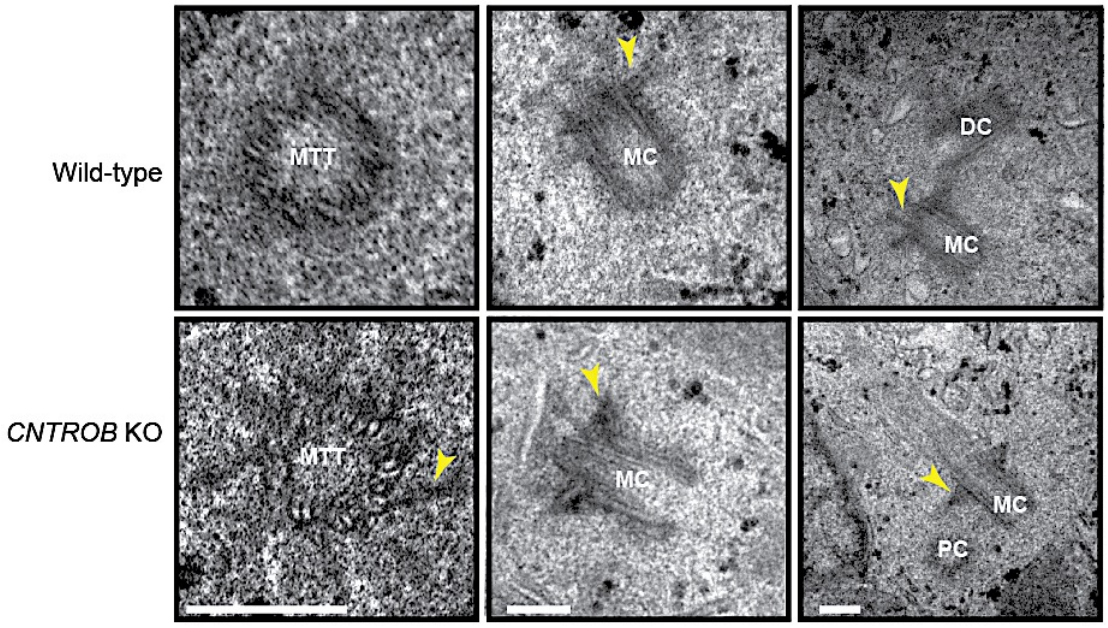

Figure 3.12: Centrobin-deficient cells show normal centrosome morphology

Transmission electron microscopy of characteristic features of the centrioles. Structures such as microtubule triplets (MTT), appendages (yellow arrowheads), mother centriole (MC), daughter centriole (DC), and procentriole (PC) can be visualised. Scale bars, 500 nm.

3.8 Centrobin-deficient cells show normal proliferation

To ascertain that any phenotype observed as a result of loss of centrobin was indeed due to its absence and not an off-target effect, we generated centrobin rescue cell lines using the pCNTROB generated in section 3.5. Western blotting analysis of the clones picked after 14 days under blasticidin selection shows variation in the level of centrobin re-expressed among stable centrobin-rescue clones (Figure 3.13A). After screening, we selected the rescue clone with centrobin expression level comparable to the wild-type (Figure 3.13A, clone 3) and this clone was selected for further experiments in this project. Using immunofluorescence microscopy, we also confirmed the re-expression of centrobin and its localisation to the centrosome in our centrobin-rescue cells (Figure 3.13B).

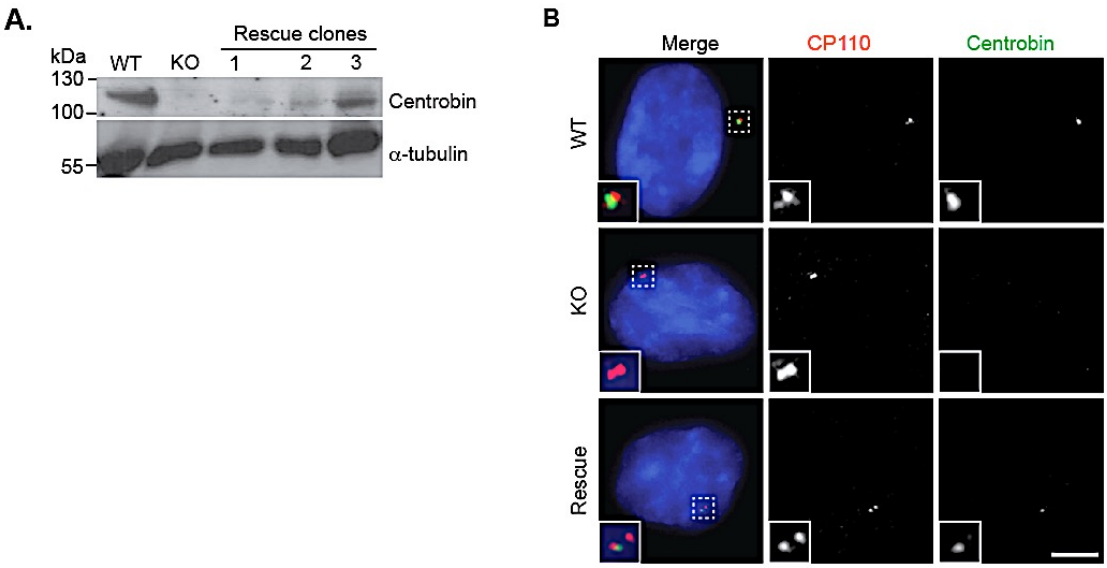

Figure 3.13: Stable re-expression of centrobin to generate rescue cell lines.

A. Cell lysates from the indicated cell lines were analysed by western blotting using monoclonal antibody against centrobin. α-tubulin was monitored as a loading control. **B.** IF microscopy images of wild-type (WT), *CNTROB* knockout (KO) and centrobin rescue (Rescue) cells after immunostaining with antibodies that detect centrobin (green) and CP110 (red). Scale bar, 5 μm.

Several studies using siRNA-mediated depletion of centrobin have reported defective centriole duplication and impaired cytokinesis (Zou et al. 2005, Lee et al. 2009, Song et al. 2010, Jeffery et al. 2010). Knockdown of centrobin in a lung cancer cell line resulted in significant p53/p38-dependent G1/S cell cycle arrest (Song et al. 2010). Since centrobin-deficient cells were viable in culture, we used proliferation and FACS analysis to detect any cell cycle aberrations in both *CNTROB* knockout and rescue cell lines. As shown in Figure 3.14 and Appendix 3, the proliferation and cell cycle profile remained unaltered in both cell lines and the doubling times were comparable to the wild-type population.

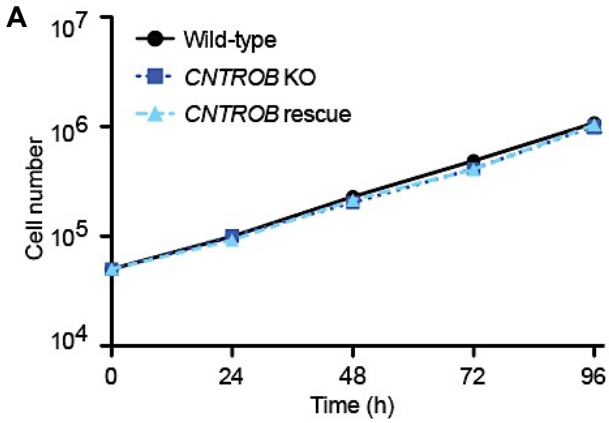

B.

Cell line	Doubling time
WT	24.3±0.6
KO	24.9±1.9
Rescue	25.2±0.8

C

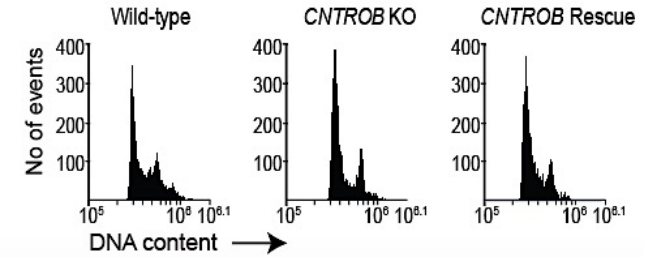

D.

Cell line	Cell cycle stage (%)		
	G1	S	G2/M
WT	55±7	18±4	21±5
KO	58±5	19±1	18±3
Rescue	57±6	23±1	14±4

Figure 3.14: Centrobin null and rescue cell lines show no proliferation defect.

A. Cells were plated at $5x10^4$ cells and counted at every 24 h for 96 h. N=at least 5 independent experiments and error bar indicates standard error of mean (SEM). No significant difference was observed between WT, KO and rescue cell line at any time point. **B.** Mean doubling time ± SEM for WT, KO and rescue cell line. No difference was observed among cell lines. **C.** Representative cell cycle profile of cells with indicated genotype analysed by FACS after staining with 20 µg/ml PI. **D.** Quantitation of the mean percentage ± SEM of cells in each stage of the cell cycle from three independent experiments where 10,000 cells were analysed per experiment per cell line.

3.9 Centrobin-deficient cells show centriole duplication defects

Centrobin has been previously reported as an essential centriole duplication factor (Zou et al. 2005). Surprisingly, our IF and EM analysis showed no defect in the localisation, distribution or abundance of centrosomal proteins investigated in this study (section 3.7). However, using Cep135 and centrin3 as centriole markers, we observed an increase in the frequency of acentriolar and monocentriolar cells in our centrobin-deficient cells (Figure 3.15). The mechanism through which these acentric and monocentric cells undergo cell division remains unclear. To understand this, we attempted to generate wild-type and centrobin null cells stably expressing GFP-centrin1 and H2B-RFP, an approach that has been successfully used in our laboratory to monitor cell and centrosome duplication (Dodson et al. 2007). Unfortunately, we obtained no positive clones after screening >100 clones by immunofluorescence analysis (data not shown). Since transient transfection of both plasmids in U2OS cells showed robust expression of the proteins encoded by cDNA on the plasmids, we speculated that there was either strict regulation of both protein expressions in hTERT-

RPE1 compared to the human carcinoma U2OS cells. This precluded us from carrying out live cell microscopy with GFP-centrin1 and H2B-RFP-expressing cells.

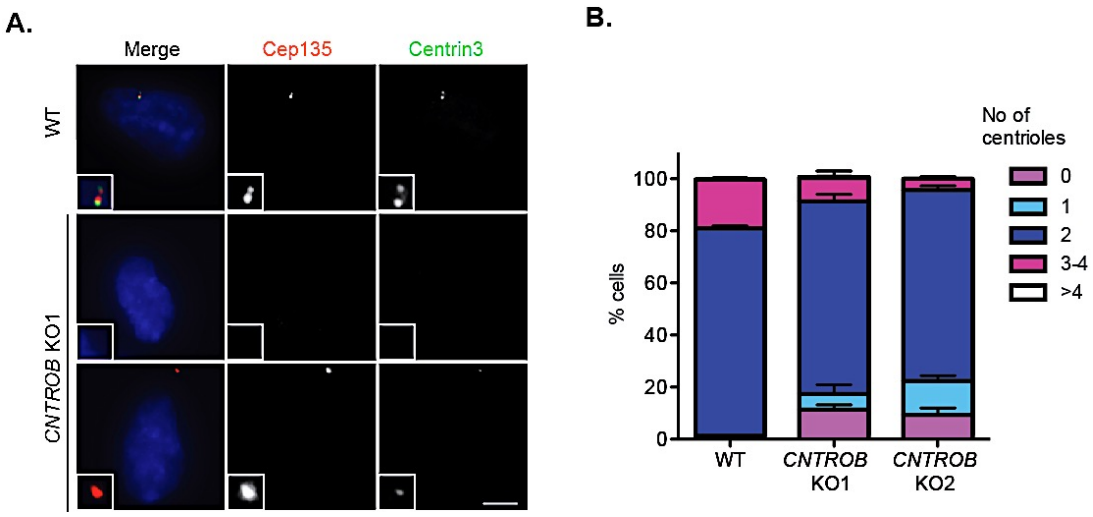

Figure 3.15: Loss of centrobin results in defective centriole duplication.

A. Representative IF micrograph of WT and *CNTROB* KO cells using antibody to centrin3 (green) and Cep135 (red). Note acentric and monocentric cells in *CNTROB* KO cells. Scale bar, 5 μm. **B.** Quantitation of number of centrioles per cell in 100 cells of 3 independent experiments. Bar graph represents mean ± SEM.

3.10 Discussion

It is widely believed that most centrosome duplication processes and proteins are highly conserved at least among vertebrates (Strnad and Gönzy, 2008; Azimzadeh and Marshall, 2010; Azimzadeh, 2014; Stearns and Fırat-Karalar, 2014). In this study, we provide bioinformatic analysis that supports the existence of high level of homology among the vertebrate centrobin orthologues. They share synteny and high degree of amino acid conservation that may be indicative of domain conservation and potentially conserved functionality. Our work also focused on the most studied centrobin isoform (alpha), although several other unconfirmed isoforms are available in the NCBI database. Proteomics and transcriptomics analyses of tissue-specific expression of centrobin show that the testis, a male organ with several tissue-specific proteins, has the highest expression level of centrobin while the endometrium has the second-highest level of expression (Fagerberg et al. 2014). However, centrobin is ubiquitously expressed (Fagerberg et al. 2014) and its expression levels fluctuate depending on the cell cycle stage (Zou et al. 2005).

We also successfully generated a novel anti-centrobin monoclonal antibody using the very well-established hybridoma technology. The loss of centrobin signal after siRNA-mediated depletion and the absence of centrobin signal in our *CNTROB* KO hTERT-RPE1 cells confirmed the specificity of our antibody. Likewise, the antibody recognised exogenous centrobin expressed from plasmid constructs that were cloned in this study. Similar to published observations, we also show here that the overexpression of centrobin causes cytosolic aggregates that were later revealed to be due to its interaction with microtubules (Zou et al. 2005, Gudi et al. 2011). In agreement with our bioinformatics analysis showing a high degree of vertebrate of centrobin conservation, we found that our monoclonal anti-centrobin antibody also detected its orthologue at the chicken centrosome and recognises *Danio rerio* centrobin but not the *Drosophila* equivalents by immunoblot (shown in Chapter 4). This also agrees with the low level of homology between human and *Drosophila* centrobin.

siRNA-mediated depletion of centrosomal proteins has been widely used to delineate the sequential order of centrosome assembly and protein functions. It has been the tool used for investigating the roles of centrobin in the centrosome duplication process. To eliminate the possibilities of off-target effects, transient depletion and residual centrobin functionality that are often presented by siRNA, we used a more robust CRISPR/Cas9 technology for disrupting the human *CNTROB* locus. Interestingly, contradicting results have been observed for centrosomal proteins using CRISPR/Cas9 and siRNA technology. For example, in our laboratory, we have shown that siRNA mediated depletion of centriole linker, C-Nap1, affects ciliation capacity, which was unaffected in *C-NAP1* knockout cells. Further investigation

carried out by transfecting the *C-NAP1* knockout cells revealed an off-target effect of the siRNA resulting in defective ciliogenesis that was previously observed (Conroy et al. 2012, Flanagan et al. 2017). For the current study, we used two independent gRNAs targeting exons 1 and 4, respectively, both of which successfully disrupted the *CNTROB* locus with similar targeting efficiency of approximately 10%. Reproducible phenotypes from our *CNTROB* KO clones with different mutations also confirm the authenticity of our reported phenotypes.

Previous studies have shown that centrobin is required for centriole duplication, faithful cytokinesis and its loss may potentially impact cell viability (Zou et al. 2005; Gudi et al. 2011, 2014; 2015). It has also been previously reported that centrobin depletion results in G1-S cell cycle arrest depending on the p53 status; *TP53* nulls did not induce cell cycle arrest when centrobin was lost (Song et al. 2010). In *Drosophila*, loss of centrobin in non-neuronal cells (such as ganglion mother cells) did not impact centriole assembly or cell proliferation (Januschke et al. 2013). Here, we observed no crucial defect on cell proliferation after centrobin ablation in non-transformed hTERT-RPE1.

Centrobin is recruited to the daughter centriole in early G1/S-phase of the cell cycle when procentriole is being assembled (Zou et al. 2005). As a core component of the centrosome, it was necessary for us to carefully investigate the centrosome composition of our *CNTROB* KO. Surprisingly, our immunofluorescence microscopy analysis showed robust localisation of cartwheel, centriole linker, appendages and PCM proteins. For example, pericentrin, a PCM marker localises to interphase centrosomes, and as expected, we noticed an increase in PCM volume in mitotic cells. This observation and the localisation of maturation markers (Kizuna, Cep164 and ninein) are indicative of efficient centriole maturation in *CNTROB* KO cells. In agreement with the immunofluorescence microscopy, electron microscopy analysis also revealed normal procentriole assembly and localisation of mother centriole appendages to only the mother centriole in proliferating *CNTROB* KO hTERT-RPE1 cells. None of our TEM analysis or immunofluorescence microscopy of the centrioles showed appendage localisation to both centrioles in an individual centrosome. This contrasts with the observation in specialised *Drosophila* neuroblast and sensory neuronal cells where loss of centrobin confers mother centriole functionality on both centrioles (Januschke et al. 2013, Gottardo et al. 2015). Interestingly, daughter centriole conversion to mother centrioles in the absence of centrobin was not observed in other *Drosophila* cell types (Januschke et al. 2013).

The integrity of the cartwheel component was revealed by the localisation of hSas6, Cep135 and CPAP to the centrosome of *CNTROB* KO cells. Cep152 and hSas6 act upstream of centrobin and are crucial for centrobin's recruitment during centriole biogenesis (Gudi et al. 2011). Cep152 interacts with Cep63 to form a complex that co-regulates their localisation to the procentriole and is essential for effective timing of hSas6 recruitment for cartwheel

assembly (Brown et al. 2013). Despite the efficient recruitment of cartwheel proteins in centrobin-deficient cells and centrobin being one of the early proteins recruited during centriole biogenesis (Gudi et al. 2011), we also observed an increase in monocentric and acentric cells in the absence of centrobin. Further investigation into centriole duplication in our *CNTROB* KO would have facilitated our understanding of the mechanism through which our cells proliferate. Although not investigated in this study, based on the available literature, it can be imagined that disruption of Cep152-centrobin-hSas6 interaction may impact the kinetics, dynamics, and stability of cartwheel and procentriole assembly to result in the defective centriole duplication observed in our *CNTROB* KO, as was the case when Cep152-Cep63 interaction was disrupted (Brown et al. 2013).

Taken together, our data confirm centrobin as a centriole duplication factor that potentially affects the assembly kinetics and stability of the procentriole during centriole biogenesis. However, it is not essential for proper proliferation and cell viability in human cells. Since centrobin interacts with other centriolar proteins, the PCM and cartwheel proteins as well as with microtubules, we next investigated the roles of centrobin in centrosome functions such as ciliogenesis and the DNA damage response. These analyses are presented in chapters 4 and 5, respectively.

4 Centrobin regulates primary ciliogenesis in vertebrate systems

4.1 Introduction

The centrosome is the major microtubule organising centre (MTOC) in animal somatic cells. It is composed of orthogonally arranged mother and daughter centrioles that are embedded in a proteinaceous PCM (Nigg and Raff, 2009; Mennella et al. 2014). The mother centriole carries the fibrous distal and sub-distal appendages which are required for plasma membrane docking, microtubule anchoring and making transition fibers during cilium formation (Sorokin, 1962; Nigg and Raff, 2009; Kobayashi and Dynlacht, 2011).

Cilia are highly conserved sensory organelles that extend from the cell surface to the extracellular space. The existence of motile and primary (immotile) cilia has been well reported; most cell types have primary cilia (Pazour and Witman, 2003). Structurally, the core of the primary cilium, the axoneme, consists of nine doublet microtubules that are surrounded by a cilium-specific phospholipid membrane that is functionally different from the cell membrane, through its enrichment for signalling molecules and receptors (Pazour and Witman 2003, Kobayashi and Dynlacht 2011). Structural components are moved from the cell body to the cilium tip to allow for ciliary axoneme and membrane extension in a highly ordered process mediated by intraflagellar transport (IFT) proteins (Hsiao et al. 2012). To facilitate axoneme nucleation and extension, centrioles migrate and dock to the cell surface of non-proliferating G0/G1 cells and they are disassembled to allow for centriolar roles in mitotic spindle assembly when the cell cycle progresses.

Primary cilia sense and transduce extracellular signals, such as Wnt and hedgehog, which are essential for cell development, differentiation and proliferation (Pazour and Witman 2003, Goetz and Anderson 2010). The importance of primary cilia in development and embryogenesis has been demonstrated experimentally in vertebrates where they are essential for viability, organogenesis and organ positioning (Huangfu et al. 2003; Goetz and Anderson, 2010). Defects in primary cilium formation or activity cause a diverse range of human developmental disorders that particularly affect the kidney, eye, liver, brain and skeleton; they are collectively termed the ciliopathies (Huangfu et al. 2003; Pazour and Witman, 2003; Goetz and Anderson, 2010; Bettencourt-Dias et al. 2011).

The mother centriole carries the appendages which play obvious roles in primary ciliogenesis (Delgehyr et al. 2005; Ishikawa et al. 2005; Graser et al. 2007; Daly et al. 2016). The distal appendages promote membrane docking during mother centriole to basal body conversion, while the subdistal appendages become the basal feet that anchors microtubules. Although the daughter centriole is still attached to the mother centriole carrying the cilium, its role in

primary cilium formation has not been well studied. The daughter centriole lacks both the distal and subdistal appendages, and interestingly, some proteins, such as centrobin, PARP-3, Neurl-4 and Cep120, have been shown to localise preferentially to the daughter centriole (Zou et al. 2005; Mahjoub et al. 2010; Li et al. 2012).

Recently, there has been increasing interest in the role of daughter centrioles in ciliogenesis. For example, live cell super-resolution microscopy of mouse brain ependymal cells was used to show that the daughter centriole is essential for deuterosome formation which contributes at least 90% of the centrioles necessary for differentiation process in multiciliated cells and refuted the existence of a *de novo* pathway of centriole duplication (Al Jord et al. 2014). Neurl-4, a daughter centriole protein that prevents ectopic microtubule organisation and interacts with CP110, has been recently implicated in ciliogenesis. Neurl-4 transiently localises to the mother centriole during ciliogenesis and cells depleted of Neurl-4 showed defective CP110 removal for proper primary cilium assembly (Li et al. 2012; Loukil et al. 2017). The cellular depletion of regulators of centrosome duplication factors such as CPAP, STIL, Cep152 and hSas6 causes ciliation defects (Wu and Tang, 2012; David et al. 2014; Loukil et al. 2017). Interestingly, monocentric cells carrying just the mother centrioles due to depletion of centriole duplication factors were unable to form cilia, thereby implicating daughter centrioles in proper cilia formation (Loukil et al. 2017).

Centrobin's preferential localisation to daughter centriole has been well described (Zou et al. 2005, Jeong et al. 2007, Januschke et al. 2013). However, its localisation to both the mother and daughter centriole in mouse hippocampal neurons has also been reported (Shin et al. 2015). Recently, the presence of a cytosolic pool of centrobin that functions in microtubule nucleaction and stabilisation, independent of the centrosomal centrobin, has been demonstrated (Shin et al. 2015). *Drosophila* centrobin has been shown to inhibit ciliation capacity at the daughter centriole and that the loss of centrobin from sensory neurons enables the daughter centriole to act as a basal body (Gottardo et al. 2015). Interestingly, when pericentrin-AKAP450 centrosomal targeting (PACT) domain-labelled centrobin was used to force the expression of *Drosophila* centrobin to the mother centriole, it prevented mother centriole to basal body conversion (Gottardo et al. 2015). A role for centrobin in vertebrate ciliogenesis is unknown. However, rat *hypodactylyl* mutants have been shown to endogenously express C-terminal centrobin truncation mutant (Liska et al. 2009). These rats show skeletal abnormalities and male infertility due to problems in the assembly of the axoneme of the sperm flagellum, phenotypes related to ciliopathy (Liska et al. 2009, 2013). Interestingly, overexpression of full-length centrobin in these mutants rescues skeletal defects but not infertility (Liska et al. 2013).

Centrobin and CPAP interact through their N-terminals (Wu and Tang 2012, Gudi et al. 2014, Zheng et al. 2016) and the N-terminal of CPAP participates in both cilia assembly and disassembly (Wu and Tang 2012, Gabriel et al. 2016). CPAP was one of the first centrosomal proteins that was identified in the pathogenesis of microcephaly and Seckel syndrome (Bond et al. 2005, Wu and Tang 2012, McIntyre et al. 2012, Gabriel et al. 2016). Previous studies have shown that CPAP-tubulin interaction is crucial for regulating centriole and ciliary length in human cells (Wu and Tang, 2012; Zheng et al. 2016). Centrobin regulates cellular levels of CPAP through regulating its availability for proteosomal degradation, depending on the cell cycle stage (Gudi et al. 2014) and both centrobin and CPAP interact and stabilise tubulin. However, the relevance of centrobin-CPAP in primary cilia formation is still unknown.

With the aim of clarifying the roles of centrobin in daughter centrioles' contribution to ciliogenesis, we studied the impact of centrobin loss on the assembly, structure and function of primary cilia in the centrobin-deficient cells generated in previous chapter. We also investigated centrobin localisation pattern and the effect of increasing cellular centrobin levels. We also determined how the loss of centrobin affects cellular levels of CPAP and CP110 during ciliogenesis. The impact of centrobin loss on embryogenesis and organ patterning in zebrafish was also studied to determine the relevance of centrobin in cilium formation and functions in an entire organism.

4.2 Dynamics of centrobin localisation in ciliated cells

The first step in investigating centrobin in ciliogenesis was to determine its localisation dynamics in serum-starved hTERT-RPE1 cells. In proliferating cells, centrobin localises preferentially to the daughter centriole (Zou et al. 2005). In our study, we used Cep164, a distal appendage marker that is required for ciliogenesis, to mark the mother centriole. In asynchronous cell populations, we observed preferential centrobin localisation to the daughter centriole (Figure 4.1A). However, in ciliated populations, we observed an increase in mother centrioles that carried a small fraction of the centrobin signal (Figure 4.1B-C). In ciliated cells, mother centrioles were identified by the presence of primary cilium markers (IFT88, detyrosinated tubulin or ARL13B). Interestingly, the transient expression of GFP-centrobin in serum-starved hTERT-RPE1 cells showed the localisation of centrobin to the mother centriole (Figure 4.1B). Quantification of mother centrioles carrying centrobin signal, based on detyrosinated tubulin staining for the ciliary axoneme, revealed that in asynchronous cells, only 4% of mother centrioles carried a centrobin signal, which increased to 44% in serum-starved populations (Figure 4.1C). These results are similar to previous observations of a daughter centriole-specific protein, Neurl-4, which transiently localises to the mother

centriole when ciliogenesis was induced in human epithelial and fibroblast cells (Loukil et al. 2017).

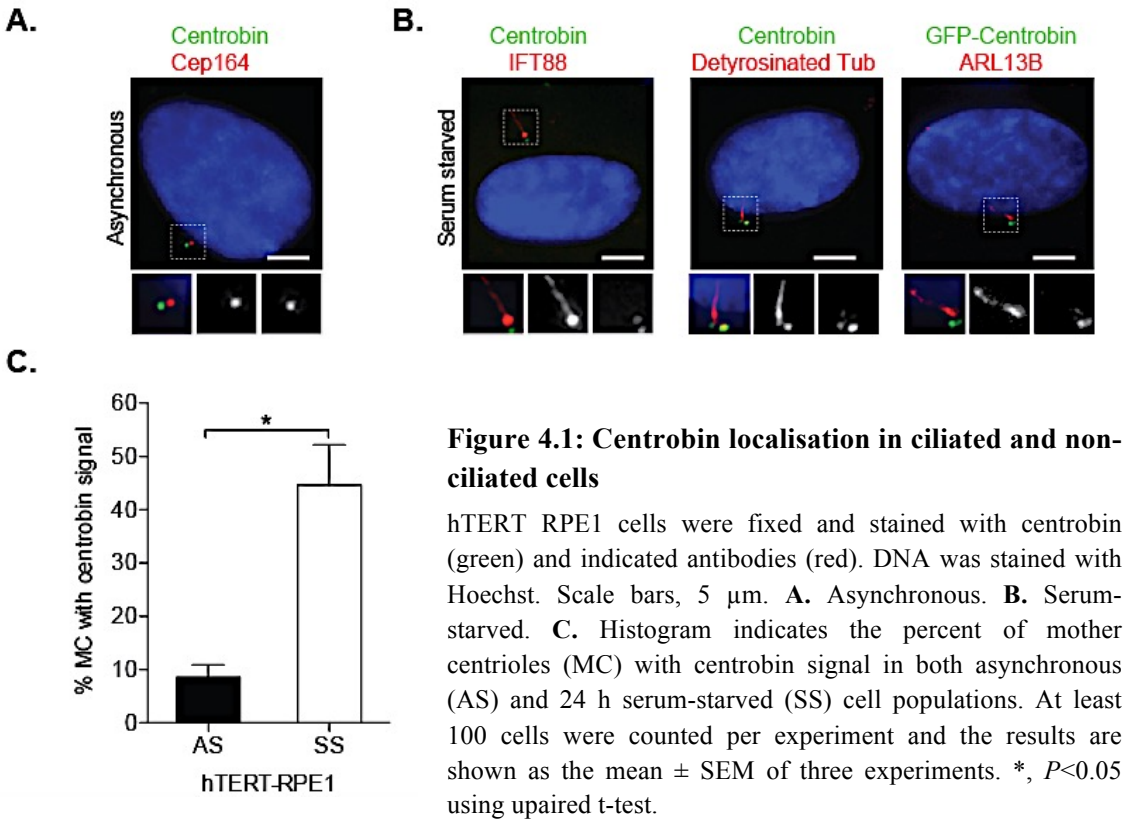

Figure 4.1: Centrobin localisation in ciliated and non-ciliated cells

hTERT RPE1 cells were fixed and stained with centrobin (green) and indicated antibodies (red). DNA was stained with Hoechst. Scale bars, 5 µm. **A.** Asynchronous. **B.** Serum-starved. **C.** Histogram indicates the percent of mother centrioles (MC) with centrobin signal in both asynchronous (AS) and 24 h serum-starved (SS) cell populations. At least 100 cells were counted per experiment and the results are shown as the mean ± SEM of three experiments. *, $P<0.05$ using upaired t-test.

4.3 Centrobin loss reduces ciliation frequency in human cells

Primary cilia are microtubule-based antenna-like organelles that assemble after the docking of mother centriole to the plasma membrane. Centrobin has been previously identified as a negative regulator of ciliogenesis in *Drosophila* (Gottardo et al. 2015) but its role in vertebrate ciliogenesis has not been previously studied. We tested the impact of centrobin loss on the assembly of primary cilia, initially, using siRNA-mediated depletion of centrobin (Figure 4.2) and then in our centrobin null hTERT-RPE1 cell line (Figure 4.3).

To first determine the impact of centrobin loss on primary cilium formation, we used RNAi to mediate protein knockdown and serum starvation to induce ciliogenesis in hTERT-RPE1 cells. Immunoblot analysis showed significant reduction in cellular level of centrobin after siRNA treatment and ciliation induction (Figure 4.2A and B). Using ARL13B to mark the ciliary membrane, we observed a marked reduction in the number of cells with protruding ciliary membrane in centrobin-depleted cell populations. Occasionally, we observed ARL13B signals in cells with partial protein knockdown. After 24 h serum deprivation, we observed no significant difference in ciliation frequency between our controls (70-80%) but we observed <20% of ciliated cells after centrobin depletion. This result suggests that centrobin is required

for primary ciliogenesis and its complete or partial loss abrogates effective ciliogenesis. In contrast to the findings in *Drosophila* where centrobin negatively regulated ciliogenesis (Gottardo et al. 2015), our result aligns with published data that support the requirement of daughter centriole specific proteins in primary cilium formation in human cells (Loukil et al. 2017).

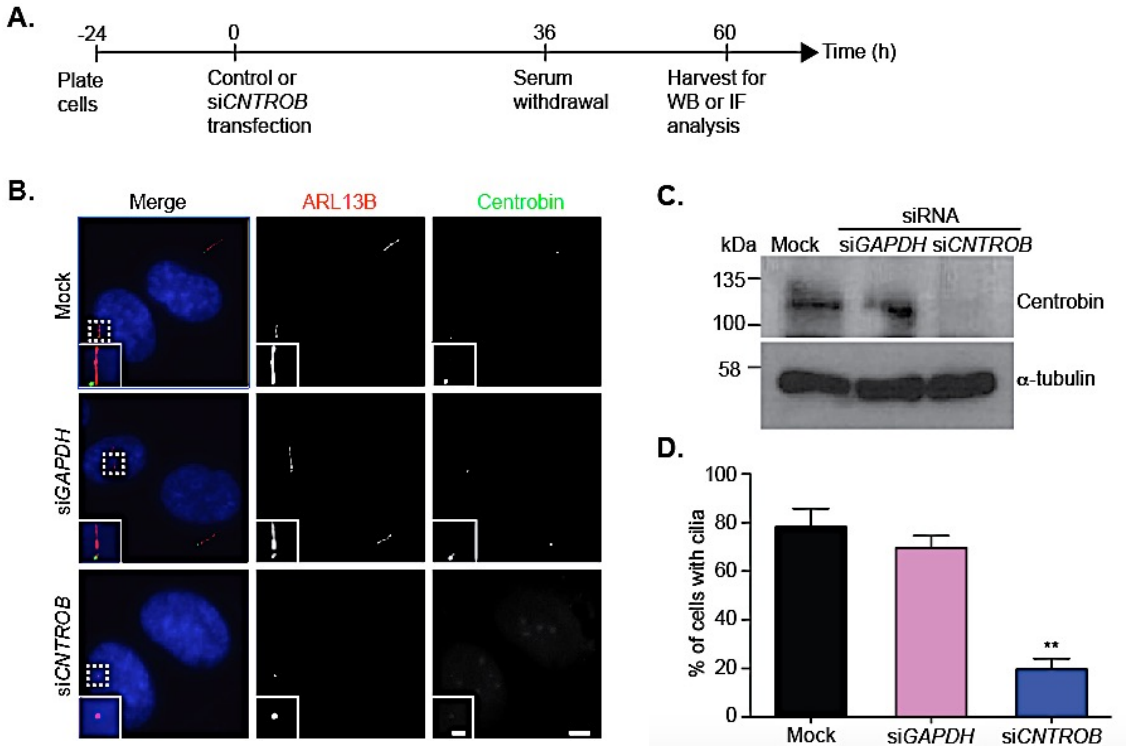

Figure 4.2: siRNA-mediated depletion of centrobin results in reduced frequency of cilia

A. Schematic diagram indicating the experimental setup of siRNA mediated protein depletion followed by serum starvation. **B.** Representative western blot showing reduced centrobin levels of centrobin in siRNA and serum starved cells. si*GAPDH* was used as siRNA control while α-tubulin was used as a loading control. **C.** Representative immunofluorescence micrograph of mock, si*GAPDH* and si*CNTROB*. Ciliary membrane was stained with antibody against ARL13B (red). Antibody to centrobin (green) was used to monitor its cellular level and DNA (blue) was stained with Hoechst. Scale bar, 5 µm, inset scale bar, 1 µm. **D.** Graph shows the percentage of ciliated cells from mock, si*GAPDH* and si*CNTROB* treated cell populations. Histogram depicts the mean ± SEM of 3 independent repeats of which at least 100 cells were counted. **, $P<0.01$; in comparison to the si*GAPDH* control by unpaired t-test.

To further establish that centrobin participates in the ciliogenesis pathway, we took advantage of our previously generated centrobin knockout and rescue cell lines (see section 3.6 and 3.8). The cells were serum-starved for 48 h and fixed for immunofluorescence microscopy. As shown in Figure 4.3A, immunofluorescence microscopy of serum-starved wild-type cells showed the presence of acetylated tubulin and ARL13B which mark the ciliary axoneme and ciliary membrane, respectively. In agreement with our previous si*CNTROB* observation,

centrobin null cells showed no ciliary structure as indicated by the absence of an ARL13B signal and a protruding axonemal acetylated tubulin signals. Interestingly, this ciliogenesis defect was rescued by stable (Figure 4.3A-B) and transient (data not shown) re-expression of centrobin in the centrobin null hTERT-RPE1 cell line. We quantified the percentages of ciliated cells and found significant reduction in cilia frequency in centrobin null cells (Figure 4.3B). These data suggest a regulatory role for centrobin in the cilium formation pathway and that it is indeed a positive regulator of ciliogenesis in human cells.

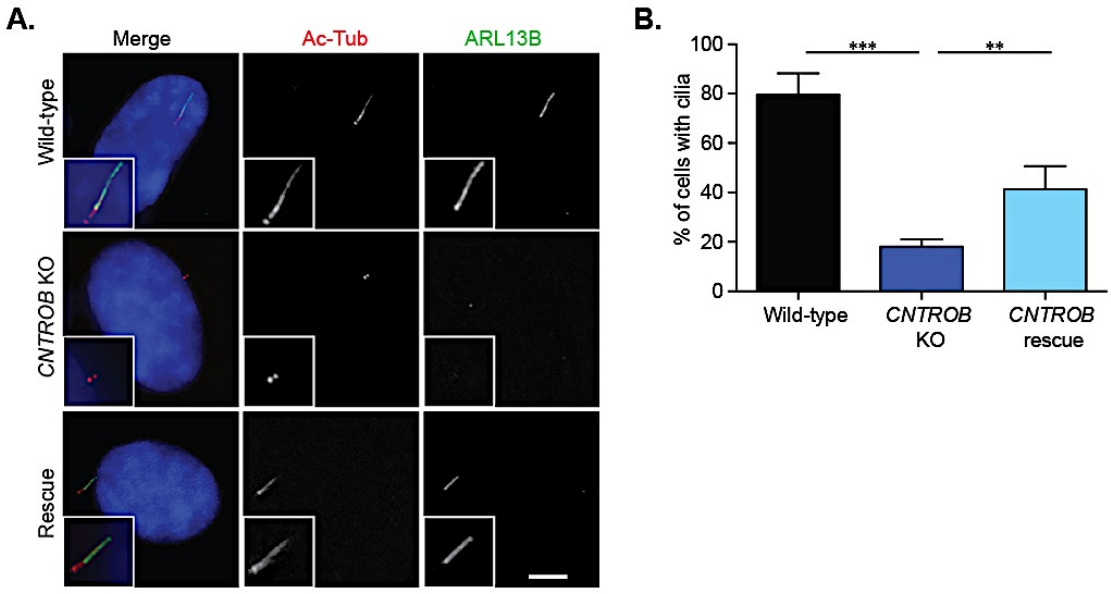

Figure 4.3: Centrobin is a positive regulator of ciliogenesis in human epithelial cells

A. Immunofluorescence micrograph of wild-type, *CNTROB* KO and centrobin rescue clones after 48 h serum starvation and stained with antibodies to acetylated tubulin (red) and ARL13B (green). DNA was visualised with Hoechst (blue). Scale bar, 5 µm**. B.** Quantitation of ciliated cells in indicated cell lines after 48 h serum starvation. Histogram shows the mean ± SEM of 3 independent repeats of which at least 100 cells were counted. **, $P<0.01$; ***, $P<0.001$; in comparison to the indicated samples by unpaired t-test.

4.4 *Drosophilia* centrobin supports human ciliogenesis

During our investigation of centrobin involvement in ciliogenesis, a concurrent but independent study of *Drosophila* sensory neurons showed that depletion of *Drosophila* centrobin (Cnb) resulted in increased frequency of biciliated cells and its forced expression abrogated ciliation (Gottardo et al. 2015). We did not observe any biciliated cells in our *CNTROB* null hTERT-RPE1 population by immunofluorescence and electron microscopy. This difference between human and *Drosophila* centrobin may be due to significant divergence of centrobin in the two organisms (22.61% homology, see Figure 3.2) or the absence of appendage proteins in *Drosophila*. Interestingly, a divergence in cilia-dependent SHh signalling in mammals and *Drosophila* has also been previously reported (Varjosalo et

al. 2006). Here, we cloned *Drosophila* centrobin and investigated its ability to rescue ciliogenesis in *CNTROB* null hTERT-RPE1 cells.

4.4.1 Cloning and transient expression of *Drosophila* centrobin

To determine if *Drosophila* and human centrobin share functional homology, we cloned *Drosophila* centrobin transcript A (NM_139423) in the into pEGFP-C1 vector (*Drosophila* mRNA was kindly gifted by Ms. Caitríona Collins). Although our cloning was successsful, the sequencing data revealed K388R, K503R and S614P mutations in the clone used. We decided to proceed with this plasmid in our rescue experiment. First, we confirmed the expression and functionality of the protein by assessing its ability to localise to human centrosomes by transient transfection into U2OS cells. We used pericentrin, an integral component of the PCM, to mark the centrosome. As evident in the immunofluorescence microscopy image, both *Drosophila* (GFP-DCnb) and human (GFP-hCNTROB) centrobin localised to the human centrosome while the untreated (UT) cells lacked centrosomal signal (Figure 4.4A). This result shows that the centrosome localising signal present on the *Drosophila* centrobin was sufficient for localising the protein in human, and thus, may retain its functions and interactions with human centrosomal proteins.

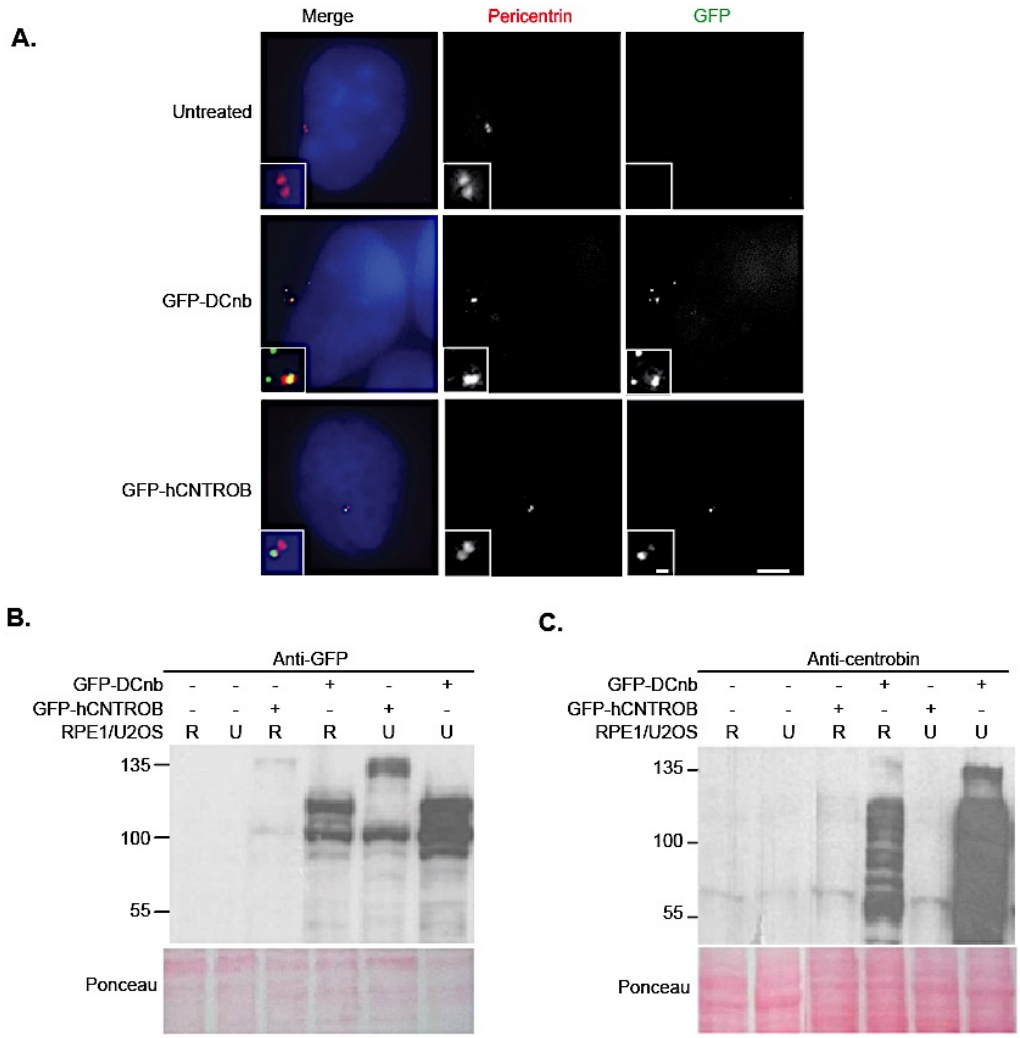

Figure 4.4: *Drosophila* centrobin localises to centrosomes in human cells

A. IF microscopy analysis confirming the expression and localisation of GFP-DCnb and GFP-hCNTROB in U2OS using pericentrin (red) to mark the centrosome and DNA was visualised using Hoechst. Scale bar, 5µm and inset bar, 1 µm. **B.** Western blot analysis of overexpression of GFP-DCnb and GFP-hCNTROB in hTERT-RPE1 (R) and U2OS (U) 24 h post-transfection. Cell lysates were probed with GFP antibody or **C.** with anti-centrobin. Ponceau was used as loading control (*Drosophila* plasmid and western blots were prepared along with Ms. Gemma Hyland).

We also analysed cell lysates of hTERT-RPE1 and U2OS cells that transiently expressed either GFP-DCnb or GFP-hCNTROB by western blotting using either GFP or centrobin antibody for visualising the protein (Figure 4.4B and C). We observed that both proteins were expressed in the two cell lines used in this experiment. They run at their respective predicted sizes of approximately 120 and 140 kDa respectively, when probed with antibody to the GFP-tag. As expected, the untransfected cell lysates showed no visible band while other bands on the immunoblot may indicate mobility shift after protein modifications or degradation products from high expression levels of the protein (Figure 4.4B). Using our previously characterised antibody, we observed the expression of the 140 kDa GFP-centrobin in both

hTERT-RPE1 and U2OS cells, with U2OS having higher protein expression levels. Although the low level of the endogenous protein in the untransfected cells could not be seen on this western blot, the very high expression level of degraded proteins makes it difficult to identify the endogenous protein (Figure 4.4C). Interestingly, our human anti-centrobin did not recognise the overexpressed *Drosophila* centrobin in any of the cell lines used. This result highlights the low protein sequence homology between centrobin in human and *Drosophila* and that the antigenic region used for our antibody was not conserved in *Drosophila* (Figure 4.4C).

4.4.2 Expression of *Drosophila* centrobin rescue ciliogenesis in hTERT-RPE1 centrobin nulls

We next explored the impact of *Drosophila* centrobin in human ciliogenesis using wild-type and centrobin null hTERT-RPE1 cells that were transiently transfected with GFP-hCNTROB, or GFP-DCnb, with empty GFP vector as a control. This was followed by serum starvation for 24 hours, staining for ARL13B to detect the ciliary membrane and staining for centrin3 to mark the basal body. We observed no significant difference in ciliation frequency after transfection of wild-type hTERT-RPE1 with GFP-DCnb or GFP-hCNTROB. Interestingly, both human and *Drosophila* centrobin rescued ciliogenesis in *CNTROB* null cells, suggesting that the regulatory role played by the protein varies with species (Figure 4.5).

As previously discussed in section 4.4.1, the *Drosophila* centrobin is recruited to the human centrosome and may interact with human centriolar proteins and participate in human centriole functions such as ciliogenesis. Strikingly, cilia that were formed in the presence of both human and *Drosophila* centrobin were not structurally different, although it was possible that the functionality may not be fully restored. While the functionality of cilia formed when *Drosophila* centrobin was transiently expressed was not tested in this study, a previous report has shown the divergence of hedgehog signalling and phosphorylation in mouse and fly. The binding and reactivity of *Drosophila* smo in a mouse model did not have any effect on the SHh signalling pathway involving mouse Cos2 (Varjosalo et al. 2006). However, our result clearly implicates the functionality of *Drosophila* centrobin in the human primary cilium assembly.

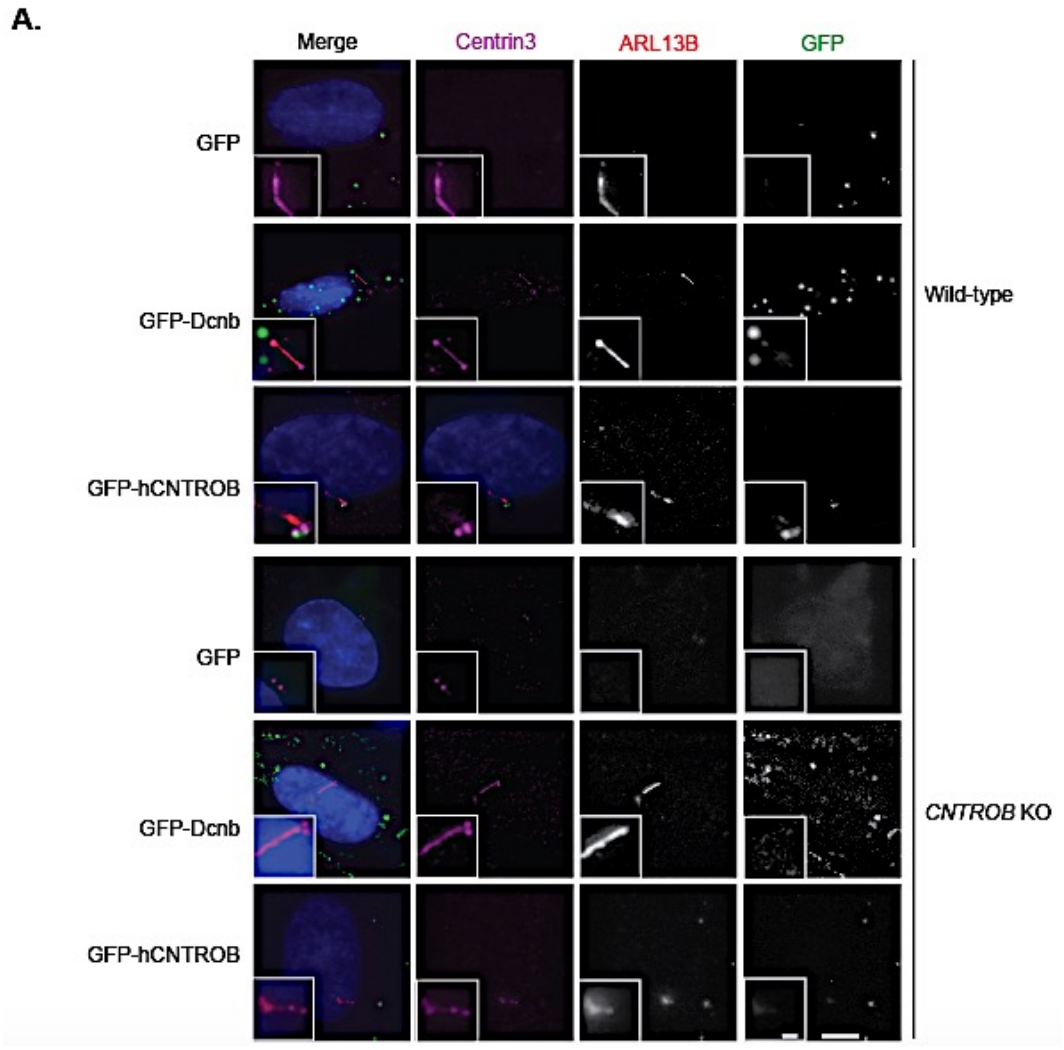

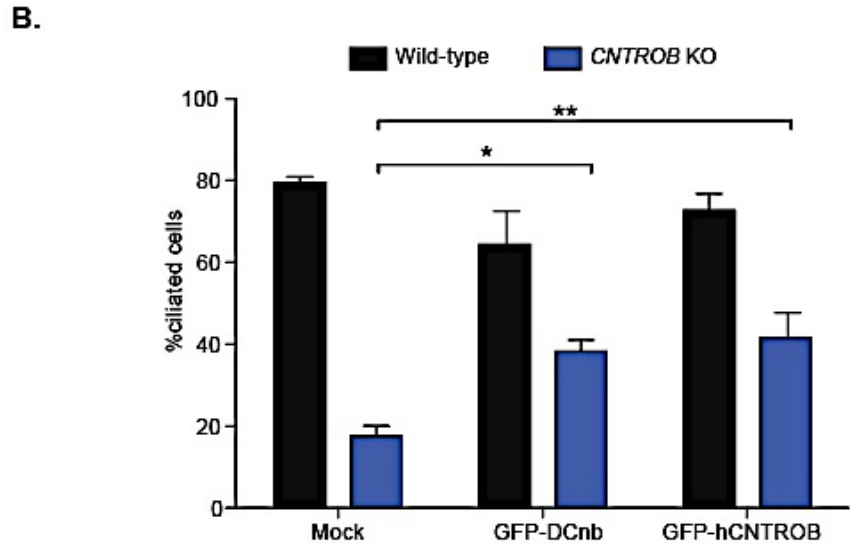

Figure 4.5: *Drosophila* centrobin rescues ciliogenesis in centrobin null hTERT-RPE1 cells

A. Immunofluorescence micrograph of wild-type and *CNTROB* KO stained with centrin3 (magenta), ARL13B (red), GFP signal (green) and DNA was visualised with Hoechst (blue). Scale bar, 5 µm, inset bar, 1 µm **B.** Quantitation of percentage of ciliated cells in wild-type and *CNTROB* KO based on

ARL13B signal. Histogram shows mean ± SEM of 3 separate experiments in which at least 100 cells were counted. **, $P<0.01$; in comparison to the indicated samples by unpaired t-test.

4.5 Zebrafish centrobin acts as a positive regulator of ciliogenesis

Most centrosomal proteins are highly conserved for their structural and functional properties (reviewed by Carvalho-Santos et al. 2011). The centrioles play dual roles, as core of the centrosome where they contribute to forming the mitotic spindle, and as basal body that template the primary cilium. The primary cilium serves important sensory functions during embryonic development and organ homeostasis that can be modeled in zebrafish embryos. The Kupffer's vesicle (KV) in zebrafish embryos is essential for left-right symmetry through modulating fluid movement (Kramer-Zucker et al. 2005). Defective primary cilium structure and function has been linked to diseases such as PKD, blindness and skeletal deformation in vertebrates (Kramer-Zucker et al. 2005, Goetz and Anderson 2010, Bettencourt-Dias et al. 2011, McIntyre et al. 2012). To investigate the consequences of centrobin ablation on vertebrate development and organogenesis, we first determined centrobin sequence using 5' RACE followed by morpholino-mediated depletion of centrobin in zebrafish embryos.

4.5.1 5'RACE, homology and sequence analysis of zebrafish centrobin

To identify zebrafish centrobin coding sequence, we performed a 5' RACE experiment using a Roche 5'/3' RACE kit. The reverse primers used were designed to regions of high conservation between human and predicted *Clupea harengus* (XP_01267307.1) and *Salmo salar* (XP_014051132.1) centrobin sequences and are indicated as GSP1, 2, 3 or 4 with red, brown, blue or teal arrows, respectively (Figure 4.6). The primers were designed based on our analysis of the transcriptome and expressed sequence tag (EST) databases. Table 4.1 shows zebrafish ESTs cloned from different zebrafish tissues and their homology to the human centrobin isoform alpha. These sequences helped in effective planning of the 5' RACE experiment.

Table 4.1: Zebrafish ESTs used in this study and their homology to the human centrobin alpha using tblastn for 2 sequences.

EST reference	Tissue Origin	Coverage (%) to human CNTROB	Identities (%)to human CNTROB
CT670105.2	Myoblast	22	31
CO356610.1	Adult testis	20	47
CT682788.2	Myoblast	15	53
EB909336.1	Testis	10	45
CK697594.1	Whole embryo	13	42

The DNA sequence obtained from the 5' RACE experiment with zebrafish mRNA (approximately 500 bp) showed a potential start codon with an in-frame upstream stop codon, which is consistent with the EST database (Figure 4.6A). Using the obtained 5'RACE sequences to design a forward primer and the EST database to predict the stop codon, we successfully used RT-PCR to clone 2610 bp full-length centrobin from zebrafish embryo cDNA. This was cloned in two fragments of approximately 1900 and 1600 bp, respectively (Figure 4.6B) that were assembled into pGEM-T-easy and sequenced. We confirmed that the sequence obtained matched the previously analysed ESTs in the NCBI database. Based on Clustalw omega estimation of sequence homology, zebrafish and human centrobin share approximately 39% homology and regions with high sequence homology are highlighted in yellow (Figure 4.6C).

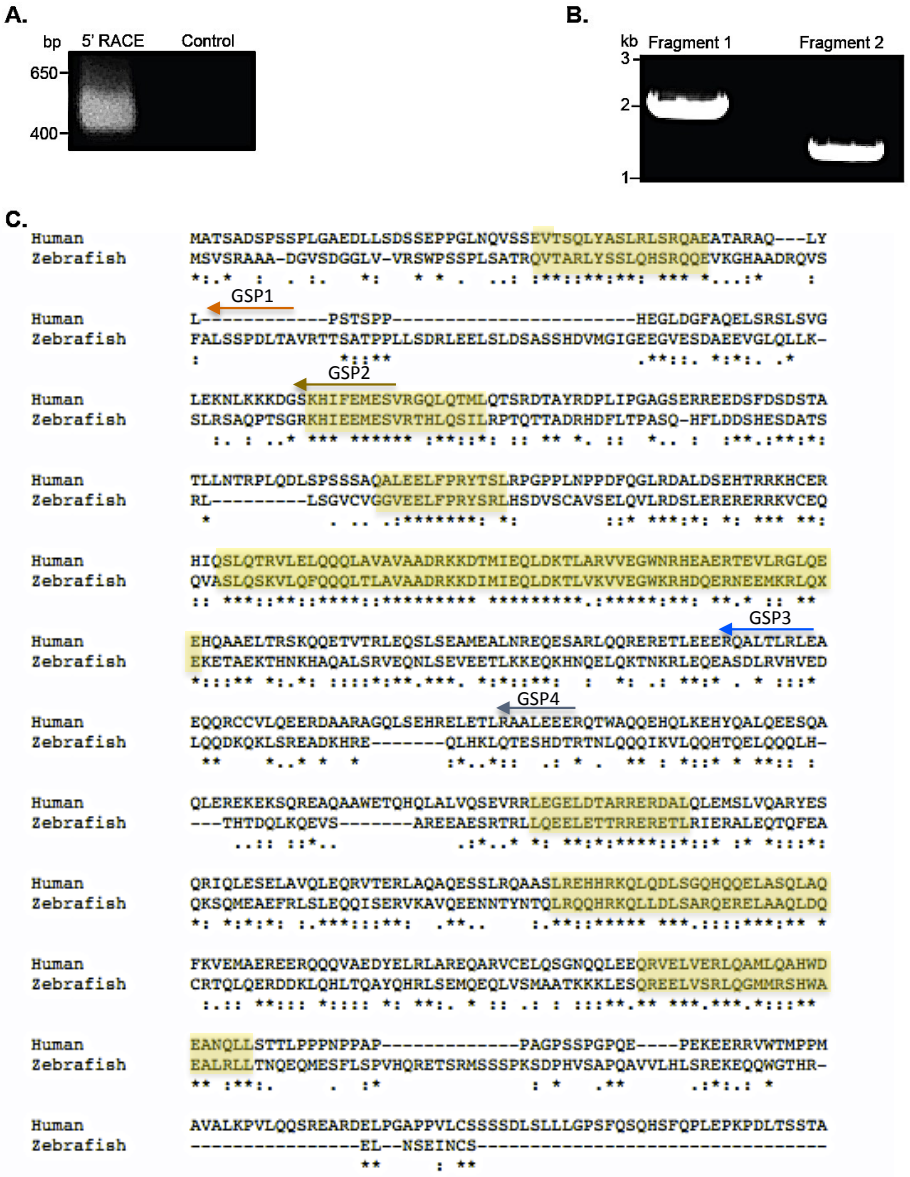

Figure 4.6: Human and zebrafish centrobin share high protein sequence identity.

A. 5' RACE product (approximately 500 bp) amplified using 5'/3' Roche kit primers and GSP 2,3 and 4. **B.** PCR amplification of full-length centrobin from zebrafish embryo cDNA in 2 fragments of

approximately 1900 and 1600 bp that we assembled into pGEM-T-Easy. **C.** Sequence alignment of human and zebrafish centrobin. The highlighted regions indicated high similarity. The red, brown, blue and teal are the regions to which primers GSP1-4 for 5' RACE were designed; * indicates the same amino acid, : indicates amino acids with similar side chains; . indicates amino acids with similar charge.

4.5.2 Zebrafish centrobin controls effective primary cilium formation

Having confirmed the zebrafish centrobin sequence, we subsequently designed two independent antisense morpholino oligonucleotides (MOs) against the ATG and the 5'UTR (MO1 and MO2, respectively) to mediate the knockdown of centrobin. We confirmed the efficacy of the MO by immunoblot analysis of centrobin levels after injecting the embryo with with standard MO control or centrobin MO (Figure 4.7A). In contrast to the *Drosophila* centrobin (Figure 4.4C), the zebrafish centrobin was detected by our monoclonal anti- human centrobin (6D4F4) antibody. This implies a closer homology between the zebrafish and human centrobin, especially in the antigenic region to which the monoclonal antibody was raised. Zebrafish centrobin contains 869 aa and has a predicted molecular weight of approximately 96 kDa. However, it runs at approximately 150 kDa on a SDS-PAGE which is higher than its predicted size and the human centrobin (903 aa). This may be due to different post-translational modifications and acidic amino acid content that result in a mobility shift.The reduced centrobin level resulted in a significant decline in the number and length of cilia in the Kupffer's vesicle (KV) (Figure 4.7B-C). A representative immunofluorescence confocal microscopy stack showing cilia of the KV is shown in Figure 4.7B. Consistent with our previous observation in human cells in which centrobin was required for ciliogenesis, these data suggest that centrobin is indeed a positive regulator of ciliogenesis in vertebrates, distinct from its function in *Drosophila*.

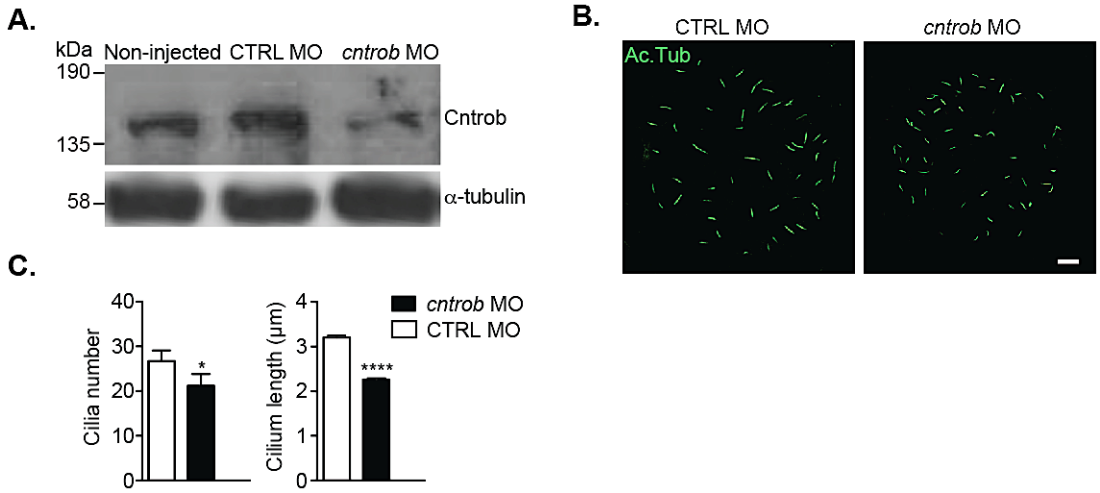

Figure 4.7: Loss of zebrafish centrobin results in reduced cilia frequency and length

A. Reduced level of zebrafish centrobin after MO treatment was confirmed by Immunoblot analysis of deyolked zebrafish embryo 24 h post fertilisation (hpf). α-tubulin was used as a loading control. **B.** Cilia in the Kupffer's vesicle (KV) were visualised by immunofluorescence microscopy staining of acetylated tubulin in 8 somite stage (ss) zebrafish embryos injected with standard control MO (CTRL MO) or MO targeting the translation start site of centrobin (*Cntrob* MO). Scale bar, 10 µm. **C.** Bar charts represent the quantification and statistical analysis of ciliation frequency and length in KV after injection with the indicated MOs at 8-ss stage. Graph shows the mean ± SEM of 4 independent experiments in which 40 CTRL MO and 33 *Cntrob* MO-treated KVs based on acetylated tubulin staining. 1067 and 750 cilia were measured in CTRL MO and *Cntrob* MO, respectively. Statistical analysis was performed using unpaired t-test. *, $P<0.01$; ****, $P<0.0001$ (Confocal images and quantifications was carried out by Dr. Teresa Casar Tena).

4.5.3 Loss of zebrafish centrobin results in microcephaly-like phenotypes

During embryo development, the primary and motile cilia transmit and receive extracellular signals for signalling pathways such as wnt and SHh. Defective cilia integrity results in a range of developmental disorders known as ciliopathies (Bettencourt-Dias et al. 2011). Ciliopathies cause abnormalities in kidney, brain, heart, retina, liver and kidney and body growth. A large cohort of core centrosome and centrosome-associated proteins have been implicated in the pathogenesis of ciliopathy (Otto et al. 2010, Keryer et al. 2011, Chaki et al. 2012, Izawa et al. 2015). Centrobin interaction with CPAP/CENPJ, a known centrosomal protein that is involved in microcephalic primordial dwarfism disorder and Seckel syndrome, has been previously reported (Bond et al. 2005, McIntyre et al. 2012, Gudi et al. 2014). Significantly, rat *hypodactyly* (*hd*) mutants with truncated centrobin have skeletal deformities and male sterility that result from defective sperm flagellar axoneme (Liška et al. 2009; Liška et al. 2013). However, the exact involvement of centrobin in ciliogenesis or ciliopathy pathogenesis has not been defined.

Using *cntrob* MO-mediated depletion in zebrafish embryo, we found that loss of centrobin results in morphological abnormalities such as smaller heads and eyes, increased frequency of

pericardiac edema and defective otolith seeding with shorter and aberrantly curved bodies (Figure 4.8 A and B). These developmental phenotypes are reminescent of those observed in zebrafish depleted of intraflagellar transport (IFT) proteins (Kramer-Zucker et al. 2005). Consistent with our previous observation of reduced ciliation frequency in the absence of centrobin in human cells and zebrafish embryo, we also have data that support that loss of centrobin results in significant increase in frequency of embryo with microcephaly/ciliopathy defects. Interestingly, these phenotypes were reproducible using the two independent MOs (data for one MO at a time are shown here, for the second MO, *see* Appendix 4) and these data also support our hypothesis of centrobin being a positive regulator of ciliogenesis.

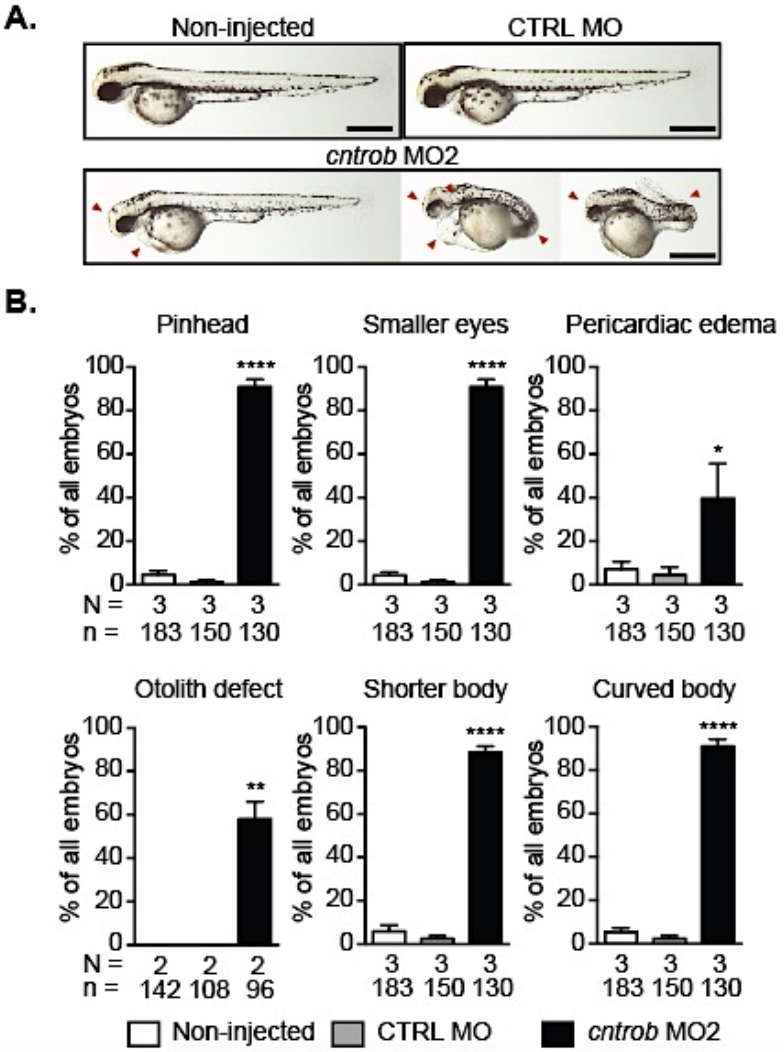

Figure 4.8: Morphological aberrations in centrobin-deficient zebrafish embryos

A. Live images of zebrafish embryos at 24 hpf. Embryos analysed were either non-injected, injected with CTRL MO or *cntrob* MO2 respectively. Arrowheads indicate morphological abnormalities. Scale bars, 500 µm. **B.** Graphical representations of frequencies of morphological abnormalities observed in either non-injected, injected with CTRL MO or *cntrob* MO2 zebrafish embryos. Number of independent experiments (N) and embryos observed (n) are indicated below each graph. Bar charts represent mean ± SEM. and statistical analysis was performed by one-way ANOVA. *, $P<0.5$; **, $P<0.01$; ****, $P<0.0001$ (These zebrafish experiments and quantifications were preformed by Dr. Teresa Casar Tena).

4.5.4 Centrobin regulates normal organogenesis in zebrafish

To gain further insight into the consequences of *cntrob* loss in zebrafish, we examined the laterality defects that are frequently observed when cilia are dysfunctional. We assayed for the expression of southpaw (*spaw*), a highly conserved left-right nodal-related gene. During the early stage of zebrafish embryogenesis, *spaw* is selectively expressed in the left lateral plate mesoderm but mislocalises when ciliary integrity is compromised (Long et al. 2003). From our analysis, we observed a significant increase in the frequency of *cntrob* morphant embryos with right-sided or bilateral *spaw* expression compared to non-injected or CTRL MO (Figure 4.9), in which *spaw* was mainly restricted to the left lateral plate mesoderm. Significantly, 40% of *Cntrob* morphant embryos lacked *spaw* expression compared to only 2% in the non-injected or CTRL MO (Figure 4.9B).

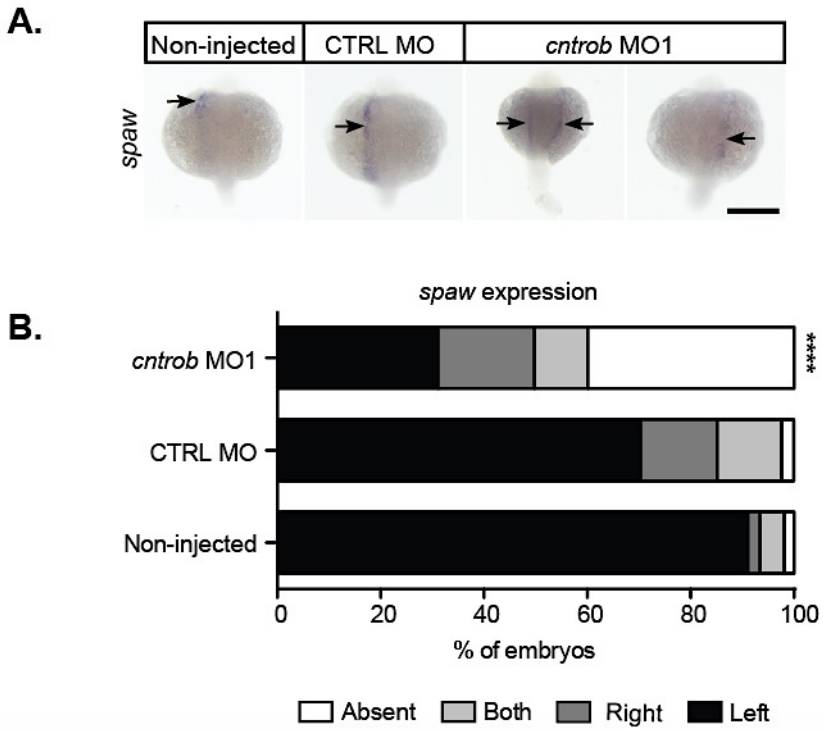

Figure 4.9: Laterality defect revealed by *spaw* randomisation in zebrafish centrobin morphant embryos.

A. WMISH micrographs showing localisation of *spaw* (purple) in the lateral plate mesoderm of 22-ss non-injected, CTRL MO or *cntrob* MO injected zebrafish embryo. Scale bars, 100 µm. **B.** Bar charts showing percentage of embryo with absent, bilateral, right and left *spaw* expression after indicated treatments. Four independent experiments were carried out and n=183-213 zebrafish embryos. Fisher's exact statistical test was used, ****. $P < 0.0001$; (The zebrafish experiments and quantifications were performed in collaboration with Dr. Teresa Casar Tena).

To substantiate the importance of centrobin in organogenesis, we analysed heart and pancreas development in zebrafish embryos. During normal vertebrate embryo development, cardiac looping occurs in such a way that the ventricle ('V') lies to the left of the atrium ('A') ('Correct') (Figure 4.10). Impairment of cilia structure and function has been associated with aberrant (inverse) or lack (no loop) of heart looping. Using WMISH to visualise *cardiac myosin light-chain 2* (*cmcl2*), during heart looping in *cntrob* morphants and control zebrafish embryos, we observed a significant increase in the frequency of inversely looped and no loop heart morphology in *cntrob*-deficient embryos (Figure 4.10B). To further establish the specificity of the MOs used in this study, we performed rescue experiments by co-injection of capped mRNA made *in vitro* from zebrafish *cntrob* cDNA (section 4.5.1). Importantly, the expression of *Cntrob* mRNA in zebrafish embryo did not affect the heart looping process (Figure 4.10B). However, co-injection of MO-resistant mRNA and *cntrob* MO rescued the cardiac defect morphology phenotype.

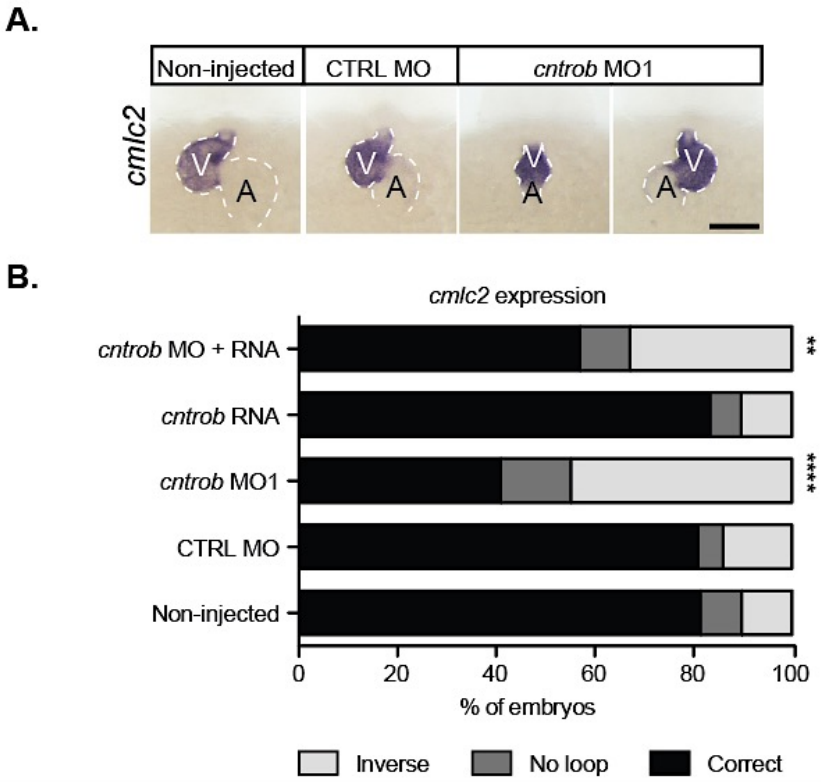

Figure 4.10: Impaired cardiac looping in *cntrob*-deficient embryos

A. Representative WMISH micrographs showing localisation of *cmcl2* (purple) in the lateral plate mesoderm of non-injected, CTRL MO or *cntrob* MO injected zebrafish embryos. Scale bar, 100 µm. **B.** Bar charts showing percentages of embryo with inverse, no loop and correct cardiac loop in non-injected zebrafish heart or after indicated treatment. *cntrob* RNA or *Cntrob* MO+RNA. Four independent experiments were carried out and n=at least 127 zebrafish embryos. Fisher's exact statistical test was used, ****. $P < 0.0001$, **. $P < 0.01$; (These zebrafish experiments and quantifications were performed by Dr. Teresa Casar Tena; Yetunde Adesanya generated pGEM-*cntrob* cDNA for *in vitro* transcription of *cntrob* mRNA used in this experiment).

Similarly, we monitored abdominal organ development by assessing the localisation of insulin-producing pancreatic β-cells using insulin as a marker in WMISH experiments. During zebrafish morphogenesis, the looping of the gut causes the pancreas precursor cells to localise to the right side of the lateral plate mesoderm in a a highly coordinated process known as 'pancreatogenesis' (Kinkel et al. 2008, Diiorio et al. 2014). Abnormal ciliogenesis leads to mislocalisation of these insulin-producing pancreatic β-cells; usually abnormally located on the left. Consistently, we observed a significantly increased frequency of abberantly localised insulin signals in *cntrob*-deficient cells (Figure 4.11). Again, we performed rescue experiments. The expression of *cntrob* mRNA in zebrafish embryos did not affect the pancreatic insulin localisation to the right (Figure 4.11B). However, co-injection of MO-resistant mRNA with *cntrob* MO rescued the correct (right) localisation of pancreatic insulin precursor cells.

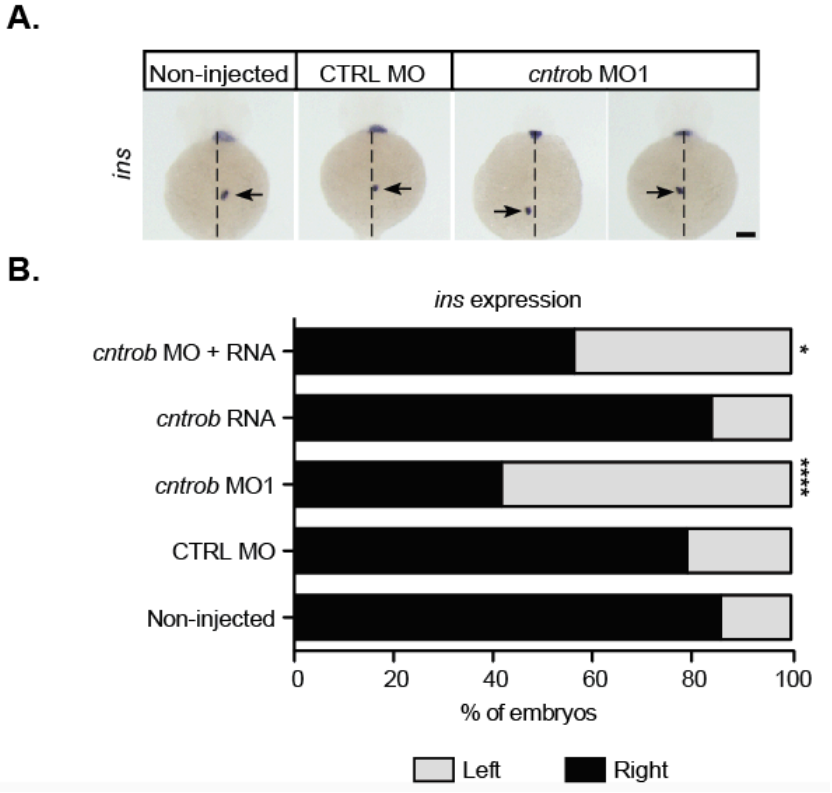

Figure 4.11: Increased pancreas mislocalisation in *cntrob* deficient embryos

A. WMISH micrographs showing localisation of *ins* (purple) in the lateral plate mesoderm of non-injected, CTRL MO or *cntrob* MO injected zebrafish embryo. Scale bars, 100 µm. **B.** Bar charts represent percentages of embryo with right or left zebrafish pancreas localisation after indicated treatments. Four independent experiments were carried out and n=at least 127 zebrafish embryos. Fisher's exact statistical test was used, ****. $P < 0.0001$, **. $P = 0.0105$; (All zebrafish experiments and quantifications were performed by Dr. Teresa Casar Tena; Yetunde Adesanya generated pGEM-*cntrob* cDNA for *in vitro* transcription of *cntrob* mRNA used in this experiment).

Collectively, these data show that depletion of Cntrob in zebrafish results in morphological features that are typical of cilia dysfunction. As a result of ciliary defect, we observed a significant increase in organ mislocalisation, an indication of embryonic developmental defects. Together, our analysis of centrobin deficiency in human cells and zebrafish embryos demonstrate that centrobin is required for effective ciliogenesis and cilium function in different vertebrate species.

4.6 Ultrastructural analysis of primary cilia in centrobin null cells

As previously described, ciliogenesis is a highly ordered, multi-stage process. At the initial stage, the centrosome migrates and docks to the plasma membrane through the interaction of the distal and subdistal appendages to the ciliary vesicle. This is then followed by the invagination of the plasma/ciliary membrane to form the ciliary pocket and the extension of microtubule-based, axoneme which protrudes from the surface of the cell. IFT is responsible for continued elongation of axonemal ciliary structures. To determine the impact of centrobin loss on ciliary ultrastructure, we examined ciliary ultrastructure by TEM analysis after 48 h of serum withdrawal. As shown in Figure 4.12, electron microscopy of 6/7 docked centrioles revealed that the mother centrioles in centrobin-deficient cells were able to dock to the ciliary vesicle and that defective ciliogenesis resulted from failed axoneme extension from the ciliary bud, leaving the nascent cilia in the 'mushroom' stage of cilium formation (Sorokin 1962).

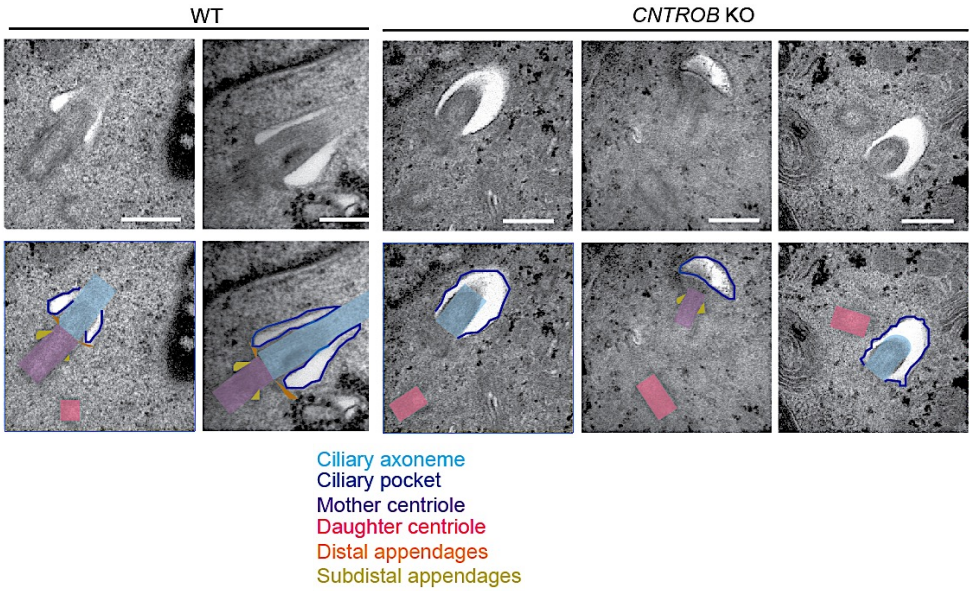

Figure 4.12: Centrobin deficient centrioles dock to ciliary vesicle but fail to extend their axoneme.

Top panel: Transmission electron micrographs of cilia in wild-type and centrobin-deficient hTERT-RPE1 cells after 48 h serum starvation. Scale bars, 500 nm. Bottom panel: show corresponding drawings to facilitate TEM data interpretation. Coloured shapes represent the structures defined in the corresponding text.

4.7 Centrobin, CP110 and ciliogenesis

Upon identifying centrobin as a positive regulator of vertebrate ciliogenesis, it was imperative that we understand the molecular mechanisms through which centrobin participates in this process. CP110 and its interacting partner, Cep97, localise to the distal end of centrioles where they regulate centriole length during centriole replication (Spektor et al. 2007, Schmidt et al. 2009). At an early stage of ciliogenesis, Cep164 recruits the protein kinase, TTBK2, to the mother centriole to mediate CP110 removal (Spektor et al. 2007, Goetz et al. 2012). Here, we first tested if centrobin depletion influences CP110 protein level during ciliogenesis. We then established novel interactions between CP110 and centrobin and mapped the interacting region.

4.7.1 Centrobin loss results in accumulation of negative regulators of ciliation

Using immunofluorescence microscopy, we monitored the distribution of negative regulators of cilia formation, CP110 and Cep97 in our centrobin knockout cells after serum starvation. We observed that in approximately 77% of serum-starved wild-type cells, CP110 and Cep97 signals were lost from the mother centriole carrying primary cilia (stained with acetylated tubuln), the signals were only detected on the daughter centriole (Figure 4.13A). In contrast, we observed aberrant localisation of CP110 and its interacting partner, Cep97, at the centrosome in 72% of serum-starved centrobin knockout cells (Figure 4.13A), which is indicative of the stabilisation of these protein complexes at the centrosome.

The presence of aberrantly-retained CP110/Cep97 complex has been reported in *CETN2*-deficient cells. However, siRNA mediated knockdown of CP110 was sufficient to rescue ciliation (Prosser and Morrison 2015). To determine whether the ciliary defect in centrobin nulls was exclusively due to CP110 dysregulation, we carried out siRNA-mediated depleting of CP110 in serum-starved wild-type hTERT-RPE1 and *CNTROB* KO. We confirmed the efficacy of siRNA knockdown of CP110 by immunofluorescence microscopy (Figure 4.13B) and western blotting of the total cell lysate (Figure 4.13C). Consistent with our observation of CP110 retention after serum starvation, we noticed the persistence of CP110 in mock and GAPDH knockdown controls after serum starvation of *CNTROB* nulls relative to the wild-type counterpart (Figure 4.13C). As shown in Figure 4.13D, there was no apparent difference in the ciliation frequencies of serum-starved wild-type treated cells, in *CNTROB* nulls, CP110 depletion resulted in partial rescue of ciliogenesis which was statistically significant when compared to *CNTROB* null mock-treated cells, but not to GAPDH knockdown controls (Figure 4.13D). Consistent with previously published findings that implicate centrobin in appropriate CP110 localisation during centriole duplication and elongation (Gudi et al. 2011),

these results show that centrobin regulates CP110 and that its stabilisation at the mother centriole contributes to defective ciliogenesis in centrobin-deficient cells. It is possible that centrobin regulates other processes during ciliogenesis; for example, its interaction with and stabilisation of tubulin have been reported (Gudi et al. 2011). This interaction may also be relevant to effective cilia assembly and extension.

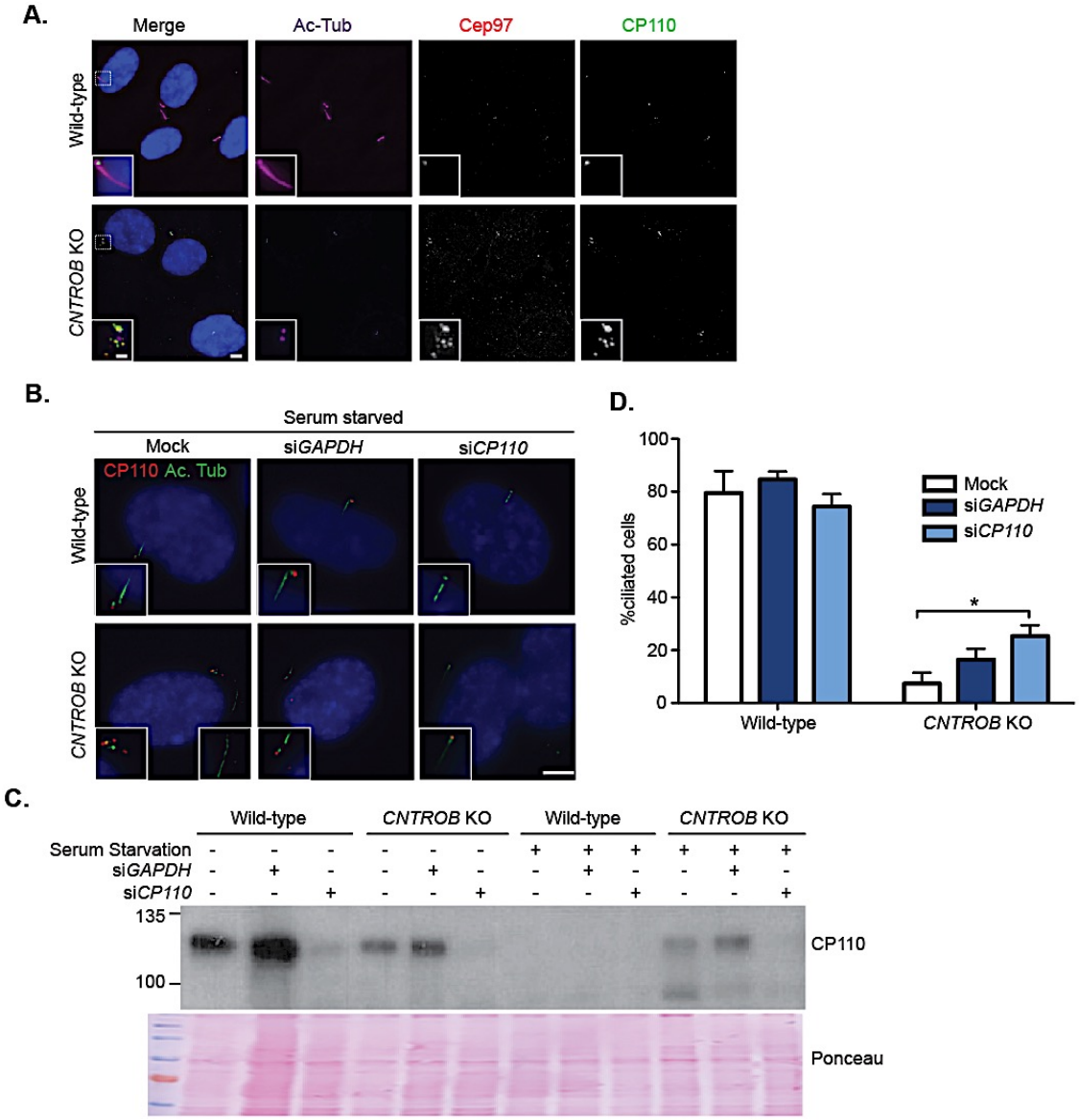

Figure 4.13: CP110 stabilisation at the mother centriole partly contribute to ciliogenesis defects in centrobin-deficient cells

A. Immunofluorescence micrograph of localisation of the negative regulators of ciliogenesis, CP110 and Cep97 in wild-type (WT) and *CNTROB* KO after 48 h serum deprivation. Antibodies against CP110 (green), Cep97 (red) and acetylated tubulin (magenta) were used for protein visualisation. Hoechst was used for visualising the DNA (blue). Scale bar, 5 µm, inset bar, 1µm. **B.** Immunofluorescence microscopy images confirming that CP110 depletion partially rescues cilia formation in *CNTROB* knockout cells. Antibodies to CP110 (red) and acetylated tubulin (green) were used for visualisation. Scale bar, 5 µm. **C.** Immunoblot confirmation of CP110 depletion in asynchronous and serum-starved wild-type and *CNTROB* KO cells after transfection with mock (M), siGAPDH (G) or siCP110 (C); Ponceau was used as loading control. **D.** Quantitation of the percentage of ciliated cells ± SEM. for serum-starved cells from **C**. *, $P<0.01$ using Student's t-test.

4.7.2 Centrobin interacts with CP110

We sought to determine if centrobin directly interacts with CP110 to modulate its activities. For this, we used co-immunoprecipitation for both the endogenous proteins to establish an interaction. First, using our centrobin knockout cell as negative control, we performed immunoprecipitation using our anti-centrobin antibody and confirmed that centrobin and CP110 interact *in vivo* (Figure 4.14A). Reciprocally, CP110 antibody immunoprecipitated endogenous centrobin in hTERT-RPE1 cell extracts, also confirming strong interaction between both proteins (Figure 4.14B). In agreement with the co-immunoprecipitation experiments, we also used an independent technique, a proximity ligation assay (PLA), to confirm interaction between CP110 and centrobin. PLA uses O-link detection system that relies on secondary antibodies that are conjugated with complementary nucleotides. In this technique, oligonucleotide tails within 40 nm distance are annealed and amplified to produce detectable fluorochrome signals. Here, red spots are indicative of interaction; centrobin knockout cells were used as negative control while established interaction between centrobin and CPAP/CENPJ was used as positive control (Figure 4.14C-D) (Gudi et al. 2014). We quantified the number of cells with > 3 red foci and observed 86% in wild-type and 13% in centrobin-deficient cells. We noticed 78% interaction-positive cells in our positive controls, indicating that CPAP and centrobin interact.

To map CP110-binding regions within the centrobin protein, HCT116 cells were transfected with GFP-centrobin fragments spanning residues 1-364 or 365-903 prior to immunoprecipitation of endogenous CP110. As shown in Figure 4.15D, immunoprecipitation with CP110 isolated centrobin fragment 365-903 but not 1-364. These observations confirm the interaction between centrobin and CP110, and the C-terminal fragment of centrobin robustly and specifically binds endogenous CP110.

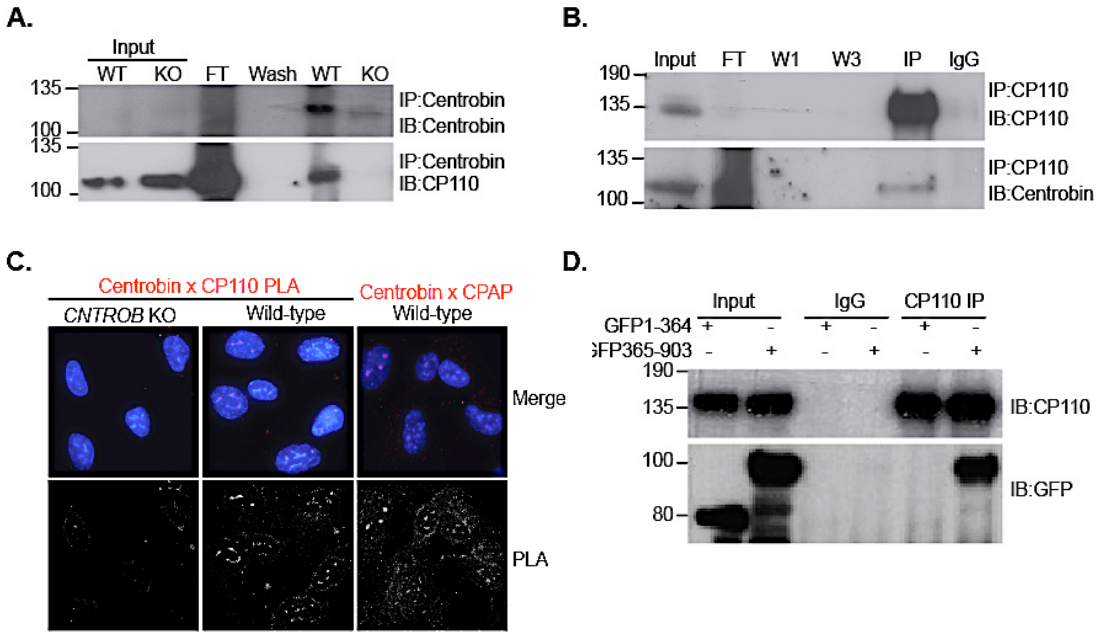

Figure 4.14: Centrobin directly interacts with CP110 via its C-terminal

A. Co-immunoprecipitation of centrobin and CP110 from hTERT-RPE1 cell lysate. Centrobin was immunoprecipitated using our novel moAb described in section 2.5.6 and *CNTROB* knockout (KO) cells were used as the negative control. Western blotting was performed using anti-centrobin and anti-CP110 antibodies. **B.** Reciprocal co-immunoprecipitation of CP110 and centrobin from hTERT-RPE1 cell lysate. CP110 was immunoprecipitated as previously described with α-rabbit IgG used as the negative immunoprecipitation control. Western blotting was performed using anti-CP110 and anti-centrobin antibodies. WT-wild-type, FT-flow through, W1 –wash 1, W3-wash 3. **C.** Proximity ligation assay using centrobin and CP110 or centrobin and CPAP as primary antibodies. Red foci indicate close proximity (<40 nm) of secondary conjugated antibodies. *CNTROB* KO cells were used as the negative controls and centrobin and CPAP interaction in wild-type cells were used as positive control (Gudi et al. 2014). **D.** Western blot showing the interaction of CP110 with GFP-centrobin fragments. Cell lysates of HCT116 transfected with GFP-centrobin fragment 1-364 aa or 365-903 aa expression vectors. Immunoprecipitation was again performed, as previously described, with anti-CP110 antibody and western blotting was performed using anti-CP110 and anti-GFP antibodies.

4.8 Mapping of the centrobin region required for ciliation

To explore the regions of centrobin that are necessary and sufficient for ciliogenesis, we dissected the 903 amino acid protein based on its known interactions as depicted in Figure 4.15A. The regions that interact with the essential centriole duplication and elongation proteins, Cep152 and CPAP, have been mapped to the amino-terminal 1-364 aa while the centrosome localising signal (CLS) and the tubulin-binding domain were mapped to the carboxy-terminal 765-903 aa (Gudi et al. 2014, 2015). The indicated fragments (Figure 4.15A) were cloned into GFP expression vectors; successful expression of these fragments was monitored by western blotting (Figure 4.15B). To map the regions of centrobin required for ciliogenesis, these expression constructs were transiently expressed in our centrobin-deficient cells. After inducing ciliogenesis, cells were prepared for immunofluorescence

microscopy to assess the impact on ciliation frequency. As previously observed, GFP-tagged full-length centrobin localised to the centrosome (section 3.5), it also localised to the basal body and axoneme of *CNTROB* nulls. Notably, its expression rescued ciliogenesis (Figure 4.15C-D). Interestingly, we observed that GFP-centrobin fragment 765-903 localised to the centrosome but was not sufficient for ciliogenesis. The expression of GFP centrobin fragment 452-903 was sufficient to rescue ciliogenesis and was the minimal C-terminal fragment required for ciliogenesis (Figure 4.15C-D). Consistent with previously reported observation of C-terminal centrobin fragments localising to microtubule bundles (Jeong et al. 2007, Gudi et al. 2011), the 365-903 and 452-903 fragments also localised to microtubule bundles and formed cytosolic aggregates (Figure 4.15D). These data show that the N-terminal CEP152 and CPAP binding region of centrobin is not necessary for ciliogenesis.

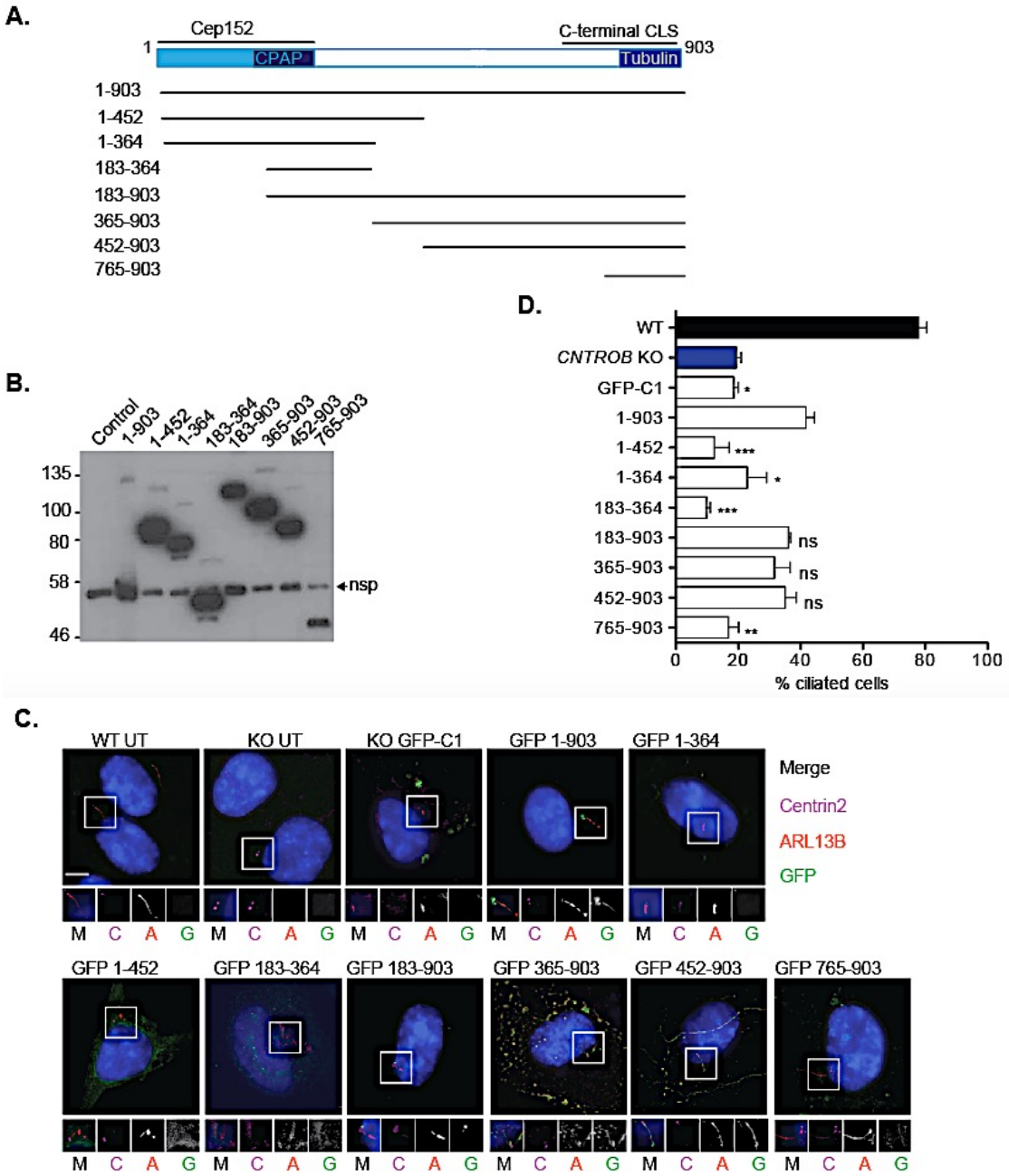

Figure 4.15: Deletion analysis shows that the N-terminal CPAP-binding region of centrobin is dispensable for ciliogenesis

A. Schematic of deletion analysis performed on centrobin. The regions required for centrosomal localisation and interaction with CPAP, Cep152 and tubulin are shown. **B.** Immunoblot showing expression of GFP-tagged fragments at 24 h after transfection in HCT116 cells. Control (UT) lane contains lysate from untransfected cells. Due to the low expression of full-length GFP-Centrobin (1-903), 200 µg total cell extracts of full-length was loaded on the gel while 20 µg of cell lysates from the fragments transfections were loaded. **C.** Immunofluorescence micrographs of *CNTROB* knockout after transient expression of GFP-tagged centrobin fragments. GFP localisation was visualised in green and antibodies against ARL13B (red), centrin2 (magenta) were used for visualisation. Hoechst was used for visualising the DNA (blue). The same order was used for all single channels in the blow-ups. Scale bar, 5 µm. **D.** Quantification of the frequency of primary cilia in *CNTROB* null cells transfected and serum-starved after 24 h. Counts were based on ARL13B staining of 100 transfected cells in 3 independent experiments. *, $P<0.05$; **, $P<0.01$; ***, $P<0.001$; ns = non-significant in comparison to full-length

rescue using one-way ANOVA and Tukey's multiple comparison test. nsp= non-specific band (*CNTROB* fragments were generated along with Mr. Kambe Takanari).

4.9 Roles of centrobin in ciliary assembly

4.9.1 Centrobin may participate in ciliary IFT transport assembly

Primary cilia are essential organelles in the hedgehog signal transduction pathway. Smoothened (Smo) is a highly conserved seven-transmembrane protein that relocalises to the primary cilium and transduces signals in response to SHh activation (Corbit et al. 2005, Goetz and Anderson 2010). To determine the functionality of the primary cilia in the residual cilia present in our *CNTROB* knockout cell population, we examined the responsiveness of these cilia to external chemical stimuli. We carried out immunofluorescence microscopy analysis of primary cilia translocation of Smo after SHh activation with smoothened agonist (SAG). In the presence of SHh ligand, we observed the translocalisation of Smo signal to 80% of SHh treated cilia in hTERT-RPE1 compared to only 23% SHh treated cilia in centrobin knockout cells. As shown in Figure 4.16, assessment of the localised Smo signal in centrobin deficient cells showed reduced localisation of Smo to the primary cilium. Consistent with the ciliogenesis defect where cells lose the ability to extend the axoneme, this result shows the possibility of signalling defects as a consequence of defective IFT in the absence of centrobin.

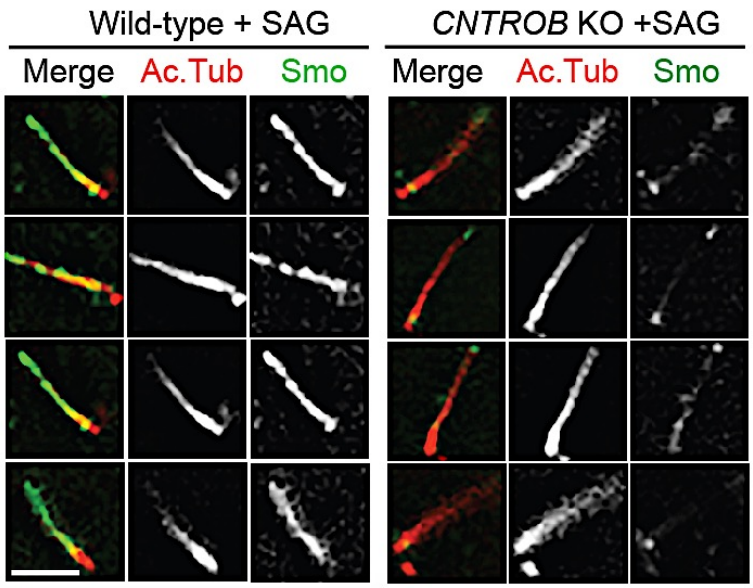

Figure 4.16: Defective smoothened localisation in residual ciliated centrobin null cells

Immunofluorescence microscopy analysis of Smoothened (Smo) in serum-starved cells after 4 h treatment with 100 mM SAG in hTERT-RPE1 and *CNTROB* KO cells. Scale bar, 1 µm; n=30 ciliated cells; N=1.

4.9.2 Overexpression of centrobin causes ARL13B protrusions

The overexpression of centrobin has been previously reported to result in cytosolic aggregates, microtubule bundling (Lee et al. 2009) and abnormally long centriole-like structures in cycling human cells (Gudi et al. 2011). Furthermore, it rescues limb malformation in *hypodactylous* rats (Liška et al. 2013). We have also shown that centrobin drives ciliogenesis positively. However, the impact of its overexpression in ciliated cells has not been reported. Therefore, we transiently overexpressed full-length *CNTROB* cDNA in hTERT-RPE1 cells to investigate the role of centrobin in human cilium assembly. Despite the low transfection and expression levels in hTERT-RPE1, after 24 h serum deprivation, we observed that elevated centrobin levels at the basal body resulted in ciliary membrane protrusions as visualised with ARL13B (Figure 4.17). We observed the ARL13B protrusions on 35% of the total cell population compared to only 4% in the empty vector control cells. These bulges were observed at random positions along the length of primary cilium and are reminenscent of those observed in ARL13B-overexpressing human cells and zebrafish embryos monitored by immunofluorescence and live cell imaging (Lu et al. 2015a). According to Lu et al. these membrane protrusions were formed prior to significant increase in length of cilia as a result of an increase in the production of membrane domain that migrates to the ciliary tip of transfected cells. Hence, this striking observation also agrees with our earlier observations that centrobin is a positive regulator of ciliogenesis in vertebrates and may mediate its effect through IFT.

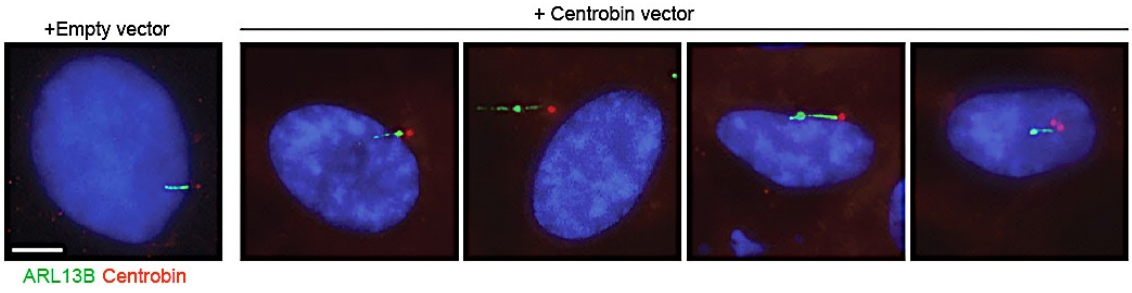

Figure 4.17: Overexpression of centrobin causes ARL13B protrusion in hTERT-RPE1

IF images of wild-type hTERT-RPE1 cells transiently transfected with full-length centrobin cDNA, fixed and stained with antibodies against centrobin (red), ARL13B (green). The ciliary membrane bulges were visible at various positions along the cilium (arrowheads). Scale bar, 5 µm.

4.10 Effect of *CNTROB* loss on cellular CPAP levels

Centrobin interacts with CPAP and regulates its cellular level by controlling CPAP centrosomal localisation and level by regulating the activities of proteasome complex on CPAP degradation, depending on the stages of the cell cycle (Gudi et al. 2014; Gudi et al. 2015). CPAP participates in primary cilium disassembly when cells re-enter cell cycle and

mutation in *CPAP* has been shown to contribute to the pathogenesis of Seckel syndrome and microcephaly (McIntyre et al. 2012, Gabriel et al. 2016). Interestingly, both CPAP and centrobin directly interact and stabilise microtubules, therefore overexpressing centrobin or CPAP proteins results in microtubule polymerisation that causes abnormal centriole elongation (Schmidt et al. 2009; Gudi et al. 2014; Gudi et al. 2015). A previous RNAi study has shown that centrobin depletion leads to centrosomal and cellular degradation of CPAP (Gudi et al. 2015), so, we sought to check the integrity of CPAP in our centrobin-deficient cells.

As evident in our immunofluorescence microscopy analysis of CPAP before and after serum deprivation, we observed the localisation of CPAP at the centrosome of centrobin deficient cells. As expected, after serum starvation, CPAP levels were reduced at the centrosome of wild-type hTERT-RPE1 cells while it was retained in centrobin deficient cells (Figure 4.18A). To confirm this increase in CPAP level, we carried out western blot analysis of the same and noticed the presence of a shorter CPAP fragment, which may indicate CPAP degradation or modification in the absence of centrobin. This modified or degraded form of CPAP may not have the ability to carry out its roles in centriole elongation or ciliogenesis (Figure 4.18B).

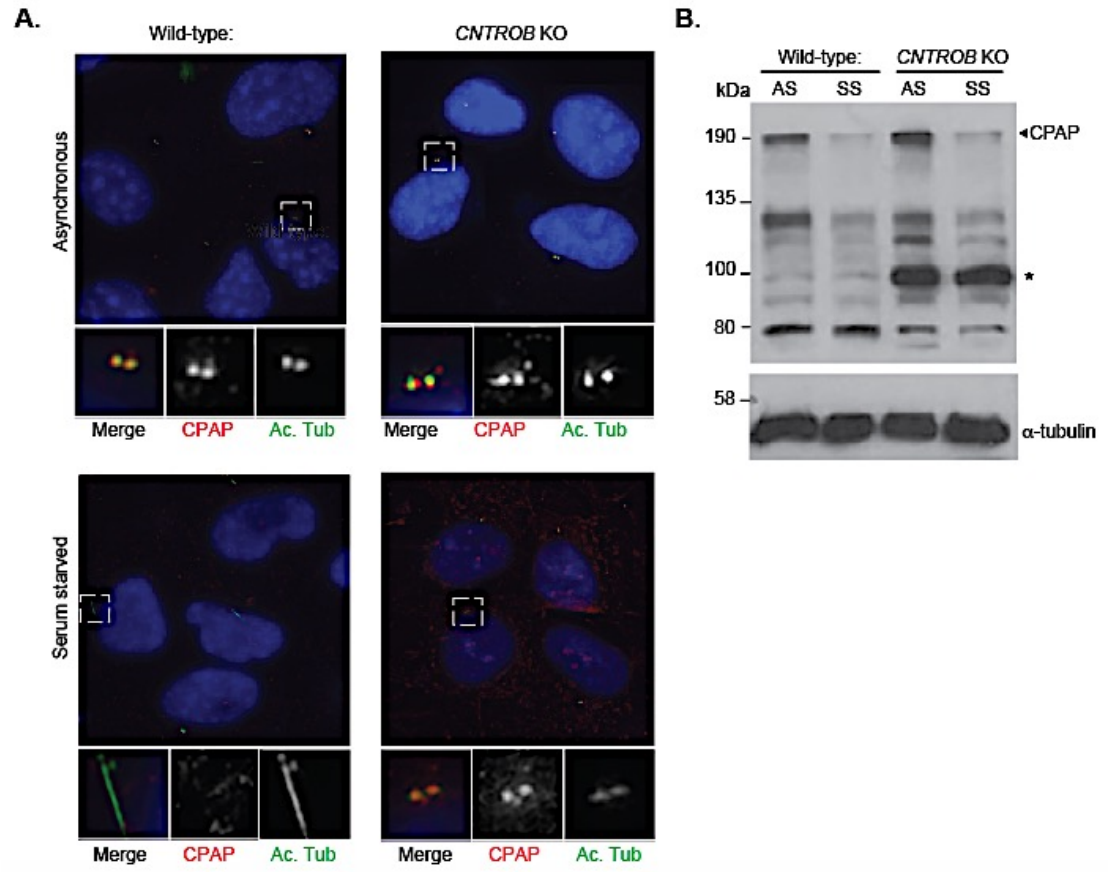

Figure 4.18: CPAP localisation and expression in centrobin-deficient cells

A. Representative immunofluorescence images showing CPAP localisation before and 48 h after serum starvation. Cells were subjected to tubulin depolymerisation, fixed and stained with antibodies raised against CPAP (red) and acetylated tubulin (green). DNA (blue) was visualised by Hoechst staining. N=2. **B.** Immunoblot analysis of CPAP before and 48 h after serum starvation. Asterisk indicates the shorter fragments or degraded form of CPAP present in the *CNTROB* KO cells but not in the wild-type cells. Alpha-tubulin was used as a loading control.

4.11 Discussion

Centrobin is a core centrosomal protein that participates in the centriole duplication process through regulating tubulin stability and CP110 localisation. Initial characterisation of centrobin has revealed its preferential localisation to the daughter centriole during interphase (Zou et al. 2005, Januschke et al. 2013). Here, we focused on the roles of centrobin in the primary cilia assembly and functionality. We show that in ciliated cells, centrobin also localises to the basal body (mother centriole) carrying the primary cilia and regulates primary cilia assembly. Our data provide support for centrobin as a positive regulator in primary cilia formation. Cells lacking centrobin were unable to efficiently assemble primary cilia. Interestingly, we sufficiently rescue this phenotype by the re-expression of centrobin in this cells and a partial rescue was observed when we depleted the negative regulator of ciliogenesis, CP110 (Spektor et al. 2007, Goetz et al. 2012).

At the time we carried out these experiments, it was unknown if centrobin and CP110 directly interact in proliferating or quiescent cells. A previous report has shown that centrobin regulates CP110 recruitment during centriole biogenesis (Gudi et al. 2011). We show here that centrobin and CP110 interact directly in proliferating cells. In the absence of centrobin, CP110 is also stabilised at the mother centriole of serum starved cells. It is possible that the interaction between CP110 and centrobin is important during centriole duplication and ciliogenesis. CP110 removal from the distal end of the mother centriole through the activities of Tau Tubulin Kinase2 (TTBK2) is a crucial step during the initiation stage of primary ciliogenesis (Goetz et al. 2012). Although several proteins are involved in the mechanism of CP110 removal (Goetz et al. 2012; Prosser and Morrison, 2015; Loukil et al. 2017); our findings identify centrobin as an interactor and participant in CP110 removal during primary ciliogenesis. Furthermore, we implicate CP110 dysregulation in centrobin-deficient cells as one of the reasons for reduced cilia frequency that we observe.

Centrobin interacts with a number of early initiation proteins that localise to the procentriole, such as CPAP, hSas6, STIL and Cep152 (Januschke et al. 2013, Gudi et al. 2014), most of which are crucial for proper cilia formation in vertebrates (Wu and Tang, 2012; David et al. 2014; Loukil et al. 2017). We next investigated the relevance of some of these interactions on centrobin's participation in ciliogenesis. Since the centrobin domains that interact with Cep152, CPAP and even tubulin have been previously mapped (Gudi et al. 2011, 2014), our centrobin fragment analysis reveals the region of centrobin that is necessary for ciliogenesis resides in its C-terminal region that also contains the tubulin binding region. We also show that the CPAP and Cep152 interactions are not crucial for centrobin's involvement in ciliogenesis. Interestingly, the tubulin-interacting region at the C-terminus was not sufficient for ciliogenesis, while the CP110-interacting region which also contains the tubulin-

interacting domain was sufficient for rescuing ciliogenesis. It is possible that centrobin regulates both the removal of CP110 at the initiation stage of ciliogenesis and the stabilisation and modification of tubulin at the base of primary cilium. It is established that post-translational polymodification of tubulins, notably, detyrosination, acetylation, glycylation and polyglutamylation, are crucial for maintain centriolar and ciliary axonemal structures (Hammond et al. 2008). Also, centrobin regulates cellular and centrosomal CPAP levels (Gudi et al. 2015), although our centrobin mapping analysis reveals that the centrobin CPAP-interacting region was not essential for its role in ciliogenesis. Given that *CPAP* has been shown to be a ciliopathy (Wu and Tang 2012) and microcephaly (Bond et al. 2005) gene, we checked the centrosomal localisation and cellular level of CPAP in our *CNTROB* KO cells before and after inducing ciliogenesis. Our immunofluorescence microscopy analysis shows CPAP localisation to the centrosome of centrobin-deficient cells; however, immunoblot analysis reveals the presence of a degraded or modified CPAP fragment which supports the published data that centrobin prevents degradation of ubiquitinated CPAP by the proteosome (Gudi .et al. 2015) and loss of centrobin results in CPAP degradation. This may also impact known CPAP contributions to primary ciliogenesis (Wu and Tang 2012).

To better understand the stage of primary ciliogenesis in which centrobin acts, we used TEM to study the ultrastructure of centrioles/cilia in our centrobin null cells before (in chapter 3) and after inducing ciliogenesis (this study). We noticed that ciliation capacity was hampered by inability of centrobin-deficient cells to efficient extend their axoneme after docking of their basal body to the ciliary vescile, leaving the nascent cilia in the 'mushroom' stage of cilium formation (as described by Sorokin, 1962). Our immunofluorescence microscopy and TEM did not show the existence of biciliated cells in the absence of centrobin as had been previously reported for specialised *Drosophila* neuronal cells (Gottardo et al. 2015). One potential explanation is the possibility of functional divergence between human and *Drosophila* centrobin as was shown by bioinformatic analysis (section 3.2). Surprisingly, *Drosophila* centrobin localises to the human centrosome and rescues ciliation frequency in centrobin-deficient cells. In this study, we did not investigate the functionality of primary cilia formed when human cells were transfected with *Drosophila* centrobin. Instead, we determine the functionality of residual cilia in centrobin-deficient cells by investigating the localisation of Smo to the primary cilium, an assay that has been commonly used to assess primary cilium functionality (reviewed by Wong and Reiter, 2008). Signalling through the Hh pathway requires Smo translocalisation to the primary cilium which then activate the Glioma (Gli) family of proteins. Prior to Hh signalling activation, its localisation to the primary cilium is prevented by the tumour suppressor Patched (PTCH1). Our analysis of Smo in the residual cilia found in centrobin-deficient cells revealed a dilution of Smo which shows the presence of a defective activation of the Hh pathway. Defective activation of Hh pathway has

been reported in cells with supernumerary cilia (Mahjoub and Stearns 2012). It could therefore be explained that the loss of centrobin affects primary ciliogenesis in vertebrates and causes defective Hh signalling in both human and *Drosophila* (Gottardo et al. 2015).

It is established that mutation in crucial ciliopathy genes or depletion of ciliary proteins causes laterality defects which are consequences of a malfunctioning cilia-dependent signalling (Goetz and Anderson 2010). Our finding that identifies centrobin as a positive regulator of ciliogenesis was reproduced in zebrafish. We observed a marked reduction in cilia number and length after MO-mediated depletion of centrobin in zebrafish embryos. Because SHh signalling is important during embryogenesis and the signals for proper organogenesis are transduced through the primary cilia, abnormal kidney, liver, heart, brain and pancreas are evident when cilia malfunction (Long et al. 2003; Corbit et al. 2005; Goetz and Anderson, 2010; Diiorio et al. 2014). A notable consequence of reduced cellular level of centrobin is defective organ localisation during development of zebrafish embryos. These observations identify ciliopathy roles for centrobin in vertebrates. To our knowledge, there is no published evidence of the clinical relevance of *CNTROB* mutations in human; however, in rats, full-length centrobin is required for proper skeletal formation and spermatogenesis (Liska et al. 2009, 2013).

Collectively, our results identify *CNTROB* as a critical regulator of vertebrate ciliogenesis and impacts the process through its C-terminal that interacts with CP110 and tubulin. Thus, our data implicate centrobin as a candidate microcephaly or ciliopathy gene. There is a growing interest in understanding the links between the centrosome, cilia and DNA damage response. A number of ciliopathy genes play have been shown to play crucial roles in the DNA damage response. For example, ATR, a key player in the DNA damage response and has been implicated in the molecular pathology of Seckel syndrome, has been recently shown to promote ciliogenesis and cilia signalling (Matsuoka et al. 2007, Stiff et al. 2016). Also, centrin2, a centrosomal protein, participates in both primary ciliogenesis and nucleotide excision repair after DNA damage (Nishi et al. 2005, Dantas et al. 2011, Prosser and Morrison 2015). Because centrobin interacts with several components of the DNA damage response (notably, BRCA2 and FANCD2) and ciliary proteins, we thought to carry out further studies (Chapter 5) to determine if centrobin links these processes.

5 A role for centrobin in the DNA damage response

5.1 Introduction

Centrosome duplication and the cell cycle are intricately linked to ensure stable centrosome numbers (Doxsey et al. 2005; Tsou and Stearns, 2006). In most non-transformed cells, procentriole assembly is restricted to S-phase. Centrosome disjunction and licensing are also essential events in the duplication steps that help to prevent centrosome hyperamplification within a cell cycle (Tsou and Stearns 2006, Tsou et al. 2009). However, the cell and centrosome cycles can be uncoupled in a process that results in centrosome amplification (Dodson et al. 2004; Harrison et al. 2011; Prosser *et al.* 2012). Centrosome number and integrity are essential for bipolar mitotic spindles and faithful chromosome segregation. Therefore, supernumerary centrosomes can result in aneuploidy and genome instability (Ganem et al. 2009). Mutation in oncogenic and tumour suppressor proteins, prolonged S-phase arrest and DNA damaging agents such as ionising radiation (IR), ultra violet radiation (UV) and hydroxyurea (HU) can induce an increase in centrosome number (Dodson et al. 2007; Nigg et al. 2009; Prosser et al. 2012).

Upon exposure to genotoxic stress, cells initiate DNA repair by engaging several interdependent repair pathways. Depending on the nature of the DNA damage, cells activate specific DNA repair pathways to restore genetic integrity or induce apoptosis if damage cannot be repaired (Ciccia and Elledge 2010). Interestingly, several key regulators of the cell cycle and DNA repair pathways localise to the centrosome and have centrosomal interacting partners (Zhang et al. 2007; Cappelli et al. 2011). Although the possibility of antibody cross-reactivity during immunofluorescence microscopy makes some of these localisations controversial, to date, good evidence exists to support centrosomal localisation of ATR, ATM, BRCA1, BRCA2, several CDKs, CHE-1, CHK1, CHK2, several PARPs, and PLK1 at all or some of the stages of the cell cycle (Fukasawa, 2007; Zhang et al. 2007).

In an attempt to determine the biological significance of DDR proteins at the centrosome, Cep63 was identified as a centrosomal substrate of ATM and ATR in *Xenopus laevis* and chicken B cells; both kinases can phosphorylate Cep63 on Ser560 to control its centrosomal localisation and role in centrosome-dependent spindle assembly checkpoint activation after exposure to genotoxic stress (Smith et al. 2009). Furthermore, BRCA2 also interacts with centrosomal proteins, such as Rho-associated coiled-coil containing protein kinase 2 (ROCK2) and nucleophosmin (NPM), to regulate the centrosome duplication process (Wang et al. 2011). Physical inhibition of the centrosomal interaction between BRCA2, NPM and ROCK2 results in centrosome amplification and genome instability. This suggests a role for BRCA2 in maintaining numerical integrity of the centrosome (Wang et al. 2011).

In addition to its role at the centrosome, BRCA2 and its interacting partner, RAD51, are crucial components of the homologous recombination (HR) pathway (Davies et al. 2001; Moynahan et al. 2001; *see* section 1.2.3). The interaction between these proteins in HR repair is mediated by BRCA2 phosphorylation in a CHK1/CHK2-dependent manner (Bahassi et al. 2008), and this interaction is required for the recruitment of RAD51 to DSBs. Loss of BRCA2 or RAD51 protein results in centrosome amplification and chromosome missegregation (Nakanishi et al. 2007, Bahassi et al. 2008, Wang et al. 2011). Ablation of RAD51 also results in centrosome amplification and defective HR that gives rise to an increase in the accumulation of unresolved damaged DNA and centriole disengagement during prolonged G2/M arrest in human and chicken B cells (Dodson et al. 2004, Katsura et al. 2009).

Given that centrosome hyperamplification after exposure to a range of genotoxic stresses is dependent on the ATR/ATM-CHK1/CHK2-CDK2 pathway activation (Dodson et al. 2004, Bourke et al. 2007, 2010, Löffler et al. 2013), this indicates a functional link between the DDR signals and centrosome cycle regulation. Recently, CHK1, but not its kinase activities, have been shown to promote PCM expansion after DNA damage and that the loss of pericentrin, a PCM component, leads to reduced level of CHK1 activation (Griffith et al. 2008, Antonczak et al. 2015). Therefore, pericentrin is believed to facilitate centrosome-dependent full activation of CHK1. Although centrosomal localisation of CHK1 is still controversial, its centrosomal interacting partners, pericentrin and microcephalin have been reported to regulate centrosome number (Wang et al. 2013b, Löffler et al. 2013, Antonczak et al. 2015).

With several recent studies emphasising a functional overlap between the DDR and centrosomal proteins (Otto et al. 2010, Chaki et al. 2012, Choi et al. 2013), it is not surprising that mutations in centrosomal and DDR proteins have been associated with a range of human inherited diseases and ciliopathies (Nigg and Raff 2009, Bettencourt-Dias et al. 2011, O'Driscoll 2012). For example, mutations in the genes that encodes the DDR protein, ATR, and centrosomal proteins, CPAP/CENPJ, CEP152 and PCNT, have been linked to microcephaly and Seckel syndrome (Bond et al. 2005, Griffith et al. 2008, Kalay et al. 2011, O'Driscoll 2012). However, the mechanisms that integrate the centrosomes, cilia and the DNA damage response are not well understood.

It is presently unclear whether centrobin, like several other centrosomal proteins, participates in centrosomal responses to genotoxic stress. Given that centrobin interacts with components of the DNA repair pathway, BRCA2 and FANCD2, and its depletion prevents HU-induced centrosome amplification (Zou et al. 2005; Gudi et al. 2014; Gupta et al. 2015), we decided to investigate a potential role of centrobin in centrosomal and cellular responses to genotoxic

stress. We also investigated a potential role of centrobin in the HR pathway by monitoring RAD51 recruitment to DSBs. Activation of the DDR was also monitored by the presence of phosphorylated histone H2AX on Ser139 (γ–H2AX) after exposure to genotoxic stress such as UV, IR and MMS (Ciccia and Elledge, 2010; Podhorecka et al. 2010).

5.2 Reduced DNA damage-induced centrosome amplification in centrobin-deficient cells

Boveri's work highlighted the relevance of centrosome in maintaining chromosome stability (Boveri, 1914, 2008). Several studies have shown that uncoupling the cell cycle and centrosome replication by IR-induced G2 or HU-induced S phase arrests results in centrosome amplification (Dodson et al. 2004; Bourke et al. 2007; Inanç et al. 2010; Prosser et al. 2012). Reduced levels of centrosome amplification after siRNA-mediated depletion of centrobin have been previously described (Zou et al. 2005). The mechanism through which centrobin promotes centrosome amplification during a prolonged S-phase is unknown. One possibility is that a centriole biogenesis step that requires centrobin is delayed, which identifies centrobin as an essential centriole duplication factor.

To determine the relevance of centrobin in DNA damage-induced centrosome amplification, we subjected our *CNTROB* KO cells to different genotoxic insults. For reliability of our analysis, it was important that we visualised both the centrioles and centrosomes after inducing centrosome amplification. We used centrin3 to mark the distal lumen of the centrioles and pericentrin to visualise the PCM of the centrosome. Using immunofluorescence microscopy, we analysed cells for centrosome amplification at 48 hours after exposure to different genotoxic stresses. As shown in Figure 5.1, there was significant reduction in the percentage of centrobin-deficient cells with robust centrosome amplification when compared to the corresponding wild-type after treatment with either 4 mM HU, 5Gy IR or 5 J/m^2 UV. These observations reinforce the importance of centrobin in centriole duplication, which is similar to published phenotypes with siRNA-mediated depletion of centrobin (Zou et al. 2005). These authors showed that in U2OS cells, siRNA-mediated knockdown of centrobin resulted in a reduced proportion of cells with amplified centrosome after HU treatment.

Although the kinetics of centrosome amplification were not determined in this study, we cannot eliminate the possibility that a slower rate of centrosome assembly in centrobin-deficient cells may result in reduced centrosome amplification. This possibility is supported by the presence of acentric and monocentric cell populations in centrobin-deficient cells, as described in section 3.9.

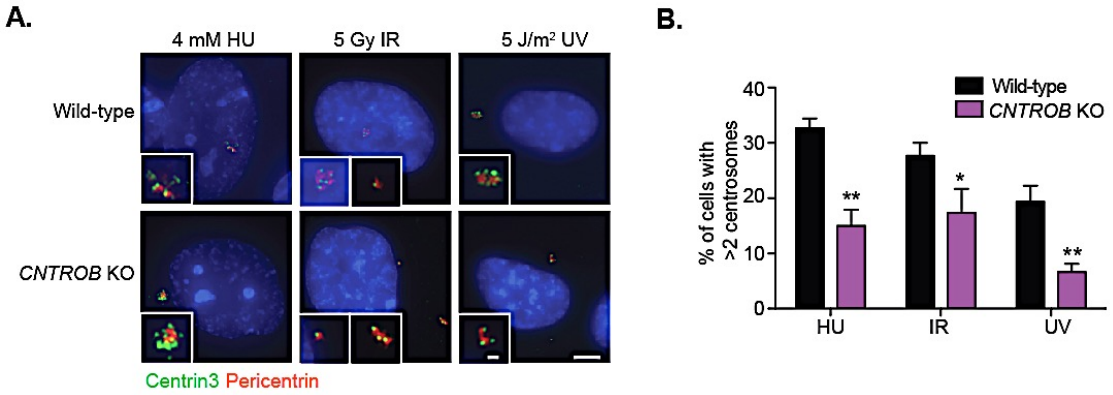

Figure 5.1: DNA-damage induced centrosome amplification is reduced in *CNTROB* KO cells

A. Immunofluorescence microscopy showing centrosome amplification in wild-type and centrobin-deficient cells stained with antibodies to centrin3 (green) and pericentrin (red) at 48 h post treatment with either 4 mM hydroxyurea (HU); 5 Gy ionising radiation (IR) or 5 J/m^2 ultraviolet radiation (UV). DNA (blue) was visualised with Hoechst. Scale bar, 5 µm and inset scale bar, 1 µm. **B.** Quantitation of wild-type and centrobin-deficient cells with abnormal centrosome after exposure to the indicated genotoxic stresses. Histogram shows mean ± SEM of at least 3 independent experiments in which a minimum of 100 cells were counted per experiment. Statistical analysis was performed using unpaired-t-test to compare wild-type and *CNTROB* KO cells separately for each treatment. *, $P<0.05$; **, $P<0.01$.

5.3 Centrobin-deficient cells are sensitive to genotoxic stress

Since DNA damage-induced centrosome amplification was attenuated in centrobin-deficient cells, we decided to carry out further investigation of the role of centrobin in the DDR. We therefore performed clonogenic survival assays on *CNTROB* KO cells to analyse the DNA repair competency after exposure to increasing doses of DNA damaging agents. Clonogenic experiments were performed as described in section 2.3.8 and a representative image of colonies formed from wild-type, *CNTROB* KO and rescue cells is shown in Figure 5.2A. As shown, there was no apparent difference in the untreated cells for all the indicated genotypes (plating efficiency ranged between 60-65%), while reduction in cell viability was observed in *CNTROB* KO after 5 Gy IR treatment. Centrobin-deficient cells show sensitivity to IR and MMS, an alkylating agent that induces DNA crosslinks (Figure 5.2B-C). ATM is one of the key players in the HR-mediated repair of DSBs and thus is necessary for proliferation and genome stability (Morrison et al. 2000, Matsuoka et al. 2007, Stracker et al. 2013). Therefore, we used the ATM kinase inhibitor, KU55933, on the wild-type cells as a control for IR sensitivity. Also, to ascertain that this phenotype was solely due to centrobin ablation, we included our centrobin rescue cells in the experiment. As evident in Figure 5.2B, IR-induced sensitivity was completely rescued by re-introduction of centrobin into *CNTROB* KO cells.

Aside from centrobin's known interaction with BRCA2, a recent proteomic study of the centriole-cilium interactomes identified FANCD2 as a centrobin-interacting protein (Zou et al. 2005, Gupta et al. 2015). FANCD2 is one of the Fanconi Anemia family of proteins. It plays crucial role in steps required for DNA strand crosslink repair, especially during S-phase (Knipscheer et al. 2009, Moldovan and D'Andrea 2009). The interaction between centrobin and FANCD2 led us to investigate the possible functions of centrobin in the repair of MMS-induced DSB . We observed that *CNTROB* KO cells have decreased viability compared to wild-type cells after exposure to MMS. This phenotype was only partially rescued by centrobin re-expression (Figure 5.2C). On the other hand, *CNTROB* KO cells have a comparable sensitivity to wild-type cells after UV-C treatment (Figure 5.2D), while centrin2 null hTERT-RPE1 cells (Prosser and Morrison 2015) were used as experimental control. Similar to previous observations in human and chicken cells, *CETN2* KO cells showed hypersensitivity to UV (Dantas et al. 2011, Daly et al. 2016). These results show centrobin is essential for successful repair of DSBs by participating in HR repair pathways through mechanisms that remain unknown but may involve its interactions with BRCA2 and FANCD2.

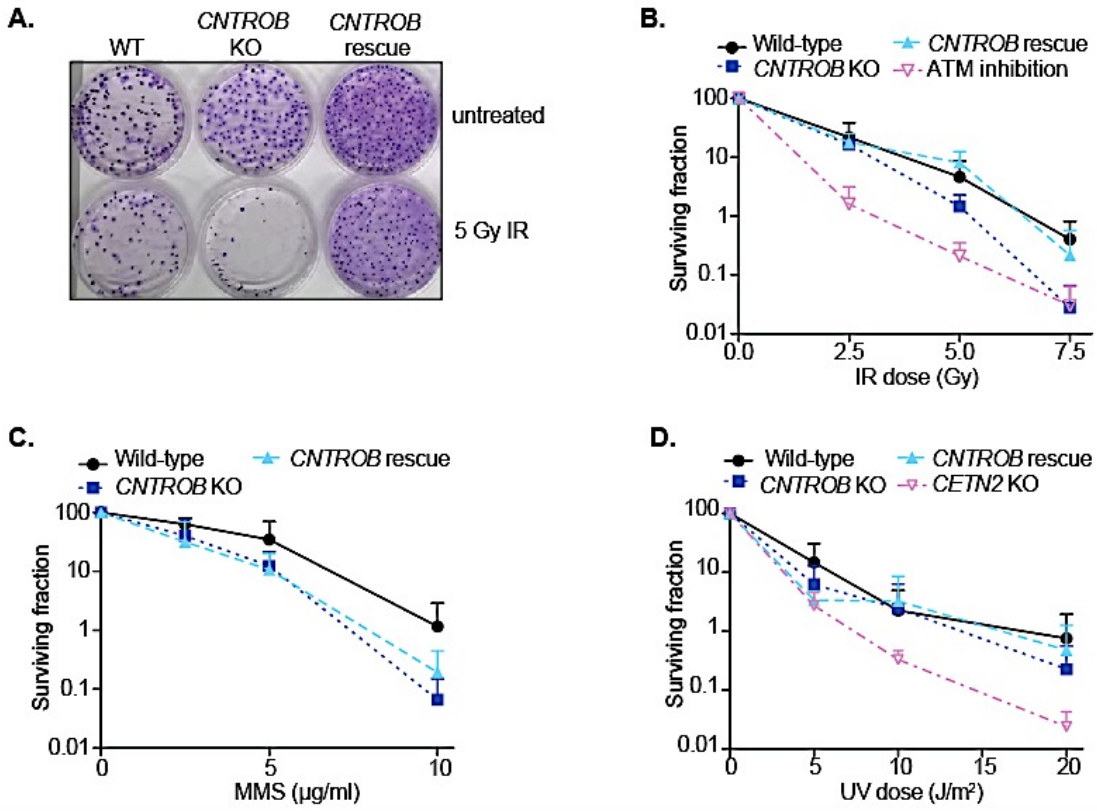

Figure 5.2: Centrobin-deficient cells are sensitive to IR- and MMS-induced DNA damage

A. Representative image of clonogenic survival plates at 12 days before (untreated) and after IR treatment (5 Gy). The image shows the difference in viability between cells of indicated genotypes. **B.** Clonogenic survival assay of wild-type, *CNTROB* KO and *CNTROB* rescue after treatment with

indicated doses of IR. ATM inhibition with KU 55933 in wild-type cells was used as a control. **C.** Clonogenic survival assay of wild-type, *CNTROB* KO and *CNTROB* rescue after treatment with indicated doses of MMS. **D.** Clonogenic survival assay of wild-type, *CNTROB* KO and *CNTROB* rescue after treatment with indicated doses of UV-C. *CETN2* knockout cells were used as experiment control. Data represent percent surviving colonies ± SEM of at least three independent experiments. Each experiment was performed in triplicate and the counts were normalised to the untreated control.

5.4 Centrobin ablation results in defective DSB repair

Following DNA damage, a number of repair and signalling factors are recruited to the site of damage to form nuclear foci which facilitate successful repair of damaged DNA. Phosphorylation and accumulation of H2AX at DNA damage sites occur within minutes of detecting DSB (Rogakou et al. 1999). γ–H2AX acts as a platform for the localisation and recruitment of downstream DNA repair and signalling factors (Rogakou et al. 1999). The interaction of RAD51 and BRCA2 is required for effective homology-dependent repair. RAD51 is a recombinase recruited and stabilised by BRCA2 at DSBs to mediate homology search and strand invasion into the homologous template during HR (Davies et al. 2001; Jensen et al. 2010). Due to the high sensitivity of centrobin nulls to IR- and MMS- induced DNA damage, we investigated the efficiency of focal recruitment of γ–H2AX and RAD51 to sites of DSBs.

5.4.1 Reduced RAD51 focal recruitment in centrobin-deficient cells

To determine if centrobin affects the HR repair pathway, we examined the ability of centrobin null cells to form γ–H2AX and RAD51 IRIF. We subjected wild-type, *CNTROB* KO and *CNTROB* rescue cells to 5 Gy IR and fixed and stained the cells for immunofluorescence microscopy. Images showing cells with typical IRIF in wild-type and knockout cells at the indicated time points are shown in Figure 5.3A and Appendix 5. The number of cells with ≥10 RAD51 IRIF was dramatically reduced in centrobin null cells. Quantification of IRIF frequency revealed a ≤30% fold reduction in the *CNTROB* KO cells with ≥10 RAD51 IRIF at 3 and 6 h when compared to the corresponding wild-type cells (Figure 5.3B). Interestingly, this phenotype was rescued in cells stably expressing transgenic centrobin (Figure 5.3B). Although we noticed impaired accumulation of γ–H2AX foci in *CNTROB* KO cells in preliminary experiments, we decided to investigate the recruitment of RAD51 and accumulation of γ–H2AX at break sites after DNA damage using automated microscopy instead of manually counting foci (sections 5.4.2 and 5.4.3 below). This is due to the laborious work and time required for manual counting and also to eliminate bias and minimise errors during quantification. However, the results of our RAD51 analysis along with

the clonogenic experiments, suggest that centrobin is involved in effective recruitment of the HR machinery to DNA damage sites.

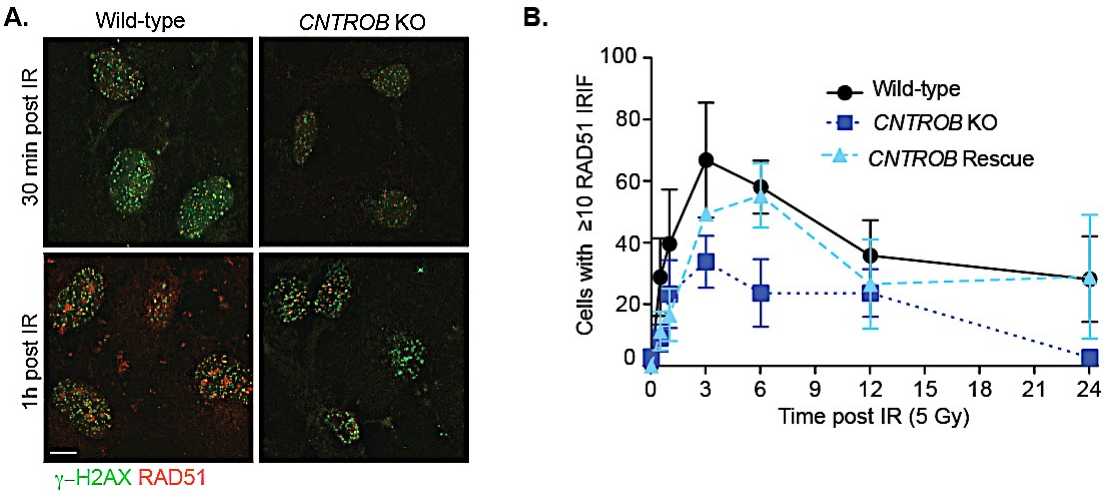

Figure 5.3: Centrobin is required for efficient DNA-damage induced RAD51 foci formation

A. Representative immunofluorescence micrograph showing RAD51 focal recruitment in wild-type and *CNTROB* knockout cells after treatment with 5 Gy IR. Cells were fixed with 4% PFA at the indicated time points. Antibodies against γ-H2AX (green) and RAD51 (red) were used. Hoechst was used to visualize DNA (blue). Scale bar, 5 µm. **B.** Quantitation of number of cells with ≥10 RAD51 foci in wild-type, *CNTROB* KO and centrobin rescue after treatment with 5 Gy IR. At least 100 cells were counted per experiment and the mean ± SEM of 3 independent experiments is shown for each of the time points.

5.4.2 Centrobin null cells show defective RAD51 and γ-H2AX foci formation after IR-induced double strand breaks

To corroborate our initial observation of centrobin's function in HR, we monitored γ-H2AX and RAD51 foci formation by automated microscopy experiments carried out in collaboration with Dr. David Gaboriau at the Faculty of Imaging by Light microscopy (FILM), Imperial College London, UK. Representative micrographs showing the defined region of interest (ROI) that determines a cell (DAPI ROI) and RAD51 foci (RAD51 foci counted) in untreated and irradiated wild-type and *CNTROB* KO cells are shown in Figure 5.4A. As shown in Figure 5.4B, the number of RAD51 and γ-H2AX foci per cell were significantly reduced in *CNTROB* KO when compared to the wild-type (Figure 5.4B-C). The number of foci per cell peaked 3 h after IR and the phenotype was particularly pronounced at 3-12 h post-IR. Notably, this phenotype was rescued in our transgenic centrobin rescue cell line (Figure 5.4B-C).

To minimise experimental variation, the cells used in this experiment were evenly irradiated on the slide prior to immunofluorescence microscopy to study IRIF. We also performed flow

cytometry analysis after treatment with IR (section 5.4.5) to ensure there were no differences in cell cycle arrest since G1 cells generally have reduced IRIF compared to cells in G2 phase of the cell cycle (Löbrich et al. 2010, Hernández et al. 2013). This increase in IRIF in G2 cells is as a result of doubled histone content after DNA replication (Löbrich et al. 2010, Hernández et al. 2013). As discussed in section 5.4.5, we observed no significant difference in cell cycle distribution of centrobin-deficient cells after IR treatment. Also, determining DAPI ROI helped to discriminate between cells at different phases of the cell cycle. This discrimination helped us to increase the reliability of our experimental findings.

γ-H2AX and RAD51 IRIF formation in irradiated cells is indicative of effective cellular DNA damage responses and ongoing HR repair, respectively. Since the dose of DNA damage induced in all the cells was the same, a similar level of response was expected. Therefore, these results implicate a defective ability to recognise break sites or a defective DNA damage response in our *CNTROB* KO cells after exposure to IR (Figure 5.3 and Figure 5.4).

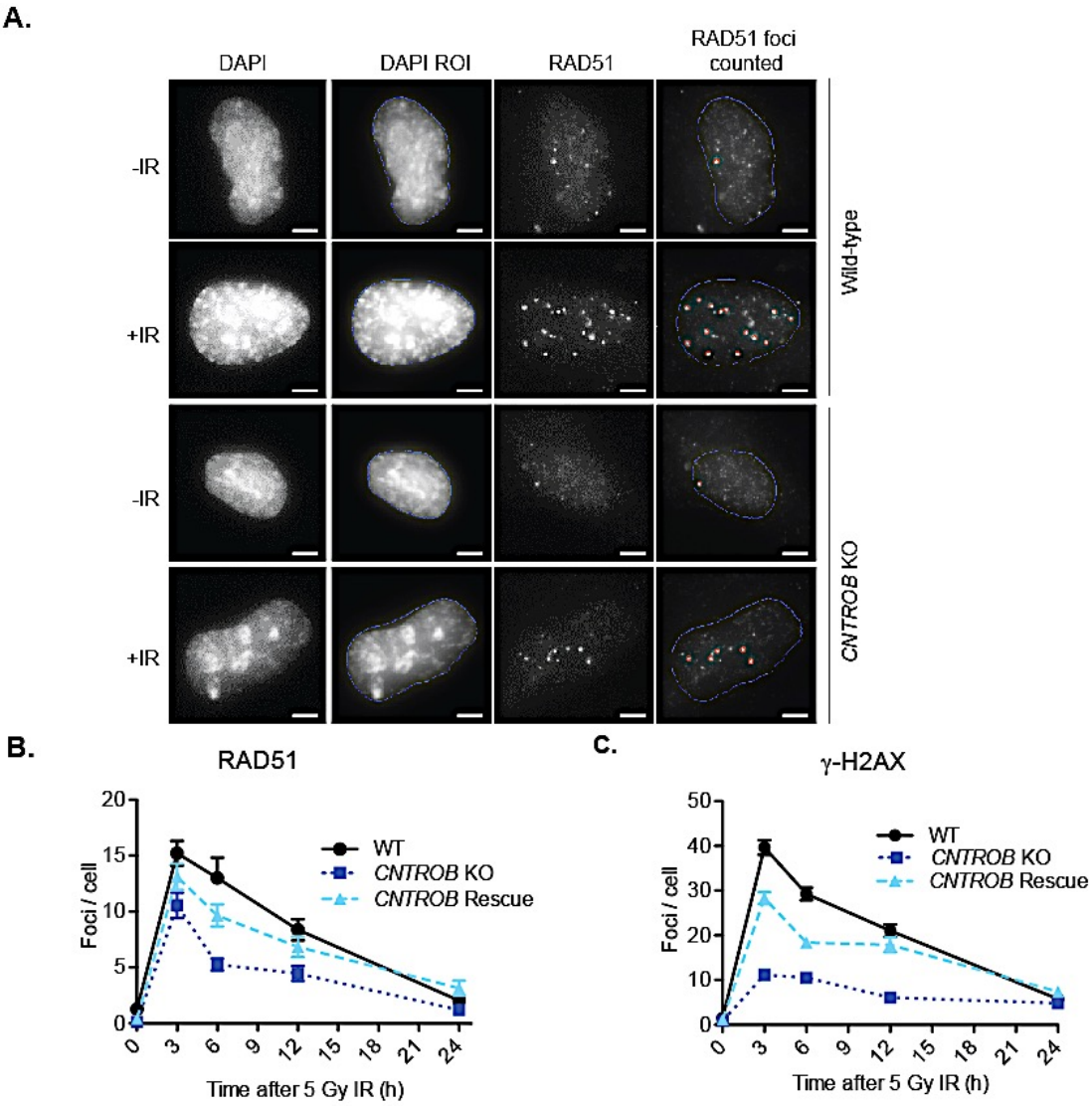

Figure 5.4: Centrobin-deficient cells show defective RAD51 and γ−H2AX foci formation after IR treatment (Automated microscopy analysis)

A. Immunofluorescence micrographs of cells showing examples of wild-type and *CNTROB* KO cells before (-IR) and after (+IR) 5 Gy IR treatment. Cells were stained with RAD51 and counterstained with Hoechst for visualising the DNA. DNA was used to define the region of interest (ROI) for automated focus quantitation. Foci counted were defined as shown on the right. Scale bars, 5 µm. **B.** Quantitation of the mean number of RAD51 foci per cell ± 95% confidence interval (CI) at the indicated time points. **C.** Quantitation of mean number of γ-H2AX foci per cell ± 95% (CI) at the indicated time points. At least 800 cells were counted per experiment and the mean of 2 independent experiments is shown for each of the time points. (Y.A prepared the slides; Dr. Gaboriau conducted imaging and analysis).

5.4.3 Centrobin-deficient cells are sensitive to MMS-induced DNA damage

The sensitivity of centrobin-deficient cells in the clonogenic survival assay led us to investigate potential role of centrobin in DNA DSB repair. Since HR-deficient mammalian cells are sensitive to alkylating agents such as methyl methanesulphonate (MMS) treatment. MMS-induced collapsed replication forks or the presence of heat-sensitive methylated DNA intermediates generate DSB that are repaired by HR (Lundin et al. 2005, Ma et al. 2011).

RAD51 and γ-H2AX are also involved in the DSBs repair induced by MMS (Nikolova et al. 2010). Again, we studied focal recruitment of RAD51 and γ-H2AX by automated immunofluorescence microscopy analysis. We noticed a dramatic reduction in the number of foci per cell after 2 h treatment with 20 μg/ml of MMS at the indicated times. Representative immunofluorescence micrographs are shown in Figure 5.5A. The DAPI ROI and RAD51 foci were defined as previously described for IR. We also observed a significant reduction in the average number of RAD51 and γ-H2AX foci per cell (Figure 5.5B-C). These results implicate centrobin in DSBs and DNA crosslink repair. Inter- or intrastrand crosslink repair is essential for efficient replication and transcription, therefore, DNA damage due to strand crosslinks is extremely toxic to cells.

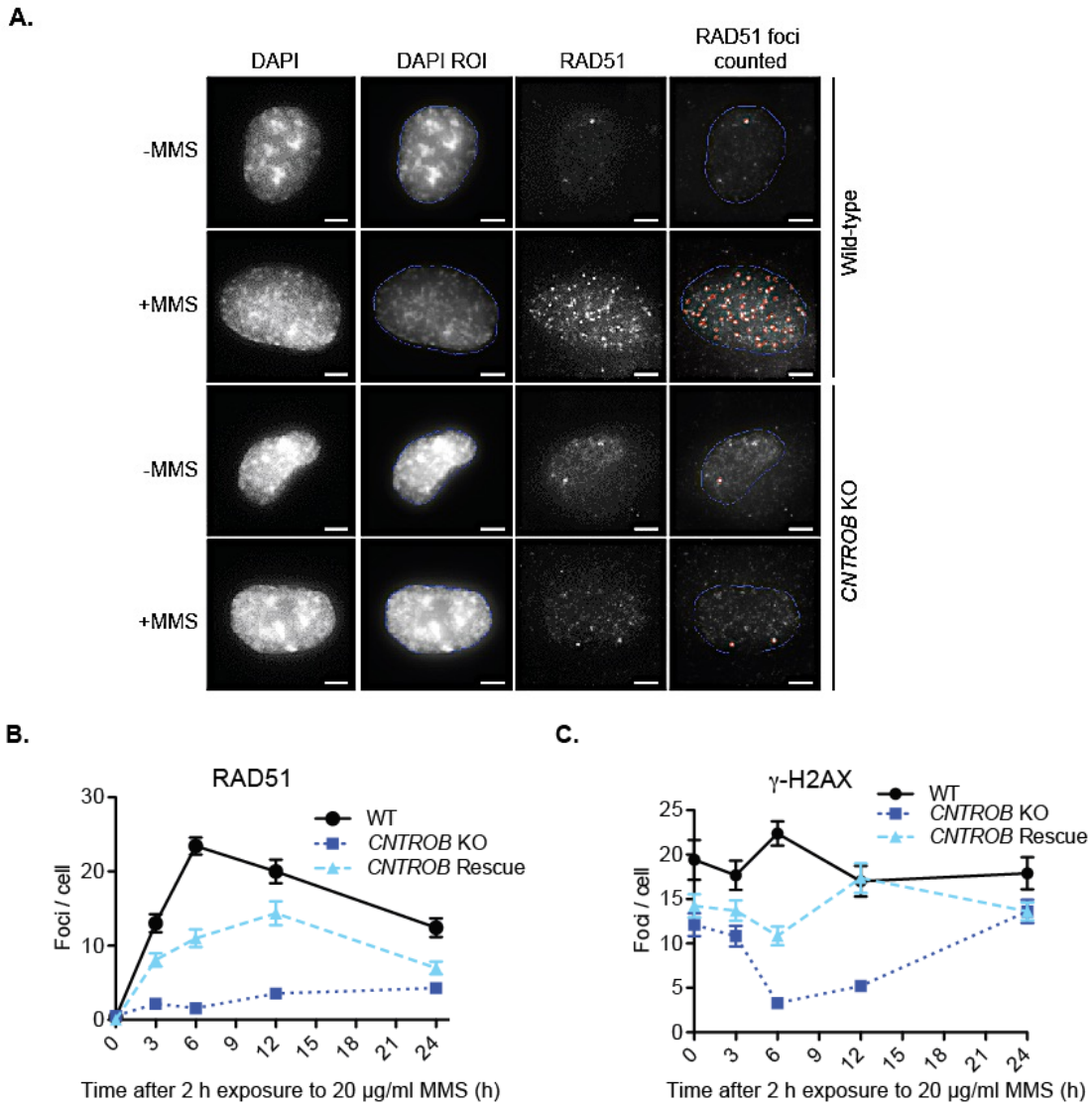

Figure 5.5: *CNTROB* KO cells show defective RAD51 and γ−H2AX foci formation after MMS treatment (Automatic microscopy analysis)

A. Immunofluorescence micrographs of cells showing examples of wild-type and *CNTROB* KO cells before (-MMS) and after (+MMS) 20 µg/ml MMS treatment. Cells were stained with RAD51 and counterstained with Hoechst for visualising the DNA. DNA was used to define the region of interest (ROI) for automated focus quantitation. Foci counted were defined as shown on the right. Scale bars, 5 µm. **B.** Quantitation of mean number of RAD51 foci per cell ± 95% confidence interval (CI). After 2 h treatment with 20 µg/ml MMS, cells were harvested for IF at the indicated time points. **C.** Quantitation of mean number of γ-H2AX foci per cell ± 95% CI. After 2 h treatment with 20 µg/ml MMS, cells were harvested for IF at the indicated time points. At least 800 cells were counted per experiment and the mean of 2 independent experiments is shown for each of the time points. (Y.A prepared the IF slides, while imaging and analysis were conducted by Dr. Gaboriau).

5.4.4 *CNTROB* KO cells show effective G2/M checkpoint activation after IR

To determine if *CNTROB* KO cells activate G2/M checkpoint after DNA damage, we carried out flow cytometry analysis after IR treatment. As shown in Figure 5.6, wild-type, *CNTROB* KO and rescue cells, were capable of activating a G2/M checkpoint response, although *CNTROB* KO and rescue cells progressed slowly into G2, as revealed by the cell cycle profile at 3 h time point post 5 Gy IR (Figure 5.6). However, the majority of the *CNTROB* KO and rescue cells accumulated in G2/M between 2 and 6 h post IR. This result suggests that centrobin-deficient cells were capable of recognising DNA damage and activating cell cycle checkpoint arrest, but they are unable to recruit DNA repair machineries to site of the DNA lesion as shown by defective RAD51 and γ-H2AX focal formation (section 5.4.2). These data also show that the reduced number of RAD51 and γ-H2AX foci were not a result of difference in cell cycle stage between wild-type and centrobin-deficient cells.

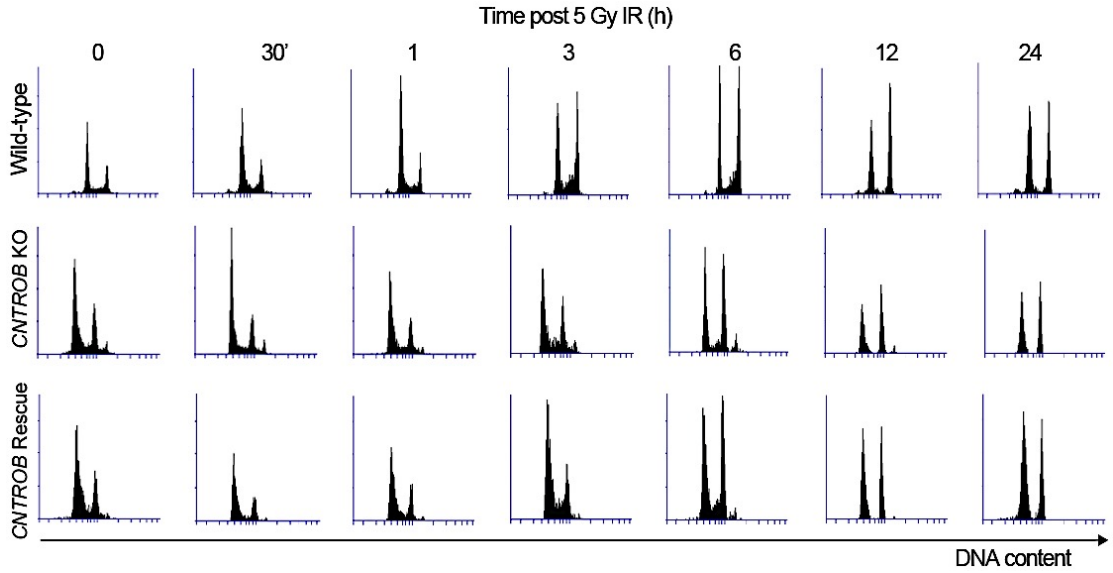

Figure 5.6: FACS analysis shows effective G2/M checkpoint activation in *CNTROB* KO cells

Flow cytometry analysis of the DNA content of wild-type, *CNTROB* KO and centrobin rescue cells before and at indicated times after 5 Gy IR. Cells were stained with propidium iodide and analysed on a BD Accuri C6 sampler and flow analysis software. 10,000 events were recorded per timepoint.

5.5 Centrobin-deficient cells show sensitivity to PARP inhibition

Given the inability of centrobin-deficient cells to effectively repair DNA damage as revealed by failure to recruit repair machineries to the site of damage, we aimed to investigate the relevance of centrobin in the two major DSBs repair pathways. NHEJ and HR are employed for DSB repair depending on the phase of the cell cycle (Takata et al. 1998). Cells deficient in HR repair machineries accumulate toxic DSBs and are sensitive to PARP inhibition (Bryant

et al. 2005, Senra et al. 2011). The PARP family of proteins is required for effective DNA damage signalling and repair (Bryant et al. 2005, Fong et al. 2009), and their inhibition can be chemically induced using olaparib. Olaparib induces nicks that are converted into DSBs during replication. On the other hand, ICRF-193 inhibits topoisomerase II activation by inducing 'close clamped' interaction between topoisomerase II and the DNA causing DSBs that are primarily repaired by NHEJ (Adachi et al. 2003). To determine the specificity of centrobin for either the HR or NHEJ repair pathways, we performed clonogenic survival assays on *CNTROB* KO cells treated with olaparib or ICRF-193. As shown in Figure 5.7, centrobin null cells were mildly sensitive to olaparib treatment at all doses used and the centrobin-rescue cell line only partially rescued the sensitivity to HR-specific breaks induced by olaparib. Here, we used ATM inhibition in wild-type cells as an experimental control since ATM inhibition compromises repair of DSBs. A characteristic feature of ATM-depleted cells is hypersensitivity to ionizing radiation that results from failure to activate the G2/M checkpoint and an accumulation of unrepaired DNA mutations that ultimately leads to cell death (Hickson et al. 2004). In contrast, wild-type and *CNTROB* KO cells showed a similar level of sensitivity to ICRF-193 (Figure 5.7B). Wild-type cells treated with DNA-PK inhibitor were sensitive due to the requirement of DNA-PK holoenzyme for NHEJ-mediated DSB repair (Ciccia and Elledge 2010, Chatterjee and Walker 2017). These preliminary data and our previous observations of defective RAD51 and γ-H2AX foci formation strongly suggest that centrobin is one of the players in the HR but not in the NHEJ DSB repair pathway, through a mechanism that remains to be defined.

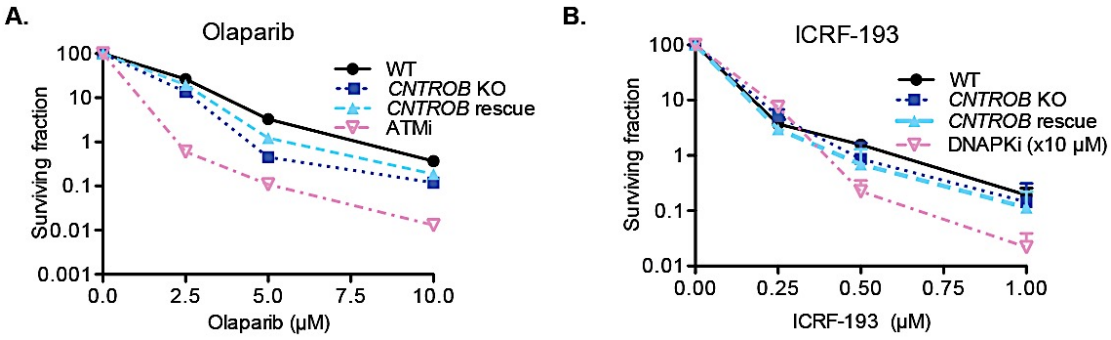

Figure 5.7: Centrobin null cells are sensitive to PARP inhibition

A. Clonogenic survival assay of wild-type, *CNTROB* KO and *CNTROB* rescue cells after treatment with indicated doses of olaparib. Each data point represents the percentage of surviving colonies of a single experiment with triplicates that were normalised to the untreated control. N=1. Wild-type cells treated with ATM inhibitor, KU55933, were used as experimental control. **B.** Clonogenic survival assay of wild-type, *CNTROB* KO, *CNTROB* rescue cells after treatment with indicated doses of ICRF-193. Wild-type cells treated with DNA-PK inhibitor, KU57788, were used as experimental control. Each data point represents the percent of surviving fraction of 2 independent experiments. Each experiment was performed in triplicate and was normalised to the untreated control.

5.6 Dynamics of centrobin localisation in damaged human cells

At this stage, we were unsure whether centrobin mediates its DDR role at the centrosome or via a yet-to-be identified nuclear pool of centrobin. To verify the possibility of centrobin localising to break sites after DNA damage, we tried different immunofluorescence microscopy conditions which included changes in pre-extraction buffer, ice-cold depolymerisation time, fixing and staining conditions before and after IR treatment. Unfortunately, we were unable to detect nuclear staining for centrobin under any of these conditions (data not shown). A representative immunofluorescence micrograph of our analyses is shown in Figure 5.8. In this particular experiment, we used cytoskeletal buffer (CSK) and wild-type and *CNTROB* KO cells were mixed on the slides and identified by centrobin staining at the centrosome. Again, we used γ–H2AX as a marker of DSBs. As shown in Figure 5.8, we did not observe any non-centrosomal colocalisation of centrobin and γ–H2AX before or after treatment with IR and CSK buffer. We believed that the localisation of γ–H2AX to the centrosome that was mainly observed after CSK treatment is a result of phospho-antibody cross-reactivity to a phosphorylated centrosomal protein and not the presence of histones at the centrosome. To our knowledge, there is no published evidence showing the localisation of, or a role for, histones at the centrosome (Marshall and Rosenbaum 2000).

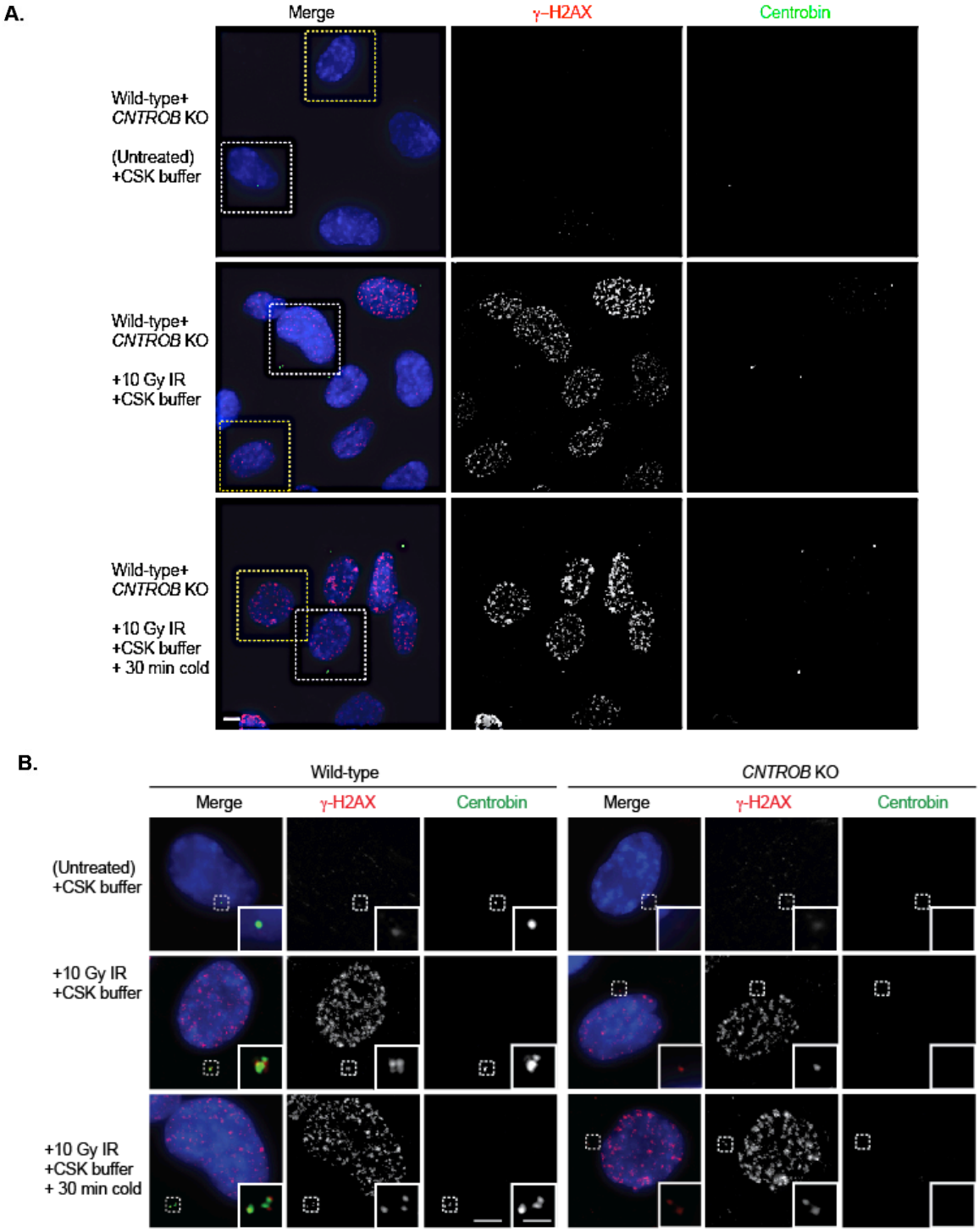

Figure 5.8: Centrobin was not detected at DSBs sites in hTERT-RPE1 cells

A. Immunofluorescence microscopy analysis of a mixture of wild-type and *CNTROB* KO before and 30 min after treatment with 10 Gy IR. Cells were fixed after cytoskeletal extraction at room temperature or on ice for 30 min. White and yellow boxes indicate wild-type (white) and *CNTROB* KO cells (yellow) used for the blow-ups in **B** below. Antibodies to γ–H2AX (red) and centrobin (green) were used and DNA was stained with Hoechst. Scale bars, 5 µm and inset scale bar, 1 µm.

5.7 Discussion

We observed defective centrosome duplication in centrobin-deficient cells (Section 3.9), and previously published reports had implicated centrobin in PLK4 overexpression- and HU-induced centrosome overduplication (Zou et al. 2005, Gudi et al. 2011). Centrosome amplification occurs when the cell cycle and centrosome duplication are dissociated by DNA damage (Dodson et al. 2004, Bourke et al. 2007, Löffler et al. 2013). We analysed centrosome amplification following treatment with genotoxic agents such as HU, IR and UV and found that centrobin-deficient cells have reduced capability to induce centrosome overduplication after exposure to these genotoxic stress inducers. These results agree with centrobin acting as a centriole duplication factor. Depletion of centrobin limits the rate of centrosome duplication (Chapter 3) and DNA damage-induced centrosome amplification. As previously discussed (Chapter 3), this reduced centrosome amplification phenotype may be due to the effects of centrobin loss on the dynamics, stability and kinetics of cartwheel and procentriole assembly during centriole duplication.

We carried out clonogenic survival assay to determine the sensitivity of centrobin-deficient cells to different DNA damage agents. The sensitivity of *CNTROB* KO cells to IR, MMS and olaparib strongly suggests the involvement of centrobin in efficient DNA repair, notably HR-mediated repair of DSBs. It is well established that cells with a compromised HR, such as BRCA2- or RAD51-deficient cells, are hypersensitive to PARP inhibition due to their reliance on PARP activity for maintenance of genomic integrity and cell survival (Tutt et al. 1999, Fong et al. 2009, Senra et al. 2011, Dziadkowiec et al. 2016). Based on this knowledge, our findings identify centrobin in the HR repair of DSBs, although further experiments, such as the DR-GFP assay (Pierce and Jasin 2005, Nakanishi et al. 2011), will be required in the future to determine the mechanism of action of centrobin as a component of the HR.

Furthermore, we also observed drastic reduction in the number of cells with efficient formation of γ-H2AX and RAD51 foci after exposure of centrobin-deficient cells to IR and MMS. Because γ-H2AX is one of the earliest modifications that is rapidly formed at the site of DSBs (Rogakou et al. 1999; Podhorecka et al. 2010), this result indicates that DSB detection and the initial stage of DDR are defective in *CNTROB* null cells. The exact mechanism through which centrobin facilitates DNA repair remains unknown. One may speculate a possible requirement for centrobin-BRCA2 interaction for the role of BRCA2 during RAD51 nucleofilament assembly on resected DNA during HR. It is interesting that similar to other HR proteins, *CNTROB* has also been described as a breast cancer predisposition gene (Moynahan et al. 2001; Lose et al. 2006; O'Driscoll, 2012; Wang et al. 2012). The insensitivity of *CNTROB* null cells to UV and ICRF-193 also suggests that

centrobin may not mediate SSB repair or NHEJ. Instead it promotes efficient HR, as may also be highlighted by its interaction with BRCA2 and FANCD2.

Our FACS analysis of centrobin-deficient cells revealed an increase in the percentage of cells in G2/M after exposure to IR. Efficient activation of the G2/M checkpoint in *CNTROB* KO cells suggests effective DNA damage-induced ATR/ATM activation, which is required for the checkpoint activation (Hoffmann 2000, Donzelli and Draetta 2003, Shaltieì et al. 2015). Based on the ability to activate the G2/M checkpoint and the observation that centrobin-deficient cells were not as sensitive to IR as the ATM-inhibited cells in a clonogenic survival assay, it can be hypothesised that centrobin acts downstream of these PIK kinases in the HR-mediated repair of DSBs. This possibility is supported by the presence of 10 potential PIK-kinase phosphorylatable SQ/TQ consensus sequences on the *CNTROB* gene product (Traven and Heierhorst 2005).

While no direct demonstration of nuclear centrobin has been published to date, its reported interaction with BRCA2 and FANCD2 (Zou et al. 2005, Gupta et al. 2015) may point to its potential nuclear localisation and DNA damage roles. Although not all DDR proteins can accumulate at DNA breaks to form distinct microscopically detectable foci (Polo and Jackson 2011), we investigated the possibility of centrobin forming nuclear foci after IR. We observed no nuclear foci of centrobin by immunofluorescence microscopy of irradiated hTERT-RPE1 cells. However, the absence of detectable nuclear centrobin foci may be as a result of the nuclear pool of centrobin not aggregating to form foci, or that the foci formed cannot be detected microscopically due to their very low cellular levels. Moreover, endogenous levels of centrobin is kept at a very low level in most human cells (Zou et al. 2005). Recently, a non-centrosomal pool of centrobin was described (Jeong et al. 2007, Shin et al. 2015). In fact, subcellular fractionation of the human KE37 whole cell extract showed that centrobin has similar distribution to that of Nek2 (Jeong et al. 2007). It is worth noting that the vast majority of Nek2 is not associated with the centrosome and that it also exhibits nuclear localisation (Fry et al. 1998; Fletcher et al. 2004; Naro et al. 2014). In addition, another interacting partner of centrobin during centriole biogenesis, CEP152, has been shown to have weak nuclear localisation and to directly participate in the DDR (Kalay et al. 2011). For example, in Seckel syndrome patient cells with impaired CEP152 functions, HU-induced replication stress leads to a significant increase in CHK2 and H2AX phosphorylations (Kalay et al. 2011). These findings further support the possibilities of low nuclear levels of centrobin that participate in the DDR.

Based on our observations, we propose three potential models through which centrobin controls the DDR (Figure 5.9). First, it is possible that a yet-to-be identified pool of nuclear centrobin directly interacts with BRCA2 and FANCD2 to facilitate centrobin's role in the

DDR. Second, since the centrosome and nucleus are physically associated in interphase cells, it is possible that the microtubule stabilising activity of centrobin may modify nuclear activities during the DDR. A final alternative model may be based on the impact of the centrosome on the nuclear envelope to modulate the subnuclear localization of damaged DNA damage or the activation of DDR signalling (Kumar et al. 2014). Recent data implicating the linker of nucleoskeleton and cytoskeleton (LINC) complex of the nuclear envelope in DSBR (Lottersberger et al. 2015; Lawrence et al. 2016) suggests a promising avenue for further exploration. The tethering of the centrosome to the LINC complex has been shown to be relevant for centrosome positioning and polarity (Chang et al. 2015). The possibility that loss of centrobin may affect the stability of the interaction between the centrosome and the LINC complex requires further investigation.

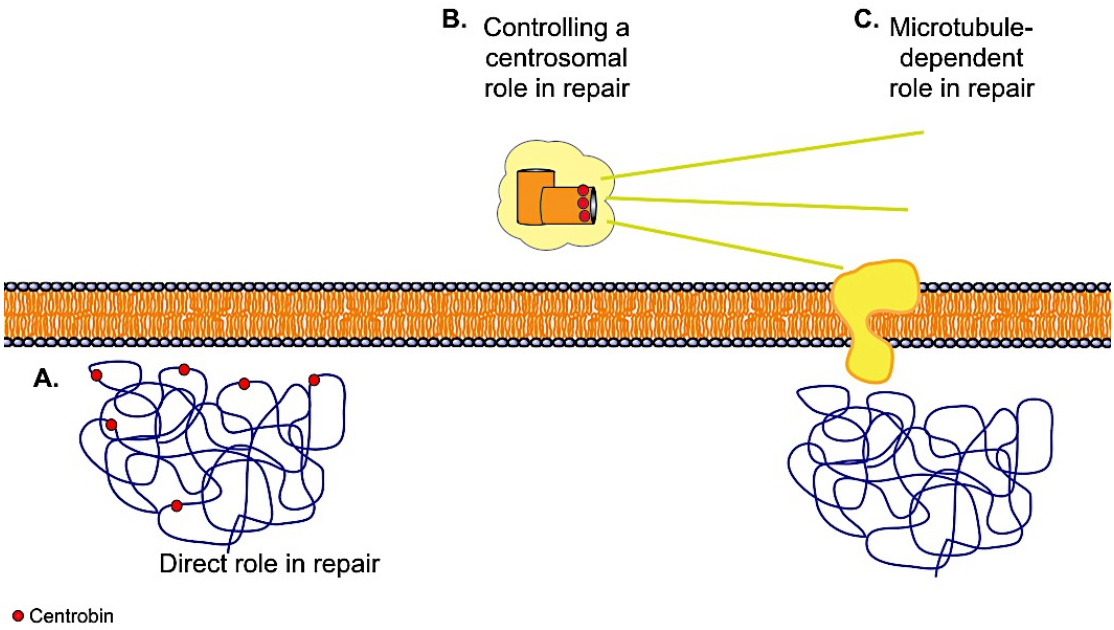

Figure 5.9: Current model of centrobin involvement in DNA-damage response

Upon DNA damage, centrobin may control DNA repair through: **A**. Its direct interaction with HR proteins inside the nucleus. **B**. Centrobin may impact the DDR through centrobin-induced centrosomal response to DSBs. **C**. Finally, it may mediate its effect by invoking microtubule-stabilising activities of centrobin that regulate nuclear localisation of DDR proteins.

The connection between the centrosome, cilia and DDR has been a recent focus of study. The link between supernumerary centrosomes and genome instability, as is observed in cancer cells, has long been suggested as an interplay between the DDR and centrosome regulation. Aside from centrobin, defects in several centrosome-associated and DDR proteins have been described in human diseases, notably in nephronophthisis-related ciliopathies, a group of genetically and clinically heterogenous autosomal-recessive cystic kidney disorders that arise

through ciliary dysfunction (Schueler et al. 2016). For example, SDCCAG8 is a centriolar component that colocalizes with TIP60, an acetylase that regulates ATM (Chaki et al. 2012). SDCCAG8 loss leads to increased DDR signalling, although the underlying mechanism is not understood (Airik et al. 2014). Therefore, our observation of a homologous recombination defect in centrobin-deficient cells provides a new instance of a centrosome-cilium regulatory protein having a role in the DDR that requires further mechanistic investigation.

6 Conclusions and future perspectives

Taken together, the data presented here strengthen the idea of a functional link between ciliogenesis and DNA repair pathways and that centrobin participates in both processes. Centrobin is an evolutionarily conserved core centrosomal protein that is ubiquitously expressed in human cells (Zou et al. 2005, Fagerberg et al. 2014). Here, we show that centrobin is a centriole duplication factor. Its depletion results in increased acentriolar and monocentric cells but has no significant effect on cell proliferation or viability. Our data, for the first time, also identify vertebrate centrobin as a positive regulator of primary ciliogenesis. We also identify centrobin as a component of the DNA damage response. It is indispensible for cell viability after genotoxic stress induced by IR, MMS and olaparib, all of which links it to the HR repair mechanism.

In this study, we used reverse genetics to examine the roles of centrobin in centriole duplication and cell cycle progression. siRNA-mediated studies of centrobin in human, normal and cancer cells, as well as rat and *Drosophila*, have shown contradicting results with regards to the roles of centrobin in centrosome duplication and ultimately cell viability (Zou et al. 2005, Liska et al. 2009, Song et al. 2010, Januschke et al. 2013). In our examination of centrobin-deficient cells, although we observed centriole duplication defects, we did not detect any specific cell cycle arrest or proliferation defects. Thus, we concluded that cellular proliferation is possible in the absence of centrobin, at least in karyotypically stable cells. Since most of the reported proliferation defects were found in U2OS and HeLa cells treated with siRNA to mediate the depletion of centrobin, it was possible that such an acute knockdown (by siRNA) of the protein may identify a non-essential but conserved role of centrobin in cell proliferation. Such role may have been compensated for in our *CNTROB* KO cells by proteins with functional redundancy to centrobin during adaptation to loss of centrobin. This phenomenon has been previously observed in mice where 'on-target' siRNA depletion of Cep131 leads to defective ciliogenesis that was not observed in *Cep131* knockout mice (Hall et al. 2013). Another possibility is that the proliferation defects were consequences of 'off-target' effect of the siRNA, a common disadvantage of siRNA (Fedorov et al. 2006, Jackson and Linsley 2010). To understand cell cycle progression and centriole duplication kinetics, it would be interesting to monitor both processes by live cell imaging of our *CNTROB* KO cells, a centrobin null cancer cell line and both cell lines with a $p53^{-/-}$ background. An independent method to validate centriole duplication would be to carefully monitor hSas6 timing and stability at the centriole biogenesis site. Centrobin is not crucial for recruitment of hSas6 and Cep152 during S-phase procentriole assembly (Gudi et al. 2014; Gudi et al. 2015). However, centrobin directly interacts with these proteins during centriole biogenesis and the exact role of centrobin in the centriole biogenesis proteins assembly remains to be answered.

The impact of PLK1 or Nek2 modifications of centrobin on cellular microtubule organisation and stabilisation has been previously described in human cells. PLK1 promotes its microtubule-stabilising activity that is required for bipolar spindle formation, while Nek2 antagonises centrobin-induced microtubule stability to regulate cell morphology and migration in interphase cells (Lee et al. 2010, Park and Rhee 2013). In our analysis of centrobin-deficient cells, we did not detect a noteworthy structural defect in the microtubule network. Here, we concluded that loss of centrobin had no significant impact on the microtubule network due to the correct composition of the centrosome. Apart from centrobin, several other centrosomal proteins, including hSas6, CPAP, ninein and the γ-TuRC complex, have been shown to control microtubule anchoring and dynamics. These proteins may have redundant roles that compensate for the loss of centrobin (Delgehyr et al. 2005; Leidel et al. 2005; O'Toole et al. 2012; Zheng et al. 2016). Determining the rate of microtubule repolymerisation after cold treatment of centrobin-deficient cells would be of great benefit to our understanding of the relevance of centrobin in microtubule stability.

To gain better understanding of the molecular mechanisms through which centrobin facilitates ciliogenesis, we carefully analysed its localisation in asynchronous and ciliated cells. We found that centrobin, which was initially characterised as a daughter centriole specific protein (Zou et al. 2005), also localises to the mother centriole after inducing ciliogenesis. The exact kinetics of centrobin translocalisation from mother to daughter centrioles is not yet clear. We also provide support for a novel role of centrobin in primary cilium formation. Human cells and zebrafish embryos deficient in centrobin were unable to efficiently form primary cilia. Interestingly, expression of either the human or *Drosophila* centrobin rescued the defect in ciliation capacity in *CNTROB* KO cells. Further analysis revealed that CP110 stabilisation at the mother centriole contributes to the ciliogenesis defect, and thus we concluded that centrobin is a component of the complex molecular mechanism that is required for efficient CP110 removal. A recent study on proteins that preferentially localise to the daughter centrioles reported that Neurl-4 also translocates to the mother centriole before primary cilium assembly and also contributes to CP110 removal during ciliogenesis (Loukil et al. 2017). However, it is still unclear how the biochemical composition of the distal ends of the mother and daughter centrioles accounts for the asymmetric removal of CP110 from the mother centriole (basal body), while it remains at the distal end of the daughter centriole.

An examination of centrobin truncation mutants revealed that the C-terminal region (aa 452-903) comprising the tubulin-interacting domains is sufficient to rescue ciliogenesis. While we did not show here that this fragment interacts with CP110, the C-terminal region (aa 365 – 903), which contains the CP110- and tubulin-binding domain, was also able to support ciliation. Importantly, expression of the tubulin-binding domain (aa 765-903), which is

crucial for its centrosomal localisation, is not sufficient to rescue the ciliogenesis defect in *CNTROB* KO cells. To fully understand the relationship between CP110 and centrobin, it would be interesting to determine the impact of these C-terminal truncation mutants on CP110 localisation. Since siRNA-mediated depletion of CP110 only partially rescues ciliogenesis, we therefore concluded that centrobin might facilitate both CP110 removal and tubulin stabilisation during ciliogenesis. The microtubule-stabilising role of centrobin at the centrioles has been well described (Jeong et al. 2007, Lee et al. 2010, Gudi et al. 2011, Shin et al. 2015). Similar to previously reported observations that transient overexpression of C-terminal fragments of centrobin leads to formation of cytosolic microtubules in proliferating cells (Jeong et al. 2007; Gudi et al. 2011), we also observed these aggregates in asynchronous and ciliated cells. It is therefore conceivable that centrobin also promotes microtubule stability during primary cilium assembly and elongation. A previous report has highlighted that centrobin organises acetylated tubulin in preference to tyrosinated tubulin (Jeong et al. 2007). Since acetylated and detyrosinated tubulin modifications are crucial for centriole elongation and primary cilium assembly (Hammond et al. 2008), it would be interesting to determine how centrobin impacts tubulin modifications during both processes.

With our data supporting centrobin as a positive regulator of ciliogenesis in hTERT-RPE1 cells, we aimed to determine its ciliary function in an entire organism by monitoring embryonic development in zebrafish. It has been well reported that defective cilia during zebrafish embryogenesis can give rise to laterality defects, incorrect organ positioning and developmental abnormalities (Kramer-Zucker et al. 2005, Kinkel et al. 2008, Goetz and Anderson 2010, Diiorio et al. 2014). We found that centrobin-depleted zebrafish embroyos showed reduced cilia frequency and organ mislocalisation. Further analysis of the involvement of centrobin in the Hh signalling pathway may help to explain the mechanism through which centrobin facilitates ciliogenesis, since components of the Hh, PDGF and Wnt signalling pathways localise to the primary cilia and are important during embryogenesis (Corbit et al. 2005; Schneider et al. 2005; Lancaster et al. 2011; Diiorio et al. 2014). So far, our data suggest a novel function for centrobin in human and zebrafish cilia-dependent signalling which provocatively raise the possibility that *CNTROB* is a ciliopathy gene that may be of clinical relevance.

In addition, our data also show that centrobin functions in DNA repair but not in G2/M checkpoint activation. A role for centrobin in DNA repair was suggested by its being initially described as a BRCA2 interactor (Zou et al. 2005). Furthermore, centrobin interaction with FANCD2 was noted in a proteomic study of the interactions of centriolar-cilium proteins (Gupta et al. 2015), consistent with the requirement we see for centrobin in efficient homologous recombination and crosslink repair. Whether centrobin localises to the nucleus to participate in the DNA damage still remains unclear. However, a non-centrosomal pool of

centrobin has been previously reported (Jeong et al. 2007, Shin et al. 2015). However, we suggest a careful analysis aimed to delineate the underlying molecular mechanisms and the subcellular localisation of centrobin in the future. Finally, as *CNTROB* (Wang et al. 2012a), *BRCA2* (Duncan et al. 1998) and *FANCD2* (Barroso et al. 2006) have been reported as breast cancer predisposition genes, further analysis of their functional interactions will define the role of centrobin in DNA repair pathways and its relation to the aetiology of human disorders such as ciliopathy, microcephaly and cancer.

7 References

Adachi, N., H. Suzuki, S. Iiizumi, & H. Koyama. (2003). Hypersensitivity of nonhomologous DNA end-joining mutants to VP-16 and ICRF-193: implications for the repair of topoisomerase II-mediated DNA damage. *J. Biol. Chem.* 278:35897–902.

Adon, A. M., X. Zeng, M. K. Harrison, S. Sannem, H. Kiyokawa, P. Kaldis, & H. I. Saavedra. (2010). Cdk2 and Cdk4 regulate the centrosome cycle and are critical mediators of centrosome amplification in p53-null cells. *Mol. Cell. Biol.* 30:694–710.

Andersen, J. S., C. J. Wilkinson, T. Mayor, P. Mortensen, E. A. Nigg, & M. Mann. (2003). Proteomic characterization of the human centrosome by protein correlation profiling. *Nature* 426:570–4.

Antonczak, A. K., L. I. Mullee, Y. Wang, D. Comartin, T. Inoue, L. Pelletier, & C. G. Morrison. (2015). Opposing effects of pericentrin and microcephalin on the pericentriolar material regulate CHK1 activation in the DNA damage response. *Oncogene* 35:2003–2010.

Arakawa, H., D. Lodygin, & J. M. Buerstedde. (2001). Mutant loxP vectors for selectable marker recycle and conditional knock-outs. *BMC Biotechnol.* 1:7.

Azimzadeh, J. (2014). Exploring the evolutionary history of centrosomes. *Philos. Trans. R. Soc. London B Biol. Sci.* 369.

Azimzadeh, J., & W. F. Marshall. (2010). Building the centriole. *Curr. Biol.* 20:R816-25.

Azimzadeh, J., M. L. Wong, D. M. Downhour, A. S. Alvarado, & W. F. Marshall. (2012). Centrosome Loss in the Evolution of Planarians. *Science (80-.).* 335.

Badano, J. L., T. M. Teslovich, & N. Katsanis. (2005). The centrosome in human genetic disease. *Nat. Rev. Genet.* 6:194–205.

Bahassi, E. M., J. L. Ovesen, A. L. Riesenberg, W. Z. Bernstein, P. E. Hasty, & P. J. Stambrook. (2008). The checkpoint kinases Chk1 and Chk2 regulate the functional associations between hBRCA2 and Rad51 in response to DNA damage. *Oncogene* 27:3977–85.

Bahe, S., Y.-D. Stierhof, C. J. Wilkinson, F. Leiss, & E. A. Nigg. (2005). Rootletin forms centriole-associated filaments and functions in centrosome cohesion. *J. Cell Biol.* 171:27–33.

Bahmanyar, S., D. D. Kaplan, J. G. Deluca, T. H. Giddings, E. T. O'Toole, M. Winey, E. D. Salmon, P. J. Casey, W. J. Nelson, A. I. M. Barth, & A. I. M. Barth. (2008). beta-Catenin is a Nek2 substrate involved in centrosome separation. *Genes Dev.* 22:91–105.

Barroso, E., R. L. Milne, L. P. Fernández, P. Zamora, J. I. Arias, J. Benítez, & G. Ribas. (2006). FANCD2 associated with sporadic breast cancer risk. *Carcinogenesis* 27:1930–1937.

Bartek, J., & J. Lukas. (2003). Chk1 and Chk2 kinases in checkpoint control and cancer. Pages 421–429Cancer Cell. Cell Press.

Basto, R., J. Lau, T. Vinogradova, A. Gardiol, C. G. Woods, A. Khodjakov, & J. W. Raff. (2006). Flies without Centrioles. *Cell* 125:1375–1386.

Benmerah, A. (2013). The ciliary pocket. *Curr. Opin. Cell Biol.* 25:78–84.

Berbari, N. F., J. S. Lewis, G. A. Bishop, C. C. Askwith, & K. Mykytyn. (2008). Bardet-Biedl syndrome proteins are required for the localization of G protein-coupled receptors to primary cilia. *Proc. Natl. Acad. Sci. U. S. A.* 105:4242–6.

Bettencourt-Dias, M. (2013). Q&A: Who needs a centrosome? *BMC Biol.* 11:28.

Bettencourt-Dias, M., & D. M. Glover. (2007). Centrosome biogenesis and function: centrosomics brings new understanding. *Nat. Rev. Mol. Cell Biol.* 8:451–63.

Bettencourt-Dias, M., F. Hildebrandt, D. Pellman, G. Woods, & S. A. Godinho. (2011). Centrosomes and cilia in human disease. *Trends Genet.* 27:307–315.

Bird, A. W., & A. A. Hyman. (2008). Building a spindle of the correct length in human cells requires the interaction between TPX2 and Aurora A. *J. Cell Biol.* 182.

Bloodgood, R. A. (2012). The future of ciliary and flagellar membrane research. *Mol. Biol. Cell* 23:2407–11.

Bobinnec, Y., A. Khodjakov, L. M. Mir, C. L. Rieder, B. Eddé, & M. Bornens. (1998). Centriole disassembly in vivo and its effect on centrosome structure and function in vertebrate cells. *J. Cell Biol.* 143:1575–89.

Bodnar, A. G., M. Ouellette, M. Frolkis, S. E. Holt, C.-P. Chiu, G. B. Morin, C. B. Harley, J. W. Shay, S. Lichtsteiner, & W. E. Wright. (1998). Extension of Life-Span by Introduction of Telomerase into Normal Human Cells. *Science (80-.).* 279.

Bond, J., E. Roberts, K. Springell, S. Lizarraga, S. Scott, J. Higgins, D. J. Hampshire, E. E. Morrison, G. F. Leal, E. O. Silva, S. M. R Costa, D. Baralle, M. Raponi, G. Karbani, Y. Rashid, H. Jafri, C. Bennett, P. Corry, C. A. Walsh, & C. Geoffrey Woods. (2005). A centrosomal mechanism involving CDK5RAP2 and CENPJ controls brain size. *Nat. Genet.* 37:353–355.

Bourke, E., J. A. L. Brown, S. Takeda, H. Hochegger, & C. G. Morrison. (2010). DNA damage induces Chk1-dependent threonine-160 phosphorylation and activation of Cdk2. *Oncogene* 29:616–24.

Bourke, E., H. Dodson, A. Merdes, L. Cuffe, G. Zachos, M. Walker, D. Gillespie, & C. G. Morrison. (2007). DNA damage induces Chk1-dependent centrosome amplification. *EMBO Rep.* 8:603–9.

Boveri, T. (2008). Concerning the Origin of Malignant Tumours by Theodor Boveri. Translated and annotated by Henry Harris. *J. Cell Sci.* 121:1–84.

Brown, N. J., M. Marjanović, J. Lüders, T. H. Stracker, & V. Costanzo. (2013). Cep63 and cep152 cooperate to ensure centriole duplication. *PLoS One* 8:e69986.

Bryant, H. E., N. Schultz, H. D. Thomas, K. M. Parker, D. Flower, E. Lopez, S. Kyle, M. Meuth, N. J. Curtin, T. Helleday, K. M. Kendrick, A. P. Da Costa, A. E. Leigh, M. R. Hinton, & J. W. Peirce. (2005). Specific killing of BRCA2-deficient tumours with inhibitors of poly(ADP-ribose) polymerase. *Nature* 434:913–917.

Bunz, F., A. Dutriaux, C. Lengauer, T. Waldman, S. Zhou, J. P. Brown, J. M. Sedivy, K. W. Kinzler, & B. Vogelstein. (1998). Requirement for p53 and p21 to sustain G2 arrest after DNA damage. *Science* 282:1497–501.

Burgess, R. C., & T. Misteli. (2015). Not All DDRs Are Created Equal: Non-Canonical DNA Damage Responses. *Cell* 162:944–7.

Burkhalter, M. D., G. B. Fralish, R. T. Premont, M. G. Caron, & M. Philipp. (2013). Grk5l controls heart development by limiting mTOR signaling during symmetry breaking. *Cell Rep.* 4:625–32.

Busch, C., O. Barton, E. Morgenstern, C. Götz, J. Günther, A. Noll, & M. Montenarh. (2007). The G2/M checkpoint phosphatase cdc25C is located within centrosomes. *Int. J. Biochem. Cell Biol.* 39:1707–13.

Cappelli, E., S. Townsend, C. Griffin, & J. Thacker. (2011). Homologous recombination proteins are associated with centrosomes and are required for mitotic stability. *Exp. Cell Res.* 317:1203–13.

Carvalho-Santos, Z., J. Azimzadeh, J. B. Pereira-Leal, & M. Bettencourt-Dias. (2011). Tracing the origins of centrioles, cilia, and flagella. *J. Cell Biol.* 194:165–175.

Chaki, M., R. Airik, A. K. Ghosh, R. H. Giles, R. Chen, G. G. Slaats, H. Wang, T. W. Hurd, W. Zhou, A. Cluckey, H. Y. Gee, G. Ramaswami, C.-J. Hong, B. A. Hamilton, I. Cervenka, R. S. Ganji, V. Bryja, H. H. Arts, J. van Reeuwijk, M. M. Oud, S. J. F. Letteboer, R. Roepman, H. Husson, O. Ibraghimov-Beskrovnaya, T. Yasunaga, G. Walz, L. Eley, J. A. Sayer, B. Schermer, M. C. Liebau, T. Benzing, S. Le Corre, I. Drummond, S. Janssen, S. J. Allen, S. Natarajan, J. F. O'Toole, M. Attanasio, S. Saunier, C. Antignac, R. K. Koenekoop, H. Ren, I. Lopez, A. Nayir, C. Stoetzel, H. Dollfus, R. Massoudi, J. G. Gleeson, S. P. Andreoli, D. G. Doherty, A. Lindstrad, C. Golzio, N. Katsanis, L. Pape, E. B. Abboud, A. A. Al-Rajhi, R. A. Lewis, H. Omran, E. Y.-H. P. Lee, S. Wang, J. M. Sekiguchi, R. Saunders, C. A. Johnson, E. Garner, K. Vanselow, J. S. Andersen, J. Shlomai, G. Nurnberg, P. Nurnberg, S. Levy, A. Smogorzewska, E. A. Otto, & F. Hildebrandt. (2012). Exome capture reveals ZNF423 and CEP164 mutations, linking renal ciliopathies to DNA damage response signaling. *Cell* 150:533–48.

Chang, W., S. Antoku, C. Östlund, H. J. Worman, & G. G. Gundersen. (2015). Linker of nucleoskeleton and cytoskeleton (LINC) complex-mediated actin-dependent nuclear positioning orients centrosomes in migrating myoblasts. *Nucleus* 6:77–88.

Chatterjee, N., & G. C. Walker. (2017). Mechanisms of DNA damage, repair, and mutagenesis. *Environ. Mol. Mutagen.* 58:235–263.

Chen, J. V., L.-R. R. Kao, S. C. Jana, E. Sivan-Loukianova, S. Mendonça, O. A. Cabrera, P. Singh, C. Cabernard, D. F. Eberl, M. Bettencourt-Dias, & T. L. Megraw. (2015). Rootletin organizes the ciliary rootlet to achieve neuron sensory function in Drosophila 211.

Choi, H. J. C., J.-R. Lin, J.-B. Vannier, G. G. Slaats, A. C. Kile, R. D. Paulsen, D. K. Manning, D. R.

Beier, R. H. Giles, S. J. Boulton, & K. A. Cimprich. (2013). NEK8 links the ATR-regulated replication stress response and S phase CDK activity to renal ciliopathies. *Mol. Cell* 51:423–39.

Ciccia, A., & S. J. Elledge. (2010). The DNA damage response: making it safe to play with knives. *Mol. Cell* 40:179–204.

Clare, D. K., J. Magescas, T. Piolot, M. Dumoux, C. Vesque, E. Pichard, T. Dang, B. Duvauchelle, F. Poirier, & D. Delacour. (2014). Basal foot MTOC organizes pillar MTs required for coordination of beating cilia. *Nat. Commun.* 5:1–9.

Conduit, P. T. (2013). The dominant force of Centrobin in centrosome asymmetry. *Nat. Cell Biol.* 15:235–7.

Cong, L., F. A. Ran, D. Cox, S. Lin, R. Barretto, N. Habib, P. D. Hsu, X. Wu, W. Jiang, L. A. Marraffini, & F. Zhang. (2013). Multiplex genome engineering using CRISPR/Cas systems. *Science* 339:819–23.

Conroy, P. C., C. Saladino, T. J. Dantas, P. Lalor, P. Dockery, & C. G. Morrison. (2012). C-NAP1 and rootletin restrain DNA damage-induced centriole splitting and facilitate ciliogenesis. *Cell Cycle* 11:3769–3778.

Corbit, K. C., P. Aanstad, V. Singla, A. R. Norman, D. Y. R. Stainier, & J. F. Reiter. (2005). Vertebrate Smoothened functions at the primary cilium. *Nature* 437:1018–1021.

Coverley, D., H. Laman, & R. A. Laskey. (2002). Distinct roles for cyclins E and A during DNA replication complex assembly and activation. *Nat. Cell Biol.* 4:523–528.

D'Silva, I., J. D. Pelletier, J. Lagueux, D. D'Amours, M. A. Chaudhry, M. Weinfeld, S. P. Lees-Miller, & G. G. Poirier. (1999). Relative affinities of poly(ADP-ribose) polymerase and DNA-dependent protein kinase for DNA strand interruptions. *Biochim. Biophys. Acta* 1430:119–26.

Daly, O. M., D. Gaboriau, K. Karakaya, S. King, T. J. Dantas, P. Lalor, P. Dockery, A. Krämer, & C. G. Morrison. (2016). Gene-targeted CEP164-deficient cells show a ciliation defect with intact DNA repair capacity. *J. Cell Sci.*

Dammermann, A., & A. Merdes. (2002). Assembly of centrosomal proteins and microtubule organization depends on PCM-1. *J. Cell Biol.* 159.

Dantas, T. J., Y. Wang, P. Lalor, P. Dockery, & C. G. Morrison. (2011). Defective nucleotide excision repair with normal centrosome structures and functions in the absence of all vertebrate centrins. *J. Cell Biol.* 193.

Dasika, G. K., S.-C. J. Lin, S. Zhao, P. Sung, A. Tomkinson, & E. Y.-H. P. Lee. (2000). DNA damage-induced cell cycle checkpoints and DNA strand break repair in development and tumorigenesis. *Oncogene* 18:7883–7899.

David, A., F. Liu, A. Tibelius, J. Vulprecht, D. Wald, U. Rothermel, R. Ohana, A. Seitel, J. Metzger, R. Ashery-Padan, H.-P. Meinzer, H.-J. Gröne, S. Izraeli, & A. Krämer. (2014). Lack of centrioles and primary cilia in *STIL* $^{-/-}$ mouse embryos. *Cell Cycle* 13:2859–2868.

Davies, A. A., J.-Y. Masson, M. J. Mcilwraith, A. Z. Stasiak, A. Stasiak, A. R. Venkitaraman, & S. C. West. (2001). Role of BRCA2 in Control of the RAD51 Recombination and DNA Repair Protein. *Mol. Cell* 7:273–282.

Davis, A. J., & D. J. Chen. (2013). DNA double strand break repair via non-homologous end-joining. *Transl. Cancer Res.* 2:130–143.

Dean, S., F. Moreira-Leite, V. Varga, & K. Gull. (2016). Cilium transition zone proteome reveals compartmentalization and differential dynamics of ciliopathy complexes. *Proc. Natl. Acad. Sci. U. S. A.* 113:E5135-43.

Delgehyr, N., J. Sillibourne, & M. Bornens. (2005). Microtubule nucleation and anchoring at the centrosome are independent processes linked by ninein function. *J. Cell Sci.* 118.

Diiorio, P., A. R. Rittenhouse, R. Bortell, & A. Jurczyk. (2014). Role of Cilia in Normal Pancreas Function and in Diseased States. *Birth Defects Res. (Part C)* 102:126–138.

Dix, C. I., & J. W. Raff. (2007). Drosophila Spd-2 recruits PCM to the sperm centriole, but is dispensable for centriole duplication. *Curr. Biol.* 17:1759–64.

Dodson, H., E. Bourke, L. J. Jeffers, P. Vagnarelli, E. Sonoda, S. Takeda, W. C. Earnshaw, A. Merdes, & C. Morrison. (2004). Centrosome amplification induced by DNA damage occurs during a prolonged G2 phase and involves ATM. *EMBO J.* 23:3864–73.

Dodson, H., S. P. Wheatley, & C. Morrison. (2007). Involvement of Centrosome Amplification in Radiation-Induced Mitotic Catastrophe. *Cell Cycle* 6:364–370.

Donzelli, M., & G. F. Draetta. (2003). Regulating mammalian checkpoints through Cdc25 inactivation. *EMBO Rep.* 4:671–7.

Doxsey, S., W. Zimmerman, & K. Mikule. (2005). Centrosome control of the cell cycle. *Trends Cell Biol.* 15:303–311.

Duncan, J. A., J. R. Reeves, & T. G. Cooke. (1998). BRCA1 and BRCA2 proteins: roles in health and disease. *Mol. Pathol.* 51:237–47.

Dziadkowiec, K. N., E. Gąsiorowska, E. Nowak-Markwitz, & A. Jankowska. (2016). PARP inhibitors: review of mechanisms of action and BRCA1/2 mutation targeting. *Prz. menopauzalny = Menopause Rev.* 15:215–219.

Fagerberg, L., B. M. Hallström, P. Oksvold, C. Kampf, D. Djureinovic, J. Odeberg, M. Habuka, S. Tahmasebpoor, A. Danielsson, K. Edlund, A. Asplund, E. Sjöstedt, E. Lundberg, C. A.-K. Szigyarto, M. Skogs, J. O. Takanen, H. Berling, H. Tegel, J. Mulder, P. Nilsson, J. M. Schwenk, C. Lindskog, F. Danielsson, A. Mardinoglu, Å. Sivertsson, K. von Feilitzen, M. Forsberg, M. Zwahlen, I. Olsson, S. Navani, M. Huss, J. Nielsen, F. Ponten, & M. Uhlén. (2014). Analysis of the Human Tissue-specific Expression by Genome-wide Integration of Transcriptomics and Antibody-based Proteomics. *Mol. Cell. Proteomics* 13:397–406.

Falck, J., C. Lukas, M. Protopopova, J. Lukas, G. Selivanova, & J. Bartek. (2001). Functional impact of concomitant versus alternative defects in the Chk2-p53 tumour suppressor pathway. *Oncogene* 20:5503–5510.

Fedorov, Y., E. M. Anderson, A. Birmingham, A. Reynolds, J. Karpilow, K. Robinson, D. Leake, W. S. Marshall, & A. Khvorova. (2006). Off-target effects by siRNA can induce toxic phenotype. *RNA* 12:1188–96.

Fisch, C., & P. Dupuis-Williams. (2011). Ultrastructure of cilia and flagella - back to the future! *Biol. Cell* 103:249–270.

Fırat-karalar, E. N., & T. Stearns. (2014). The centriole duplication cycle. *Philos. Trans. R. Soc. London B Biol. Sci.* 369.

Flanagan, A.-M., E. Stavenschi, S. Basavaraju, D. Gaboriau, D. A. Hoey, & C. G. Morrison. (2017). Centriole splitting caused by loss of the centrosomal linker protein C-NAP1 reduces centriolar satellite density and impedes centrosome amplification. *Mol. Biol. Cell* 28:736–745.

Fletcher, L., G. J. Cerniglia, E. A. Nigg, T. J. Yend, & R. J. Muschel. (2004). Inhibition of centrosome separation after DNA damage: a role for Nek2. *Radiat. Res.* 162:128–35.

Fong, P. C., D. S. Boss, T. A. Yap, A. Tutt, P. Wu, M. Mergui-Roelvink, P. Mortimer, H. Swaisland, A. Lau, M. J. O'Connor, A. Ashworth, J. Carmichael, S. B. Kaye, J. H. M. Schellens, & J. S. de Bono. (2009). Inhibition of Poly(ADP-Ribose) Polymerase in Tumors from *BRCA* Mutation Carriers. *N. Engl. J. Med.* 361:123–134.

Franken, N. A. P., H. M. Rodermond, J. Stap, J. Haveman, & C. van Bree. (2006). Clonogenic assay of cells in vitro. *Nat. Protoc.* 1:2315–2319.

Fry, A. M. (2014). Solving the centriole disengagement puzzle. *Nat. Cell Biol.* 17:3–5.

Fry, A. M., T. Mayor, P. Meraldi, Y.-D. Stierhof, K. Tanaka, & E. A. Nigg. (1998a). C-Nap1, a Novel Centrosomal Coiled-Coil Protein and Candidate Substrate of the Cell Cycle–regulated Protein Kinase Nek2. *J. Cell Biol.* 141.

Fry, A. M., P. Meraldi, & E. A. Nigg. (1998b). A centrosomal function for the human Nek2 protein kinase, a member of the NIMA family of cell cycle regulators. *EMBO J.* 17:470–81.

Fu, J., & D. M. Glover. (2012). Structured illumination of the interface between centriole and peri-centriolar material. *Open Biol.* 2:120104.

Fu, J., I. M. Hagan, & D. M. Glover. (2015). The centrosome and its duplication cycle. *Cold Spring Harb. Perspect. Biol.* 7:a015800.

Fukasawa, K. (2007). Oncogenes and tumour suppressors take on centrosomes. *Nat. Rev. Cancer* 7:911–24.

Gabriel, E., A. Wason, A. Ramani, L. M. Gooi, P. Keller, A. Pozniakovsky, I. Poser, F. Noack, N. S. Telugu, F. Calegari, T. Šarić, J. Hescheler, A. A. Hyman, M. Gottardo, G. Callaini, F. S.

Alkuraya, & J. Gopalakrishnan. (2016). CPAP promotes timely cilium disassembly to maintain neural progenitor pool. *EMBO J.* 35:803–19.

Ganem, N. J. J., S. A. A. Godinho, & D. Pellman. (2009). A Mechanism Linking Extra Centrosomes to Chromosomal Instability. *Nature* 460:278–282.

Garcia-Gonzalo, F. R., K. C. Corbit, M. S. Sirerol-Piquer, G. Ramaswami, E. A. Otto, T. R. Noriega, A. D. Seol, J. F. Robinson, C. L. Bennett, D. J. Josifova, J. M. García-Verdugo, N. Katsanis, F. Hildebrandt, & J. F. Reiter. (2011). A transition zone complex regulates mammalian ciliogenesis and ciliary membrane composition. *Nat. Genet.* 43:776–84.

Genois, M.-M., A. Mukherjee, J.-M. Ubeda, R. Buisson, E. Paquet, G. Roy, M. Plourde, Y. Coulombe, M. Ouellette, & J.-Y. Masson. (2012). Interactions between BRCA2 and RAD51 for promoting homologous recombination in Leishmania infantum. *Nucleic Acids Res.* 40:6570–84.

Gerdes, J. M., E. E. Davis, & N. Katsanis. (2009). The vertebrate primary cilium in development, homeostasis, and disease. *Cell* 137:32–45.

Gibbons, I. R., & A. J. Rowe. (1965). Dynein: A Protein with Adenosine Triphosphatase Activity from Cilia. *Science* 149:424–6.

Giráldez, S., J. Herrero-Ruiz, M. Mora-Santos, M. Á. Japón, M. Tortolero, & F. Romero. (2014). SCF(FBXW7α) modulates the intra-S-phase DNA-damage checkpoint by regulating Polo like kinase-1 stability. *Oncotarget* 5:4370–83.

Goetz, S. C., & K. V Anderson. (2010). The primary cilium: a signalling centre during vertebrate development. *Nat. Rev. Genet.* 11:331–44.

Goetz, S. C., K. F. Liem, & K. V. Anderson. (2012). The Spinocerebellar Ataxia-Associated Gene Tau Tubulin Kinase 2 Controls the Initiation of Ciliogenesis. *Cell* 151:847–858.

Gottardo, M., G. Pollarolo, S. Llamazares, J. Reina, M. G. Riparbelli, G. Callaini, & C. Gonzalez. (2015). Loss of Centrobin Enables Daughter Centrioles to Form Sensory Cilia in Drosophila. *Curr. Biol.* 25:2319–2324.

Graser, S., Y.-D. Stierhof, S. B. Lavoie, O. S. Gassner, S. Lamla, M. Le Clech, & E. A. Nigg. (2007). Cep164, a novel centriole appendage protein required for primary cilium formation. *J. Cell Biol.* 179:321–30.

Griffith, E., S. Walker, C.-A. Martin, P. Vagnarelli, T. Stiff, B. Vernay, N. Al Sanna, A. Saggar, B. Hamel, W. C. Earnshaw, P. A. Jeggo, A. P. Jackson, & M. O'Driscoll. (2008). Mutations in pericentrin cause Seckel syndrome with defective ATR-dependent DNA damage signaling. *Nat. Genet.* 40:232–6.

Gudi, R., C. J. Haycraft, P. D. Bell, Z. Li, & C. Vasu. (2015a). Centrobin-mediated regulation of CPAP level limits centriole length during elongation stage. *J. Biol. Chem.*:jbc.M114.603423.

Gudi, R., C. J. Haycraft, P. D. Bell, Z. Li, & C. Vasu. (2015b). Centrobin-mediated regulation of the centrosomal protein 4.1-associated protein (CPAP) level limits centriole length during elongation stage. *J. Biol. Chem.* 290:6890–902.

Gudi, R., C. Zou, J. Dhar, Q. Gao, & C. Vasu. (2014). Centrobin-CPAP interaction promotes CPAP localization to the centrioles during centriole duplication. *J. Biol. Chem.*

Gudi, R., C. Zou, J. Li, & Q. Gao. (2011). Centrobin-tubulin interaction is required for centriole elongation and stability. *J. Cell Biol.* 193:711–25.

Gupta, G. D., É. Coyaud, J. Gonçalves, B. A. Mojarad, Y. Liu, Q. Wu, L. Gheiratmand, D. Comartin, J. M. Tkach, S. W. T. Cheung, M. Bashkurov, M. Hasegan, J. D. Knight, Z.-Y. Lin, M. Schueler, F. Hildebrandt, J. Moffat, A.-C. Gingras, B. Raught, & L. Pelletier. (2015). A Dynamic Protein Interaction Landscape of the Human Centrosome-Cilium Interface. *Cell* 163:1484–1499.

Hall, E. A., M. Keighren, M. J. Ford, T. Davey, A. P. Jarman, L. B. Smith, I. J. Jackson, & P. Mill. (2013). Acute Versus Chronic Loss of Mammalian Azi1/Cep131 Results in Distinct Ciliary Phenotypes. *PLoS Genet.* 9:e1003928.

Hammond, J. W., D. Cai, & K. J. Verhey. (2008). Tubulin modifications and their cellular functions. *Curr. Opin. Cell Biol.* 20:71–6.

Hardy, T., M. Lee, R. S. Hames, S. L. Prosser, D.-M. Cheary, M. D. Samant, F. Schultz, J. E. Baxter, K. Rhee, & A. M. Fry. (2014). Multisite phosphorylation of C-Nap1 releases it from Cep135 to trigger centrosome disjunction. *J. Cell Sci.* 127:2493–2506.

Haren, L., M.-H. Remy, I. Bazin, I. Callebaut, M. Wright, & A. Merdes. (2006). NEDD1-dependent recruitment of the gamma-tubulin ring complex to the centrosome is necessary for centriole duplication and spindle assembly. *J. Cell Biol.* 172:505–15.

Harper, J. W., S. J. Elledge, K. Keyomarsi, B. Dynlacht, L. H. Tsai, P. Zhang, S. Dobrowolski, C. Bai, L. Connell-Crowley, E. Swindell, P. M. Fox, & N. Wei. (1995). Inhibition of cyclin-dependent kinases by p21. *Mol. Biol. Cell* 6:387–400.

Harrison, M. K., A. M. Adon, & H. I. Saavedra. (2011). The G1 phase Cdks regulate the centrosome cycle and mediate oncogene-dependent centrosome amplification. *Cell Div.* 6:2.

Hatch, E. M., A. Kulukian, A. J. Holland, D. W. Cleveland, & T. Stearns. (2010). Cep152 interacts with Plk4 and is required for centriole duplication. *J. Cell Biol.* 191:721–9.

Hatch, E., & T. Stearns. (2010). The life cycle of centrioles. *Cold Spring Harb. Symp. Quant. Biol.* 75:425–31.

Hermeking, H. (2003). The 14-3-3 cancer connection. *Nat. Rev. Cancer* 3:931–943.

Hernández, L., M. Terradas, M. Martín, L. Tusell, & A. Genescà. (2013). Highly sensitive automated method for DNA damage assessment: gamma-H2AX foci counting and cell cycle sorting. *Int. J. Mol. Sci.* 14:15810–26.

Hickson, I., Y. Zhao, C. J. Richardson, S. J. Green, N. M. B. Martin, A. I. Orr, P. M. Reaper, S. P. Jackson, N. J. Curtin, & G. C. M. Smith. (2004). Identification and characterization of a novel and specific inhibitor of the ataxia-telangiectasia mutated kinase ATM. *Cancer Res.* 64:9152–9.

Hildebrandt, F., T. Benzing, & N. Katsanis. (2011). Ciliopathies. *N. Engl. J. Med.* 364:1533–43.

Ho, G. P. H., S. Margossian, T. Taniguchi, & A. D. D'Andrea. (2006). Phosphorylation of FANCD2 on two novel sites is required for mitomycin C resistance. *Mol. Cell. Biol.* 26:7005–15.

Hoey, D. A., J. C. Chen, & C. R. Jacobs. (2012). The primary cilium as a novel extracellular sensor in bone. *Front. Endocrinol. (Lausanne).* 3:75.

Hoffmann, I. (2000). The role of Cdc25 phosphatases in cell cycle checkpoints. *Protoplasma* 211:8–11.

Honda, R., & H. Yasuda. (2000). Activity of MDM2, a ubiquitin ligase, toward p53 or itself is dependent on the RING finger domain of the ligase. *Oncogene* 19:1473–1476.

Hooper, J. E., & M. P. Scott. (2005). Communicating with Hedgehogs. *Nat. Rev. Mol. Cell Biol.* 6:306–317.

Hsiao, Y.-C., K. Tuz, & R. J. Ferland. (2012). Trafficking in and to the primary cilium. *Cilia* 1:4.

Hu, Q., L. Milenkovic, H. Jin, M. P. Scott, M. V Nachury, E. T. Spiliotis, & W. J. Nelson. (2010). A septin diffusion barrier at the base of the primary cilium maintains ciliary membrane protein distribution. *Science* 329:436–9.

Huangfu, D., A. Liu, A. S. Rakeman, N. S. Murcia, L. Niswander, & K. V. Anderson. (2003). Hedgehog signalling in the mouse requires intraflagellar transport proteins. *Nature* 426:83–87.

Hurd, T. W., F. Hildebrandt, & H. Hughes. (2011). Mechanisms of Nephronophthisis and Related Ciliopathies. *Nephron Exp Nephrol* 118:9–14.

Inanç, B., H. Dodson, & C. G. Morrison. (2010), November 15. A centrosome-autonomous signal that involves centriole disengagement permits centrosome duplication in G2 phase after DNA damage.

Inoko, A., M. Matsuyama, H. Goto, Y. Ohmuro-Matsuyama, Y. Hayashi, M. Enomoto, M. Ibi, T. Urano, S. Yonemura, T. Kiyono, I. Izawa, & M. Inagaki. (2012). Trichoplein and Aurora A block aberrant primary cilia assembly in proliferating cells. *J. Cell Biol.* 197:391–405.

Ishikawa, H., A. Kubo, S. Tsukita, & S. Tsukita. (2005). Odf2-deficient mother centrioles lack distal/subdistal appendages and the ability to generate primary cilia. *Nat. Cell Biol.* 7:517–524.

Izawa, I., H. Goto, K. Kasahara, & M. Inagaki. (2015). Current topics of functional links between primary cilia and cell cycle. *Cilia* 4:12.

Jackman, M., C. Lindon, E. A. Nigg, & J. Pines. (2003). Active cyclin B1–Cdk1 first appears on centrosomes in prophase. *Nat. Cell Biol.* 5:143–148.

Jackson, A. L., & P. S. Linsley. (2010). Recognizing and avoiding siRNA off-target effects for target identification and therapeutic application. *Nat. Rev. Drug Discov.* 9:57–67.

Jackson, S. P. (2002). Sensing and repairing DNA double-strand breaks. *Carcinogenesis* 23:687–696.

Jacobson, A., & S. W. Peltz. (1996). INTERRELATIONSHIPS OF THE PATHWAYS OF mRNA DECAY AND TRANSLATION IN EUKARYOTIC CELLS. *Annu. Rev. Biochem.* 65:693–739.

Jain, A. K., K. Allton, A. D. Duncan, & M. C. Barton. (2014). TRIM24 is a p53-induced E3-ubiquitin ligase that undergoes ATM-mediated phosphorylation and autodegradation during DNA damage. *Mol. Cell. Biol.* 34:2695–709.

Jana, S. C., G. Marteil, & M. Bettencourt-Dias. (2014). Mapping molecules to structure: unveiling secrets of centriole and cilia assembly with near-atomic resolution. *Curr. Opin. Cell Biol.* 26:96–106.

Januschke, J., J. Reina, S. Llamazares, T. Bertran, F. Rossi, J. Roig, & C. Gonzalez. (2013). Centrobin controls mother-daughter centriole asymmetry in Drosophila neuroblasts. *Nat. Cell Biol.* 15:241–8.

Jeffery, J. M., I. Grigoriev, I. Poser, A. van der Horst, N. Hamilton, N. Waterhouse, J. Bleier, V. N. Subramaniam, I. V Maly, A. Akhmanova, & K. K. Khanna. (2013). Centrobin regulates centrosome function in interphase cells by limiting pericentriolar matrix recruitment. *Cell Cycle* 12:899–906.

Jeffery, J. M., A. J. Urquhart, V. N. Subramaniam, R. G. Parton, & K. K. Khanna. (2010). Centrobin regulates the assembly of functional mitotic spindles. *Oncogene* 29:2649–58.

Jensen, R. B., A. Carreira, & S. C. Kowalczykowski. (2010). Purified human BRCA2 stimulates RAD51-mediated recombination. *Nature* 467.

Jeong, Y., J. Lee, K. Kim, J. C. Yoo, & K. Rhee. (2007). Characterization of NIP2/centrobin, a novel substrate of Nek2, and its potential role in microtubule stabilization. *J. Cell Sci.* 120:2106–16.

Jin, H., & M. V Nachury. (2009). The BBSome. *Curr. Biol.* 19:R472-3.

Johnson, C. A., & S. J. Collis. (2016). Ciliogenesis and the DNA damage response: a stressful relationship. *Cilia* 5:19.

Al Jord, A., A.-I. Lemaître, N. Delgehyr, M. Faucourt, N. Spassky, & A. Meunier. (2014). Centriole amplification by mother and daughter centrioles differs in multiciliated cells. *Nature* 516:104–7.

Joukov, V., J. C. Walter, & A. De Nicolo. (2014). The Cep192-Organized Aurora A-Plk1 Cascade Is Essential for Centrosome Cycle and Bipolar Spindle Assembly. *Mol. Cell* 55:578–591.

Kalay, E., G. Yigit, Y. Aslan, K. E. Brown, E. Pohl, L. S. Bicknell, H. Kayserili, Y. Li, B. Tüysüz, G. Nürnberg, W. Kiess, M. Koegl, I. Baessmann, K. Buruk, B. Toraman, S. Kayipmaz, S. Kul, M. Ikbal, D. J. Turner, M. S. Taylor, J. Aerts, C. Scott, K. Milstein, H. Dollfus, D. Wieczorek, H. G. Brunner, M. Hurles, A. P. Jackson, A. Rauch, P. Nürnberg, A. Karagüzel, & B. Wollnik. (2011). CEP152 is a genome maintenance protein disrupted in Seckel syndrome. *Nat. Genet.* 43:23–6.

Katoh, Y., S. Michisaka, S. Nozaki, T. Funabashi, T. Hirano, R. Takei, & K. Nakayama. (2017). Practical method for targeted disruption of cilia-related genes by using CRISPR/Cas9-mediated, homology-independent knock-in system. *Mol. Biol. Cell* 28:898–906.

Katsura, M., T. Tsuruga, O. Date, T. Yoshihara, M. Ishida, Y. Tomoda, M. Okajima, M. Takaku, H. Kurumizaka, A. Kinomura, H. K. Mishima, & K. Miyagawa. (2009). The ATR-Chk1 pathway plays a role in the generation of centrosome aberrations induced by Rad51C dysfunction. *Nucleic Acids Res.* 37:3959–68.

Keller, L. C., S. Geimer, E. Romijn, J. Yates, I. Zamora, W. F. Marshall, & W. F. Marshall. (2009). Molecular architecture of the centriole proteome: the conserved WD40 domain protein POC1 is required for centriole duplication and length control. *Mol. Biol. Cell* 20:1150–66.

Keryer, G., J. R. Pineda, G. Liot, J. Kim, P. Dietrich, C. Benstaali, K. Smith, F. P. Cordelières, N. Spassky, R. J. Ferrante, I. Dragatsis, & F. Saudou. (2011). Ciliogenesis is regulated by a huntingtin-HAP1-PCM1 pathway and is altered in Huntington disease. *J. Clin. Invest.* 121:4372–4382.

Kim, K., S. Lee, J. Chang, & K. Rhee. (2008). A novel function of CEP135 as a platform protein of C-NAP1 for its centriolar localization. *Exp. Cell Res.* 314:3692–700.

Kim, S., K. Lee, J.-H. Choi, N. Ringstad, & B. D. Dynlacht. (2015). Nek2 activation of Kif24 ensures cilium disassembly during the cell cycle. *Nat. Commun.* 6:8087.

Kim, S., N. A. Zaghloul, E. Bubenshchikova, E. C. Oh, S. Rankin, N. Katsanis, T. Obara, & L.

Tsiokas. (2011). Nde1-mediated inhibition of ciliogenesis affects cell cycle re-entry. *Nat. Cell Biol.* 13:351–360.

Kinkel, M. D., S. C. Eames, M. R. Alonzo, & V. E. Prince. (2008). Cdx4 is required in the endoderm to localize the pancreas and limit beta-cell number. *Development* 135:919–929.

Kitagawa, R., C. J. Bakkenist, P. J. McKinnon, & M. B. Kastan. (2004). Phosphorylation of SMC1 is a critical downstream event in the ATM-NBS1-BRCA1 pathway. *Genes Dev.* 18:1423–38.

Kleylein-Sohn, J., J. Westendorf, M. Le Clech, R. Habedanck, Y.-D. Stierhof, & E. A. Nigg. (2007). Plk4-induced centriole biogenesis in human cells. *Dev. Cell* 13:190–202.

Knipscheer, P., M. Räschle, A. Smogorzewska, M. Enoiu, T. V. Ho, O. D. Schärer, S. J. Elledge, & J. C. Walter. (2009). The Fanconi anemia pathway promotes replication-dependent DNA interstrand cross-link repair. *Science* 326:1698–701.

Kobayashi, T., & B. D. Dynlacht. (2011). Regulating the transition from centriole to basal body.

Kong, D., V. Farmer, A. Shukla, J. James, R. Gruskin, S. Kiriyama, & J. Loncarek. (2014). Centriole maturation requires regulated Plk1 activity during two consecutive cell cycles. *J. Cell Biol.* 206:855–65.

Kramer-Zucker, A. G., F. Olale, C. J. Haycraft, B. K. Yoder, F. Schier, Alexander, & I. A. Drummond. (2005). Cilia-driven fluid flow in the zebrafish pronephros, brain and Kupffer's vesicle is required for normal organogenesis. *development* 132:1907–1921.

Krämer, A., B. Maier, & J. Bartek. (2011). Centrosome clustering and chromosomal (in)stability: a matter of life and death. *Mol. Oncol.* 5:324–35.

Krock, B. L., & B. D. Perkins. (2008). The intraflagellar transport protein IFT57 is required for cilia maintenance and regulates IFT-particle-kinesin-II dissociation in vertebrate photoreceptors. *J. Cell Sci.* 121:1907–15.

Kuhns, S., K. N. Schmidt, J. Reymann, D. F. Gilbert, A. Neuner, B. Hub, R. Carvalho, P. Wiedemann, H. Zentgraf, H. Erfle, U. Klingmüller, M. Boutros, & G. Pereira. (2013). The microtubule affinity regulating kinase MARK4 promotes axoneme extension during early ciliogenesis. *J. Cell Biol.* 200:505–22.

Lachaud, C., A. Moreno, F. Marchesi, R. Toth, J. J. Blow, & J. Rouse. (2016). Ubiquitinated Fancd2 recruits Fan1 to stalled replication forks to prevent genome instability. *Science* 351:846–9.

Lancaster, M. A., J. Schroth, & J. G. Gleeson. (2011). Subcellular spatial regulation of canonical Wnt signalling at the primary cilium. *Nat. Biotechnol.* 13:702–709.

Lane, H. A., & E. A. Nigg. (1996). Antibody microinjection reveals an essential role for human polo-like kinase 1 (Plk1) in the functional maturation of mitotic centrosomes. *J. Cell Biol.* 135:1701–13.

Lattao, R., L. Kovács, & D. M. Glover. (2017). The Centrioles, Centrosomes, Basal Bodies, and Cilia of Drosophila melanogaster. *Genetics* 206:33–53.

Lawo, S., M. Hasegan, G. D. Gupta, & L. Pelletier. (2012). Subdiffraction imaging of centrosomes reveals higher-order organizational features of pericentriolar material. *Nat. Cell Biol.* 14:1148–1158.

Lee, J., Y. Jeong, S. Jeong, & K. Rhee. (2010). Centrobin/NIP2 is a microtubule stabilizer whose activity is enhanced by PLK1 phosphorylation during mitosis. *J. Biol. Chem.* 285:25476–84.

Lee, J., S. Kim, Y. Jeong, & K. Rhee. (2009). Centrobin/Nip2 expression in vivo suggests its involvement in cell proliferation. *Mol. Cells* 28:31–6.

Lee, K., & K. Rhee. (2011). PLK1 phosphorylation of pericentrin initiates centrosome maturation at the onset of mitosis. *J. Cell Biol.* 195:1093–101.

Lee, K., & K. Rhee. (2012). Separase-dependent cleavage of pericentrin B is necessary and sufficient for centriole disengagement during mitosis. *Cell Cycle* 11:2476–2485.

Leidel, S., M. Delattre, L. Cerutti, K. Baumer, & P. Gönczy. (2005). SAS-6 defines a protein family required for centrosome duplication in C. elegans and in human cells. *Nat. Cell Biol.* 7:115–125.

Li, J., S. Kim, T. Kobayashi, F.-X. Liang, N. Korzeniewski, S. Duensing, & B. D. Dynlacht. (2012). Neurl4, a novel daughter centriole protein, prevents formation of ectopic microtubule organizing centres. *EMBO Rep.* 13:547–53.

Liang, Y., D. Meng, B. Zhu, & J. Pan. (2016). Mechanism of ciliary disassembly. *Cell. Mol. Life Sci.* 73:1787–1802.

Lieber, M. R. (2010). The mechanism of double-strand DNA break repair by the nonhomologous DNA end-joining pathway. *Annu. Rev. Biochem.* 79:181–211.

Lindqvist, A., V. Rodríguez-Bravo, & R. H. Medema. (2009). The decision to enter mitosis: feedback and redundancy in the mitotic entry network. *J. Cell Biol.* 185:193–202.

Liska, F., C. Gosele, E. Popova, B. Chylíková, D. Křenová, V. Křen, M. Bader, L. L. Tres, N. Hubner, & A. L. Kierszenbaum. (2013). Overexpression of Full-Length Centrobin Rescues Limb Malformation but Not Male Fertility of the Hypodactylous (hd) Rats. *PLoS One* 8:e60859.

Liska, F., C. Gosele, E. Rivkin, L. Tres, M. C. Cardoso, P. Domaing, E. Krejcí, P. Snajdr, M. A. Lee-Kirsch, D. G. de Rooij, D. G. de Rooij, V. Kren, D. Krenová, A. L. Kierszenbaum, & N. Hubner. (2009). Rat hd mutation reveals an essential role of centrobin in spermatid head shaping and assembly of the head-tail coupling apparatus. *Biol. Reprod.* 81:1196–205.

Löbrich, M., A. Shibata, A. Beucher, A. Fisher, M. Ensminger, A. A. Goodarzi, O. Barton, & P. A. Jeggo. (2010). γH2AX foci analysis for monitoring DNA double-strand break repair: Strengths, limitations and optimization. *Cell Cycle* 9:662–669.

Löffler, H., a Fechter, F. Y. Liu, S. Poppelreuther, & A. Krämer. (2013). DNA damage-induced centrosome amplification occurs via excessive formation of centriolar satellites. *Oncogene* 32:2963–72.

Loncarek, J., P. Hergert, V. Magidson, & A. Khodjakov. (2008a). Control of daughter centriole formation by the pericentriolar material. *Nat. Cell Biol.* 10:322–8.

Loncarek, J., P. Hergert, V. Magidson, & A. Khodjakov. (2008b). Control of daughter centriole formation by the pericentriolar material. *Nat. Cell Biol.* 10:322–328.

Long, S., N. Ahmad, & M. Rebagliati. (2003). The zebrafish nodal-related gene southpaw is required for visceral and diencephalic left-right asymmetry. *Development* 130:2303–2316.

Lopes, C. A., S. C. Jana, I. Cunha-Ferreira, S. Zitouni, I. Bento, P. Duarte, S. Gilberto, F. Freixo, A. Guerrero, M. Francia, M. Lince-Faria, J. Carneiro, & M. Bettencourt-Dias. (2015). PLK4 trans-Autoactivation Controls Centriole Biogenesis in Space. *Dev. Cell* 35:222–235.

Lose, F., P. Lovelock, G. Chenevix-Trench, G. J. Mann, G. M. Pupo, A. B. Spurdle, & Kathleen Cuningham Foundation Consortium for Research into Familial Breast Cancer. (2006). Variation in the RAD51 gene and familial breast cancer. *Breast Cancer Res.* 8:R26.

Loukil, A., K. Tormanen, & C. Sütterlin. (2017). The daughter centriole controls ciliogenesis by regulating Neurl-4 localization at the centrosome. *J. Cell Biol.* 216:1287–1300.

Lu, H., M. T. Toh, V. Narasimhan, S. K. Thamilselvam, S. P. Choksi, & S. Roy. (2015a). A function for the Joubert syndrome protein Arl13b in ciliary membrane extension and ciliary length regulation. *Dev. Biol.* 397:225–236.

Lu, Q., C. Insinna, C. Ott, J. Stauffer, P. A. Pintado, J. Rahajeng, U. Baxa, V. Walia, A. Cuenca, Y.-S. Hwang, I. O. Daar, S. Lopes, J. Lippincott-Schwartz, P. K. Jackson, S. Caplan, & C. J. Westlake. (2015b). Early steps in primary cilium assembly require EHD1-and EHD3- dependent ciliary vesicle formation. *Nat. Cell Biol.* 17:228–240.

Lu, X., O. Ma, T.-A. Nguyen, S. N. Jones, M. Oren, & L. A. Donehower. (2007). The Wip1 Phosphatase acts as a gatekeeper in the p53-Mdm2 autoregulatory loop. *Cancer Cell* 12:342–54.

Lundin, C., M. North, K. Erixon, K. Walters, D. Jenssen, A. S. H. Goldman, & T. Helleday. (2005). Methyl methanesulfonate (MMS) produces heat-labile DNA damage but no detectable in vivo DNA double-strand breaks. *Nucleic Acids Res.* 33:3799–811.

Ma, H., M.- Gutierrez, S.-W. Park, J. Wu, Y. Lee, K. Suzuki, A. Koski, D. Ji, T. Hayama, R. Ahmed, H. Darby, C. Van Dyken, Y. Li, E. Kang, A.-R. Park, D. Kim, S.-T. Kim, J. Gong, Y. Gu, X. Xu, D. Battaglia, S. A. Krieg, D. M. Lee, D. H. Wu, D. P. Wolf, S. B. Heitner, J. Carlos Izpisua Belmonte, P. Amato, J.-S. Kim, S. Kaul, & S. Mitalipov. (2017). Correction of a pathogenic gene mutation in human embryos. *Nature* 0:1–7.

Ma, W., J. W. Westmoreland, D. A. Gordenin, & M. A. Resnick. (2011). Alkylation Base Damage Is Converted into Repairable Double-Strand Breaks and Complex Intermediates in G2 Cells Lacking AP Endonuclease. *PLOS Genet.* 7:e1002059.

Mahjoub, M. R., & T. Stearns. (2012). Report Supernumerary Centrosomes Nucleate Extra Cilia and Compromise Primary Cilium Signaling. *Curr. Biol.* 22:1628–1634.

Mahjoub, M. R., Z. Xie, & T. Stearns. (2010). Cep120 is asymmetrically localized to the daughter centriole and is essential for centriole assembly. *J. Cell Biol.* 191:331–46.

Mali, P., L. Yang, K. M. Esvelt, J. Aach, M. Guell, J. E. DiCarlo, J. E. Norville, & G. M. Church. (2013). RNA-guided human genome engineering via Cas9. *Science* 339:823–6.

Mao, Z., Y. Jiang, X. Liu, A. Seluanov, & V. Gorbunova. (2009). DNA repair by homologous recombination, but not by nonhomologous end joining, is elevated in breast cancer cells. *Neoplasia* 11:683–91.

Mardin, B. R., & E. Schiebel. (2012). Breaking the ties that bind: new advances in centrosome biology. *J. Cell Biol.* 197:11–8.

Maréchal, A., & L. Zou. (2015). RPA-coated single-stranded DNA as a platform for post-translational modifications in the DNA damage response. *Cell Res.* 25:9–23.

Marshall, W. F., & J. L. Rosenbaum. (2000). Are there nucleic acids in the centrosome? *Curr. Top. Dev. Biol.* 49:187–205.

Matsumoto, Y., & J. L. Maller. (2004). A centrosomal localization signal in cyclin E required for Cdk2-independent S phase entry. *Science* 306:885–8.

Matsuoka, S., B. A. Ballif, A. Smogorzewska, E. R. McDonald, K. E. Hurov, J. Luo, C. E. Bakalarski, Z. Zhao, N. Solimini, Y. Lerenthal, Y. Shiloh, S. P. Gygi, & S. J. Elledge. (2007). ATM and ATR substrate analysis reveals extensive protein networks responsive to DNA damage. *Science* 316:1160–6.

Matsuoka, S., M. Huang, & S. J. Elledge. (1998). Linkage of ATM to cell cycle regulation by the Chk2 protein kinase. *Science* 282:1893–7.

McIntyre, R. E., P. Lakshminarasimhan Chavali, O. Ismail, D. M. Carragher, G. Sanchez-Andrade, J. V. Forment, B. Fu, M. Del Castillo Velasco-Herrera, A. Edwards, L. van der Weyden, F. Yang, R. Ramirez-Solis, J. Estabel, F. A. Gallagher, D. W. Logan, M. J. Arends, S. H. Tsang, V. B. Mahajan, C. L. Scudamore, J. K. White, S. P. Jackson, F. Gergely, D. J. Adams, & D. J. Adams. (2012). Disruption of Mouse Cenpj, a Regulator of Centriole Biogenesis, Phenocopies Seckel Syndrome. *PLoS Genet.* 8:e1003022.

Mennella, V., D. A. Agard, B. Huang, & L. Pelletier. (2014). Amorphous no more: subdiffraction view of the pericentriolar material architecture. *Trends Cell Biol.* 24:188–97.

Mennella, V., B. Keszthelyi, K. L. McDonald, B. Chhun, F. Kan, G. C. Rogers, B. Huang, & D. A. Agard. (2012). Subdiffraction-resolution fluorescence microscopy reveals a domain of the centrosome critical for pericentriolar material organization. *Nat. Cell Biol.* 14:1159–68.

Meraldi, P., & E. A. Nigg. (2001). Centrosome cohesion is regulated by a balance of kinase and phosphatase activities. *J. Cell Sci.* 114:3749–3757.

Mi, J., C. Guo, D. L. Brautigan, & J. M. Larner. (2007). Protein Phosphatase-1α Regulates Centrosome Splitting through Nek2. *Cancer Res.* 67.

Miyamoto, T., K. Hosoba, B. D. Dynlacht, & S. M. Correspondence. (2015). The Microtubule-Depolymerizing Activity of a Mitotic Kinesin Protein KIF2A Drives Primary Cilia Disassembly Coupled with Cell Proliferation Constitutive activation of PLK1-KIF2A pathway impairs ciliogenesis. *CellReports* 10:664–673.

Moldovan, G.-L., & A. D. D'Andrea. (2009). FANCD2 hurdles the DNA interstrand crosslink. *Cell* 139:1222–4.

Molla-Herman, A., R. Ghossoub, T. Blisnick, A. Meunier, C. Serres, F. Silbermann, C. Emmerson, K. Romeo, P. Bourdoncle, A. Schmitt, S. Saunier, N. Spassky, P. Bastin, & A. Benmerah. (2010). The ciliary pocket: an endocytic membrane domain at the base of primary and motile cilia. *J. Cell Sci.* 123:1785–95.

Moritz, M., M. B. Braunfeld, V. Guénebaut, J. Heuser, & D. A. Agard. (2000). Structure of the γ-tubulin ring complex: a template for microtubule nucleation. *Nat. Cell Biol.* 2:365–370.

Morrison, C., E. Sonoda, N. Takao, A. Shinohara, K. Yamamoto, & S. Takeda. (2000). The controlling role of ATM in homologous recombinational repair of DNA damage. *EMBO J.* 19:463–71.

Moynahan, M. E., A. J. Pierce, & M. Jasin. (2001). BRCA2 Is Required for Homology-Directed Repair

of Chromosomal Breaks. *Mol. Cell* 7:263–272.

Mullee, L. I., & C. G. Morrison. (2016). Centrosomes in the DNA damage response—the hub outside the centre. *Chromosom. Res.* 24:35–51.

Nakamura, A., H. Arai, & N. Fujita. (2009). Centrosomal Aki1 and cohesin function in separase-regulated centriole disengagement. *J. Cell Biol.* 187:607–14.

Nakanishi, A., X. Han, H. Saito, K. Taguchi, Y. Ohta, S. Imajoh-Ohmi, & Y. Miki. (2007). Interference with BRCA2, which localizes to the centrosome during S and early M phase, leads to abnormal nuclear division. *Biochem. Biophys. Res. Commun.* 355:34–40.

Nakanishi, K., F. Cavallo, E. Brunet, & M. Jasin. (2011). Homologous recombination assay for interstrand cross-link repair. *Methods Mol. Biol.* 745:283–91.

Naro, C., F. Barbagallo, P. Chieffi, C. F. Bourgeois, M. P. Paronetto, & C. Sette. (2014). The centrosomal kinase NEK2 is a novel splicing factor kinase involved in cell survival. *Nucleic Acids Res.* 42:3218–27.

Nigg, E. A. (2001). MITOTIC KINASES AS REGULATORS OF CELL DIVISION AND ITS CHECKPOINTS. *Mol. Cell Biol.* 2:21–32.

Nigg, E. A., & J. W. Raff. (2009). Centrioles, centrosomes, and cilia in health and disease. *Cell* 139:663–78.

Nigg, E. A., & T. Stearns. (2011). The centrosome cycle: Centriole biogenesis, duplication and inherent asymmetries. *Nat. Cell Biol.* 13:1154–1160.

Nikolova, T., M. Ensminger, M. Löbrich, & B. Kaina. (2010). Homologous recombination protects mammalian cells from replication-associated DNA double-strand breaks arising in response to methyl methanesulfonate. *DNA Repair (Amst).* 9:1050–1063.

Nishi, R., Y. Okuda, E. Watanabe, T. Mori, S. Iwai, C. Masutani, K. Sugasawa, & F. Hanaoka. (2005). Centrin 2 stimulates nucleotide excision repair by interacting with xeroderma pigmentosum group C protein. *Mol. Cell. Biol.* 25:5664–74.

O'Driscoll, M. (2012). Diseases associated with defective responses to DNA damage. *Cold Spring Harb. Perspect. Biol.* 4.

O'Rourke, B. P., M. A. Gomez-Ferreria, R. H. Berk, A. M. U. Hackl, M. P. Nicholas, S. C. O'Rourke, L. Pelletier, & D. J. Sharp. (2014). Cep192 controls the balance of centrosome and non-centrosomal microtubules during interphase. *PLoS One* 9:e101001.

O'Toole, E., G. Greenan, K. I. Lange, M. Srayko, & T. Müller-Reichert. (2012). The role of γ-tubulin in centrosomal microtubule organization. *PLoS One* 7:e29795.

Oshimori, N., M. Ohsugi, & T. Yamamoto. (2006). The Plk1 target Kizuna stabilizes mitotic centrosomes to ensure spindle bipolarity. *Nat. Cell Biol.* 8:1095–1101.

Otto, E. A., T. W. Hurd, R. Airik, M. Chaki, W. Zhou, C. Stoetzel, S. B. Patil, S. Levy, A. K. Ghosh, C. A. Murga-Zamalloa, J. van Reeuwijk, S. J. F. Letteboer, L. Sang, R. H. Giles, Q. Liu, K. L. M. Coene, A. Estrada-Cuzcano, R. W. J. Collin, H. M. McLaughlin, S. Held, J. M. Kasanuki, G. Ramaswami, J. Conte, I. Lopez, J. Washburn, J. Macdonald, J. Hu, Y. Yamashita, E. R. Maher, L. M. Guay-Woodford, H. P. H. Neumann, N. Obermüller, R. K. Koenekoop, C. Bergmann, X. Bei, R. A. Lewis, N. Katsanis, V. Lopes, D. S. Williams, R. H. Lyons, C. V Dang, D. A. Brito, M. B. Dias, X. Zhang, J. D. Cavalcoli, G. Nürnberg, P. Nürnberg, E. A. Pierce, P. K. Jackson, C. Antignac, S. Saunier, R. Roepman, H. Dollfus, H. Khanna, & F. Hildebrandt. (2010). Candidate exome capture identifies mutation of SDCCAG8 as the cause of a retinal-renal ciliopathy. *Nat. Genet.* 42:840–50.

Pagan, J. K., A. Marzio, M. J. K. Jones, A. Saraf, P. V Jallepalli, L. Florens, M. P. Washburn, & M. Pagano. (2014). Degradation of Cep68 and PCNT cleavage mediate Cep215 removal from the PCM to allow centriole separation, disengagement and licensing. *Nat. Cell Biol.* 17:31–44.

Panic, M., S. Hata, A. Neuner, E. Schiebel, & H. Zentgraf. (2015). The Centrosomal Linker and Microtubules Provide Dual Levels of Spatial Coordination of Centrosomes. *PLOS Genet.* 11:e1005243.

Park, J., & K. Rhee. (2013). NEK2 phosphorylation antagonizes the microtubule stabilizing activity of centrobin. Page Biochemical and Biophysical Research Communications.

Pazour, G. J., B. L. Dickert, Y. Vucica, E. S. Seeley, J. L. Rosenbaum, G. B. Witman, & D. G. Cole.

(2000). Chlamydomonas IFT88 and its mouse homologue, polycystic kidney disease gene tg737, are required for assembly of cilia and flagella. *J. Cell Biol.* 151:709–18.

Pazour, G. J., & G. B. Witman. (2003). The vertebrate primary cilium is a sensory organelle. *Curr. Opin. Cell Biol.* 15:105–110.

Pedersen, L. B., & J. L. Rosenbaum. (2008). Intraflagellar Transport (IFT): Role in Ciliary Assembly, Resorption and Signalling. *Curr. Dev. Biol.* 85:23–61.

Peng, C., P. R. Graves, R. S. Thoma, Z. Wu, A. S. Shaw, H. Piwnica-Worms, & S. J. Elledge. (1997). Mitotic and G2 Checkpoint Control: Regulation of 14-3-3 Protein Binding by Phosphorylation of Cdc25C on Serine-216. *Science (80-.).* 277:1501–1505.

Perler, F. B. (1998). Protein splicing of inteins and hedgehog autoproteolysis: structure, function, and evolution. *Cell* 92:1–4.

Perler, F. B., J. A. Porter, D. P. von Kessler, S. C. Ekker, K. E. Young, J. J. Lee, K. Moses, & P. A. Beachy. (1995). The product of hedgehog autoproteolytic cleavage active in local and long range signalling. *Nature* 374:363–366.

Pierce, A. J., & M. Jasin. (2005). Measuring Recombination Proficiency in Mouse Embryonic Stem Cells. Pages 373–384Molecular Toxicology Protocols. Humana Press, New Jersey.

Pihan, G. A. (2013). Centrosome dysfunction contributes to chromosome instability, chromoanagenesis, and genome reprograming in cancer. *Front. Oncol.* 3:277.

Podhorecka, M., A. Skladanowski, & P. Bozko. (2010). H2AX Phosphorylation: Its Role in DNA Damage Response and Cancer Therapy. *J. Nucleic Acids* 2010.

Polo, S. E., & S. P. Jackson. (2011). Dynamics of DNA damage response proteins at DNA breaks: a focus on protein modifications. *Genes Dev.* 25:409–33.

Prosser, S. L., & C. G. Morrison. (2015). Centrin2 regulates CP110 removal in primary cilium formation. *J. Cell Biol.* 208:693–701.

Prosser, S. L., M. D. Samant, J. E. Baxter, C. G. Morrison, & A. M. Fry. (2012). Oscillation of APC/C activity during cell cycle arrest promotes centrosome amplification. *J. Cell Sci.* 125:5353–68.

Pugacheva, E. N., S. A. Jablonski, T. R. Hartman, E. P. Henske, & E. A. Golemis. (2007). HEF1-dependent Aurora A activation induces disassembly of the primary cilium. *Cell* 129:1351–63.

Purohit, A., S. H. Tynan, R. Vallee, & S. J. Doxsey. (1999). Direct Interaction of Pericentrin with Cytoplasmic Dynein Light Intermediate Chain Contributes to Mitotic Spindle Organization. *J. Cell Biol.* 147:481–491.

Qin, H., D. R. Diener, S. Geimer, D. G. Cole, & J. L. Rosenbaum. (2004). Intraflagellar transport (IFT) cargo: IFT transports flagellar precursors to the tip and turnover products to the cell body. *J. Cell Biol.* 164:255–66.

Ran, A. F., D. A. Scott, J. Wright, P. D. Hsu, V. Agarwala, & F. Zhang. (2013). Genome engineering using CRISPR-Cas system. *Nat. Protoc.* 8:2281–2308.

Rogakou, E. P., C. Boon, C. Redon, & W. M. Bonner. (1999). Megabase chromatin domains involved in DNA double-strand breaks in vivo. *J. Cell Biol.* 146:905–16.

Sánchez, I., & B. D. Dynlacht. (2016). Cilium assembly and disassembly. *Nat. Cell Biol.* 18:711–717.

Sanchez, Y., C. Wong, R. S. Thoma, R. Richman, Z. Wu, H. Piwnica-Worms, & S. J. Elledge. (1997). Conservation of the Chk1 checkpoint pathway in mammals: linkage of DNA damage to Cdk regulation through Cdc25. *Science* 277:1497–501.

Satyanarayana, A., & P. Kaldis. (2009). Mammalian cell-cycle regulation: several Cdks, numerous cyclins and diverse compensatory mechanisms. *Oncogene* 28:2925–2939.

Scheer, U. (2014). Historical roots of centrosome research: discovery of Boveri's microscope slides in Würzburg. *Philos. Trans. R. Soc. London B Biol. Sci.* 369.

Schmidt, T. I., J. Kleylein-Sohn, J. Westendorf, M. Le Clech, S. B. Lavoie, Y.-D. Stierhof, & E. A. Nigg. (2009). Control of centriole length by CPAP and CP110. *Curr. Biol.* 19:1005–11.

Schneider, L., C. A. Clement, S. C. Teilmann, G. J. Pazour, E. K. Hoffmann, P. Satir, & S. T. Christensen. (2005). PDGFRαα Signaling Is Regulated through the Primary Cilium in Fibroblasts. *Curr. Biol.* 15:1861–1866.

Schöckel, L., M. Möckel, B. Mayer, D. Boos, & O. Stemmann. (2011). Cleavage of cohesin rings coordinates the separation of centrioles and chromatids. *Nat. Cell Biol.* 13:966–972.

Seeley, E. S., & M. V Nachury. (2010). The perennial organelle: assembly and disassembly of the primary cilium. *J. Cell Sci.* 123:511–8.

Senra, J. M., B. A. Telfer, K. E. Cherry, C. M. McCrudden, D. G. Hirst, M. J. O'Connor, S. R. Wedge, & I. J. Stratford. (2011). Inhibition of PARP-1 by olaparib (AZD2281) increases the radiosensitivity of a lung tumor xenograft. *Mol. Cancer Ther.* 10:1949–58.

Seo, S., Q. Zhang, K. Bugge, D. K. Breslow, C. C. Searby, M. V. Nachury, & V. C. Sheffield. (2011). A Novel Protein LZTFL1 Regulates Ciliary Trafficking of the BBSome and Smoothened. *PLoS Genet.* 7:e1002358.

Sept, D. (2007). Microtubule Polymerization: One Step at a Time. *Curr. Biol.* 17:R764–R766.

Shah, A. S., Y. Ben-Shahar, T. O. Moninger, J. N. Kline, & M. J. Welsh. (2009). Motile cilia of human airway epithelia are chemosensory. *Science* 325:1131–4.

Shaltieì, I. A., L. Krennin, W. Bruinsma, & R. H. Medema. (2015). The same, only different – DNA damage checkpoints and their reversal throughout the cell cycle. *J. Cell Sci.* 128:607–620.

Sherr, C. J., & J. M. Roberts. (2004). Living with or without cyclins and cyclin-dependent kinases. *Genes Dev.* 18:2699–711.

Shieh, S. Y., M. Ikeda, Y. Taya, & C. Prives. (1997). DNA damage-induced phosphorylation of p53 alleviates inhibition by MDM2. *Cell* 91:325–34.

Shin, W., N.-K. Yu, B.-K. Kaang, & K. Rhee. (2015). The microtubule nucleation activity of centrobin in both the centrosome and cytoplasm. *Cell Cycle* 14:1925–31.

Sillibourne, J. E., I. Hurbain, T. Grand-Perret, B. Goud, P. Tran, & M. Bornens. (2013). Primary ciliogenesis requires the distal appendage component Cep123. *Biol. Open* 2:535–45.

Sir, J.-H., M. Pütz, O. Daly, C. G. Morrison, M. Dunning, J. V Kilmartin, & F. Gergely. (2013). Loss of centrioles causes chromosomal instability in vertebrate somatic cells. *J. Cell Biol.* 203:747–56.

Smith, E., D. Dejsuphong, A. Balestrini, M. Hampel, C. Lenz, S. Takeda, A. Vindigni, & V. Costanzo. (2009). An ATM- and ATR-dependent checkpoint inactivates spindle assembly by targeting CEP63. *Nat. Cell Biol.* 11:278–285.

Song, L., T. Dai, H. Xiong, C. Lin, H. Lin, T. Shi, & J. Li. (2010). Inhibition of centriole duplication by centrobin depletion leads to p38–p53 mediated cell-cycle arrest. *Cell. Signal.* 22:857–864.

Sonn, S., Y. Jeong, & K. Rhee. (2009). Nip2/centrobin may be a substrate of Nek2 that is required for proper spindle assembly during mitosis in early mouse embryos. *Mol. Reprod. Dev.* 76:587–592.

Sonnen, K. F., A.-M. Gabryjonczyk, E. Anselm, Y.-D. Stierhof, & E. A. Nigg. (2013). Human Cep192 and Cep152 cooperate in Plk4 recruitment and centriole duplication. *J. Cell Sci.* 126:3223–33.

Sorino, C., T. Bruno, A. Desantis, M. G. Di Certo, S. Iezzi, F. De Nicola, V. Catena, A. Floridi, L. Chessa, C. Passananti, E. Cundari, & M. Fanciulli. (2013). Centrosomal Che-1 protein is involved in the regulation of mitosis and DNA damage response by mediating pericentrin (PCNT)-dependent Chk1 protein localization. *J. Biol. Chem.* 288:23348–57.

Sorokin, S. (1962a). Centrioles and the formation of rudimentary cilia by fibroblast and smooth muscle cells. *J. Cell Biol.* 15:363–77.

Sorokin, S. (1962b). Centrioles and the formation of rudimentary cilia by fibroblasts and smooth muscle cells. *J. Cell Biol.* 15:363–377.

Sorokin, S. P. (1968). Reconstructions of centriole formation and ciliogenesis in mammalian lungs. *J. Cell Sci* 3:207–230.

Spektor, A., W. Y. Tsang, D. Khoo, & B. D. Dynlacht. (2007). Cep97 and CP110 Suppress a Cilia Assembly Program. *Cell* 130:678–690.

Stiff, T., T. Casar Tena, M. O'Driscoll, P. A. Jeggo, & M. Philipp. (2016). ATR promotes cilia signalling: links to developmental impacts. *Hum. Mol. Genet.* 25:1574–87.

Stracker, T. H., & J. H. J Petrini. (2011). The MRE11 complex: starting from the ends. *Nat. Publ. Gr.* 12:90–103.

Stracker, T. H., I. Roig, P. A. Knobel, & M. Marjanović. (2013). The ATM signaling network in

development and disease. *Front. Genet.* 4:37.

Stracker, T. H., T. Usui, & J. H. J. Petrini. (2009). Taking the time to make important decisions: the checkpoint effector kinases Chk1 and Chk2 and the DNA damage response. *DNA Repair (Amst).* 8:1047–54.

Strnad, P., & P. Gönzy. (2008). Mechanisms of procentriole formation. *Trends Cell Biol.* 18:389–396.

Strnad, P., S. Leidel, T. Vinogradova, U. Euteneuer, A. Khodjakov, P. Gönczy, A. Paoletti, & M. Bornens. (2007). Regulated HsSAS-6 levels ensure formation of a single procentriole per centriole during the centrosome duplication cycle. *Dev. Cell* 13:203–13.

Szymanska, K., & C. A. Johnson. (2012). The transition zone: an essential functional compartment of cilia. *Cilia* 1.

Takata, M., M. S. Sasaki, E. Sonoda, C. Morrison, M. Hashimoto, H. Utsumi, Y. Yamaguchi-Iwai, A. Shinohara, & S. Takeda. (1998). Homologous recombination and non-homologous end-joining pathways of DNA double-strand break repair have overlapping roles in the maintenance of chromosomal integrity in vertebrate cells. *EMBO J.* 17:5497–508.

Tang, J., R. L. Erikson, & X. Liu. (2006). Checkpoint kinase 1 (Chk1) is required for mitotic progression through negative regulation of polo-like kinase 1 (Plk1). *Proc. Natl. Acad. Sci. U. S. A.* 103:11964–9.

Tang, L., Y. Zeng, H. Du, M. Gong, J. Peng, B. Zhang, M. Lei, F. Zhao, W. Wang, X. Li, & J. Liu. (2017). CRISPR/Cas9-mediated gene editing in human zygotes using Cas9 protein. *Mol. Genet. Genomics* 292:525–533.

Tang, Z., M. G. Lin, T. R. Stowe, S. Chen, M. Zhu, T. Stearns, B. Franco, & Q. Zhong. (2013). Autophagy promotes primary ciliogenesis by removing OFD1 from centriolar satellites. *Nature* 502:254–257.

Tanos, B. E., H.-J. Yang, R. Soni, W.-J. Wang, F. P. Macaluso, J. M. Asara, & M.-F. B. Tsou. (2013). Centriole distal appendages promote membrane docking, leading to cilia initiation. *Genes Dev.* 27:163–8.

Traven, A., & J. Heierhorst. (2005). SQ/TQ cluster domains: concentrated ATM/ATR kinase phosphorylation site regions in DNA-damage-response proteins. *BioEssays* 27:397–407.

Tsou, M.-F. B., & T. Stearns. (2006). Mechanism limiting centrosome duplication to once per cell cycle. *Nature, Publ. online 19 July 2006; | doi10.1038/nature04985* 442:947.

Tsou, M. F. B., W. J. Wang, K. A. George, K. Uryu, T. Stearns, & P. V. Jallepalli. (2009). Polo Kinase and Separase Regulate the Mitotic Licensing of Centriole Duplication in Human Cells. *Dev. Cell* 17:344–354.

Tutt, A., A. Gabriel, D. Bertwistle, F. Connor, H. Paterson, J. Peacock, G. Ross, & A. Ashworth. (1999). Absence of Brca2 causes genome instability by chromosome breakage and loss associated with centrosome amplification. *Curr. Biol.* 9:1107-S1.

Varjosalo, M., S.-P. Li, & J. Taipale. (2006). Divergence of Hedgehog Signal Transduction Mechanism between Drosophila and Mammals. *Dev. Cell* 10:177–186.

Vogelstein, B., D. Lane, & A. J. Levine. (2000). Surfing the p53 network. *Nature* 408:307–310.

Vorobjev, I., & Y. S. Chentsov. (1982). Centrioles in the Cell Cycle . I . Epithelial Cells. *J. Cell Biol.* 93:938–49.

Wang, G., Q. Chen, X. Zhang, B. Zhang, X. Zhuo, J. Liu, Q. Jiang, & C. Zhang. (2013a). PCM1 recruits Plk1 to the pericentriolar matrix to promote primary cilia disassembly before mitotic entry. *J. Cell Sci.* 126:1355–65.

Wang, G., Q. Jiang, & C. Zhang. (2014). The role of mitotic kinases in coupling the centrosome cycle with the assembly of the mitotic spindle. *J. Cell Sci.* 127:4111–4122.

Wang, H.-F., K. Takenaka, A. Nakanishi, & Y. Miki. (2011). BRCA2 and nucleophosmin coregulate centrosome amplification and form a complex with the Rho effector kinase ROCK2. *Cancer Res.* 71:68–77.

Wang, H., Y.-T. Xie, J.-Y. Han, Y. Ruan, A.-P. Song, L.-Y. Zheng, W.-Z. Zhang, C. Sajdik, Y. Li, X.-X. Tian, & W.-G. Fang. (2012). Genetic polymorphisms in centrobin and Nek2 are associated with breast cancer susceptibility in a Chinese Han population. *Breast Cancer Res. Treat.* 136:241–51.

Wang, Y., T. J. Dantas, P. Lalor, P. Dockery, & C. G. Morrison. (2013b). Promoter hijack reveals pericentrin functions in mitosis and the DNA damage response. *Cell Cycle* 12:635–46.

Wei, Q., Y. Zhang, Y. Li, Q. Zhang, K. Ling, & J. Hu. (2012). The BBSome controls IFT assembly and turnaround in cilia. *Nat. Cell Biol.* 14:950–958.

Wiese, C., Y. Zheng, C. Detraves, M. Julian, A. Moisand, C. Gueth-Hallonet, A. Debec, I. Salles-Passador, A. Puget, & H. Mazarguil. (2006). Microtubule nucleation: gamma-tubulin and beyond. *J. Cell Sci.* 119:4143–53.

Winey, M., & E. T. O'Toole. (2014). Centriole structure. *Philos. Trans. R. Soc. London B Biol. Sci.* 369.

Wong, S. Y., & J. F. Reiter. (2008). The primary cilium at the crossroads of mammalian hedgehog signaling. *Curr. Top. Dev. Biol.* 85:225–60.

Woodruff, J. B., O. Wueseke, & A. A. Hyman. (2014). Pericentriolar material structure and dynamics. *Philos. Trans. R. Soc. Lond. B. Biol. Sci.* 369:20130459-.

Wu, K.-S., & T. K. Tang. (2012). CPAP is required for cilia formation in neuronal cells. *Biol. Open* 1:559–65.

Yagi, T., I. Minoura, A. Fujiwara, R. Saito, T. Yasunaga, M. Hirono, & R. Kamiya. (2005). An axonemal dynein particularly important for flagellar movement at high viscosity. Implications from a new Chlamydomonas mutant deficient in the dynein heavy chain gene DHC9. *J. Biol. Chem.* 280:41412–20.

Yang, J., M. Adamian, & T. Li. (2006). Rootletin interacts with C-Nap1 and may function as a physical linker between the pair of centrioles/basal bodies in cells. *Mol. Biol. Cell* 17:1033–40.

Yen, H.-J., M. K. Tayeh, R. F. Mullins, E. M. Stone, V. C. Sheffield, & D. C. Slusarski. (2006). Bardet-Biedl syndrome genes are important in retrograde intracellular trafficking and Kupffer's vesicle cilia function. *Hum. Mol. Genet.* 15:667–677.

Yoder, B. K., X. Hou, & L. M. Guay-Woodford. (2002). The polycystic kidney disease proteins, polycystin-1, polycystin-2, polaris, and cystin, are co-localized in renal cilia. *J. Am. Soc. Nephrol.* 13:2508–16.

Zhang, S., P. Hemmerich, & F. Grosse. (2007). Centrosomal localization of DNA damage checkpoint proteins. *J. Cell. Biochem.* 101:451–65.

Zheng, X., A. Ramani, K. Soni, M. Gottardo, S. Zheng, L. M. Gooi, W. Li, S. Feng, A. Mariappan, A. Wason, P. Widlund, A. Pozniakovsky, I. Poser, H. Deng, G. Ou, M. Riparbelli, C. Giuliano, A. A. Hyman, M. Sattler, J. Gopalakrishnan, & H. Li. (2016). Molecular basis for CPAP-tubulin interaction in controlling centriolar and ciliary length. *Nat. Commun.* 7.

Zhu, F., S. Lawo, A. Bird, D. Pinchev, A. Ralph, C. Richter, T. Mü Ller-Reichert, R. Kittler, A. A. Hyman, & L. Pelletier. (2008). The Mammalian SPD-2 Ortholog Cep192 Regulates Centrosome Biogenesis. *Curr. Biol.* 18:136–141.

Zimmermann, K. W. (1898). Beiträge zur Kenntniss einiger Drüsen und Epithelien. *Arch. für Mikroskopische Anat.* 52:552–706.

Zitouni, S., C. Nabais, S. C. Jana, A. Guerrero, & M. Bettencourt-Dias. (2014). Polo-like kinases: structural variations lead to multiple functions. *Nat. Rev. Mol. Cell Biol.* 15:433–452.

Zou, C., J. Li, Y. Bai, W. T. Gunning, D. E. Wazer, V. Band, & Q. Gao. (2005). Centrobin: a novel daughter centriole-associated protein that is required for centriole duplication. *J. Cell Biol.* 171:437–45.

8 Appendix

8.1 Supporting data

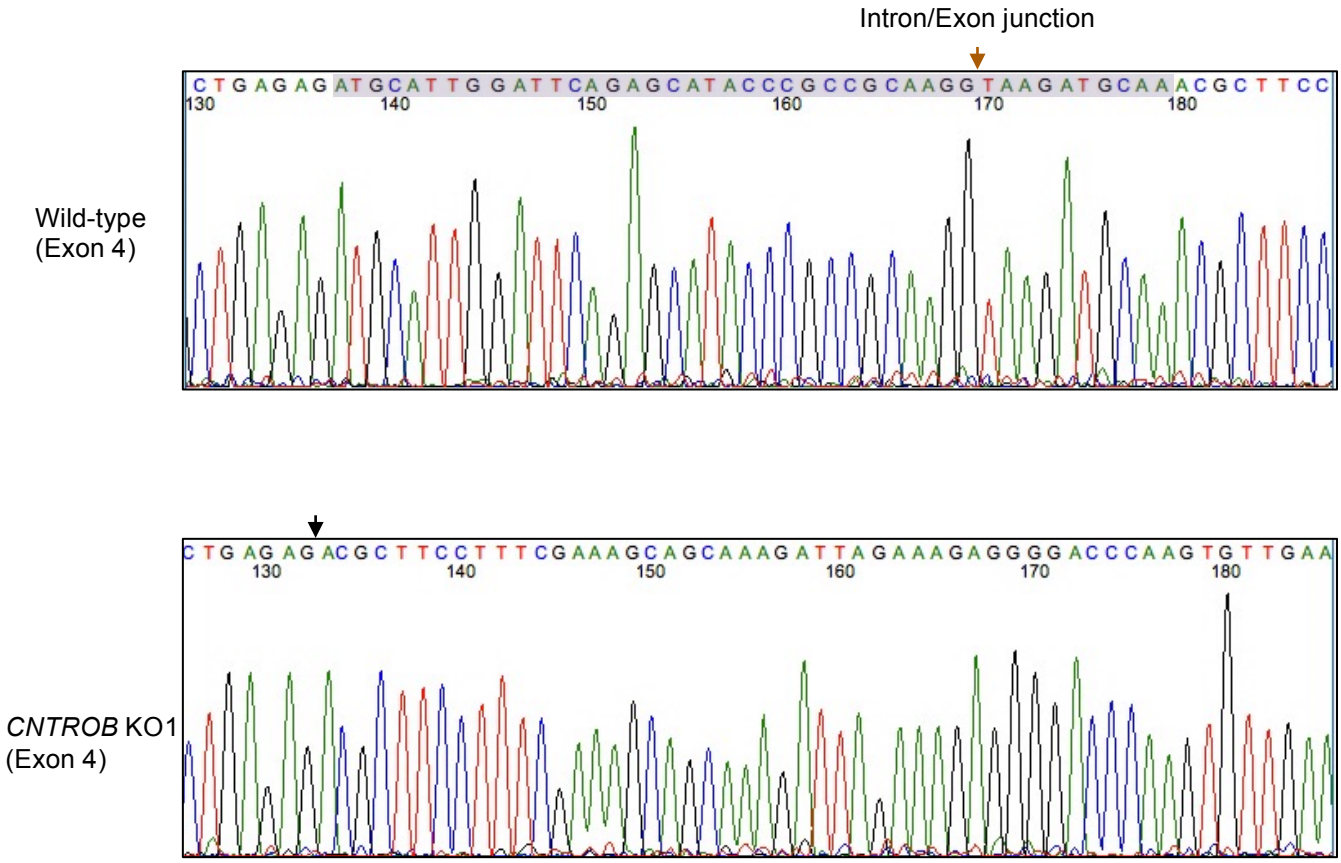

Appendix 1: Genomic DNA sequence trace of comparison of wild-type and *CNTROB* KO 1

Top panel shows the DNA sequence trace of exon 4 in wild-type hTERT-RPE1 cells. The region that is deleted in *CNTROB* KO 1 clone is highlighted in light-purple. The intron/exon junction that is also deleted after CRISPR/Cas9-mediated genome editing is pointed by brown arrow. Bottom panel shows the DNA sequence trace from *CNTROB* KO 1. The altered region is pointed by black arrow.

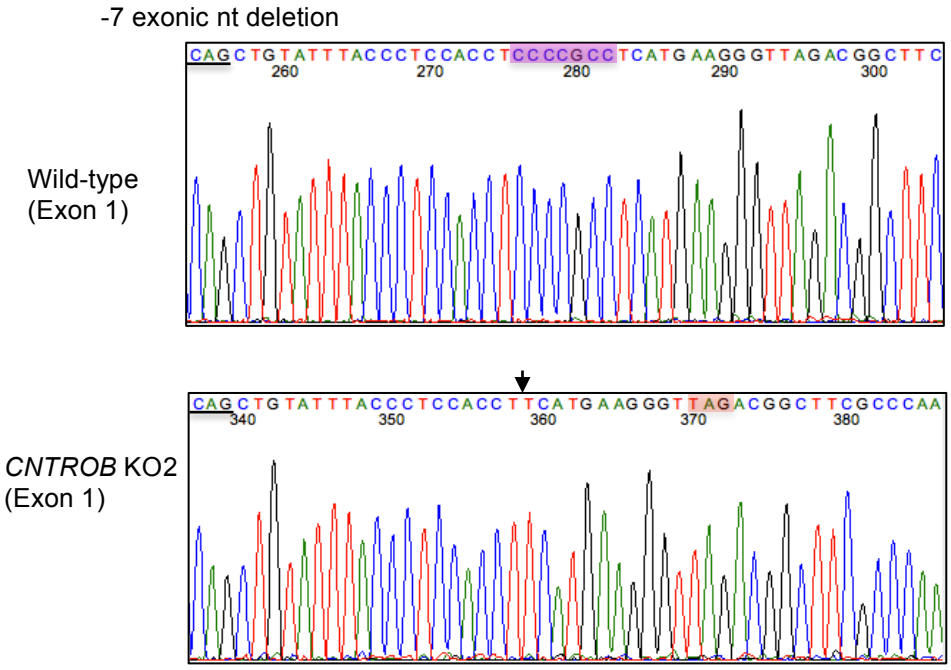

Appendix 2: Genomic DNA sequence trace of comparison of wild-type and *CNTROB* KO 2

Top panel shows the DNA sequence trace of exon 1 in wild-type hTERT-RPE1 cells. The region that is deleted after CRISPR/Cas9-mediated genome editing in *CNTROB* KO 2 clone is highlighted in purple. A codon is underlined to indicate the reading frame. Bottom panel shows the DNA sequence trace from *CNTROB* KO 2. The altered region is pointed by black arrow and the stop codon introduced is highlighted in pink.

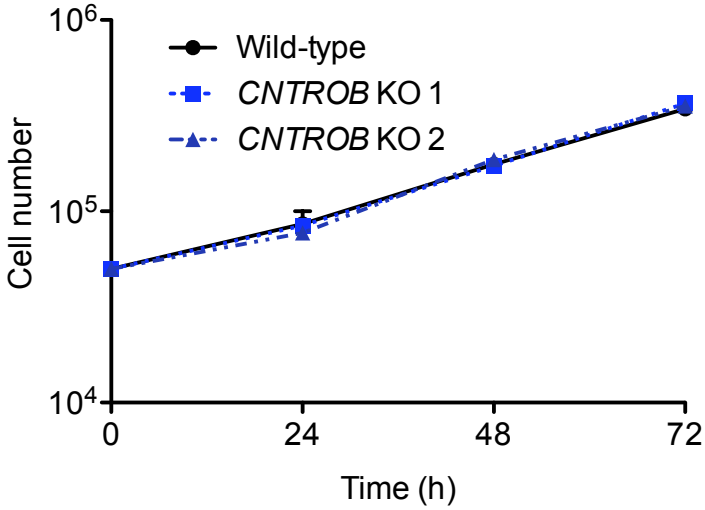

Appendix 3: Neither *CNTROB* KO clone shows a proliferation defect

Cells were plated at $5x10^4$ cells and counted every 24 h for 72 h. Each point represent mean of two independent experiments and error bar indicates standard error of mean. No significant difference was observed between wild-type, *CNTROB* KO 1 and *CNTROB* KO 2 at any time point.

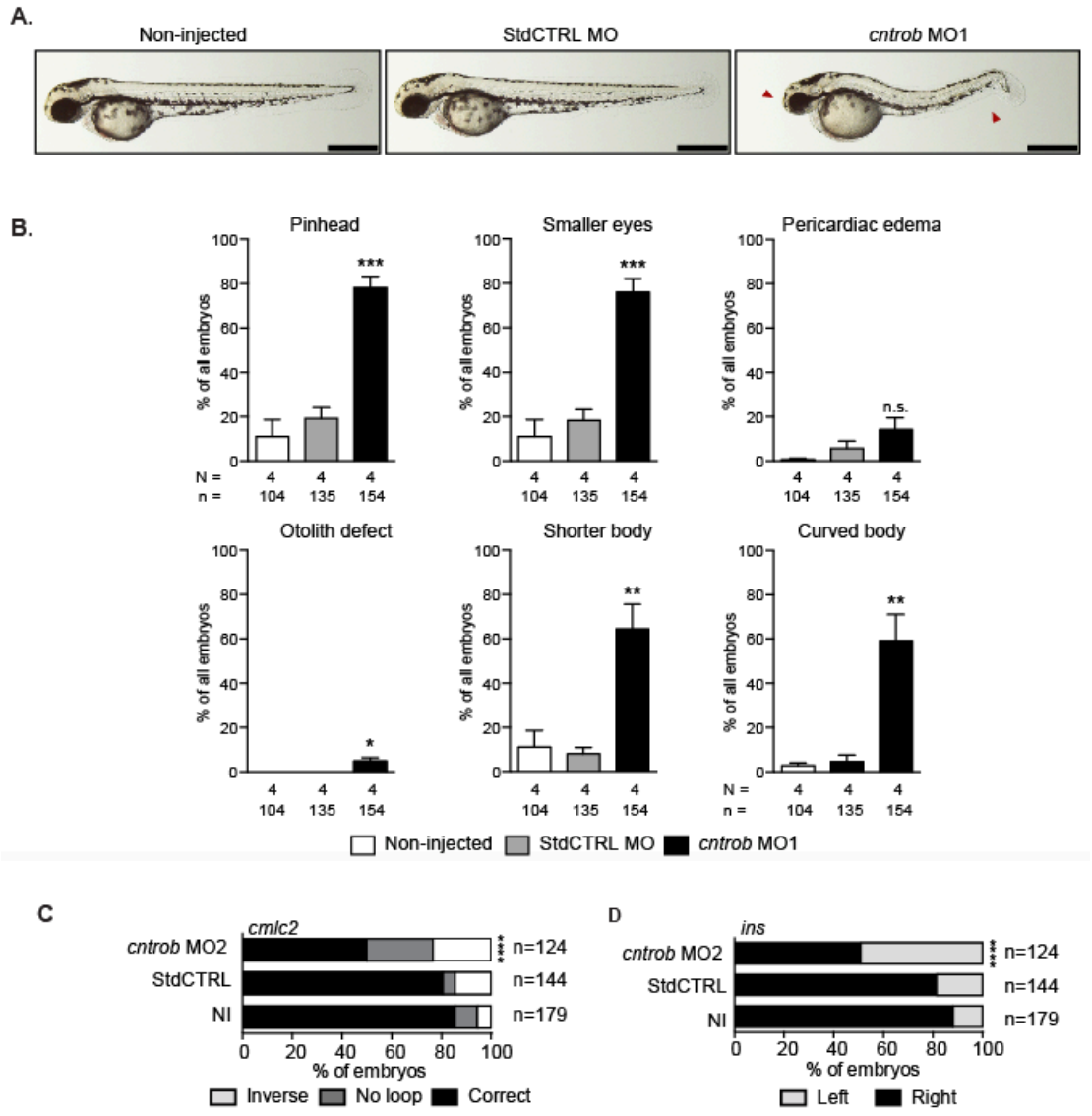

Appendix 4: Reproduction of the zebrafish phenotypes with a second MO

MO1 was directed to the *centrobin* ATG, MO2 to the 5' UTR **A.** Live images show gross phenotypes of zebrafish embryos injected with control or *centrobin* MOs at 48 hpf. Arrowheads indicate morphological abnormalities. Scale bars, 500 nm. **B.** Quantitation of developmental phenotypes in Centrobin-deficient embryos. Each phenotype was quantitated over 3 experiments in the indicated number of zebrafish embryos and graphs indicate means ± S.E.M.*, $P<0.05$; **, $P<0.01$; ****, $P<0.0001$; by one-way ANOVA. **C.** Quantitation of appropriate heart looping in wild-type embryos and embryos injected as indicated at 48 hpf. ****, $P<0.0001$. Significances were assessed using Fisher's exact test. **D.** Quantitation of pancreas placement in wild-type embryos and embryos injected as indicated at 48 hpf. Correct placement is at right.****, $P<0.0001$. Significances were assessed using Fisher's exact test.

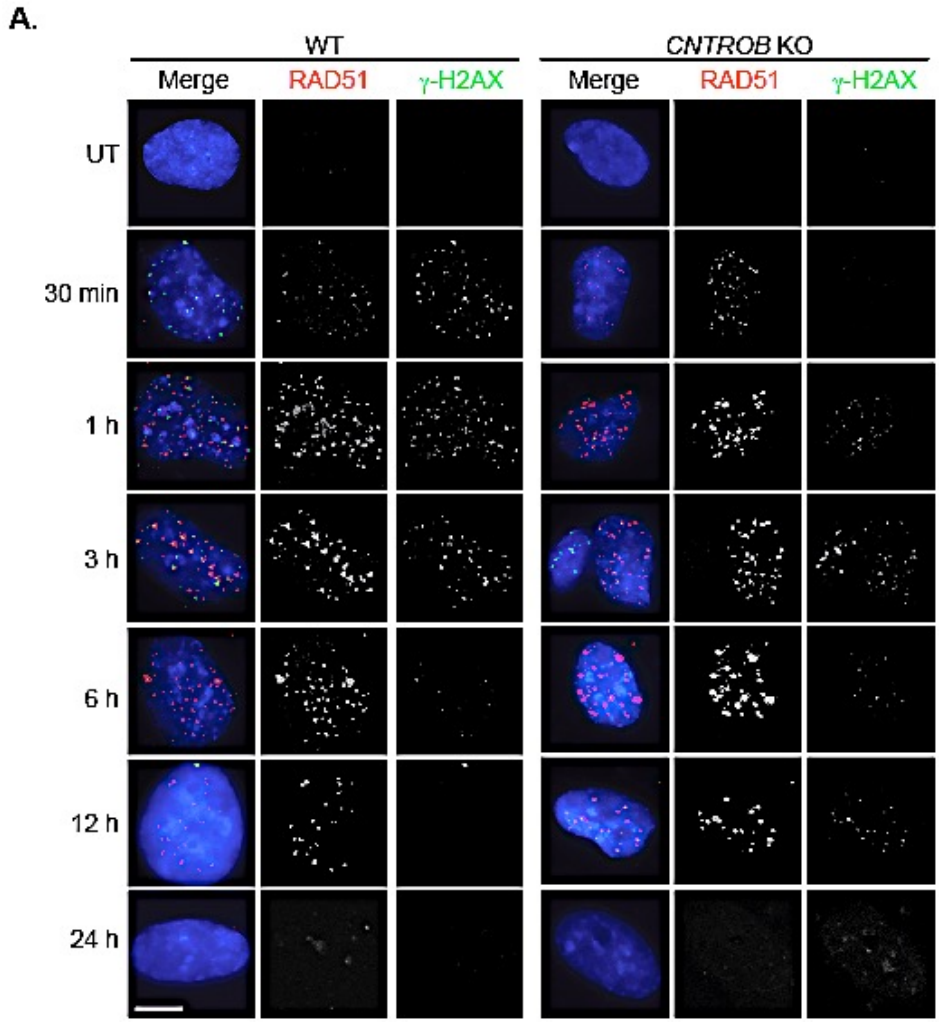

Appendix 5: Representative immunofluorescence microscopy analysis of RÀD51 and γ-H2AX after IR treatment

Representative immunofluorescence micrograph showing RAD51 focal recruitment in wild-type and *CNTROB* knockout cells after treatment with 5 Gy IR. Cells were fixed with 4% PFA at the indicated time points. Antibodies against γ-H2AX (green) and RAD51 (red) were used with Hoechst to visualize DNA (blue). Scale bar, 5 µm.

8.2 Scientific communications

8.2.1 International oral and poster presentations

Ogungbenro Adesanya, Y., Tena, TC, Breslin, L., Mullee, L., Antonczak, A., Dantas, T; Daly, OM., Cuffe, S., Prosser, SL., Wang Jr, Y., Gaboriau, D., Philipp, M and Morrison, CG. Linking primary ciliogenesis and DNA damage responses, 10th meeting: Cilia, Flagella and Centrosome Conference, Nice, France –Keynote lecture, Oct 10-12th, 2017.

Ogungbenro Adesanya, Y., Tena, TC, Gaboriau, D., Philipp, M and and Morrison, CG. Centrobin links primary ciliogenesis and homologous recombinational repair in vertebrates, EMBO Centrosome and Spindle Pole Bodies conference, EMBL, Heidelberg, Germany – poster presentation, 24 – 27th Sept 2017.

Adesanya, YB, Tena, TC, Gaboriau, D., Philipp, M and Morrison, CG. The BRCA2 interactor, centrobin participates in ciliogenesis and DNA repair, Mammalian DNA Repair, Gordon Research Conference, Ventura, california, USA February 19-24, 2017.

Adesanya, YB., Tena, TC, Gaboriau, D., Philipp, M and Morrison, CG. The BRCA2 interactor, centrobin participates in ciliogenesis, EMBO Cilia Conference, Amsterdam, The Netherland -Poster presentation, October 4-7th 2016.

Adesanya, YB, Gaboriau, D. and and Morrison, CG. Functional analysis of centrobin, EMBO Centrosome Conference, Lisbon – Poster presentation, 30th Sept – 4th Oct 2014.

8.2.2 National oral and poster presentations

Adesanya, YB., Tena, TC, Gaboriau, D., Philipp, M and and Morrison, CG. Functional analysis of centrobin in DNA repair and cilia formation, Annual CCB talk, Centre for Chromosome Biology, NUI Galway, Ireland –Oral presentation, 19th April 2017.

Adesanya, YB, Tena, TC, Gaboriau, D., Philipp, M and Morrison, CG. The BRCA2 interactor, centrobin participates in ciliogenesis and DNA repair, CCB-IFOM symposium, NUI Galway, Ireland –Poster presentation, 15th February 2017.

Adesanya, YB, Gaboriau, D. and and Morrison, CG. Functional analysis of centrobin in DNA damage response and cilia formation, Annual CCB talk, Centre for Chromosome Biology, NUI Galway, Ireland –Oral presentation, 8th June 2016.

Adesanya YB., Gaboriau, D. and Morrison, CG. Reverse genetic analysis of centrobin functions, Irish Cilia Biology Network Meeting, University College Dublin, Dublin, Ireland - – Oral and Poster presentations, Nov 2015.

Adesanya YB., Gaboriau, D. and Morrison, CG. A role for centrobin in Ciliation, Science Advisory Board, Centre for Chromosome Biology, NUI Galway, Ireland – Poster presentations, Nov 2015.

Adesanya, YB, Gaboriau, D. and and Morrison, CG. Functional analysis of centrobin in DNA damage response and cilia formation, Annual CCB talk, Centre for Chromosome Biology, NUI Galway, Ireland –Oral presentation, 19th August 2015.

Adesanya, YB, Gaboriau, D. and and Morrison, CG. Functional analysis of centrobin, Annual CCB talk, Centre for Chromosome Biology, NUI Galway, Ireland –Oral presentation, 20th Aug 2014.

8.2.3 Publications/submissions

Ogungbenro Adesanya, Y., Tena, TC, Gaboriau, D., Lalor, P., Dockery, P., Philipp, M and and Morrison, CG. Centrobin controls primary ciliogenesis in vertebrates; *Journal of Cell Biology*. 217, jcb.201706095. (Published 13th February 2018). PMID: 29440264.

Ogungbenro Adesanya, Y., Tena, TC., Philipp, M and and Morrison, CG. Identification of zebrafish centrobin coding sequence. GenBank: MF461638.

The original data of this report is available on:

http://jcb.rupress.org/content/early/2018/02/12/jcb.201706095

JCB

Report

Centrobin controls primary ciliogenesis in vertebrates

Yetunde Adesanya Ogungbenro,[1] Teresa Casar Tena,[3] David Gaboriau,[1,4] Pierce Lalor,[2] Peter Dockery,[2] Melanie Philipp,[3] and Ciaran G. Morrison[1]

[1]Centre for Chromosome Biology, School of Natural Sciences and [2]Anatomy, School of Medicine, National University of Ireland Galway, Galway, Ireland
[3]Institute of Biochemistry and Molecular Biology, Ulm University, Ulm, Germany
[4]Facility for Imaging by Light Microscopy, Imperial College London, London, England, UK

The BRCA2 interactor, centrobin, is a centrosomal protein that has been implicated in centriole duplication and microtubule stability. We used genome editing to ablate *CNTROB* in hTERT-RPE1 cells and observed an increased frequency of monocentriolar and acentriolar cells. Using a novel monoclonal antibody, we found that centrobin primarily localizes to daughter centrioles but also associates with mother centrioles upon serum starvation. Strikingly, centrobin loss abrogated primary ciliation upon serum starvation. Ultrastructural analysis of centrobin nulls revealed defective axonemal extension after mother centriole docking. Ciliogenesis required a C-terminal portion of centrobin that interacts with CP110 and tubulin. We also depleted centrobin in zebrafish embryos to explore its roles in an entire organism. Centrobin-depleted embryos showed microcephaly, with curved and shorter bodies, along with marked defects in laterality control, morphological features that indicate ciliary dysfunction. Our data identify new roles for centrobin as a positive regulator of vertebrate ciliogenesis.

Introduction

Centrosomes are the major microtubule organizing center in animal somatic cells and contribute to cell division, cell movement, and cell polarity. Mature centrosomes consist of two centrioles, cylindrical assemblies of triplet microtubules arranged with a ninefold symmetry, within the pericentriolar material. The centrioles differ from one another: the older of the two carries distal and subdistal appendages and is termed the mother centriole, as distinct from the younger, daughter centriole (Vorobjev and Chentsov, 1982; Nigg and Stearns, 2011).

Primary cilia are membrane-bounded, antenna-like structures that transduce extracellular signals at the surface of most human cell types (Goetz and Anderson, 2010). Defects in primary cilium formation or activity cause a diverse range of human developmental disorders that particularly affect the kidney, eye, liver, brain, and skeleton, collectively termed the ciliopathies (Waters and Beales, 2011; Braun and Hildebrandt, 2017). The centrosome has an important function in primary ciliation (Sorokin, 1962; Seeley and Nachury, 2010; Ishikawa and Marshall, 2011): the basal body, the structure at the base of the cilium, is established during primary ciliogenesis by plasma membrane docking of the mother centriole (Anderson, 1972; Ishikawa et al., 2005; Tanos et al., 2013).

Centrobin (also known as NIP2 or LIP8) is a centrosome component first described as an in vitro interactor of the C-terminal region of the BRCA2 tumor suppressor (Zou et al., 2005; Jeffery et al., 2010). Centrobin was initially described as a component of daughter centrioles and is required for efficient centriole duplication, which is at least partly because of its interactions with tubulin (Zou et al., 2005; Jeong et al., 2007; Jeffery et al., 2010; Lee et al., 2010; Gudi et al., 2011). Work in *Drosophila melanogaster* has indicated centrobin as a negative regulator of ciliogenesis in specialized sensory neurons (Gottardo et al., 2015). Here we describe the function of centrobin in vertebrate ciliogenesis.

Results and discussion

Centrobin-deficient cells show centriole duplication and ciliogenesis defects

We generated monoclonal antibody 6D4F4 against amino acids 113–361 of the human protein (Fig. S1 A). 6D4F4 recognized a centrosomal protein slightly larger than 100 kD (Fig. S1 B). To confirm 6D4F4's specificity, we used siRNA to deplete centrobin and lost the signal seen in immunoblot and immunofluorescence (IF) microscopy analyses (Fig. S1, B and C). This signal localized to the interphase microtubule organizing center and to the spindle poles, and predominantly to one of the two centrioles detected by CEP135 and CPAP staining, within the pericentriolar material revealed by pericentrin labeling (Fig. S1 D). Centrobin localized adjacently to the ninein signal, consistent with its being associated with the daughter centriole, as previously observed (Zou et al., 2005).

We then used CRISPR-Cas9 genome editing to disrupt exons 1 and 4 of *CNTROB* in the immortalized hTERT-RPE1

Correspondence to Ciaran G. Morrison: Ciaran.Morrison@nuigalway.ie

Supplemental material can be found at:
http://doi.org/10.1083/jcb.201706095

The Rockefeller University Press
J. Cell Biol.
https://doi.org/10.1083/jcb.201706095

cell line. Immunoblot screening of candidates yielded four clones that lacked detectable centrobin. Genomic PCR and DNA sequencing was used to confirm that *CNTROB* disruption generated premature stop codons that we verified in RT-PCR experiments. The analysis presented in this paper is based predominantly on a clone in which targeting of exon 4 led to a 43-nucleotide deletion (KO1), but we also examined a second clone where exon 1 disruption caused deletion of seven bases (KO2) and found no difference in the phenotypes we observed (Fig. S2, A–C). Western blotting and IF microscopy confirmed the absence of centrobin, and stable expression of full-length centrobin was used to obtain rescue clones (Fig. 1, A and B). Proliferative analysis showed no significant impact on cell doubling times in the absence of centrobin (Fig. 1 C), with a similar cell cycle profile being observed in *CNTROB* nulls and in WT cells (Fig. 1 D). Although centriole proteins, centriolar appendage proteins, and the centriolar satellites localized normally in the absence of centrobin, we observed an increased number of acentriolar and monocentriolar centrobin null cells (Fig. 1, E and F), confirming the requirement for centrobin in centriole duplication (Zou et al., 2005). Although it is possible that a more significant impact on centriole duplication may have been selected against in the p53-positive hTERT-RPE1 cells, the centriole duplication phenotypes seen in our knockout cells were similar to those seen in the original study of siRNA-treated HeLa cells, which have defective p53 signaling (Zou et al., 2005).

A negative role in ciliogenesis had been indicated for centrobin in *Drosophila* (Gottardo et al., 2015). Therefore, we examined the localization of centrobin after serum starvation, which induces ciliogenesis in RPE1 cells. Although centrobin was largely restricted to the daughter centriole in asynchronous cells, a small fraction was found at the basal body in ciliated cells (Fig. 2 A). We observed this association with both the endogenous centrobin protein and with GFP-tagged, overexpressed centrobin. Although centrobin has mainly been observed at daughter centrioles, it localized to both centrioles in cultured mouse hippocampal neurons (Jeong et al., 2007; Gudi et al., 2011; Shin et al., 2015). Strikingly, we found that centrobin-deficient cells had a marked defect in forming primary cilia, which could be rescued by reexpression of centrobin (Fig. 2, B and C). RNAi knockdown of centrobin in hTERT-RPE1 cells also reduced primary ciliation (Fig. 2 D). GFP-tagged *Drosophila* centrobin localized to centrosomes and overexpression of *Drosophila* centrobin in human *CNTROB* null cells restored ciliogenesis (Fig. 2, E and F). This suggests that there may be species- or tissue-specific determinants of centrobin function that differ between vertebrates and flies (Gottardo et al., 2015). For example, the roles of CP110 in controlling centriole overduplication differ between human cells and flies (Franz et al., 2013). Electron microscopy analysis revealed that 6 of 7 centrioles docked to the primary ciliary vesicle had failed to extend the axoneme from the ciliary bud, leaving the nascent cilia in the "mushroom" stage of cilium formation (Sorokin, 1962; Fig. 2 G).

Centrobin microtubule binding and CP110 interaction regions are required for ciliogenesis

To explore how centrobin controls ciliogenesis, we dissected the protein on basis of its known interactions, as diagramed in Fig. 3 A. The tubulin-binding and centrosome-targeting region of centrobin has been mapped to amino acids 765–903 (Gudi et al., 2011) and the region required for interaction with the key centriole duplication and extension regulators, CEP152 and CPAP (CENPJ), within amino acids 1–364 (Gudi et al., 2014, 2015). Transiently expressed, GFP-tagged full-length centrobin localized to the basal body in *CNTROB* nulls and rescued ciliogenesis (Fig. 3, B–D). We also observed GFP-centrobin along the axoneme, a location that was only rarely seen with the endogenous protein. Strikingly, overexpression of centrobin in WT cells caused bulges along the axoneme (Fig. S2 D), suggestive of defects in cilium assembly or intraflagellar transport. Centrobin 1–452 was neither required nor sufficient for ciliogenesis, indicating that the N-terminal CEP152 and CPAP-binding region of centrobin is not necessary for ciliogenesis. Expression of centrobin 452–903 supported ciliogenesis, with the transgene product also localizing to microtubule bundles (Fig. 3, B–D), as was seen in HeLa cells transfected with centrobin 445–903 (Jeong et al., 2007). Centrobin 365–903 localized to cytoplasmic aggregates similar to those described in previous transfection experiments in HeLa cells (Gudi et al., 2014). These data indicate that the C-terminal 451 amino acids of centrobin are sufficient to allow ciliogenesis, although the centrosome-targeting region 765–903 alone was not. It remains to be determined whether centrosome localization of centrobin is required for ciliogenesis. Appropriate regulation of microtubule stability is an obvious candidate mechanism by which centrobin may contribute to ciliogenesis (Jeong et al., 2007; Gudi et al., 2011; Shin et al., 2015).

We next examined the relationship between centrobin and CP110, a key negative regulator of ciliogenesis. CP110 and its partner, CEP97, were aberrantly localized around the distal end of the centriole after serum starvation of centrobin-deficient cells (Fig. 3 E), rather than being removed, as is the case during normal ciliogenesis (Spektor et al., 2007; Tsang et al., 2008). Immunoprecipitation of full-length centrobin copurified CP110 (Fig. 3 F), whereas coimmunoprecipitation with CP110 was observed with centrobin 365–903 but not with centrobin 1–364 (Fig. 3 G). Notably, expression of full-length centrobin or the ciliation-permissive 452–903 fragment led to the absence of CP110 from the distal end of the centriole (Fig. S2 E). Together, these findings indicate that the C-terminal region of centrobin interacts with CP110 and suggest that the centrobin–CP110 interaction regulates CP110 removal during ciliogenesis, possibly by facilitating access of another regulatory protein to CP110. We tested whether CP110 ablation could restore ciliogenesis in *CNTROB* nulls, as in *CETN2* nulls (Prosser and Morrison, 2015). CP110 knockdown in *CNTROB* nulls rescued ciliogenesis to an extent that was significant compared with mock-treated cells but not to *GAPDH* knockdown controls (Fig. S2, E–G). This indicates that both microtubule stabilization and CP110 regulation by the C-terminal region of centrobin are required for ciliogenesis. Thus, our model is that centrobin contributes to the removal of CP110 from the mother centriole, as distinct from inhibiting its recruitment, although we do not know the mechanism for this.

Centrobin deficiency causes ciliopathy defects in zebrafish

Next, to test whether centrobin is required for ciliary functions in another vertebrate system, we injected zebrafish embryos with two nonoverlapping antisense morpholinos (MOs) against the ATG and 5′-UTR of *cntrob*. As shown in Fig. 4 (A–C), Cntrob MO injection caused a decline in the levels of centrobin in embryos, along with significant declines in cilium number and length in the Kupffer's vesicle (KV), an organelle that contains

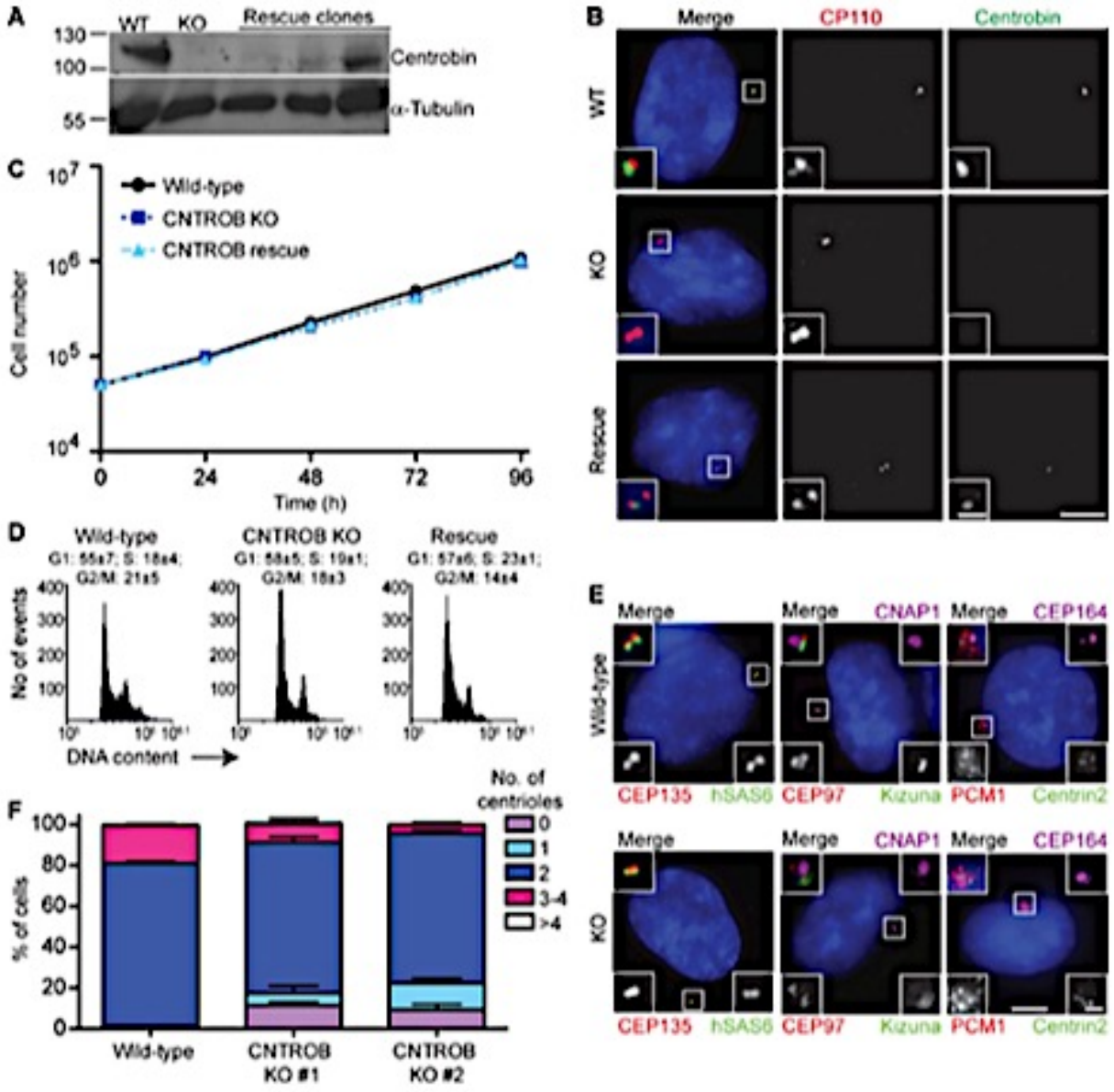

Figure 1. **CNTROB null cells are viable but show a defect in centriole duplication.** (A) *CNTROB*-edited clones and rescue candidates were identified by immunoblot for centrobin. (B) Confirmation of loss of centrobin protein expression by IF microscopy using antibodies to CP110 (red) and centrobin (green). Bars: 5 µm; (inset) 1 µm. (C) Growth curves show mean ± SEM of five independent experiments. No significant difference was observed between WT and centrobin-deficient cells at any time point. (D) Flow cytometry analysis of cell cycle profiles in asynchronous cells. Numbers indicate the mean percentage ± SEM of cells in each cell cycle phase (n = 3). (E) IF microscopy of the indicated PCM, centriole, and centriolar satellite makers in asynchronous WT and centrobin null cells. Bars: 5 µm; (inset) 1 µm. (F) The number of centrioles per cell were counted in 100 cells in three separate experiments. Centrioles were visualized by centrin2 and CEP135 staining. Bar graph shows mean + SEM.

a ciliated epithelium critical for left–right asymmetry during development (Essner et al., 2005). Moreover, Cntrob MO-injected embryos showed morphological abnormalities impacted by ciliary defects, such as smaller heads and eyes, pericardiac edema, and defective otolith seeding, with shorter and aberrantly curved bodies (Fig. 4, D and E; and Fig. S3, A and B).

We also observed marked impacts on laterality, another feature observed in ciliopathies. Cntrob MO injection caused randomization of the localization of *southpaw* (*spaw*) expression, which is normally restricted to the left lateral plate mesoderm (Fig. 5, A and B). Zebrafish deficient in left–right asymmetry determination, however, possess mirror-imaged *spaw* expression right of the midline, or exhibit bilateral *spaw* expression. Consistently, analysis of heart development in Cntrob MO-treated embryos showed declines in the fraction with normal positioning of the ventricle to the left of the atrium, as determined by visualization of cardiac myosin light chain 2 (*cmlc2*; Fig. 5, C and D; and Fig. S3 C). Abdominal organ asymmetry was also disturbed, as the correct positioning of the endocrine pancreas was impaired during the development of centrobin-deficient embryos, as determined by *insulin* (*ins*) localization (Fig. 5, E and F; and Fig. S3 D). Importantly, normal heart and pancreas location was rescued by reexpression of *cntrob* in Cntrob MO-injected embryos, demonstrating the specificity of the MO phenotypes we describe here (Fig. 5, D and F). These phenotypes reveal defects in cilium formation

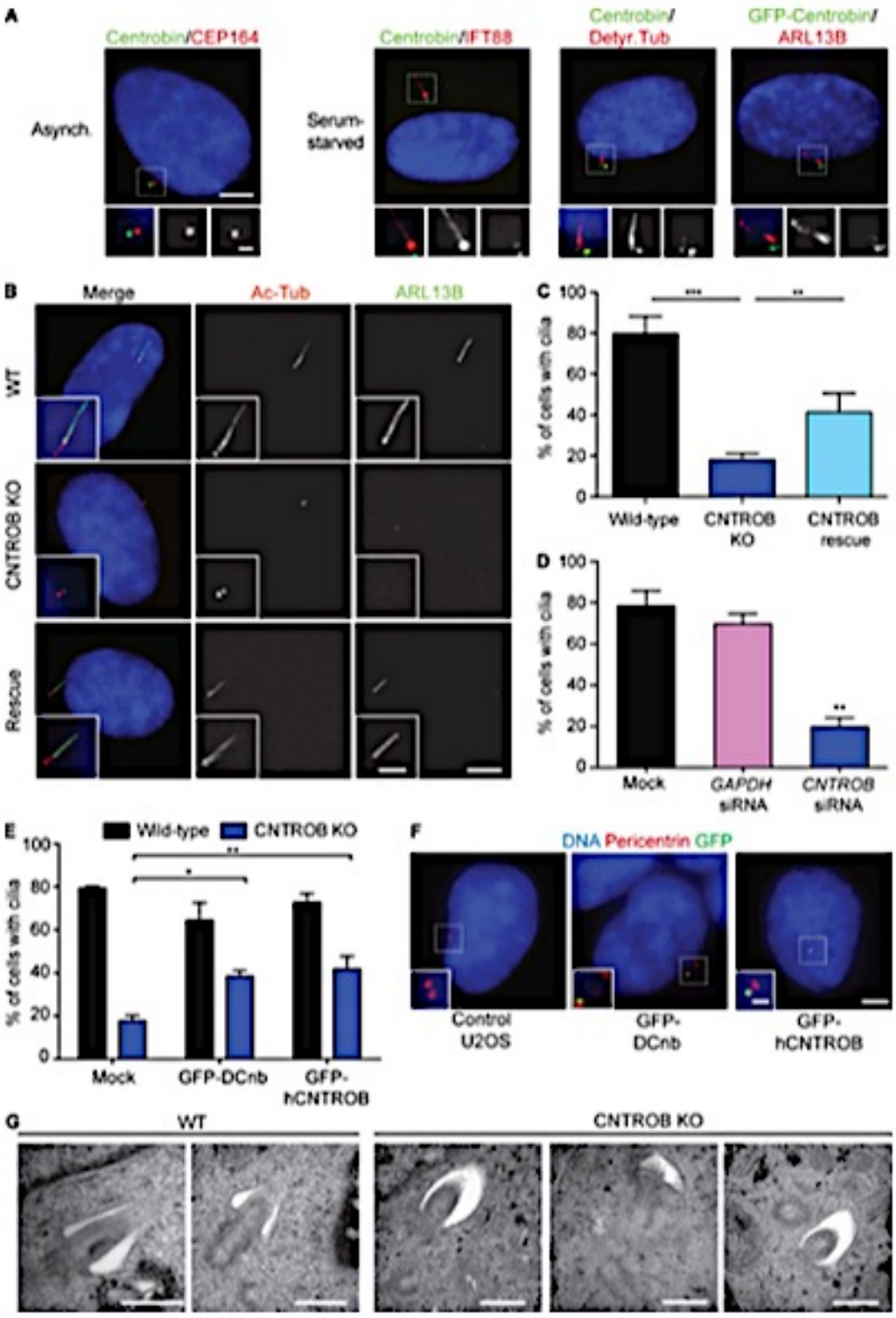

Figure 2. ***CNTROB* null cells are defective in primary ciliogenesis.** (A) Localization of centrobin (green) in asynchronous (Asynch.) or 48-h serum-starved cells. Detyr. Tub, detyrosinated tubulin. Bars: 5 µm; (inset) 1 µm. (B) IF microscopy of the cilium markers ARL13B (green) and acetylated tubulin (red) in cells after 48-h serum starvation. Bars: 5 µm; (inset) 2 µm. (C) Quantitation of the ciliation frequency after 48-h serum starvation showing mean + SEM of three independent experiments in which at least 100 cells were quantitated by acetylated tubulin staining. **, $P < 0.01$; ***, $P < 0.001$, in comparison to indicated samples by unpaired *t* test. (D) siRNA knockdown of *CNTROB* was used to ablate centrobin, with a *GAPDH* siRNA used as negative control (siGAPDH). Bar chart shows quantitation of the ciliation frequency after 24 h serum starvation. (E) Quantitation of the ciliation frequency after 48-h serum starvation of cells transiently transfected with GFP-tagged centrobin constructs. Bar charts show mean + SEM of three independent experiments in which at least 100 cells were quantitated by ARL13B staining. *, $P < 0.05$; **, $P < 0.01$, in comparison to controls by unpaired *t* test. (F) IF microscopy of U2OS cells transiently transfected with GFP-tagged human or *Drosophila* centrobin (green) with pericentrin (red) as a marker for centrosomes. Bars: 5 µm; (inset) 1 µm. (G) Transmission electron microscopy analysis of WT and centrobin null (knockout [KO]) cells after 48-h serum starvation. Bars, 500 nm.

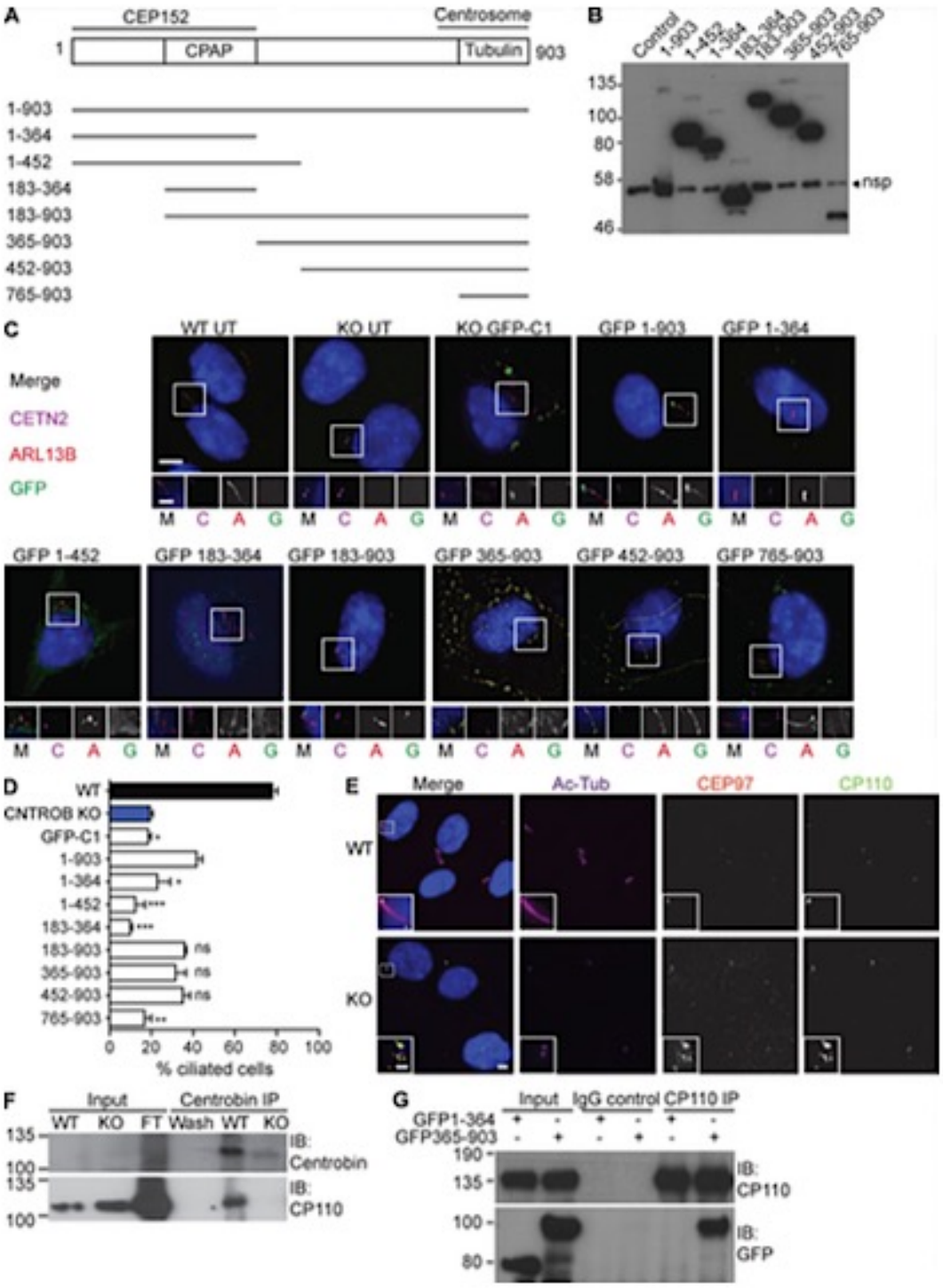

Figure 3. **The N-terminal CPAP-binding region of centrobin is dispensable for ciliogenesis.** **(A)** Schematic of deletion analysis performed on centrobin, indicating regions required for CPAP, CEP152, or tubulin interactions or localization to the centrosome. **(B)** Immunoblot showing expression of each of the GFP-tagged centrobin fragments at 24 h after transfection into HCT116 cells. The control lane is from untransfected cells. The lane with full-length protein is overloaded relative to the others. Nsp, nonspecific band. **(C)** Fluorescence micrographs of *CNTROB* null cells 24 h after transfection with GFP-tagged expression constructs that were tested in B. In the merged images, GFP localization is shown in green, ARL13B in red, and centrin2 in magenta. The same order is used for all single channels in the blowups. Bars: 5 µm; (inset) 2 µm. **(D)** Quantitation of the frequency of primary cilia in *CNTROB* null cells transfected with the indicated constructs. Cells were serum starved for 24 h, starting 24 h after transfection. Scoring was based on ARL13B staining and bar chart shows mean + SEM from 100 transfected cells in each of three experiments. **, $P < 0.01$; ***, $P < 0.001$, compared with full-length rescue using one-way ANOVA and Tukey's multiple comparison test. **(E)** IF microscopy of CP110 and CEP97 localization in WT and centrobin-null hTERT-RPE1 cells. Bars: 5 µm; (inset) 2 µm. **(F)** Coimmunoprecipitation (Co-IP) of endogenous CNTROB and CP110 from hTERT-RPE1 cell extract using anticentrobin monoclonal antibody 6D4F4 for the pulldown. *CNTROB*-null cells were used as the negative control. **(G)** Coimmunoprecipitation experiment using polyclonal anti-CP110 for pulldown 24 h after transfection of HCT116 WT cells with the indicated GFP constructs. IgG incubated with cell extracts was used as negative control. Size markers are in kilodaltons.

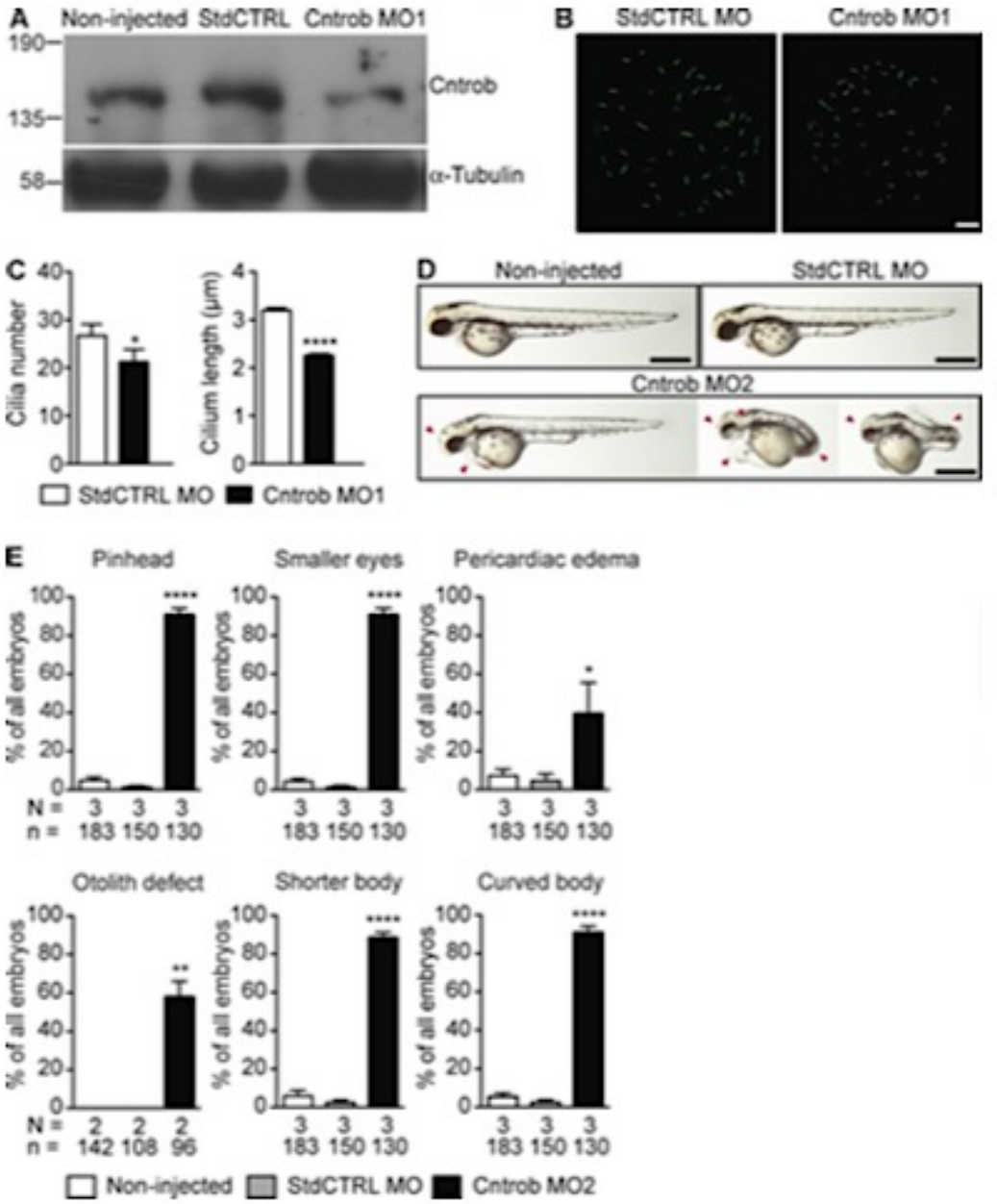

Figure 4. **Centrobin loss causes ciliary and developmental defects in zebrafish embryos.** MO1 was directed to the centrobin ATG and MO2 to the 5′ UTR. **(A)** Immunoblot analysis of efficacy of the centrobin knockdown in zebrafish embryos at 24 hpf. **(B)** Confocal stacks of cilia in KV in 8 ss zebrafish embryos injected with the standard control MO (StdCTRL MO) or MO targeting the translation start site of centrobin. Cilia were visualized with an antibody to acetylated tubulin (green). Bar, 10 µm. **(C)** Quantitation of ciliation frequency and length in KV after injection with the indicated MOs showing mean + SEM of four independent experiments in which 40 standard control MO and 33 Cntrob MO-treated KVs were quantitated by acetylated tubulin staining. In standard control embryos, 1067 cilia were measured, and in Cntrob MO embryos, 750 cilia. *, $P < 0.01$; ***, $P < 0.0001$; unpaired *t* test. **(D)** Live images show gross phenotypes of zebrafish embryos injected with control or Cntrob MOs at 24 hpf. Arrowheads indicate morphological abnormalities. Bars, 500 nm. **(E)** Quantitation of developmental phenotypes in centrobin-deficient embryos. Each phenotype was quantitated over three experiments in the indicated number of zebrafish embryos and graphs indicate means + SEM. *, $P < 0.05$; **, $P < 0.01$; ****, $P < 0.0001$, by one-way ANOVA.

and a range of developmental abnormalities that are consistent with defects in ciliation in the absence of centrobin. Together, our analyses of centrobin deficiency demonstrate that in vertebrates centrobin is required for ciliogenesis and cilium function.

CNTROB as a candidate microcephaly or ciliopathy gene

Defects in centrosome regulation are implicated in primary microcephaly and primordial dwarfism, disorders that do not have ciliopathy features (Nigg and Raff, 2009; Klingseisen and Jackson, 2011). However, cilia assemble on the mother centriole, so there is clearly potential for overlap in the molecular pathology of these diseases. Mutations in *PLK4*, which encodes the key kinase that directs centriole duplication, were described in cases of microcephalic primordial dwarfism, and MO knockdown of *plk4* in zebrafish led to ciliopathy phenotypes like those we describe for *cntrob* (Martin et al., 2014). Mutations in *ATR* give rise to Seckel syndrome, a microcephaly disorder (O'Driscoll

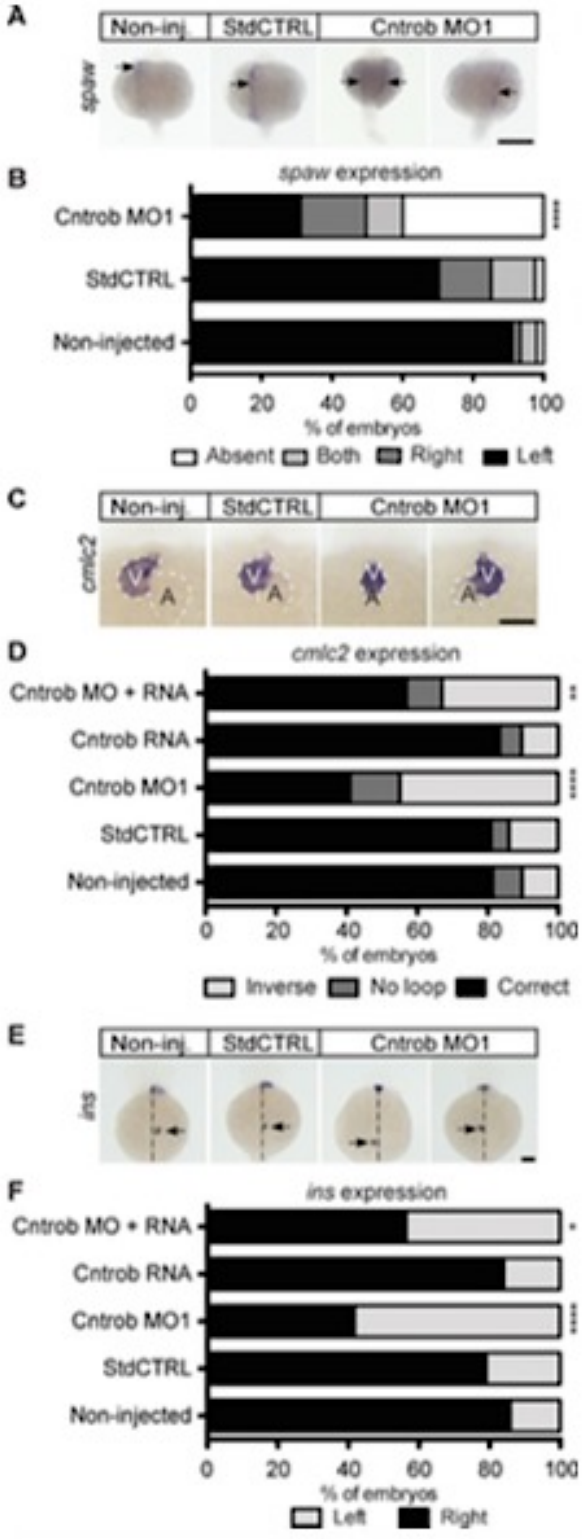

Figure 5. **Centrobin loss causes laterality defects in zebrafish embryos.** **(A, C, and E)** WMISH micrographs of showing localization of the messages of *spaw* for left lateral plate mesoderm, *cmlc2* to indicate heart looping, and *ins* to label pancreata and assess abdominal situs development. Dashed line indicates midline. A, atrium; V, ventricle. Bars, 100 µm. **(B)** Quantitation of laterality of *spaw* expression (arrows) in WT embryos and embryos injected as indicated at 20–22 ss. Appropriate asymmetric expression is to the left. **(D)** Quantitation of appropriate heart looping in WT embryos and embryos injected as indicated at 48 hpf. **(F)** Quantitation of pancreas placement in WT embryos and embryos injected as indicated at 48 hpf. Correct placement is on the right side from the midline. *, $P < 0.05$; **, $P < 0.01$; ****, $P < 0.0001$. Significances were assessed using Fisher's exact test.

et al., 2003). Recent work has demonstrated defects in ciliary signaling in ATR-SS cells and atr-depleted zebrafish embryos showed phenotypes indicative of ciliary dysfunction (Stiff et al., 2016). Although there is no published evidence of the clinical impact of *CNTROB* mutation to our knowledge, rat *hypodactyly* mutants, which have a truncating mutation in *Cntrob*, show skeletal abnormalities and male infertility caused by defective sperm flagellar axoneme assembly, a ciliopathy-related phenotype (Liska et al., 2009; Liška et al., 2013). The roles of centrobin in centriole duplication and its interactions with CPAP/CENPJ, a known microcephaly gene (Bond et al., 2005), link it to primary microcephaly. A human disease role for centrobin remains to be determined.

Material and methods

Cell culture and transfections

hTERT-RPE1 and U2OS cells were acquired from the American Type Culture Collection. hTERT-RPE1s were cultured in DMEM/F12 1:1 and U2OS in DMEM (Lonza). Matched HCT116 (colon carcinoma) *TP53*$^{+/+}$ (40–16) and *TP53*$^{-/-}$ (379.2) clones were provided by B. Vogelstein (Johns Hopkins University, Baltimore, MD; Bunz et al., 1998) and cultured in DMEM. Media were supplemented with 10% vol/vol FBS (Sigma-Aldrich) and penicillin-streptomycin (100 U/ml and 100 µg/ml, respectively; Sigma-Aldrich). Cell lines were cultured in a humidified 5% CO_2 atmosphere at 37°C, and mycoplasma testing was performed every 3 mo. Primary cilium formation was induced in hTERT-RPE1 by culturing cells in DMEM F-12 supplemented with 0.1% FBS and 1% penicillin-streptomycin for up to 48 h.

For transient transfections, we used Lipofectamine 2000 (Thermo Fisher Scientific) complexed with DNA at a 2:1 ratio in Opti-MEM (Gibco) for 20 min. For stable transfections, linearized plasmid was cotransfected with pLox-Bsr or pLox-Neo (Arakawa et al., 2001). Cells were incubated with the lipid–DNA complexes for 4–6 h, after which the medium was replaced and cells were allowed to recover for 24 h before trypsinization and serial dilution into media containing the necessary antibiotic (5 µg/ml Blasticidin S [Sigma-Aldrich] or 1 mg/ml G418 [Invivogen]) for 3 d. Single colonies were picked after 10–14 d and expanded using 3-mm Scienceware cloning discs (Sigma-Aldrich) before microscopy or immunoblot analysis.

Flow cytometry

Cells were fixed with ice-cold 70% ethanol at −20°C for at least 2 h or overnight. After fixation, cells were washed twice with 1× PBS, then resuspended in PBS containing 200 µg/ml RNase A and 40 µg/ml propidium iodide (Sigma-Aldrich) for 30 min. Cytometry was performed on an Accuri C6 Sampler (BD Biosciences).

Cloning

To clone human *CNTROB* cDNA isoform α (NM_053051), hTERT-RPE1 RNA was isolated using TRIzol (Invitrogen). Reverse transcription was performed using the High Capacity RNA to cDNA kit (Applied Biosystems) according to the manufacturer's instructions, and PCR was performed using KOD Hot Start (EMD Millipore) with the primers 5′-AAAAAGAATTCTATGGCAACATCAGCTGAC-3′ and 5′-AAAAAGGTACCTCATCTCCAGACTCCC-3′. PCR products were

cloned into pGEM-T Easy (Promega), sequenced, and subcloned into pEGFP-C1 (Clontech) using EcoRI and KpnI restriction sites. To generate pCNTROB-blasticidin, the EGFP coding sequence was removed using AgeI and XhoI, and a blasticidin resistance cassette was cloned into the neomycin resistance gene by blunt end ligation. CNTROB fragments were generated by PCR from pGEM-T Easy-hCNTROB and restriction cloned into pEGFP-C1. Primers used for fragment generation were as follows: hCNTROB-183-EcoR1F, 5′-TTTGGAATTCTT TTCAGGGGCTGAGAGATGCATTGG-3′; hCNTROB-365-EcoR1F, 5′-AAAAGAATTCACAAGAGCACCAGCTTAAGGAACACTACC AGG-3′; hCNTROB-452-EcoR1F, 5′-TTATGAATTCTGCTG TGCAGCTGGAGCAGCGGGTGAC-3′; hCNTROB-765-EcoR1F, 5′-TTTAGAATTCCGCCATGGCATCCAGTCTTTTCCGGGTCCC-3′; hCNTROB-364-Sal1R, 5′-TTTGTCGACCTACTGGGCCCAGGT CTGCCGTTCTTCTTCTAG-3′; and hCNTROB-452-Sal1R, 5′-AAT GTCGACGCCAGCTCCGACTCCAGCTGGATCCGC-3′.

For CRISPR/Cas targeting of *CNTROB* in hTERT-RPE1 cells, we used the human exome Cas9 site catalog (Mali et al., 2013) to generate guide RNAs targeting *CNTROB* exons 1 and 4. We cloned the following annealed primers into pX330-U6-Chimeric_BB-CBh-hSpCas9 vector (Plasmid 43330; Addgene; Cong et al., 2013): exon 1, 5′-CAC CGGTCTAACCCTTCATGAGGCG-3′ and 5′-AAACCGCCTCAT GAAGGGTTAGACc-3′; and exon 4, 5′-CACCGGTTTGCATCTTAC CTTGCCGG-3′ and 5′-AAACCCGCAAGGTAAGATGCAAACc-3′.

To identify zebrafish *centrobin* EST sequence, we used Basic Local Alignment Search Tool (BLAST) comparison with the human *CNTROB* cDNA sequence. Rapid Amplification of cDNA ends (RACE) primers were designed within cDNA sequences that encode regions predicted to be highly conserved between mammals and fish. Next, we used a 5′/3′ RACE kit (Roche) to amplify *centrobin* sequences from zebrafish embryos at 8 h after fertilization (hpf) using the following primers: GSP1_ZF5, 5′-CAGCGGTGAGATCAGGAGAGGACAGAG CG-3′; GSP2_ZF5, 5′-CACTTTCCATCTCCTCTATGTGCTTCC TGC-3′; GSP3_ZF5, 5′-CCTCCACATGCACACGCAGATCAGACG CC-3′; and GSP4_ZF5, 5′-CGTCCGTGTGTCATGCGACTCTGT CTGG-3′. We then predicted a 2,610-bp full-length *centrobin* cDNA sequence and deposited this sequence in GenBank under accession no. MF461638. We then cloned the full-length cDNA in two fragments that we assembled into pGEM-T Easy after RT-PCR of 8-hpf embryo mRNA with the following primers: ZF CNTROB full F, 5′-ATG TCTGTGAGCCGAGCTGCTGCTGATGG-3′; ZF CNTROB full R, 5′-TCAGTGTTGTCCAGCTGTGGCTCCAGTG-3′; ZF CNTROB full R3, 5′-TCAGTACAGAAACTCCAACCTGCTCAGCCC-3′; and ZF7 CNTROB HindIII frag F, 5′-AGCAAAAGCTTAGCAGAGAAG CAGATAAACACAGAG-3′. A mutant form with a silent mutation to ensure MO resistance was cloned using the following primer: ZF7 CNTROB mut F, 5′-ATGTCAGTCAGTCGCGCTGCAGCAG-3′.

To generate pGFP-DCnb, reverse transcription was performed on *Drosophila* mRNA provided by C. Collins (National University of Ireland Galway, Galway, Ireland) as described above and the centrobin transcript cloned into pEGFP-C1 after PCR with primers we designed from centrobin transcript variant A (NM_139423): DCnb-Fwd, 5′-CCCTCA AGCTTCCATGAGTGATACCGATACGGACGAC-3′ and DCnb-Rev, 5′-GCCTTGGTACCTCAGCACTTCCAAGGTGGAGGCTTACT-3′.

Monoclonal antibody generation

A fragment of the human *CNTROB* cDNA encoding amino acids 113–361 was cloned into pGEX4T3 (GE Healthcare) and expressed in bacteria as a GST fusion protein. The centrobin fragment was purified from a glutathione column by thrombin cleavage and used for hybridoma preparation (Dundee Cell Products). The best-performing clone 6D4 was expanded and subcloned to give 6D4F4, which produces IgG1κ.

RNA-mediated interference

hTERT-RPE1 cells were plated to attain 30–40% confluency on the day of transfection. On the next day, 50 nmol of custom siRNA (5′-AAG GAUGGUUCUAAGCAUAUC-3′; Jeong et al., 2007) or Silencer Select siRNA oligonucleotides specific to *GAPDH* (s5573; Ambion) was complexed with Oligofectamine (Invitrogen) in Opti-MEM (Gibco) for 20 min before addition to cells. After 4-h incubation of cells with the Oligofectamine-siRNA complexes, medium supplemented with 30% FBS was added, and cells were incubated for 48 h. Where indicated, cells were transfected for 36 h before serum starvation for 24 h.

Zebrafish husbandry and manipulations

Zebrafish were housed in a fully automated water-circulating rack system (Tecniplast) and exposed to a 14-h light and 10-h dark cycle. Embryos from EK and AB WT strains were generated using natural matings and raised until the desired stage in an incubator set to 28.5°C. Microinjections of MOs or capped RNAs were done with the help of an Eppendorf Femtojet and a Narishige micromanipulator at the 1–2 cell stage. MOs were designed based on submitted sequences and synthesized by Gene Tools. Two nonoverlapping MOs against the ATG and 5′-UTR of zebrafish *centrobin* were used: MO1, 5′-GTCTGTGAG ATGTCTGTGAGCCGAG-3′; and MO2, 5′-ATGAGAGTTTGTTTA CCGTCCGAGT-3′. As control, the standard control MO was used. Capped RNAs for reconstitution experiments were in vitro transcribed from linearized plasmids using the mMessage mMachine SP6 kit (Ambion) according to the manufacturer's instructions. All husbandry and experiments herein have been approved by local authorities and adhered to current European law.

IF microscopy

hTERT-RPE1 cells were grown on sterile coverslips and fixed in methanol containing 5 mM EGTA at −20 °C for 10 min or 4% paraformaldehyde for 10 min at room temperature followed by permeabilization with 0.15% Triton X-100 in 1× PBS for 2 min. To stain with antibodies against modified tubulins, cells were incubated on ice for 30 min to depolymerize microtubules. The cells were blocked in 1% BSA in 1× PBS before incubation in primary antibody for 1 h followed by 45 min incubation with fluorescently labeled secondary antibodies (Jackson Immunoresearch Laboratories Inc.). DNA was stained with Hoechst 33258 (Sigma-Aldrich), and slides were mounted in 80% vol/vol glycerol containing 3% N-propyl-gallate in 1× PBS. Cells were imaged using an IX81 microscope (Olympus) with a C4742-80-12AG camera (Hamamatsu) with a 100× oil objective, NA 1.35, using Volocity software (Perkin-Elmer). Images are presented as maximum intensity projections of z-stacks after deconvolution. Merges and individual channel images were exported as tagged image file formats (TIFFs) for publication and then cropped for publication using Photoshop CS6 (Adobe).

Primary antibodies used on human cells in this study were as follows: acetylated tubulin (1:2,000; T6793, clone 6-11B-1; Sigma-Aldrich); ARL13B (17711–1-AP; 1:2,000; ProteinTech); CP110 (1:2,000; 12780-1-AP; ProteinTech); IFT88 (13967–1-AP; 1:800; ProteinTech); detyrosinated tubulin (1:2,000; Ab48389; Abcam); pericentrin (Ab4448; 1:10,000; Abcam); Centrin2 (Poly6288; 1:1,000; Biolegend); Centrin (1:1,000; 20H5; Millipore); Centrin3 (1:1,000; 3E6; Abnova); CEP164 (Daly et al., 2016; 1F3G10; 1:100,000); α tubulin (1:2,000; B512, Sigma-Aldrich); CEP135 (Bird and Hyman, 2008; 1420 738; 1:1,000); CPAP (1:1,000; 11517-1-AP; ProteinTech); Ninein (Ab4447; 1:250; Abcam); SDCCAG8 (1:250; 13471-1-AP; ProteinTech); γ-tubulin (1:1,000; T3559; Sigma-Aldrich); centrobin (this study; 6D4F4; 1:10,000); CEP97 (1:1,000; 22050-1-AP; ProteinTech); hSAS6 (1:500; H00163786-B01P; Novus Biologicals); Kizuna (Oshimori et al., 2006; 1:2,000); C-NAP1 (Flanagan et al., 2017;

6F2C8; 1:2); PCM1 (Dammermann and Merdes, 2002; 817; 1:10,000); CEP164 (1:1,000; HPA037606, Sigma-Aldrich); and CEP97 (1:250; N-17; Santa Cruz Biotechnology).

For microscopy of zebrafish cilia, eight somite stage (ss) embryos were fixed overnight at 4°C using 4% PFA buffered in PBS and processed for cilia staining as previously described (Burkhalter et al., 2013). Cilia were labeled using anti-acetylated tubulin antibody (1:1,000; T6793; Sigma-Aldrich). An Alexa Fluor 488–labeled secondary antibody was used for detection (1:1,000; Molecular Probes). After staining, zebrafish embryos were manually deyolked using forceps, and the posterior part of the embryo was mounted in Vectashield (Vectorlabs) between two coverslips. Cilia were analyzed with a TCS SP5II confocal microscope (Leica). Cilia length was measured from confocal stacks using ImageJ.

Whole-mount in situ hybridization (WMISH)

Zebrafish embryos were fixed at the desired stages using 4% PFA buffered in PBS, dehydrated in a graded methanol series and stored at −20°C until further processing. For WMISH, embryos were gradually rehydrated and then processed according to standard protocols. WMISH probes against *cmlc2*, *ins*, and *spaw* have been described previously (Burkhalter et al., 2013). For detection of *centrobin* transcripts, a DIG-labeled in situ probe covering the whole coding sequence of centrobin was generated from the pGEM-T Easy plasmid after linearization with ApaI and using SP6 for in vitro transcription. Live embryos and those processed by WMISH were imaged on an M125 upright microscope (Leica) equipped with an IC80 HD camera (Lecia).

Transmission electron microscopy

Cells were harvested by trypsinization and pelleted at 250 *g* for 5 min. Cells were washed twice in 1× PBS, and then twice in 0.1 M sodium cacodylate buffer, pH 7.2 (Sigma-Aldrich), followed by overnight incubation at 4°C in primary fixative (2% glutaraldehyde and 2% paraformaldehyde [Electron Microscopy Sciences] in cacodylate buffer). The next day, cells were pelleted, washed, and fixed in secondary fixative (2% osmium tetroxide [Sigma-Aldrich] in cacodylate buffer) for a minimum of 2 h in the dark at room temperature until the cell pellet turned black. Cell pellets were washed three times in cacodylate buffer before dehydration through ethanol gradient (15 min each of 30, 60, and 90%), after which cells were further dehydrated three times for 30 min in 100% ethanol. To remove all of the alcohol, cell pellets were incubated in propylene oxide (Sigma-Aldrich) for 30 min followed by 4-h incubation in 50:50 propylene oxide/resin (TAAB) and overnight incubation in a 25:75 propylene oxide/resin mixture. The next day, samples were embedded in 100% low viscosity resin (TAAB). The blocks were sectioned on a microtome (Reichert-Jung Ultracut E; Leica) and stained with uranyl acetate and lead citrate before transmission electron microscopy (H-7000; Hitachi) with an ORCA-HRL camera (Hamamatsu). Images were processed using AMT version 6 (AMT Imaging).

Immunoblotting

Total cell extracts were prepared by lysing cells in lysis buffer (50 mM Tris HCl, pH 7.4, 150 mM NaCl, 5% glycerol, 1 mM EDTA, 0.5% sodium deoxycholate, 1% IGEPAL, protease inhibitor cocktail [Roche], and phosphatase inhibitors [Sigma-Aldrich]) for 20 min on ice. Samples were then centrifuged for 20 min at 18,000 *g* at 4°C, and supernatant was transferred to a fresh tube. 24-hpf zebrafish embryos were manually dechorionated, deyolked (Burkhalter et al., 2013), and lysed in the same way. Protein concentration was determined by Bradford assay on a Nanodrop 2000c spectrophotometer (Thermo Fisher Scientific). For loading on SDS-PAGE gel, 20–80 µg of whole cell lysate was transferred into a fresh tube and 5× sample buffer containing 20% β-mercaptoethanol was added to the samples and boiled at 95°C for 5 min. After proteins were resolved on 6–10% SDS–polyacrylamide gels, they were transferred to a nitrocellulose membrane (GE Healthcare) using a semidry transfer unit (Hoeffer TE77) at 1 mA/cm^2 for 2 h or a TransBlot wet transfer unit (BioRad) at 350 mA for 3 h. Blot detection was performed using ECL (GE Healthcare) after blocking and incubation in primary and secondary antibodies.

The primary antibodies used in this study were as follows: centrobin (6D4F4; 1:1,000), CP110 (1:2,000; 12780-1-AP; ProteinTech), α-tubulin (1:10,000; B512; Sigma-Aldrich), GFP (1:15,000; 66002-1-Ig; Proteintech), and GAPDH (1:10,000; 2118; Cell Signaling). HRP-labeled goat anti–mouse or anti–rabbit secondary antibodies were used at 1:10,000 (Jackson Immunoresearch Laboratories Inc.).

Coimmunoprecipitation

After trypsinization of HCT116 (WT) or hTERT-RPE1 cells, whole cell extracts were prepared by lysing cells in lysis buffer (50 mM Tris HCl, pH 7.4, 150 mM NaCl, 20% glycerol, 1 mM EDTA, 0.5% sodium deoxycholate, 1% IGEPAL, protease inhibitor cocktail [Roche], 1 mM sodium orthovanadate, 5 mM sodium fluoride, 1:10,000 dilution of benzonase nuclease [Sigma-Aldrich], and 1 mM PMSF) for 45 min at 4°C on a rotating wheel. Samples were then centrifuged for 20 min at 18,000 *g* at 4°C and supernatants transferred to a fresh tube. Protein concentration was determined by Bradford assay on a Thermo Fisher Scientific Nanodrop 2000c Spectrophotometer. Meanwhile, 20 µl of prewashed protein A/G beads (Santa Cruz Biotechnology) were incubated with 3–5 µg of primary antibody for 1 h at 4 °C with gentle agitation. The beads–antibody complex was washed twice with lysis buffer followed by incubation with 3–5 mg total cell extract for a further 2 h. After incubation, immunoprecipitates were spun down at 155 *g* for 3 min and the supernatant discarded. Beads were washed four times in lysis buffer, then boiled in 5× Laemmli buffer for 10 min and pelleted at 18,000 *g* before immunoblot analysis.

Quantification and statistical analysis

Data were analyzed using Prism v5.0 and v6.0 (GraphPad) with the statistical tests as indicated in the figure legends.

Online supplemental material

Fig. S1 shows generation and characterization of a monoclonal antibody for centrobin. Fig. S2 shows confirmation of *CNTROB* disruption by genome editing. Fig. S3 shows reproduction of the zebrafish phenotypes with a second MO.

Acknowledgments

We thank Caitriona Collins for *Drosophila* mRNA and Sandra Burczyk and Cornelia Donow for excellent fish care.

This work was funded by Science Foundation Ireland Principal Investigator award 10/IN.1/B2972 and European Commission grant SEC-2009-4.3-02, project 242361 "BOOSTER." Y.A. Ogungbenro received a Government of Ireland Postgraduate Scholarship from the Irish Research Council (GOIPG/2013/318). We acknowledge the National Biophotonics and Imaging Platform Ireland and the National Centre for Biomedical Engineering Sciences Flow Cytometry core facility, which were supported by the Irish Government Program for Research in Third-Level Institutions. Zebrafish experiments were funded by Deutsche Forschungsgemeinschaft grant PH144/4-1.

The authors declare no competing financial interests.

Author contributions: Y.A. Ogungbenro and C.G. Morrison conceptualized the project. Methodology was by Y.A. Ogungbenro, T.C. Tena, D. Gabor Miklos, M. Philipp and C.G. Morrison. Investigation

was by Y.A. Ogungbenro, T.C. Tena, D. Gaboriau, and P. Lalor. C.G. Morrison wrote the original draft. Y.A. Ogungbenro, T.C. Tena, D. Gaboriau, M. Philipp, and C.G. Morrison wrote, reviewed, and edited the paper. Funding acquisition was by M. Philipp, P. Dockery, and C.G. Morrison. M. Philipp, P. Dockery, and C.G. Morrison provided resources. M. Philipp, P. Dockery, and C.G. Morrison supervised the project.

Submitted: 15 June 2017
Revised: 19 July 2017
Accepted: 17 January 2018

References

Anderson, R.G. 1972. The three-dimensional structure of the basal body from the rhesus monkey oviduct. *J. Cell Biol.* 54:246–265. https://doi.org/10.1083/jcb.54.2.246

Arakawa, H., D. Lodygin, and J.M. Buerstedde. 2001. Mutant loxP vectors for selectable marker recycle and conditional knock-outs. *BMC Biotechnol.* 1:7. https://doi.org/10.1186/1472-6750-1-7

Bird, A.W., and A.A. Hyman. 2008. Building a spindle of the correct length in human cells requires the interaction between TPX2 and Aurora A. *J. Cell Biol.* 182:289–300. https://doi.org/10.1083/jcb.200802005

Bond, J., E. Roberts, K. Springell, S.B. Lizarraga, S. Scott, J. Higgins, D.J. Hampshire, E.E. Morrison, G.F. Leal, E.O. Silva, et al. 2005. A centrosomal mechanism involving CDK5RAP2 and CENPJ controls brain size. *Nat. Genet.* 37:353–355. https://doi.org/10.1038/ng1539

Braun, D.A., and F. Hildebrandt. 2017. Ciliopathies. *Cold Spring Harb. Perspect. Biol.* 9:a028191. https://doi.org/10.1101/cshperspect.a028191

Bunz, F., A. Dutriaux, C. Lengauer, T. Waldman, S. Zhou, J.P. Brown, J.M. Sedivy, K.W. Kinzler, and B. Vogelstein. 1998. Requirement for p53 and p21 to sustain G2 arrest after DNA damage. *Science.* 282:1497–1501. https://doi.org/10.1126/science.282.5393.1497

Burkhalter, M.D., G.B. Fralish, R.T. Premont, M.G. Caron, and M. Philipp. 2013. Grk5l controls heart development by limiting mTOR signaling during symmetry breaking. *Cell Reports.* 4:625–632. https://doi.org/10.1016/j.celrep.2013.07.036

Cong, L., F.A. Ran, D. Cox, S. Lin, R. Barretto, N. Habib, P.D. Hsu, X. Wu, W. Jiang, L.A. Marraffini, and F. Zhang. 2013. Multiplex genome engineering using CRISPR/Cas systems. *Science.* 339:819–823. https://doi.org/10.1126/science.1231143

Daly, O.M., D. Gaboriau, K. Karakaya, S. King, T.J. Dantas, P. Lalor, P. Dockery, A. Kramer, and C.G. Morrison. 2016. CEP164-null cells generated by genome editing show a ciliation defect with intact DNA repair capacity. *J. Cell Sci.* 129:1769–1774. https://doi.org/10.1242/jcs.186221

Dammermann, A., and A. Merdes. 2002. Assembly of centrosomal proteins and microtubule organization depends on PCM-1. *J. Cell Biol.* 159:255–266. https://doi.org/10.1083/jcb.200204023

Essner, J.J., J.D. Amack, M.K. Nyholm, E.B. Harris, and H.J. Yost. 2005. Kupffer's vesicle is a ciliated organ of asymmetry in the zebrafish embryo that initiates left-right development of the brain, heart and gut. *Development.* 132:1247–1260. https://doi.org/10.1242/dev.01663

Flanagan, A.M., E. Stavenschi, S. Basavaraju, D. Gaboriau, D.A. Hoey, and C.G. Morrison. 2017. Centriole splitting caused by loss of the centrosomal linker protein C-NAP1 reduces centriolar satellite density and impedes centrosome amplification. *Mol. Biol. Cell.* 28:736–745. https://doi.org/10.1091/mbc.E16-05-0325

Franz, A., H. Roque, S. Saurya, J. Dobbelaere, and J.W. Raff. 2013. CP110 exhibits novel regulatory activities during centriole assembly in *Drosophila*. *J. Cell Biol.* 203:785–799. https://doi.org/10.1083/jcb.201305109

Goetz, S.C., and K.V. Anderson. 2010. The primary cilium: a signalling centre during vertebrate development. *Nat. Rev. Genet.* 11:331–344. https://doi.org/10.1038/nrg2774

Gottardo, M., G. Pollarolo, S. Llamazares, J. Reina, M.G. Riparbelli, G. Callaini, and C. Gonzalez. 2015. Loss of Centrobin Enables Daughter Centrioles to Form Sensory Cilia in Drosophila. *Curr. Biol.* 25:2319–2324. https://doi.org/10.1016/j.cub.2015.07.038

Gudi, R., C. Zou, J. Li, and Q. Gao. 2011. Centrobin-tubulin interaction is required for centriole elongation and stability. *J. Cell Biol.* 193:711–725. https://doi.org/10.1083/jcb.201006135

Gudi, R., C. Zou, J. Dbar, Q. Gao, and C. Vasu. 2014. Centrobin-centrosomal protein 4.1-associated protein (CPAP) interaction promotes CPAP localization to the centrioles during centriole duplication. *J. Biol. Chem.* 289:15166–15178. https://doi.org/10.1074/jbc.M113.531152

Gudi, R., C.J. Haycraft, P.D. Bell, Z. Li, and C. Vasu. 2015. Centrobin-mediated regulation of the centrosomal protein 4.1-associated protein (CPAP) level limits centriole length during elongation stage. *J. Biol. Chem.* 290:6890–6902. https://doi.org/10.1074/jbc.M114.603423

Ishikawa, H., and W.F. Marshall. 2011. Ciliogenesis: building the cell's antenna. *Nat. Rev. Mol. Cell Biol.* 12:222–234. https://doi.org/10.1038/nrm3085

Ishikawa, H., A. Kubo, S. Tsukita, and S. Tsukita. 2005. Odf2-deficient mother centrioles lack distal/subdistal appendages and the ability to generate primary cilia. *Nat. Cell Biol.* 7:517–524. https://doi.org/10.1038/ncb1251

Jeffery, J.M., A.J. Urquhart, V.N. Subramaniam, R.G. Parton, and K.K. Khanna. 2010. Centrobin regulates the assembly of functional mitotic spindles. *Oncogene.* 29:2649–2658. https://doi.org/10.1038/onc.2010.37

Jeong, Y., J. Lee, K. Kim, J.C. Yoo, and K. Rhee. 2007. Characterization of NIP2/centrobin, a novel substrate of Nek2, and its potential role in microtubule stabilization. *J. Cell Sci.* 120:2106–2116. https://doi.org/10.1242/jcs.03458

Klingseisen, A., and A.P. Jackson. 2011. Mechanisms and pathways of growth failure in primordial dwarfism. *Genes Dev.* 25:2011–2024. https://doi.org/10.1101/gad.169037

Lee, J., Y. Jeong, S. Jeong, and K. Rhee. 2010. Centrobin/NIP2 is a microtubule stabilizer whose activity is enhanced by PLK1 phosphorylation during mitosis. *J. Biol. Chem.* 285:25476–25484. https://doi.org/10.1074/jbc.M109.099127

Liska, F., C. Gosele, E. Rivkin, L. Tres, M.C. Cardoso, P. Domaing, E. Krejci, P. Snajdr, M.A. Lee-Kirsch, D.G. de Rooij, et al. 2009. Rat bd mutation reveals an essential role of centrobin in spermatid head shaping and assembly of the head-tail coupling apparatus. *Biol. Reprod.* 81:1196–1205. https://doi.org/10.1095/biolreprod.109.078980

Liška, F., C. Gosele, E. Popova, B. Chylíková, D. Křenová, V. Křen, M. Bader, L.L. Tres, N. Hubner, and A.L. Kierszenbaum. 2013. Overexpression of full-length centrobin rescues limb malformation but not male fertility of the hypodactylous (hd) rats. *PLoS One.* 8:e60859. https://doi.org/10.1371/journal.pone.0060859

Mali, P., L. Yang, K.M. Esvelt, J. Aach, M. Guell, J.E. DiCarlo, J.E. Norville, and G.M. Church. 2013. RNA-guided human genome engineering via Cas9. *Science.* 339:823–826. https://doi.org/10.1126/science.1232033

Martin, C.A., I. Ahmad, A. Klingseisen, M.S. Hussain, L.S. Bicknell, A. Leitch, G. Nürnberg, M.R. Toliat, J.E. Murray, D. Hunt, et al. 2014. Mutations in PLK4, encoding a master regulator of centriole biogenesis, cause microcephaly, growth failure and retinopathy. *Nat. Genet.* 46:1283–1292. https://doi.org/10.1038/ng.3122

Nigg, E.A., and J.W. Raff. 2009. Centrioles, centrosomes, and cilia in health and disease. *Cell.* 139:663–678. https://doi.org/10.1016/j.cell.2009.10.036

Nigg, E.A., and T. Stearns. 2011. The centrosome cycle: Centriole biogenesis, duplication and inherent asymmetries. *Nat. Cell Biol.* 13:1154–1160. https://doi.org/10.1038/ncb2345

O'Driscoll, M., V.L. Ruiz-Perez, C.G. Woods, P.A. Jeggo, and J.A. Goodship. 2003. A splicing mutation affecting expression of ataxia-telangiectasia and Rad3-related protein (ATR) results in Seckel syndrome. *Nat. Genet.* 33:497–501. https://doi.org/10.1038/ng1129

Oshimori, N., M. Ohsugi, and T. Yamamoto. 2006. The Plk1 target Kizuna stabilizes mitotic centrosomes to ensure spindle bipolarity. *Nat. Cell Biol.* 8:1095–1101. https://doi.org/10.1038/ncb1474

Prosser, S.L., and C.G. Morrison. 2015. Centrin2 regulates CP110 removal in primary cilium formation. *J. Cell Biol.* 208:693–701. https://doi.org/10.1083/jcb.201411070

Seeley, E.S., and M.V. Nachury. 2010. The perennial organelle: assembly and disassembly of the primary cilium. *J. Cell Sci.* 123:511–518. https://doi.org/10.1242/jcs.061093

Shin, W., N.K. Yu, B.K. Kaang, and K. Rhee. 2015. The microtubule nucleation activity of centrobin in both the centrosome and cytoplasm. *Cell Cycle.* 14:1925–1931. https://doi.org/10.1080/15384101.2015.1041683

Sorokin, S. 1962. Centrioles and the formation of rudimentary cilia by fibroblasts and smooth muscle cells. *J. Cell Biol.* 15:363–377. https://doi.org/10.1083/jcb.15.2.363

Spektor, A., W.Y. Tsang, D. Khoo, and B.D. Dynlacht. 2007. Cep97 and CP110 suppress a cilia assembly program. *Cell.* 130:678–690. https://doi.org/10.1016/j.cell.2007.06.027

Stiff, T., T. Casar Tena, M. O'Driscoll, P.A. Jeggo, and M. Philipp. 2016. ATR promotes cilia signalling: links to developmental impacts. *Hum. Mol. Genet.* 25:1574–1587. https://doi.org/10.1093/hmg/ddw034

Tanos, B.E., H.J. Yang, R. Soni, W.J. Wang, F.P. Macaluso, J.M. Asara, and M.F. Tsou. 2013. Centriole distal appendages promote membrane docking, leading to cilia initiation. *Genes Dev.* 27:163–168. https://doi.org/10.1101/gad.207043.112

Tsang, W.Y., C. Bossard, H. Khanna, J. Perälnen, A. Swaroop, V. Malhotra, and B.D. Dynlacht. 2008. CP110 suppresses primary cilia formation through its interaction with CEP290, a protein deficient in human ciliary disease. *Dev. Cell.* 15:187–197. https://doi.org/10.1016/j.devcel.2008.07.004

Vorobjev, I.A., and Y.S. Chentsov. 1982. Centrioles in the cell cycle. I. Epithelial cells. *J. Cell Biol.* 93:938–949. https://doi.org/10.1083/jcb.93.3.938

Waters, A.M., and P.L. Beales. 2011. Ciliopathies: an expanding disease spectrum. *Pediatr. Nephrol.* 26:1039–1056. https://doi.org/10.1007/s00467-010-1731-7

Zou, C., J. Li, Y. Bai, W.T. Gunning, D.E. Wazer, V. Band, and Q. Gao. 2005. Centrobin: A novel daughter centriole-associated protein that is required for centriole duplication. *J. Cell Biol.* 171:437–445. https://doi.org/10.1083/jcb.200506185

Supplemental material

JCB

Ogungbenro et al., https://doi.org/10.1083/jcb.201706095

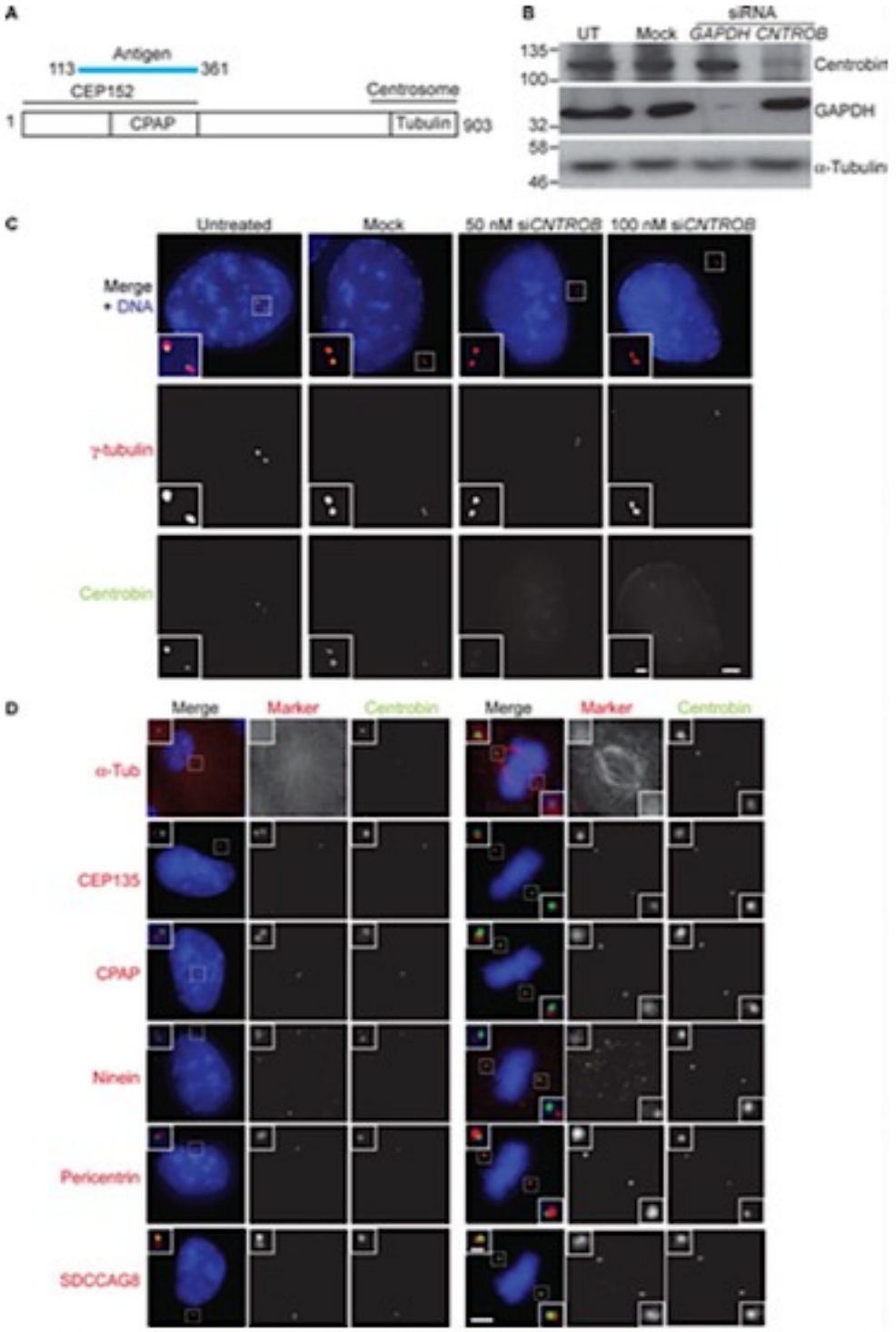

Figure S1. **Generation and characterization of a monoclonal antibody for centrobin. (A)** Diagram of centrobin indicating fragment of the protein used for generation of the monoclonal 6D4F4 and the regions required for CPAP, CEP152, or tubulin interactions or localization to the centrosome. **(B)** RNAi confirmation of the specificity of 6D4F4 using immunoblot analysis of control hTERT-RPE1 cells or of *CNTROB* knockdown cells 48 h after siRNA transfection with the indicated siRNA. UT, untreated. **(C)** Micrograph confirmation of the specificity of 6D4F4. *CNTROB* knockdown or control hTERT-RPE1 cells were stained for centrobin (green) and γ-tubulin (red) 48 h after siRNA transfection. Bars: 5 µm; (inset) 1 µm. **(D)** IF localization of centrobin. Interphase or mitotic cells were stained with the monoclonal antibody 6D4F4 to centrobin (green) and the indicated markers (red). Bars: 5 µm; (inset) 1 µm.

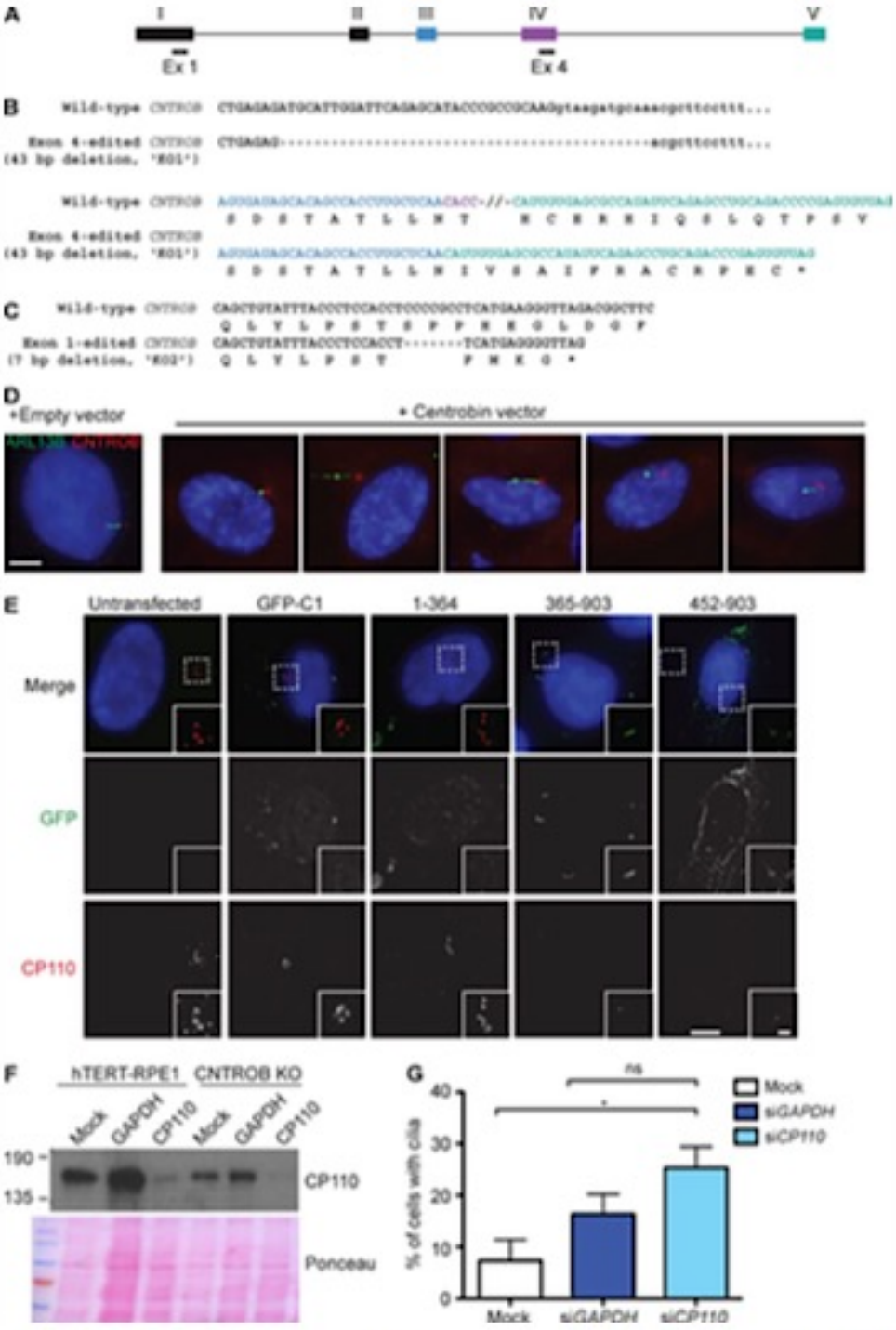

Figure S2. **Confirmation of *CNTROB* disruption by genome editing. (A)** Diagram of exons 1–5 of the 19 exons in the *CNTROB* locus showing the location of the guide RNAs used for CRISPR-directed genome editing (Ex 1 and Ex 4; not to scale). Exons are based on sequence NM_053051.3 and are indicated in color to clarify splicing in B. **(B)** Genome editing of *CNTROB* genomic sequence with the resultant transcript and predicted protein sequence for KO1 (exon 4 guide). Sequences are colored according to their respective exon as in A, and part of the WT exon 4 sequence is omitted. The 43-bp deletion at the 3′ end of exon 4 in KO1 led to splicing between directly exons 3 and 5, as indicated. **(C)** Genome editing of *CNTROB* genomic sequence with the resultant transcript and predicted protein sequence for KO2 (exon 1 guide). **(D)** IF micrographs of cells 48 h after transfection with the indicated plasmid. Cells were fixed and stained with antibodies to centrobin (red) and ARL13B (green), then counterstained for DNA with DAPI (blue). 35% of 100 cells transfected with the centrobin plasmid showed the "bulge," which was seen in only 4% of the control transfectants. Bar, 5 µm. **(E)** IF micrographs of *CNTROB* null cells after 24 h serum starvation imposed 16 h after transfection with the indicated GFP control or GFP-tagged centrobin fragment. Cells were fixed and stained with antibodies to CP110 (red) and GFP (green), then counterstained for DNA with DAPI (blue). Bars: 5 µm; (inset) 1 µm. Images are representative of two experiments in which CP110 accumulation was seen in a mean 65% of CNTROB knockout cells; 59% of the GFP-transfected cells; 65% of cells transfected with 1–364; 25% with 365–903; and 22% with 452–903. **(F)** Immunoblot showing the knockdown of CP110 in cells treated as indicated. Ponceau staining of the membrane after transfer was used as a loading control. **(G)** Bar chart shows quantitation of the ciliation frequency in *CNTROB* null cells after 48 h serum starvation with mock transfection, *CP110* knockdown and control *GAPDH* knockdown. Histogram shows mean + SEM of three independent experiments in which at least 100 cells were quantitated for ciliation by staining for acetylated tubulin. *, $P < 0.05$, in comparison to the indicated samples by unpaired *t* test.

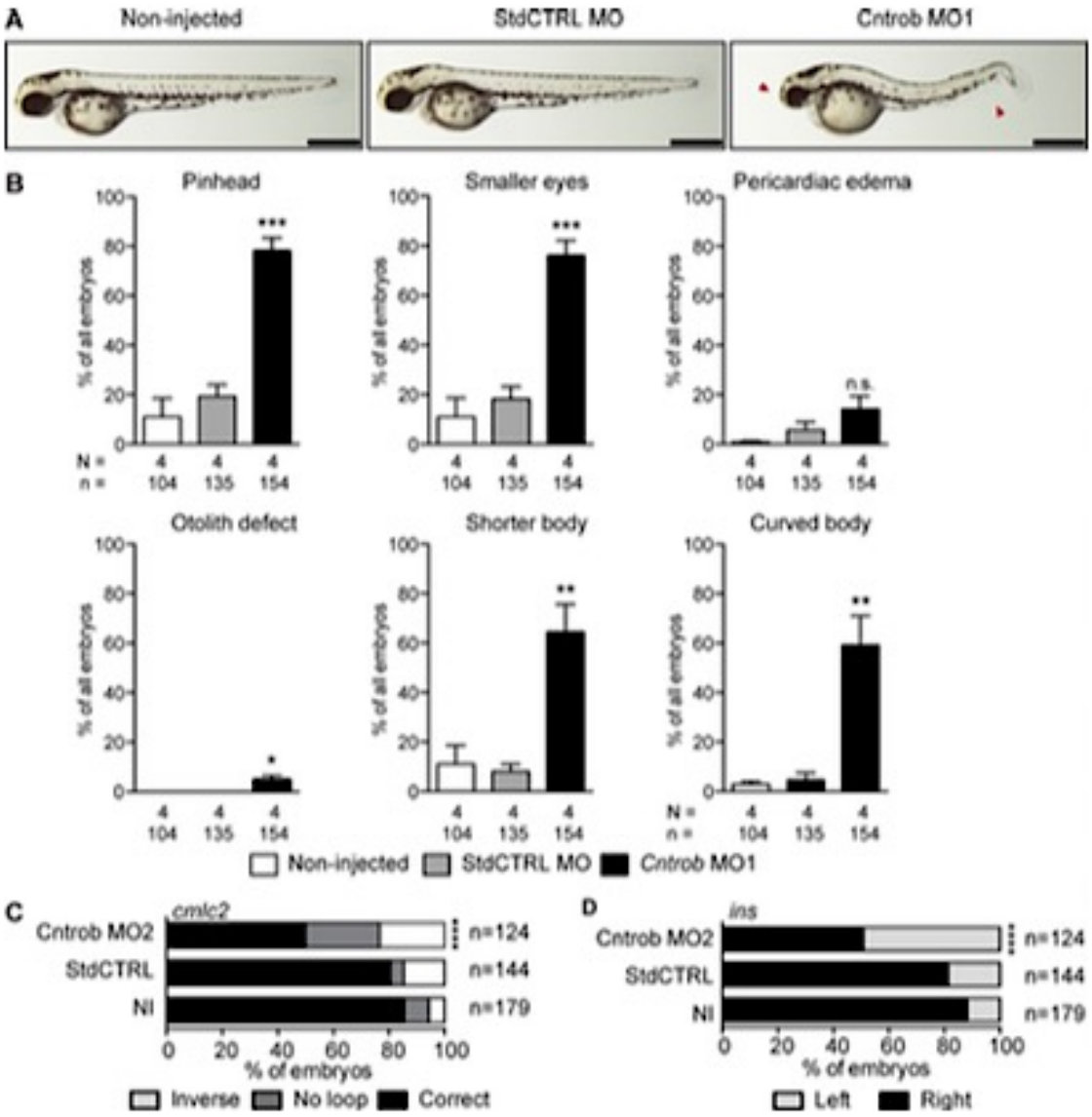

Figure S3. **Reproduction of the zebrafish phenotypes with a second MO.** MO1 was directed to the centrobin ATG and MO2 to the 5′ UTR. **(A)** Live images show gross phenotypes of zebrafish embryos injected with control or centrobin MOs at 48 hpf. Arrowheads indicate morphological abnormalities. Bars, 500 nm. **(B)** Quantitation of developmental phenotypes in centrobin-deficient embryos. Each phenotype was quantitated over three experiments in the indicated number of zebrafish embryos, and graphs indicate means + SEM. *, $P < 0.05$; **, $P < 0.01$; ****, $P < 0.0001$, by one-way ANOVA. **(C)** Quantitation of appropriate heart looping in WT embryos and embryos injected as indicated at 48 hpf. ****, $P < 0.0001$. Significances were assessed using Fisher's exact test. **(D)** Quantitation of pancreas placement in WT embryos and embryos injected as indicated at 48 hpf. Correct placement is at right. ****, $P < 0.0001$. Significances were assessed using Fisher's exact test.

Danio rerio centrobin (cntrob) mRNA, complete cds

GenBank: MF461638.1

FASTA Graphics

Go to:

```
LOCUS       MF461638                2706 bp    mRNA    linear   VRT 10-FEB-2018
DEFINITION  Danio rerio centrobin (cntrob) mRNA, complete cds.
ACCESSION   MF461638
VERSION     MF461638.1
KEYWORDS    .
SOURCE      Danio rerio (zebrafish)
  ORGANISM  Danio rerio
            Eukaryota; Metazoa; Chordata; Craniata; Vertebrata; Euteleostomi;
            Actinopterygii; Neopterygii; Teleostei; Ostariophysi;
            Cypriniformes; Cyprinidae; Danio.
REFERENCE   1  (bases 1 to 2706)
  AUTHORS   Ogungbenro,Y.A., Casar Tena,T., Gaboriau,D., Lalor,P., Dockery,P.,
            Philipp,M. and Morrison,C.G.
  TITLE     Centrobin controls primary ciliogenesis in vertebrates
  JOURNAL   J. Cell Biol. (2018) In press
REFERENCE   2  (bases 1 to 2706)
  AUTHORS   Ogungbenro,Y.A., Casar Tena,T., Philipp,M. and Morrison,C.G.
  TITLE     Direct Submission
  JOURNAL   Submitted (10-JUL-2017) Biochemistry, National University of
            Ireland Galway, Centre for Chromosome Biology, Biomedical Sciences
            Building, Dangan, Galway, Galway H91 TK33, Ireland
FEATURES             Location/Qualifiers
     source          1..2706
                     /organism="Danio rerio"
                     /mol_type="mRNA"
                     /strain="AB"
                     /db_xref="taxon:7955"
                     /chromosome="23"
                     /dev_stage="8 hpf"
     gene            1..2706
                     /gene="cntrob"
     5'UTR           1..39
                     /gene="cntrob"
     CDS             40..2649
                     /gene="cntrob"
                     /function="required for centriole duplication,
                     ciliogenesis and cytokinesis"
                     /note="encodes a core centrosomal protein that interacts
                     with BRCA2"
                     /codon_start=1
                     /product="centrobin"
                     /protein_id="AUZ17047.1"
                     /translation="MSVSRAAADGVSDGGLVVRSWPSSPLSATRQVTARLYSSLQHSR
                     QQEVKGHAADRQVSFALSSPDLTAVRTTSATPPLLSDRLEELSLDSASSHDVMGIGEE
                     GVESDAEEVGLQLLKSLRSAQPTSGRKHIEEMESVRTHLQSILRPTQTTADRHDFLTP
                     ASQHFLDDSHESDATSRLLSGVCVGGVEELFPRYSRLHSDVSCAVSELQVLRDSLERE
                     RERRKVCEQQVASLQSKVLQFQQQLTLAVAADRKKDIMIEQLDKTLVKVVEGWKRHDQ
                     ERNEEMKRLQEEKETAEKTHNKHAQALSRVEQNLSEVEETLKKEQKHNQELQKTNKRL
                     EQEASDLRVHVEDLQQDKQKLSREADKHREQLHKLQTESHDTRTNLQQQIKVLQQHTQ
                     ELQQQLHTHTDQLKQEVSAREEAESRTRLLQEELETTRRERETLRIERALEQTQFEAQ
                     KSQMEAEFRLSLEQQISERVKAVQEENNTYNTQLRQQHRKQLLDLSARQERELAAQLD
                     QCRTQLQERDDKLQHLTQAYQHRLSEMQEQLVSMAATKKKLESQREELVSRLQGMMRS
                     HWAEALRLLTNQEQMESFLSPVHQRETSRMSSSPKSDPHVSAPQAVVLHLSREKEQQW
                     GTHRELNSEINCSNTFSPLEPQLDNTELTALSDCSALWVRPMFTIDESMKEQSEERRE
                     TQSNLKHNLNYSQCEPKLKHSHTDAWTNHNSAADNVQDRGGASVLKQSHAPSDTWTNN
                     SSAPDSGLGRGGASVLKQSHAPLDTLTIHSSTADSGLARGGASVLKQSHTPSDQWANH
                     SSTAESGLGRGGVSVVKQSNAPSDTWTNHCSAAESGLGRVVFCTETEPRPLRHTTIRS
                     APESGLSRLEFLY"
```

```
     3'UTR           2650..2706
                     /gene="cntrob"
ORIGIN
        1 taaacaaact ctcatcaaac tccacaaact gtctgtgaga tgtctgtgag ccgagctgct
       61 gctgatggtg ttagtgatgg tggtctggtg gtgcgctcat ggccctcgtc tcctctgtct
      121 gcgactcgtc aggtcaccgc tcgcctctac agctcattac agcacagccg acagcaggag
      181 gtcaaaggtc acgctgcaga caggcaggtg tcattcgctc tgtcctctcc tgatctcacc
      241 gctgtcagga cgacctcagc cacgcctcct ctgctctctg ataggctgga ggagctcagt
      301 ttggactccg cctcctctca tgatgtgatg ggcataggag aggagggggt ggagtcagat
      361 gcagaagagg tggggcttca acttttgaag agcctgagat ctgcacaacc gacgagtggc
      421 aggaagcaca tagaggagat ggaaagtgtg aggacacact tgcagtctat actgaggcca
      481 acacagacaa ctgcagacag acacgatttt ctgactcctg catcacagca cttcctggat
      541 gattcacatg agagtgatgc cacgtcacgc ctgctcagtg gtgtgtgtgt aggtggtgtg
      601 gaggagttgt tccctcgtta ttcccgtctt cattcagatg tgagctgcgc agtttctgag
      661 ctgcaggtgc tgagagacag tctagagaga gagcgagagc gccgcaaggt gtgtgagcag
      721 caggtggcgt ctctccaaag taaagttctt cagtttcagc agcagttaac actcgctgta
      781 gccgccgacc gcaagaaaga catcatgatt gaacagttgg acaagacgct ggtgaaggtg
      841 gttgagggct ggaagaggca cgatcaggag cgaaatgagg agatgaaacg gctgcaggag
      901 gagaaggaga ccgctgagaa aacacacaac aaacatgcac aggctctgtc tcgtgttgag
      961 cagaatctct ctgaggttga ggaaactctg aagaaggagc agaaacacaa tcaggagctg
     1021 cagaagacca acaaacgact ggagcaagag gcgtctgatc tgcgtgtgca tgtggaggac
     1081 ttacagcaag acaagcaaaa gcttagcaga gaagcagata aacacagaga gcagctccac
     1141 aaactccaga cagagtcgca tgacacacgg acgaatctac aacaacaaat caaggtgctg
     1201 cagcagcaca cacaagaatt acagcagcag ctgcacacac acacggatca gctgaaacag
     1261 gaagtgtctg cgcgtgaaga ggcagaaagc agaactcggc tgttacagga agagctggag
     1321 acgacaagga gagagcgaga gacactgaga atagagcgag cactggagca gacgcagttc
     1381 gaggcgcaga agtctcagat ggaggctgag tttcgtctgt cattggagca gcagatcagt
     1441 gaaagagtga aggctgtgca ggaggagaac aacacataca acacacaact acgacagcag
     1501 cacaggaagc agctactgga tctaagtgca cggcaggagc gagagctggc ggctcagctg
     1561 gatcagtgca gaacacagtt acaggagaga gacgacaaac tgcagcatct cacacaggct
     1621 taccagcaca gactgtcgga gatgcaggag cagctggttt ccatggcagc gactaaaaag
     1681 aagctagaat cgcagaggga ggagcttgtg tctcgtcttc agggaatgat gcgctctcat
     1741 tgggcggagg ctttacggct gctgaccaat caggagcaga tggagagttt tttatcaccc
     1801 gtccatcaga gggaaacatc cagaatgtcg tcatctccta agagtgaccc acatgtatca
     1861 gctccgcagg ctgtggttct gcatctgtcc agagagaagg agcagcagtg gggaacacac
     1921 cgagagctga actcagagat caactgcagc aacacattca gcccactgga gccacagctg
     1981 gacaacactg agctcacagc actcagtgac tgcagtgcat tgtgggtcag gccgatgttc
     2041 acaatagatg aatccatgaa agagcagagt gaggagagga gagaaactca gtcaaacctg
     2101 aagcacaatc tgaattacag tcagtgtgaa cccaagctga aacacagcca cacagacgca
     2161 tggaccaatc acaactcagc tgcagataat gtgcaggaca ggggcggagc ttctgtactg
     2221 aaacagagcc acgccccctc agacacgtgg accaataaca gctcagctcc agatagtggg
     2281 ctgggcaggg gcggagcttc tgtactaaaa cagagccacg ccccccttaga cacattgact
     2341 attcacagct caactgcaga tagtgggctg gccaggggcg gagcttctgt actgaagcag
     2401 agccacaccc cctcagacca atgggccaat cacagctcaa ctgcagagag tgggctgggc
     2461 aggggcggtg tttctgtagt gaagcagagc aacgccccct cagacacatg gaccaatcac
     2521 tgctcagctg cagagagtgg gctgggcagg gtggtgttct gtactgaaac agagccacgc
     2581 cccctcagac acacgactat acgctcagct ccagaaagtg ggctgagcag gttggagttt
     2641 ctgtactgaa caagcatgcc ctcctcagaa cacatgacca tccacagctc aactgccaga
     2701 attgtt
//
```